CHALMERS
UNIVERSITY OF TECHNOLOGY

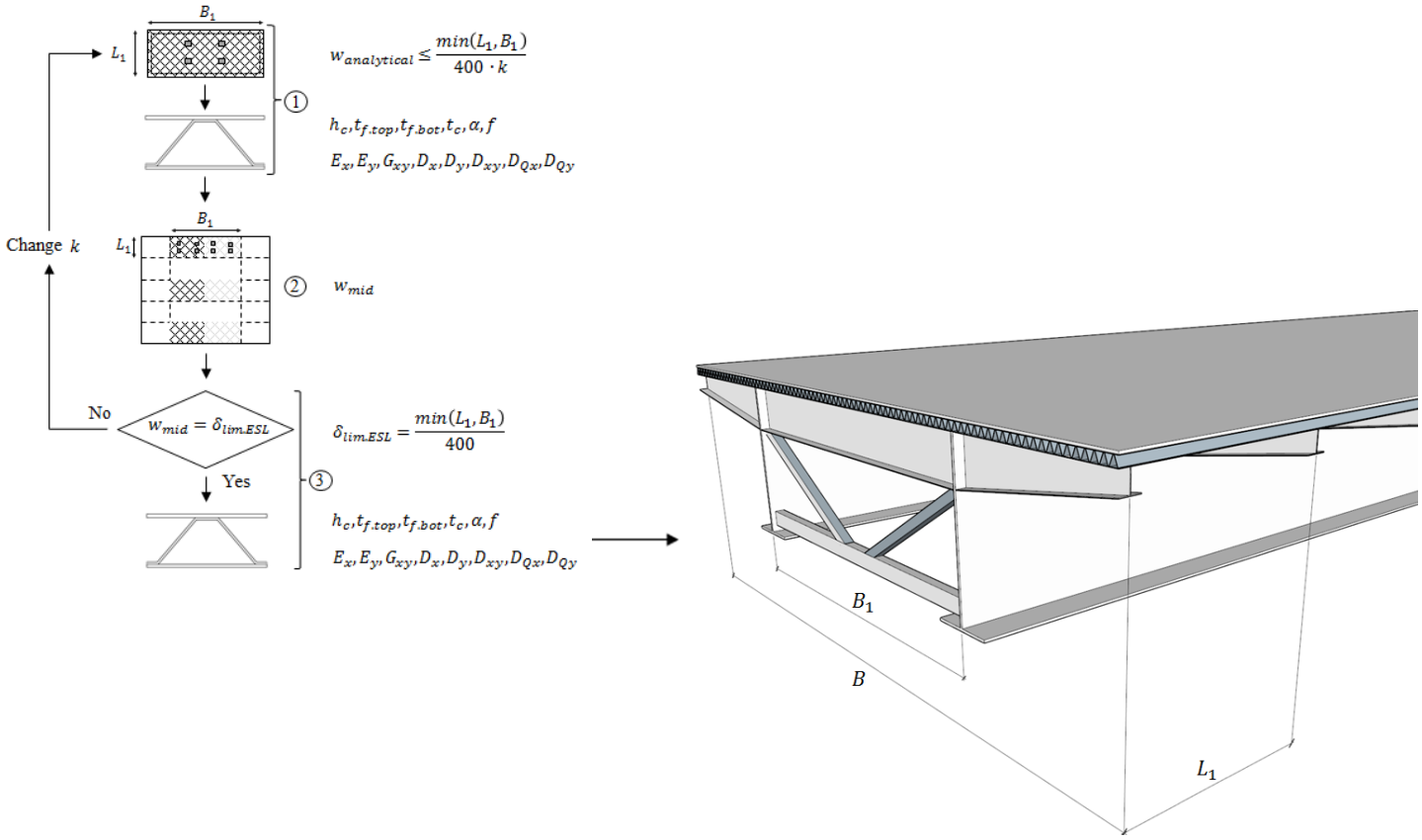

Steel sandwich decks in medium span bridges

A case study

Master's Thesis in the Master's Programme Structural Engineering and Building Technology

David Dackman
Walter Ek

Department of Civil and Environmental Engineering
Division of Structural Engineering
Steel and Timber structures
CHALMERS UNIVERSITY OF TECHNOLOGY
Gothenburg, Sweden 2015
Master's Thesis 2015:145

MASTER'S THESIS 2015:145

Steel sandwich decks in medium span bridges

A case study

Master's Thesis in the Master's Programme Structural Engineering and Building Technology

David Dackman

Walter Ek

Department of Civil and Environmental Engineering
Division of Structural Engineering
Steel and Timber structures
CHALMERS UNIVERSITY OF TECHNOLOGY
Göteborg, Sweden 2015

Steel sandwich decks in medium span bridges
A case study

Master's Thesis in the Master's Programme Structural Engineering and Building Technology

David Dackman

Walter Ek

Examensarbete 2015:145/ Institutionen för bygg- och miljöteknik,
Chalmers tekniska högskola 2015

Department of Civil and Environmental Engineering
Division of Structural Engineering
Steel and Timber structures
Chalmers University of Technology
SE-412 96 Göteborg
Sweden
Telephone: + 46 (0)31-772 1000

Cover:
Flowchart of preliminary design of SSD configuration

Chalmers Reproservice / Department of Civil and Environmental Engineering
Göteborg, Sweden, 2015

Steel sandwich decks in medium span bridges

A case study

Master's thesis in the Master's Programme Structural Engineering and Building Technology

David Dackman
Walter Ek
Department of Civil and Environmental Engineering
Division of Structural Engineering
Steel and Timber structures
Chalmers University of Technology

ABSTRACT

Steel-concrete composite bridges offer several benefits compared to concrete bridges, mainly with regard to reduced construction time and disturbance of the surrounding area. In most cases the weight of the concrete deck makes launching of the whole composite section difficult, and therefore the deck needs to be cast or lifted on the steelwork in a second step. If the steel girders instead could be launched together with the bridge deck, the construction time could be significantly reduced. The use of steel sandwich decks (SSD) in bridges is a concept developed over recent years. SSD's are composed of two stiff outer face plates attached to a core and the high stiffness-to-weight ratio allows for a weight reduction compared to concrete decks.

The purpose of this thesis was to evaluate SSD's as an alternative to concrete decking in composite bridges. An existing steel-concrete composite bridge was used as a case study, to evaluate the performance of SSD's and investigate the possibility of launching the main girders together with the deck.

In a preliminary design it was investigated how different distances between transverse girders influenced the dimensions of the SSD. The 3D SSD was idealised as a homogeneous orthotropic plate and the area of the SSD was optimised.

The SSD obtained from the preliminary design was used to model the whole bridge in the finite element software Abaqus/CAE and the performance of the SSD was studied in more detail. The existing composite bridge was modelled as well in order to compare stresses in the main girders. Finally, the performance during launching was verified.

It was concluded that the SSD could be a valid alternative to concrete decks in composite bridges, especially when reduction of the construction time is of importance.

Key words: Steel sandwich decks, bridge decks, optimisation, finite element analysis

Contents

Preface

In this Master's thesis, the application of steel sandwich decks in bridges was studied. It was written in the spring of 2015, and the project was carried out in the cooperation between the Department of Civil and Environmental Engineering at Chalmers University of Technology and WSP Bridge and Hydraulic design in Gothenburg.

We would like to thank Roland Olsson and his co-workers at WSP Bridge and Hydraulic design for giving us the opportunity to complete this project at their department.

Gratitude is given to our examiner Mohammad Al-Emrani, for the support and encouragement he has given us during the project. The input from our opponent group consisting of Adam Johansson and Johan Fredberg has been valuable as well.

Finally, the deepest gratitude is given to our supervisor Peter Nilsson. Without his support, this project would not have been possible to complete. His great dedication and commitment have inspired us to perform at the top of our ability.

Gothenburg June 2015

David Dackman

Walter Ek

Notations

Roman upper case letters

A_c, A_f	Area per unit width of corrugation and face plates respectively, [m]
B	Total width of the bridge, [m]
B_1	Distance between the main girders, [m]
D_x, D_y	Bending stiffness per unit width of corrugated SSD, for bending around the x- and y-axis respectively, [Nm]
D_{xy}	Torsional stiffness per unit width of corrugated SSD, [Nm]
D_{Qx}, D_{Qy}	Transverse shear stiffness per unit width of corrugated SSD, in the x- and y-direction respectively, [Nm]
E_c	Modulus of elasticity of core material, [Pa]
E_{conc}	Modulus of elasticity of concrete, [Pa]
E_f	Modulus of elasticity of face plate material, [Pa]
E_s	Modulus of elasticity of steel, [Pa]
E_x, E_y	Axial stiffness per unit width of corrugated SSD, in the x- and y-direction respectively, [N/m]
$E_x^{e\prime}$, $E_y^{e\prime}$	Engineering constants, related to axial stiffness, for in-plane loading, [Pa]
E_x^e, E_y^e	Engineering constants, related to bending stiffness, for out-of-plane loading, [Pa]
G_f	Shear modulus of elasticity of face plate material, [Pa]
G_c	Shear modulus of elasticity of core material, [Pa]
G_{xy}	Horizontal shear stiffness per unit width of corrugated SSD, [N/m]
$G_{xy}^{e\prime}$	Engineering constant, related to horizontal shear stiffness, for in-plane loading, [Pa]
G_{xy}^e	Engineering constant, related to torsional stiffness, for out-of-plane loading, [Pa]
G_{xz}^e, G_{yz}^e	Engineering constants, related to transverse shear stiffness, [Pa]
I_f	Moment of inertia per unit width of face plates, [m^3]
I_c	Moment of inertia per unit width of corrugation, [m^3]
L	Total length of bridge, [m]
L_1	Length between the transverse girders, [m]
L_{span1}	Length of edge span, [m]
L_{span2}	Length of middle span, [m]
M_{xx}, M_{yy}	Bending moments per unit width, in x- and y-direction respectively, [N]

M_{xy} Twisting moment per unit width, [N]

N_{xx}, N_{yy} Membrane forces per unit width, in x- and y-direction respectively, [N/m]

N_{xy} Membrane shear force per unit width, [N/m]

Q_{ik} Characteristic axle load in traffic lane i, [N]

S Non-dimensional coefficient used for calculation of D_{Qy}, [-]

V_x, V_y Shear force per unit width, in x- and y-direction respectively, [N/m]

V_{MG} Volume per meter of main girders, from preliminary design, [m^2]

V_{SSP} Volume per meter of SSD, from preliminary design, [m^2]

V_{TG} Volume per meter of transverse girders, from preliminary design, [m^2]

V_{tot} Total volume of bridge per meter, from preliminary design, [m^2]

P_{plc} Plastic collapse load of corrugation under patch load, [N]

Roman lower case letters

b Width of the interval considered in calculation of b_e, [m]

b_e Effective width, [m]

b_{EB} Width of edge beam flange, [m]

$b_{MG.bf}$ Width of main girder bottom flange, [m]

$b_{TG.bf}$ Width of transverse girder bottom flange, [m]

$b_{TGS.bf}$ Width of transverse support girder bottom flange, [m]

c Loaded length of the corrugation in calculation of P_{plc}, [m]

f Length of horizontal corrugation segment [m]

$f_{u.f.top}$ Ultimate strength of top face plate, [Pa]

$f_{y.f.top}$ Yield strength of top face plate, [Pa]

$f_{y.f.bot}$ Yield strength of bottom face plate, [Pa]

$f_{y.c}$ Yield strength of SSD corrugation, [Pa]

g_k Self-weight of bridge deck, [N/m^2]

h Distance between middle surfaces of face plates, [m]

h_c Height of corrugation, measured vertically from centre line of crest to centre line at trough, [m]

h_{EB} Height of edge beam, [m]

$h_{MG.w}$ Height of main girder web, [m]

$h_{TG.w}$ Height of transverse girder web, [m]

$h_{TGS.w}$ Height of transverse support girder web, [m]

k_{GJ} Ratio depending on the distance to the zero-shear plane of SSD, [-]

k_c Ratio depending on the distance to the shear centre of the corrugation, [-]

l_c Length of one corrugation leg, measured along the centre line, [m]

l_o Length of corrugation opening, [m]

p Half of the corrugation pitch, [m]

q_{ik} Characteristic uniformly distributed load in traffic lane i, [N/m^2]

t_c Thickness of corrugation, [m]

$t_{f.top}$ Thickness of top face plate, [m]

$t_{f.bot}$ Thickness of bottom face plate, [m]

t_{EB} Thickness of edge beam, [m]

$t_{MG.bf}$ Thickness of main girder bottom flange, [m]

$t_{MG.w}$ Thickness of main girder web, [m]

$t_{TG.bf}$ Thickness of transverse girder bottom flange, [m]

$t_{TG.w}$ Thickness of transverse girder web, [m]

$t_{TGS.bf}$ Thickness of transverse support girder bottom flange, [m]

$t_{TGS.w}$ Thickness of transverse support girder web, [m]

w_{cant} Deflection of cantilever part of SSD, [m]

w_{mid} Deflection of SSD between main and transverse girders, [m]

w_{lane} Width of traffic lane, [m]

Greek lower case letters

α Angle of corrugation, [deg]

α_Q Correction factor for axle loads, [-]

α_q Correction factor for uniformly distributed traffic load, [-]

γ_G Partial coefficient for permanent ULS load, [-]

γ_Q Partial coefficient for variable ULS load, [-]

γ_{M0} Partial factor for resistance check, [-]

γ_{M1} Partial factor for instability checks, [-]

ε Coefficient considering the yield strength, [-]

η_{cant} Utilisation ratio for w_{cant}, [-]

η_{mid} Utilisation ratio for w_{mid}, [-]

η_1 Utilisation ratio for bending, [-]

η_2 Utilisation ratio for patch loading, [-]

η_{LT} Utilisation ratio for lateral torsional buckling, [-]

λ Buckling load factor, [-]

ν_c	Poisson's ratio of core material, [-]
ν_{conc}	Poisson's ratio of concrete, [-]
ν_f	Poisson's ratio of face plate material, [-]
ν'_x	Poisson's ratio, associated with extension, in x-direction, [-]
ν_x	Poisson's ratio, associated with bending, in x-direction, [-]
ν'_y	Poisson's ratio, associated with extension, in y-direction, [-]
ν_y	Poisson's ratio, associated with bending, in y-direction, [-]
ξ	Reduction factor for self-weight, [-]
$\sigma_{vM.f.top}$	von Mises stress in top face plate, [Pa]
$\sigma_{x.f.top}$	Stress in top face plate, in x-direction, [Pa]
$\sigma_{x.f.bot}$	Stress in bottom face plate, in x-direction, [Pa]
$\sigma_{y.f.top}$	Stress in bottom face plate, in y-direction, [Pa]
$\sigma_{yb.f.top}$	Bending stress component in top face plate, in y-direction, [Pa]
$\sigma_{yn.f.top}$	Normal stress component in top face plate, in y-direction, [Pa]
$\psi_{0,1}$	Factor for combination of variable ULS loads [-]
$\psi_{1,1}$	Factor for frequent load combination, [-]

Abbreviations

ESL	Equivalent Single Layer
FEM	Finite Element Method
GMAW	Gas Metal Arc Welding
HAZ	Heat Affected Zone
HLAW	Hybrid Laser Arc Welding
LM1	Load Model 1
SLS	Service Limit State
SSD	Steel Sandwich Deck
TS	Tandem System
UDL	Uniformly Distributed Load
ULS	Ultimate Limit State

1 Introduction

1.1 Background

Steel-concrete composite bridges offer several benefits compared to concrete bridges, mainly with regard to reduced construction time and disturbance of the surrounding area (Collin & Lundmark, 2002). The need for formwork from the ground, when constructing concrete bridges, can be avoided since the steel girders can be launched or lifted and then act as support of the formwork. These advantages have contributed to the growing popularity of composite bridges during the last decades.

In most cases the weight of the concrete deck makes launching of the whole composite section difficult and therefore the deck slab needs to be cast or lifted on the steelwork in a second step (Collings, 2008). If the steel girders instead could be launched together with the bridge deck, the construction time would be significantly reduced. A weight reduction of the deck could make launching of the whole bridge feasible and also reduce the dimensions of the main girders and the substructure.

The use of steel sandwich decks (SSD) in bridges is a concept developed over recent years. SSD's are composed of two stiff outer face plates attached to a core. The core can have various geometrical configurations and is supposed to resist shear forces only, while the face plates resist bending moments. One important feature of the SSD is the high stiffness-to-weight ratio, which allows for a weight reduction compared to concrete decks.

The traditional steel decks used in bridge construction are the so-called orthotropic decks, consisting of a top plate with longitudinal stiffeners. A significant feature of orthotropic steel decks is the large amount of manual welding and problem with fatigue cracks.

SSD's are manufactured using laser welding which allows for welding from one side and a more automated welding process (Caccese & Yorulmaz, 2009). The laser welding process also improves the fatigue resistance compared to the orthotropic steel decks (Bright & Smith, 2007). The use of laser welding for larger sections, like bridge decks, is a relatively new technique but recent developments make SSD's a potential cost effective alternative to conventional decking.

1.2 Aim and objectives

The purpose of this thesis was to evaluate SSD decks as an alternative to concrete decking in composite bridges. This is done through a case study in which the objectives were to:

- Obtain a SSD configuration optimised with regard to weight, without the loss of structural performance.
- Study how the dimensions of the main girders were influenced by replacing the concrete deck with SSD's.
- Investigate if the construction time could be reduced, by allowing for launching of the bridge with the deck included.

1.3 Method

The thesis started with a literature study about SSD's. The main focus was on the structural behaviour and performance of the decks including properties like stiffness, orthotropy, fatigue and instability. The history, applications and production processes of SSD's were covered briefly, as well as the construction and behaviour of steel-concrete composite bridges.

To evaluate the potential of SSD's a case study of a bridge over Bergeforsen was carried out in two steps. The bridge was designed and built as a composite bridge consisting of two launched I-girders and a cast in-situ concrete slab. The total length of 166 m is divided into in three spans and the total width of the traffic lanes is 11.25 m.

In the first step a preliminary design was carried out with the purpose of finding a low weight SSD configuration. Different configurations of the SSD and distances between the transverse girders were investigated in order to find the combination resulting in the lowest steel volume in the bridge. An optimisation routine developed by Beneus & Koc (2014) was further developed and used to minimise the area of the SSD. A part of the bridge deck was analysed with a finite element (FE) model in Abaqus/CAE to check that the deflection of the SSD was below the requirement. In the preliminary FE-analysis the 3D SSD was idealised as a homogeneous orthotropic thick plate in order to reduce the modelling and calculation times.

In the second step the whole bridge was modelled and analysed in Abaqus/CAE with the SSD from the preliminary design. A FE-model of the existing composite bridge over Bergeforsen was created as well in order to be able to compare stresses in the main girder bottom flanges of the two bridges. First, the dimensions of the bottom flanges in the SSD bridge were adjusted until the bottom flange stresses in the two models corresponded. Next, the edge beam was designed so that the cantilever part of the SSD met the local deflection requirement. In addition to designing the main girders and the edge beams, verification of the SSD capacity was done at critical sections. Finally, it was investigated if the SSD deck could be launched together with the main girders.

1.4 Outline

The first chapter describes the background, methodology and purpose of the thesis. In the following chapter the literature study is covered. The main focus of the literature study was the structural performance of the SSD. The elastic stiffness constants for modelling the SSD as an equivalent single layer (ESL) was presented followed by a description of the behaviour of thick orthotropic plates following Mindlin-Reissner kinematics. Furthermore, an analytical solution for the deflection of the SSD modelled as an ESL was presented.

In chapter three the preliminary design of the SSD was covered. The preliminary design procedure of the SSD was explained and the configuration used for further analysis was presented.

In the fourth chapter the bridge used as a case study was modelled in Abaqus/CAE. Different models with either a SSD deck or a concrete deck were analysed. The performance of the SSD deck was verified and in addition, the possibility to launch the SSD deck together with the main girders was investigated.

In chapter five the methods and results were discussed and in chapter six conclusions from the thesis were drawn and suggestions for further studies recommended.

1.5 Limitations

No complete design of the bridge was carried out. A comparative study of the two bridge configurations was performed with respect to stress levels in the main girders.

The structural performance of the SSD deck was verified at critical sections but no connections were designed and the fatigue strength was not considered. Furthermore, only traffic loads and self-weight were considered.

The material needed for construction of the two bridges was compared but a cost comparison was omitted.

2 Literature study

2.1 Composite bridges

Composite bridges are structures that combine materials. The materials can be concrete, steel and glass or carbon-reinforced plastic. One of the most common composite bridge types consist of steel girders with a cast in-situ concrete slab (Collings, 2008). The steel-concrete composite bridge holds many advantages compared to a concrete bridge such as lower self-weight of the superstructure, no need of falsework on the ground and shorter construction time.

In most cases the weight of the concrete deck makes launching/lifting of the whole composite section difficult and therefore the deck slab needs to be cast or lifted on the steelwork in a second step. To ensure stability before the concrete has been cast the steelwork needs bracing.

I-girders are frequently used in composite bridges, and a typical composite bridge with I-girders are shown in Figure 2.1. The longitudinal and transverse stiffeners are used to transfer and distribute concentrated loads and to prevent local buckling of plate elements. The cross bracing provides lateral stability and distributes vertical loads to the main girders.

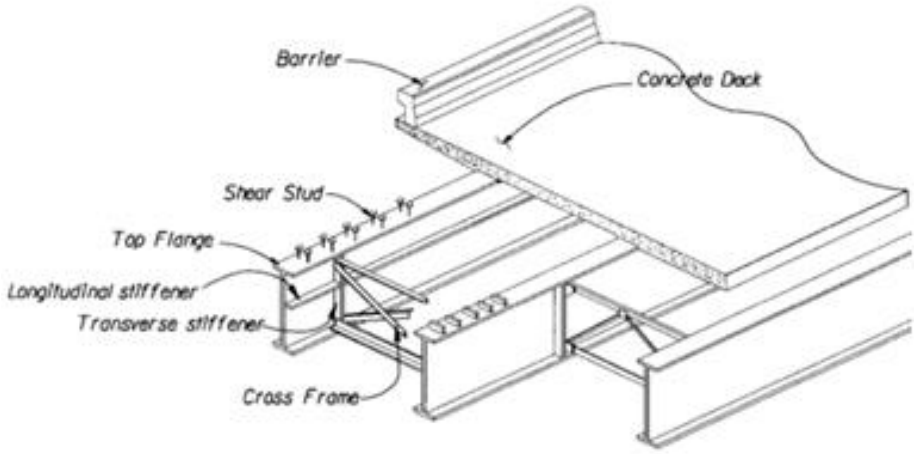

Figure 2.1 Typical components of I-girder composite bridges (Saleh & Duan, 2000).

2.2 Shear lag

Shear lag arises because the in-plane shear straining of a flange cause the parts closest to the web to develop higher longitudinal stresses then the parts further away (Vayas & Iliopoulos, 2014). Low in-plane shear stiffness G_{xy} therefore increases the shear lag effect. Elementary beam theory cannot capture this phenomenon correctly since the assumption that plane sections remain plane after bending is not true. Due to the shear lag the stresses at the web-flange intersection are larger than those calculated with beam theory. In design this effect is accounted for by introducing an effective width b_e (see Figure 2.2).

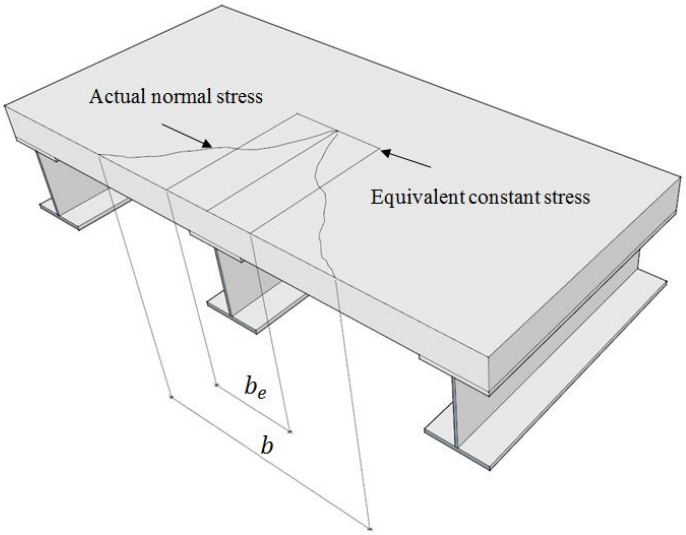

Figure 2.2 Shear lag effect and effective flange width.

The effective width can be calculated with equation (2.1), obtained from Zou et al. (2011), as the integral of the normal stress distribution divided by the maximum stress in a given interval.

$$b_e = \frac{\int_{-b/2}^{b/2} \sigma_x dx}{\sigma_{max}} \tag{2.1}$$

where:

b_e Effective width, [m]

b Width of the interval considered, [m]

σ_x Normal stress distribution, [Pa]

σ_{max} Maximum normal stress, [m]

Moffatt & Dowling (1975) performed a parametric study on the shear lag effect in steel box girders using finite element (FE) analysis. It was concluded that increased flange width to span length ratio b/L_{span} and increased axial stiffness to in-plane shear stiffness ratio E_x/G_{xy}, lead to a more pronounced shear lag effect. Furthermore it was shown that the shear lag was influenced by the type of loading and boundary conditions, while independent of the type of cross section (box, I-, T- or U-).

A parametric study of the shear lag effect in orthotropic steel beam flanges was conducted by Tenchev (1996) in order to establish a formula for a shear lag coefficient b_e/b. The conclusions by Moffatt & Dowling (1975) were confirmed and it was also shown that the transverse axial stiffness of the flange E_y, had negligible influence on the shear lag. Figure 2.3 shows the relation between b_e/b, E_x/G_{xy} and b/L_{span}.

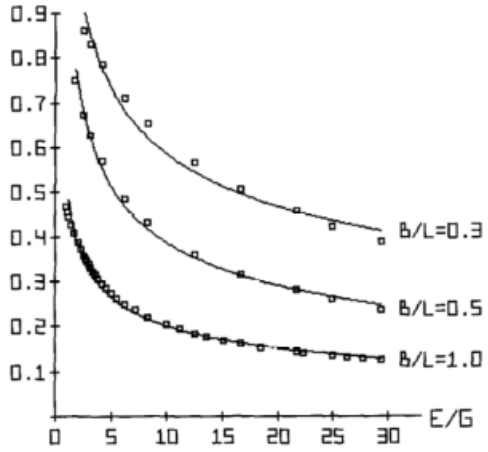

Figure 2.3 Shear lag coefficient (Tenchev, 1996).

Zou et al. (2011) proposed equation (2.2) as an analytical model for calculating the effective flange width for orthotropic bridge decks supported on steel girders. The shear lag model was verified with a finite element (FE) model, for different truck load positions.

$$b_e = \frac{\int_0^{b/2} \cosh(\xi_1 y)\, dy}{\cosh\left(\frac{\xi_1 b}{2}\right)} \tag{2.2}$$

where:

$$\xi_1 = \frac{\pi}{L_{span}} \sqrt{\frac{E_x}{G_{xy}}}$$

b_e Effective width, [m]

b Width of the interval considered, [m]

L_{span} Span length, [m]

E_x Axial stiffness, [N/m]

G_{xy} In-plane shear stiffness, [N/m]

2.3 Steel sandwich decks

A steel sandwich deck (SSD) is composed of two stiff plates that resist bending moments, separated by a low density core that resists shear forces (Caccese & Yorulmaz, 2009). The high stiffness-to-weight ratio allows for considerable weight reduction and faster construction compared to bridge decks made of concrete.

The core can have many different configurations with different properties (see Figure 2.4). Alwan & Järve (2012) studied the axial, bending and shear stiffness in ten different core configurations and concluded that the corrugated V-core (see Figure 2.6) was the most promising one for bridge deck applications.

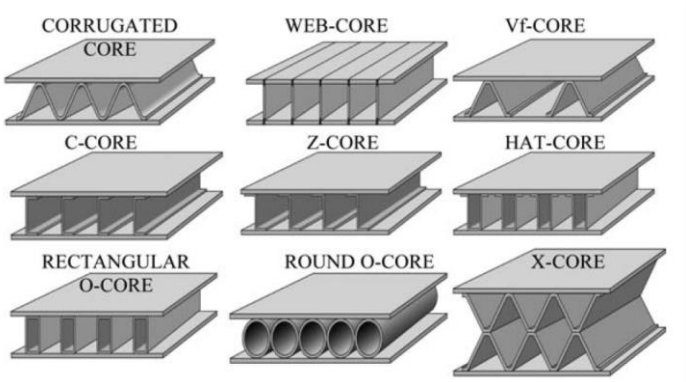

Figure 2.4 Different types of core configurations (Romanoff & Varsta, 2006).

2.3.1 History and application

Sandwich-like components were proposed for construction already in the 1950s. The development of laser welded sandwich panels was initiated in 1988 by the U.S. Navy and resulted in the use of stake welds to attach the face plates to the core (Abbott et al., 2007). Stake welds penetrates the plates from one side and connects them (see Figure 2.5). This concept was first used on the USS Mt. Whitey in 1994 and resulted in weight savings of 40% compared to classical stiffened plate structures. Even if the weight savings were significant, the research was abandoned since the manufacturing price was to high.

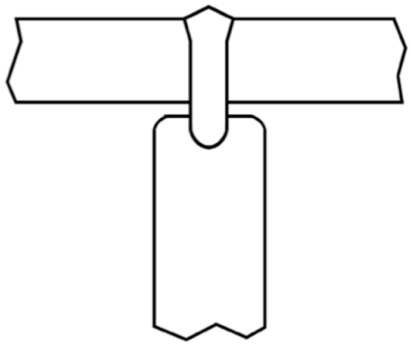

Figure 2.5 Laser stake weld connecting the face plate and core.

During recent years there has been on-going research on the behaviour and production of SSD's. In the 1990s, European research projects investigated the production and application of SSD's in ship building (Kujala et al., 2004). A German research project conducted by Meyer Werft resulted in the development of web-core panels. Furthermore, two factories producing corrugated core sandwich panels have been established in Finland.

2.3.2 Production of SSD

The development of new laser welding techniques has made it possible to produce products with better static and dynamic performance, in a faster and more cost efficient way. Traditional welding methods alone, like spot welding or gas metal arc welding (GMAW), have certain disadvantages that causes problem when it comes to

the production of SSD's. In the GMAW process an electrode wire is continuously fed through a conduit and welding gun to the base metal. High weld quality can be obtained but there are limitations to the minimum metal thickness (Philips, 1961).

Laser welding is a high energy density process capable of welding many different metals and alloys. It has many advantages compared to GMAW such as higher welding speed, increased process reliability and no requirement of fill material (Caccese et al., 2006). Furthermore, the heat affected zone (HAZ) and residual stresses are reduced. However, the lack of filler material can lead to stress concentrations due to the geometry of the weld, especially in sharp corners.

The hybrid laser arc welding (HLAW) is a combination of laser welding and GMAW, utilising features from both methods (see Figure 2.6). The laser weld method provides deep weld penetration, high speed, low heat input and small heat affected zones. In addition the GMAW improves the weld geometry and gives wide tolerances for the joint gaps, surface conditions and impurities (Abbott et al., 2007).

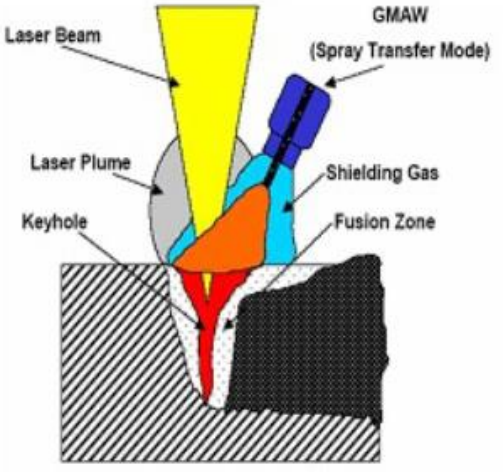

Figure 2.6 Hybrid laser arc welding (Abbott et al., 2007).

Even though HLAW has many benefits and is available on the market, the practical implication is not widely spread (Beneus & Koc, 2014). The investment costs and risks involved when changing from well-established methods of welding, leads to a conservative attitude in many companies.

2.4 Elastic stiffness constants of SSD

Libove & Hubka (1951) derived formulas and investigated the elastic constants for corrugated core sandwich plates, used to idealise the 3D sandwich plate as a homogeneous orthotropic plate (see Figure 2.7). In the derivations the modulus of elasticity in z-direction was assumed to be infinite. Straight lines normal to the middle surface were assumed to remain straight, but not necessarily normal to the middle surface, during distortion of the plate. Furthermore, the corrugation was assumed to be connected to the face plates through rigid joints at its crests and troughs.

The behaviour of a SSD can be described by the following elastic constants: two extensional stiffnesses E_x and E_y , two bending stiffnesses D_x and D_y, a twisting

stiffness D_{xy}, two transverse shear stiffnesses D_{Qx} and D_{Qy}, a horizontal shear stiffness G_{xy} and two Poisson's ratios υ_x and υ_y.

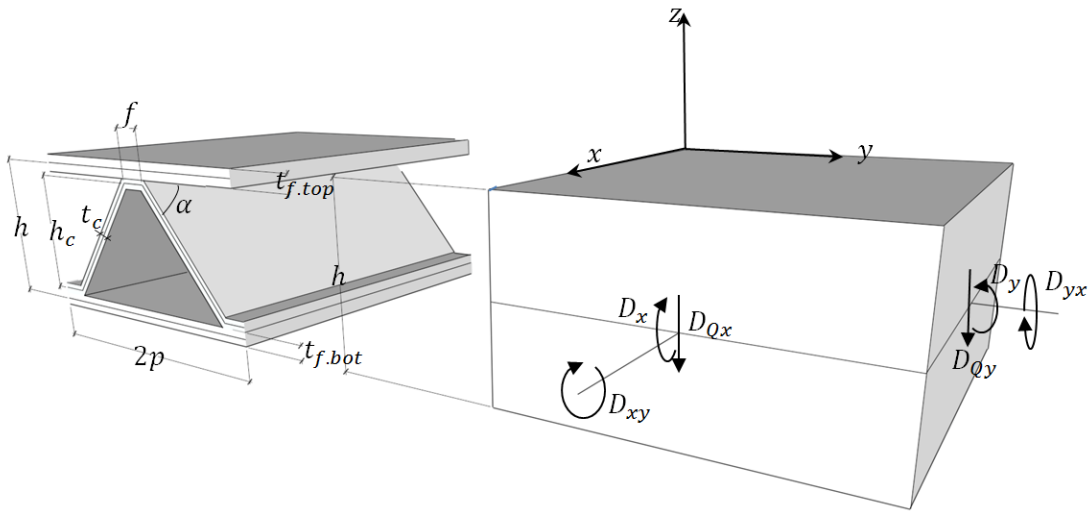

Figure 2.7 Dimensions of corrugated V-core SSD (left) and equivalent elastic constants of a homogeneous orthotropic plate (right).

2.4.1 Axial stiffness

The axial stiffnesses per unit width [N/m] are given in equations (2.3) and (2.4):

$$E_x = E_f A_f + E_c A_c \tag{2.3}$$

$$E_y = \frac{E_f A_f}{1 - \nu_f^2 \left(1 - \frac{E_f A_f}{E_x}\right)} \tag{2.4}$$

where:

$A_f = t_{f.top} + t_{f.bot}$

E_c Modulus of elasticity of core material, [Pa]

E_f Modulus of elasticity of face plate, [Pa]

$t_{f.top}$ Thickness of top face plate, [m]

$t_{f.bot}$ Thickness of bottom face plate, [m]

A_c Area, per unit width, of corrugation cross section, [m]

ν_f Poisson's ratio of face plate material, [-]

The Poisson's ratios associated with extension are given in equations (2.5) and (2.6):

$$\nu_x' = \nu_f \tag{2.5}$$

$$\nu_y' = \nu_x' \frac{E_y}{E_x} \tag{2.6}$$

2.4.2 Bending stiffness

The bending stiffnesses per unit width [Nm] of a corrugated SSD are given in equations (2.7) and (2.8):

$$D_x = E_f I_f + E_c I_c \tag{2.7}$$

$$D_y = \frac{E_f I_f}{1 - \nu_f^2 \left(1 - \frac{E_f I_f}{D_x}\right)} \tag{2.8}$$

where:

I_f Moment of inertia, per unit width, of face plates, [m^3]

I_c Moment of intertia, per unit width, of corrugation, [m^3]

The Poisson's ratios associated with bending are given in equations (2.9) and (2.10):

$$\nu_x = \nu_f \tag{2.9}$$

$$\nu_y = \nu_x \frac{D_y}{D_x} \tag{2.10}$$

2.4.3 Torsional stiffness

The torsional stiffness per unit width [Nm] of a corrugated SSD is given in equation (2.11):

$$D_{xy} = 2\left[G_f t_{f.top} k_{GJ}^2 + \frac{G_c t_c}{A_c}\left(k_{GJ} - k_c\right)^2 + G_f t_{f.top}\left(1 - k_{GJ}\right)^2\right] h^2 \tag{2.11}$$

where:

G_f Shear modulus of elasticity of face plate material, [Pa]

G_c Shear modulus of elasticity of core material, [Pa]

t_c Thickness of corrugated core plate, [m]

k_{GJ} Ratio depending on the distance to the zero-shear plane, [-]

k_c Ratio depending on the distance to the shear centre of the corrugation, [-]

2.4.4 Horizontal shear stiffness

The horizontal shear stiffness per unit width [N/m] of a corrugated SSD is given in equation (2.12):

$$G_{xy} = \frac{G_c t_c^2}{A_c} + G_f A_f \tag{2.12}$$

2.4.5 Transverse shear stiffness

The transverse shear stiffness per unit width [N/m] in y-direction is given in equation (2.13):

$$D_{Qy} = Sh\left(\frac{E_c}{1-\nu_c^2}\right)\left(\frac{t_c}{h_c}\right)^3 \tag{2.13}$$

where:

h_c Height of corrugation, measured vertically from centre line of crest to centre line at trough, [m]

ν_c Poisson's ratio of core material, [-]

S Non-dimensional coefficient depending on the shape of corrugation, relative proportions of sandwich cross section, and the material properties of the component parts, [-]

The transverse shear stiffness per unit width [N/m] in the x-direction is given in equation (2.14):

$$D_{Qx} = \frac{G_c I t_c h}{p\int_0^{l_c} Q ds} \tag{2.14}$$

where:

Q Static moment of hatched area (see Figure 2.8) about the neutral axis, [m^3]

I Moment of inertia of cross section of width $2p$ about centroidal axis, [m^4]

h Distance between middle surfaces of face plates, [m]

p Half of the corrugation pitch, [m]

l_c Length of one corrugation leg, measured along the centre line, [m]

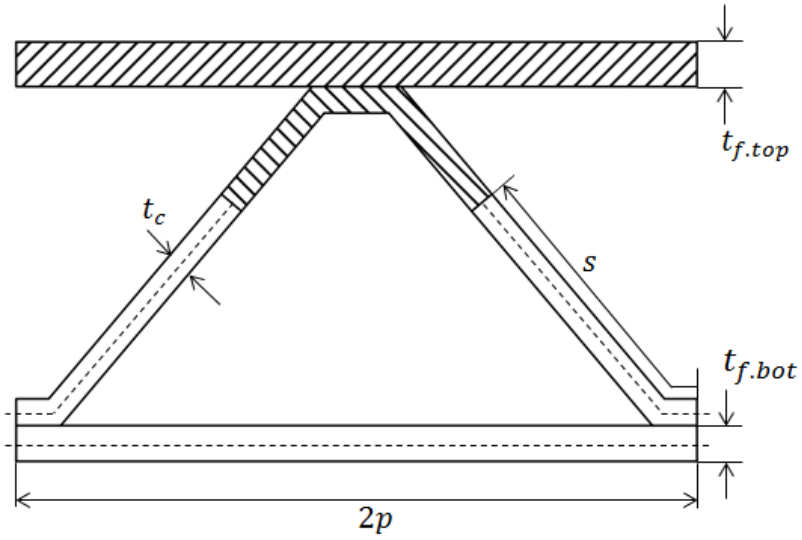

Figure 2.8 Area used when calculating the static moment of area.

If it is assumed that the face plates resist the entire bending moment and that the corrugation therefore carries no normal stress, equation (2.14) can simplified to equation (2.15):

$$D_{Qx} \approx \frac{G_c t_c^2}{A_c} \left(\frac{h}{p}\right)^2 \tag{2.15}$$

2.5 Mindlin-Reissner plate theory

Plate theory is a simplification of 3D elasticity analogous to beam theory but with extension in two directions. The two most common plate theories are the so called Kirchoff theory for thin plates and Mindlin-Reissner theory for thick plates. In the Kirchoff theory it is assumed that the normal remains straight and orthogonal to the middle plane after deformation (Oñate, 2013). The assumption that the normal remains orthogonal to the middle plane after deformation means that the transverse shear deformations do not contribute to the out-of-plane displacements. When analysing a SSD the transverse shear deformations are too large to neglect and the Mindlin-Reissner kinematics has to be adopted.

The Mindlin-Reissner kinematics assumes that the normal to the plate remains straight but not orthogonal to the middle plane. Blaauwendraad (2010) made a distinction between plates loaded in their plane and plates loaded perpendicular to the plane and presented the theory for both. For plates loaded in their plane, the plane stress state is called the membrane state while plates subjected to load perpendicular to the plane are in a state of bending and transverse shear. In addition to the assumption about the middle plane, the stress σ_{zz} in the direction normal to the mid-plane is assumed to be negligibly small compared to the bending stresses σ_{xx} and σ_{yy} and is set to zero. Furthermore, the middle plane is assumed to remain unstrained due to bending.

2.5.1 Plate acting as membrane

In the membrane state, all stress components are parallel to the middle plane and the membrane forces per unit width N_{xx}, N_{yy} and N_{xy} are obtained by multiplying the stress components σ_{xx}, σ_{yy} and σ_{xy} with the thickness t (see Figure 2.9).

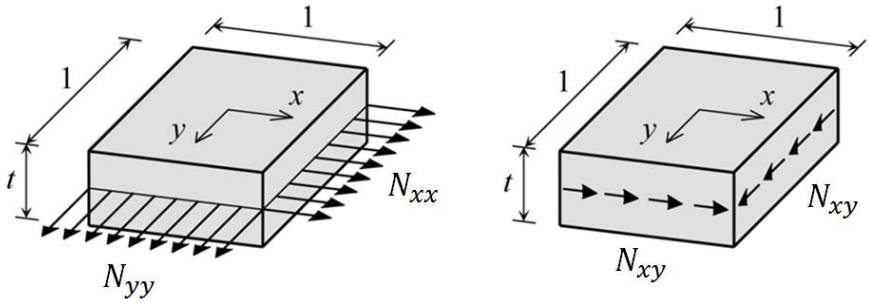

Figure 2.9 Membrane forces in a thick plate (Blaauwendraad, 2010)

Using the elastic stiffness constants from section 3.2 and accounting for material orthotropy result in the following relation between the deformations and stress resultants:

$$\varepsilon_{xx} = \frac{N_{xx}}{E_x} - \nu_y' \frac{N_{yy}}{E_y} \tag{2.16}$$

$$\varepsilon_{yy} = \frac{N_{yy}}{E_y} - \nu_x' \frac{N_{xx}}{E_x} \tag{2.17}$$

$$\gamma_{xy} = \frac{N_{xy}}{G_{xy}} \tag{2.18}$$

Or with matrix notation:

$$\begin{Bmatrix} \varepsilon_{xx} \\ \varepsilon_{yy} \\ \gamma_{xy} \end{Bmatrix} = \begin{bmatrix} 1/E_x & -\nu_y'/E_y & 0 \\ -\nu_x'/E_x & 1/E_y & 0 \\ 0 & 0 & 1/G_{xy} \end{bmatrix} \begin{Bmatrix} N_{xx} \\ N_{yy} \\ N_{xy} \end{Bmatrix} \tag{2.19}$$

By inverting equation (2.19) the following stiffness formulation is obtained:

$$\begin{Bmatrix} N_{xx} \\ N_{yy} \\ N_{xy} \end{Bmatrix} = \begin{bmatrix} E_{xx} & \nu_y' E_{xx} & 0 \\ \nu_x' E_{yy} & E_{yy} & 0 \\ 0 & 0 & G_{xy} \end{bmatrix} \begin{Bmatrix} \varepsilon_{xx} \\ \varepsilon_{yy} \\ \gamma_{xy} \end{Bmatrix} \tag{2.20}$$

where:

$$E_{xx} = \frac{E_x}{1 - \nu_x' \nu_y'}$$

$$E_{yy} = \frac{E_y}{1 - \nu_x' \nu_y'}$$

2.5.2 Plates in bending and shear

A plate loaded perpendicular to its plane will be subjected to a displacement w in z-direction, and rotations φ_x and φ_y. A distributed load q is associated with the displacement w and distributed couples $q_{\varphi x}$ and $q_{\varphi y}$ are associated with the rotations φ_x and φ_y. The load components and stress resultants are shown in Figure 2.10.

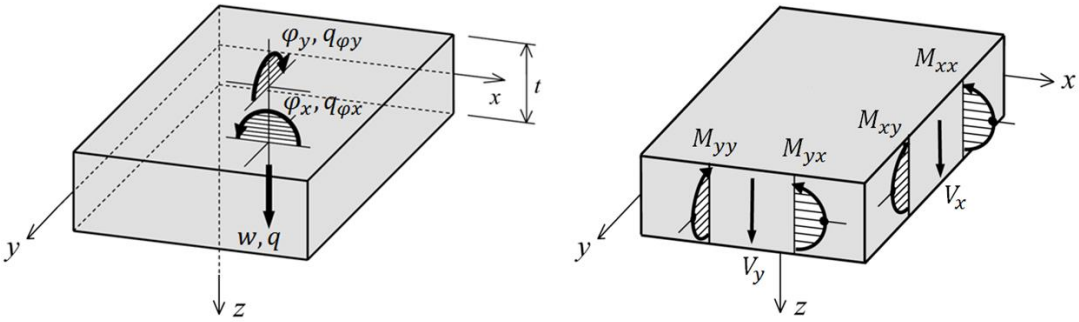

Figure 2.10 Load components with associated displacement and rotations on plate subjected to bending and shear (left) and stress resultants in the plate (right) (Blaauwendraad, 2010).

By introducing three curvatures κ_{xx}, κ_{yy} and κ_{xy}, the strains in a horizontal plane at distance z from the middle plane can be written as:

$$\varepsilon_{xx} = z\kappa_{xx} \tag{2.21}$$

$$\varepsilon_{yy} = z\kappa_{yy} \tag{2.22}$$

$$\gamma_{xy} = z\kappa_{xy} \tag{2.23}$$

where:

$$\kappa_{xx} = \frac{\partial \varphi_x}{\partial x}$$

$$\kappa_{yy} = \frac{\partial \varphi_y}{\partial y}$$

$$\kappa_{xy} = \frac{\partial \varphi_x}{\partial y} + \frac{\partial \varphi_y}{\partial x}$$

Due to the assumption that σ_{zz} is zero, all horizontal layers of the plate are in a state of plane stress. The same constitutive relation as in equation (2.20) can therefore be applied to each layer, but with the Poisson's ratios associated with bending ν_x and ν_y. Integration of the stress components σ_{xx}, σ_{yy} and σ_{xy} over the thickness will then give the bending moments per unit width M_{xx} and M_{yy} and a twisting moment per unit width M_{xy}. With the bending and torsional stiffnesses from Section 2.4, the following stiffness formulation is obtained according to Zenktert (1995):

$$M_{xx} = D_{xx}\left(\kappa_{xx} + \nu_y \kappa_{yy}\right) \tag{2.24}$$

$$M_{yy} = D_{yy}\left(\kappa_{yy} + \nu_x \kappa_{xx}\right) \tag{2.25}$$

$$M_{xy} = \frac{D_{xy}}{2}\kappa_{xy} \tag{2.26}$$

where:

$$D_{xx} = \frac{D_x}{1 - \nu_x \nu_y}$$

$$D_{yy} = \frac{D_y}{1 - \nu_x \nu_y}$$

Or with matrix notation:

$$\begin{Bmatrix} M_{xx} \\ M_{yy} \\ M_{xy} \end{Bmatrix} = \begin{bmatrix} D_{xx} & \nu_y D_{xx} & 0 \\ \nu_x D_{yy} & D_{yy} & 0 \\ 0 & 0 & \frac{D_{xy}}{2} \end{bmatrix} \begin{Bmatrix} \kappa_{xx} \\ \kappa_{yy} \\ \kappa_{xy} \end{Bmatrix} \tag{2.27}$$

The shear forces per unit length V_x and V_y are obtained by integration of the vertical shear stress components σ_{xz} and σ_{yz} over the thickness of the plate. With the transverse shear stiffnesses from Section 2.4, the relations between shear forces and shear deformations are given below:

$$V_x = D_{Qx}\gamma_x \tag{2.28}$$

$$V_y = D_{Qy}\gamma_y \tag{2.29}$$

where:

$$\gamma_x = \varphi_x + \frac{\partial w}{\partial x}$$

$$\gamma_y = \varphi_y + \frac{\partial w}{\partial y}$$

2.5.3 Coupling between membrane action and bending

To define the constitutive law for coupled membrane action and bending, equation (2.20) and (2.27) can be combined. If a common reference plane R is chosen equation (2.30) is obtained according to Blaauwendraad (2010).

$$\begin{Bmatrix} N_{yy} \\ N_{yy} \\ N_{xy} \\ M_{xx}^{R} \\ M_{yy}^{R} \\ M_{xy}^{R} \end{Bmatrix} = \begin{bmatrix} E_x x & \nu_y' E_{xx} & 0 & * & * & 0 \\ \nu_x' E_{yy} & E_{yy} & 0 & * & * & 0 \\ 0 & 0 & G_{xy} & 0 & 0 & * \\ * & * & 0 & D_{xx} & \nu_y D_{xx} & 0 \\ * & * & 0 & \nu_x D_{yy} & D_{yy} & 0 \\ 0 & 0 & * & 0 & 0 & \frac{D_{xy}}{2} \end{bmatrix} \begin{Bmatrix} \varepsilon_{xx}^{R} \\ \varepsilon_{yy}^{R} \\ \gamma_{xy}^{R} \\ \kappa_{xx} \\ \kappa_{yy} \\ \rho_{xy} \end{Bmatrix} \quad (2.30)$$

In the general case, the coupling terms denoted with * in the stiffness matrix of equation (2.30) will be non-zero and depend on the distance to the reference plane. If a material is homogeneous or has symmetrical stiffness properties with regard to the middle plane, there is no difference between the reference planes for membrane action and bending. The reference plane R is then chosen as the common reference plane and membrane action will be fully uncoupled with bending, resulting in zeros at the positions denoted * in the stiffness matrix of equation (2.30).

2.6 Analytical analysis of a simply supported SSD

Chang (2004) proposed a closed-form analytical solution to calculate the deflection of a simply supported SSD subjected to out-of-plane traffic loading. The sandwich plate theory used is based on the Mindlin-Reissner kinematics described in Section 2.5, in which the 3D SSD is idealised as an equivalent orthotropic plate.

2.6.1 Governing equations

Chang (2004) derived the following system of governing differential equations for an orthotropic sandwich plate:

$$\left(D_{xx}\frac{\partial^2}{\partial x^2} + \frac{D_{xy}}{2}\frac{\partial^2}{\partial y^2} - D_{Qx}\right)\varphi_x + \left(\frac{D_{xy}}{2} + D_{xx}\upsilon_y\right)\frac{\partial^2 \varphi_y}{\partial x \partial y} + D_{Qx}\frac{\partial w}{\partial x} = 0 \quad (2.31)$$

$$\left(\frac{D_{xy}}{2} + D_{yy}\upsilon_x\right)\frac{\partial^2 \varphi_x}{\partial x \partial x} + \left(D_{yy}\frac{\partial^2}{\partial y^2} + \frac{D_{xy}}{2}\frac{\partial^2}{\partial x^2} - D_{Qy}\right)\varphi_y + D_{Qy}\frac{\partial w}{\partial y} = 0 \quad (2.32)$$

$$-D_{Qx}\frac{\partial \varphi_x}{\partial x} - D_{Qy}\frac{\partial \varphi_y}{\partial y} + \left(D_{Qx}\frac{\partial^2}{\partial x^2} + D_{Qy}\frac{\partial^2}{\partial y^2}\right)w + q = 0 \quad (2.33)$$

where:

$$D_{xx} = \frac{D_x}{1 - \nu_x \nu_y}$$

$$D_{yy} = \frac{D_y}{1 - \nu_x \nu_y}$$

$$\nu_y = \nu_x \frac{D_y}{D_x}$$

2.6.2 Boundary conditions

Three boundary conditions should be prescribed at any point of the sandwich plate edge. For a simply supported edge, two of the boundary conditions prescribe deflections in z-direction and bending moments to zero. The third boundary condition can be either a so called soft or hard type boundary condition (see Figure 2.11). For the former, the twisting moment is zero and shearing of the edge is permitted. For the hard boundary condition, shearing is not permitted and a twisting moment will be present.

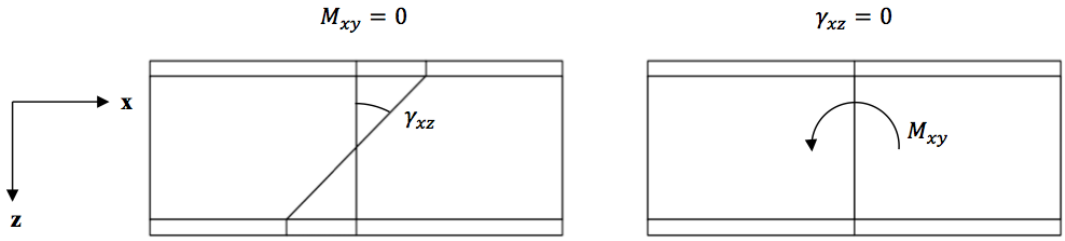

Figure 2.11 Definition of soft (left) and hard (right) boundary condition.

2.6.3 Deflection of a simply supported SSD

For rectangular plate (length a and width b) with hard type simply supported edges, the deflection, slopes and transverse load can be expanded with the double infinite Fourier series given in equations (2.34) to (2.37):

$$w = \sum_{m=1}^{\infty}\sum_{n=1}^{\infty} w_{mn} \sin\left(\frac{m\pi x}{a}\right)\sin\left(\frac{n\pi x}{b}\right) \tag{2.34}$$

$$\varphi_x = \sum_{m=1}^{\infty}\sum_{n=1}^{\infty} A_{mn} \cos\left(\frac{m\pi x}{a}\right)\sin\left(\frac{n\pi x}{b}\right) \tag{2.35}$$

$$\varphi_y = \sum_{m=1}^{\infty}\sum_{n=1}^{\infty} B_{mn} \sin\left(\frac{m\pi x}{a}\right)\sin\left(\frac{n\pi x}{b}\right) \tag{2.36}$$

$$q = \sum_{m=1}^{\infty}\sum_{n=1}^{\infty} q_{mn} \sin\left(\frac{m\pi x}{a}\right)\sin\left(\frac{n\pi x}{b}\right) \tag{2.37}$$

For a uniformly distributed load q_{mn} can be determined by equation (2.38):

$$\begin{aligned} q_{mn} &= \frac{4}{ab}\int_0^a\int_0^b q \sin\left(\frac{m\pi x}{a}\right)\sin\left(\frac{n\pi x}{b}\right) dxdy \\ &= \frac{4q}{mn\pi^2}[1-(-1)^m][1-(-1)^n] \end{aligned} \tag{2.38}$$

For a point load acting at a point $(x, y) = (x', y')$, q_{mn} is obtained by equation (2.39):

$$q_{mn} = \frac{4P}{ab} \sin\left(\frac{m\pi x'}{a}\right) \sin\left(\frac{n\pi x'}{b}\right) \tag{2.39}$$

By substituting equations (2.34) to (2.37) into equations (2.31) to (2.33), the following system of equations in terms of the unknown coefficients w_{mn}, A_{mn} and B_{mn} was obtained:

$$\begin{bmatrix} K_{11} & K_{12} & K_{13} \\ K_{21} & K_{22} & K_{23} \\ K_{31} & K_{32} & K_{33} \end{bmatrix} \begin{Bmatrix} w_{mn} \\ A_{mn} \\ B_{mn} \end{Bmatrix} = \begin{Bmatrix} 0 \\ 0 \\ q_{mn} \end{Bmatrix} \tag{2.40}$$

where:

$$K_{11} = D_{xx}\left(\frac{m\pi}{a}\right)^2 + \frac{D_{xy}}{2}\left(\frac{n\pi}{b}\right)^2 + D_{Qx}\,, \quad K_{12} = \left[\frac{D_{xy}}{2} + D_{xx}\nu_y\right]\left(\frac{mn\pi^2}{ab}\right)$$

$$K_{13} = -D_{Qx}\left(\frac{m\pi}{a}\right)$$

$$K_{21} = K_{12}\,, \quad K_{22} = D_{yy}\left(\frac{n\pi}{b}\right)^2 + \frac{D_{xy}}{2}\left(\frac{m\pi}{a}\right)^2 + D_{Qy}\,, \quad K_{23} = -D_{Qy}\left(\frac{n\pi}{b}\right)$$

$$K_{31} = K_{13}\,, \quad K_{32} = K_{23}\,, \quad K_{33} = D_{Qx}\left(\frac{m\pi}{a}\right)^2 + D_{Qy}\left(\frac{n\pi}{b}\right)^2$$

w_{mn} is then obtained by solving equation (2.40) and used in equation (2.34) for calculating the deflection of a simply supported SSD.

2.7 Equivalent single layer FE-model of SSD

For a plate to be analysed with other boundary conditions and geometries, a FE-software is needed. In the FE-software the SSD can be modelled with single layer shell elements, assigned with stiffnesses equivalent to those of the SSD. In this thesis the FE-software Abaqus/CAE was used. Two different material models were considered.

2.7.1 Lamina material model

The lamina material model in Abaqus/CAE considers orthotropic materials under plane stress conditions. The lamina model works for either in-plane or out-of-plane loading but cannot consider both at the same time. For the in-plane components of the stress and strain, the stress-strain relation is of the following form:

$$\begin{Bmatrix} \varepsilon_{11} \\ \varepsilon_{22} \\ \gamma_{12} \end{Bmatrix} = \begin{bmatrix} 1/E_x^{e\prime} & -\nu_x'/E_x^{e\prime} & 0 \\ -\nu_x'/E_x^{e\prime} & 1/E_y^{e\prime} & 0 \\ 0 & 0 & 1/G_{xy}^{e\prime} \end{bmatrix} \begin{Bmatrix} \sigma_{11} \\ \sigma_{22} \\ \tau_{12} \end{Bmatrix} \tag{2.41}$$

The inputs for the material model are the engineering constants $E_x^{e\prime}$, $E_x^{e\prime}$, $G_{xy}^{e\prime}$, G_{xz}^{e}, G_{yz}^{e} and Poisson's ratio ν_x', where the terms G_{xz}^{e} and G_{yz}^{e} are used to model the transverse shear deformation. In case of out-of-plane loading the bending-curvature relationship is given by changing $E_x^{e\prime}$, $E_y^{e\prime}$, $G_{xy}^{e\prime}$ and ν_x' to E_x^{e} , E_y^{e}, G_{xy}^{e} and ν_x in equation (3.47).

The engineering constants were obtained from Lok & Cheng (1999). For in-plane loading conditions equations (2.42) to (2.44) were used:

$$E_x^{e\prime} = \frac{E_x}{h} \tag{2.42}$$

$$E_y^{e\prime} = \frac{E_y}{h} \tag{2.43}$$

$$G_{xy}^{e\prime} = \frac{G_{xy}}{h} \tag{2.44}$$

The engineering constants for out-of-plane loading conditions were obtained by equations (2.45) to (2.47):

$$E_x^{e} = \frac{12D_x}{h^3} \tag{2.45}$$

$$E_y^{e} = \frac{12D_y}{h^3} \tag{2.46}$$

$$G_{xy}^{e} = \frac{6D_{xy}}{h^3} \tag{2.47}$$

The engineering constants related to the transverse shear stiffnesses were obtained by equations (2.48) and (2.49), where k is a shear correction factor taken as 5/6:

$$G_{xz}^{e} = \frac{D_{Qx}}{kh} \tag{2.48}$$

$$G_{yz}^{e} = \frac{D_{Qx}}{kh} \tag{2.49}$$

2.7.2 General shell section

If in-plane and out-of-plane loading needs to be considered at the same time the lamina model is insufficient for a geometrically orthotropic plate. Instead, a general shell section has to be used in which shell section response is defined by equation (2.50):

$$\{\boldsymbol{N}\} = [\boldsymbol{D}]\{\boldsymbol{E}\} \tag{2.50}$$

where:

$\{\boldsymbol{N}\}$ Membrane forces and bending moments per unit length acting on the shell section

$[\boldsymbol{D}]$ Section stiffness matrix

$\{\boldsymbol{E}\}$ Generalised section strains in the shell

Equation (2.50) can be written as:

$$\begin{Bmatrix} N_{xx} \\ N_{yy} \\ N_{xy} \\ M_{xx} \\ M_{yy} \\ M_{xy} \end{Bmatrix} = \begin{bmatrix} D_{11} & D_{12} & 0 & 0 & 0 & 0 \\ D_{21} & D_{22} & 0 & 0 & 0 & 0 \\ 0 & 0 & D_{33} & 0 & 0 & 0 \\ 0 & 0 & 0 & D_{44} & D_{45} & 0 \\ 0 & 0 & 0 & D_{54} & D_{55} & 0 \\ 0 & 0 & 0 & 0 & 0 & D_{66} \end{bmatrix} \begin{Bmatrix} \varepsilon_{xx} \\ \varepsilon_{yy} \\ \gamma_{xy} \\ \kappa_{xx} \\ \kappa_{yy} \\ \kappa_{xy} \end{Bmatrix} \tag{2.51}$$

where the stiffness terms are given as (see Section 2.5):

$$D_{11} = \frac{E_x}{1 - \nu_x' \nu_y'}, \quad D_{12} = D_{21} = \frac{\nu_x' E_y}{1 - \nu_x' \nu_y'} = \frac{\nu_y' E_x}{1 - \nu_x' \nu_y'}$$

$$D_{22} = \frac{E_y}{1 - \nu_x' \nu_y'}, \quad D_{33} = G_{xy}$$

$$D_{44} = \frac{D_x}{1 - \nu_x \nu_y}, \quad D_{45} = D_{54} = \frac{\nu_x D_y}{1 - \nu_x \nu_y} = \frac{\nu_y D_x}{1 - \nu_x \nu_y}$$

$$D_{55} = \frac{D_y}{1 - \nu_x \nu_y}, \quad D_{66} = \frac{1}{2} D_{xy}$$

$$\nu_y' = \nu_x' \frac{E_y}{E_x}$$

$$\nu_y = \nu_x \frac{D_y}{D_x}$$

If out-of-plane or in-plane loading is considered separately, the general shell section and lamina material model should yield the same results.

2.8 Structural behaviour and performance of SSD

Chang et al. (2005) analysed the bending behaviour of a V-core SSD and investigated how the corrugation angle α, corrugation depth to core thickness ratio h_c/t_c, pitch to corrugation depth p/h_c, and core to face thickness t_c/t_f influenced the stiffness of the plate. The sandwich plate theory used was based on the Mindlin-Reissner plate

theory, in which the 3D SSD was idealised as an equivalent orthotropic 2D plate. The theory was used together with the elastic constants derived by Libove & Hubka (1951). The results from the study showed that the corrugation angle α was the parameter with most influence on the stiffness. Increasing α slightly increased the bending stiffnesses D_y and D_x, but drastically decreased the shear stiffnesses D_{Qy}. This lead to an reduction of the overall stiffness.

In addition, the investigations confirmed a phenomenon observed in experiments done by Tan et al. (1989). High ratios of h_c/t_c and p/h_c, together with a large corrugation angle α might result in a negative moment M_y at the central point in the span of the deck. This is a consequence of a much higher stiffness in the direction of the corrugation, due to high D_{Qx} and low D_{Qy}. Most of the bending is therefore resisted in the x-direction and causes small or negative M_y. Although, since the transverse shear deformation is much greater than the bending deformation, the net deflection of the plate was downward.

Beneus & Koc (2014) developed an optimisation routine in Mathcad, in which a SSD was optimised compared to an orthotropic steel deck of similar size. The elastic constants used were based on expressions from Libove & Hubka (1951). The optimisation routine included constraints to ensure that the compression parts of the deck were in cross section class three and that the local deflections were below a given limit.

Two different optimisations were performed. The first one maximised D_x with the same area as the orthotropic steel deck and the second one minimised the cross-sectional area with the same D_x as the orthotropic steel deck. A significant increase of both bending stiffness D_x and torsional stiffness D_{xy} was obtained for the case with the same cross-sectional area. The area optimisation resulted in a weight reduction of 23% compared to the orthotropic steel deck. Furthermore, the bending stiffness in the direction perpendicular to the corrugation D_y, was significantly increased in both optimisation studies.

In addition to the optimisation studies, Beneus & Koc (2014) performed FE-analyses in order to evaluate the structural performance of the SSD when utilised as a bridge deck. The bridge in the analysis was modelled with two simply supported steel I-girders as main girders, together with transverse steel girders. As a result from the analyses the effective flange widths b_e due to shear lag, and shear lag coefficient b_e/b were calculated. The SSD with maximised D_x had a shear lag coefficient of 66% and the SSD with minimised area a shear lag coefficient of 59%. A significant increase of the effective width was obtained in both cases, when compared to an utilisation ratio of 37% for the orthotropic steel deck.

In the analyses performed by Chang et al. (2005) and Beneus & Koc (2014), the elastic stiffness constants derived Libove & Hubka (1951) were used. Rigid joints were therefore assumed between the face plates and corrugation. In reality the stiffness of the weld itself will affect the behaviour of the SSD. The influence of weld configuration for one specific V-core sandwich deck was studied by Caccese & Yorulmaz (2009), using 3D FE-models. The continuous stake welds were modelled with shell elements and four different configurations were analysed (see Figure 2.12).

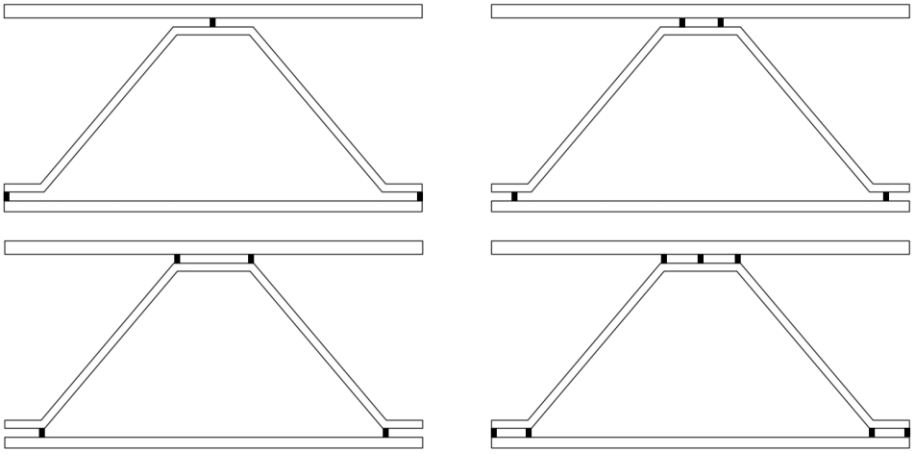

Figure 2.12 Different weld configurations with one weld in the centre (top left), two welds in between the corners and centre (top right), two welds in the corner (bottom left) and welds in both corners and centre (bottom right).

The increasing shear rigidity gained from placing the welds at the corners had large influence on the overall stiffness. One weld at the centre line increased the displacement at the top centre line with 62% compared to the case with welds at the corner and centre and with 47% compared to the case with corner welds only. The effect of weld link thickness was also investigated. The analysis showed that the weld link thickness did not contribute significantly to the overall stiffness of the model if it was chosen between 0.1 and 50 times the face plate thickness.

2.8.1 Failure modes

A sandwich plate will have different failure modes depending on the geometry and type of loading. Zenkert (1997) listed the most common failure modes and presented some analytical expressions. For a corrugated-core sandwich deck the failure modes were identified as global buckling, shear crimping, yielding, local buckling, face wrinkling and plastic collapse.

The shear crimping is a shear instability failure with the same limit as the global buckling mode, when the critical load equals the shear stiffness. The general global buckling failure and shear crimping failure are illustrated in Figure 2.13.

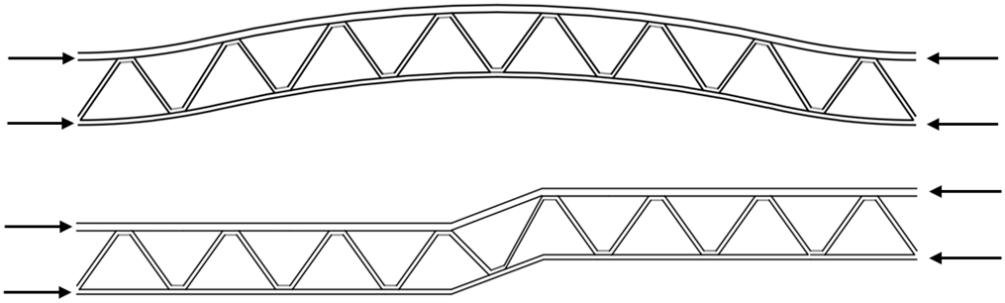

Figure 2.13 Global buckling failure (top) and shear crimping (bottom).

If the SSD is loaded parallel to the corrugations, local buckling can be avoided by assigning compression parts to cross section class three, according to SS-EN 1993-1-1 (2005). Face wrinkling on the other hand is a type of local buckling that can occur either when the plate is subjected to in-plane compressive load perpendicular to the corrugation, or in the compressed face during bending as shown in Figure 2.14.

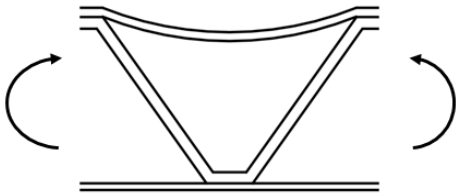

Figure 2.14 Face wrinkling of compressed face plate due to bending.

When the SSD is subjected to patch loads a possible failure mode is plastic collapse of the corrugation. The plastic collapse load was given by Naar (1997) and presented by Kujala (1998) as:

$$P_{plc} = 2\left(4\frac{M_f}{\beta} + 4\frac{M_c}{\beta}\left(\frac{k_1\beta c + \frac{M_f}{2M_c}}{1 + k_1 k_3 t_c}\right)\right)\left(1 - \left(\frac{\sigma_{x.f.top}}{f_{y.c}}\right)^2\right)^{0.5} \qquad (2.52)$$

where:

$$M_f = \frac{f_{y.f.top} p t_{f.top}^2}{2}$$

$$M_c = \frac{f_{y,c} t_c^2}{4}$$

$$I_f = \frac{p t_{f.top}}{6}$$

$$k_2 = \frac{M_f^2}{12 E I_f M_w}$$

$$\phi = arctan\left(\frac{2k_2 \sin^2\alpha}{\sin^2\alpha - k_2^2}\right)$$

$$k_1 = \frac{f_{y.f.top}}{40 t_c f_{y.c}} \frac{\sqrt{\sin^2\alpha - \sin^2\phi}}{\sin\phi cos\phi}$$

$$\beta = \sqrt{\frac{M_f}{4M_c k_1}}$$

$\sigma_{x.f.top}$ Stress in the top plate parallel to the corrugation, [Pa]

$f_{y.f.top}$ Yield strength of top plate, [Pa]

$f_{y.c}$	Yield strength of corrugation, [Pa]
$t_{f.top}$	Thickness of top plate, [m]
t_c	Thickness of corrugation, [m]
p	Half of the corrugation pitch, [m]
α	Corrugation angle, [rad]
c	Loaded length of the corrugation, [m]

Naar (1997) conducted laboratory tests in order to verify the plastic collapse formulation. The tests were conducted by applying a patch load on simply supported SSD's with different configurations. For top, bottom and core plate thicknesses above 1 mm, the accuracy of the formulation was typically within the region of 10-15%.

Biagi & Bart-Smith (2012) studied the in-plane compressive response of a truss core sandwich column when the load was applied either parallel or perpendicular to the corrugations. Different failure modes were identified depending on the direction of the applied load and if strain hardening was considered or not. Failure maps were constructed as functions of the column length L, face plate thickness h, corrugation thickness t, corrugation angle α and length of the corrugation leg l. The core slenderness ratio t/l and corrugation angle α were kept constant and the principle of the failure maps is shown in Figure 2.15. Increasing the corrugation angle or lowering the core slenderness ratio will expand the macro elastic buckling region.

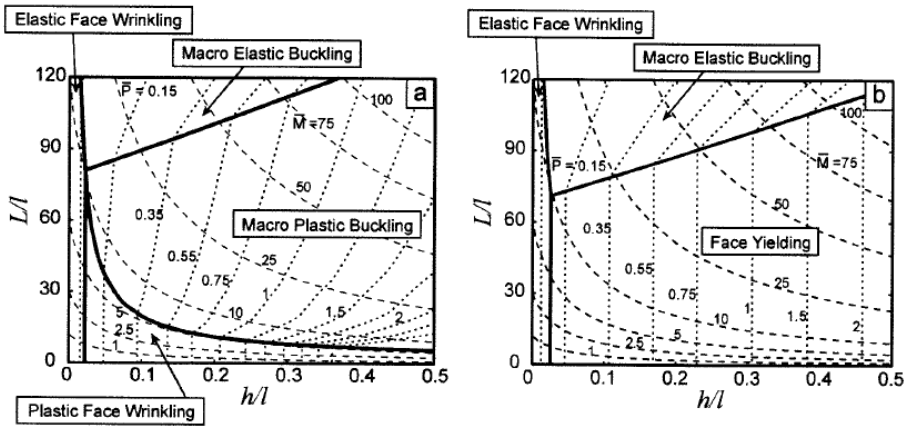

Figure 2.15 Failure mechanism maps for a corrugated core sandwich column with (a) a strain hardening material and (b) an elastic-perfectly plastic material (Biagi, 2010).

2.8.2 Fatigue resistance

Fatigue resistance is critical when designing steel bridges and for the traditional orthotropic steel deck problems with fatigue cracks are a significant feature. Geometrical stress concentrations due to the weld profile together with weld defects are factors that strongly influence the fatigue life. The use of HLAW when manufacturing the SSD's reduces the HAZ and improves the weld geometry (Caccese & Yorulmaz, 2009).

Kozak (2005) identified five different types of fatigue cracks that can occur for laser welded web-core sandwich decks (see Figure 2.16). The occurrence of the different cases is determined by the stiffness, load and boundary conditions of the structure.

Case 1: Fatigue crack in the laser weld toe in the top plate, parallel to the web, as a result of global bending.

Case 2: Fatigue crack in the laser welded toe in the top plate, transverse to the web, as a result of global bending.

Case 3: Fatigue crack in top plate caused by local bending or buckling.

Case 4: Fatigue crack in the laser welded contact area of the web and the plates, as a result of transverse bending.

Case 5: Fatigue crack in the laser welded contact area of the web and the plates due to longitudinal shearing.

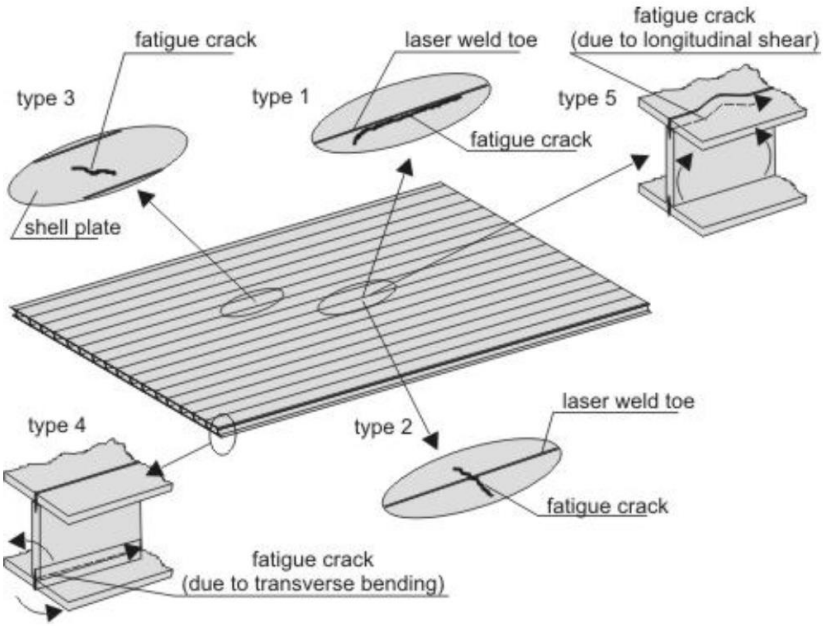

Figure 2.16 Fatigue crack occurrences in laser-welded web core sandwich decks (Kozak, 2005).

Caccese et al. (2006) performed fatigue testing on different series of cruciform specimens fabricated with the HLAW technique (see Figure 2.17). Test results were also compared to historical data. In Figure 2.18 the results are plotted along with S-N curves based on results for cruciform joints with conventional welding from Munse et al. (1983) and Kihl (2002). The purpose of the specimen series A to C was to study the effects of fillet size and shape of the weld. The investigation resulted in the final detail, series D, and it was concluded that the fatigue life for this detail was significantly better compared to similar specimens with conventional welds.

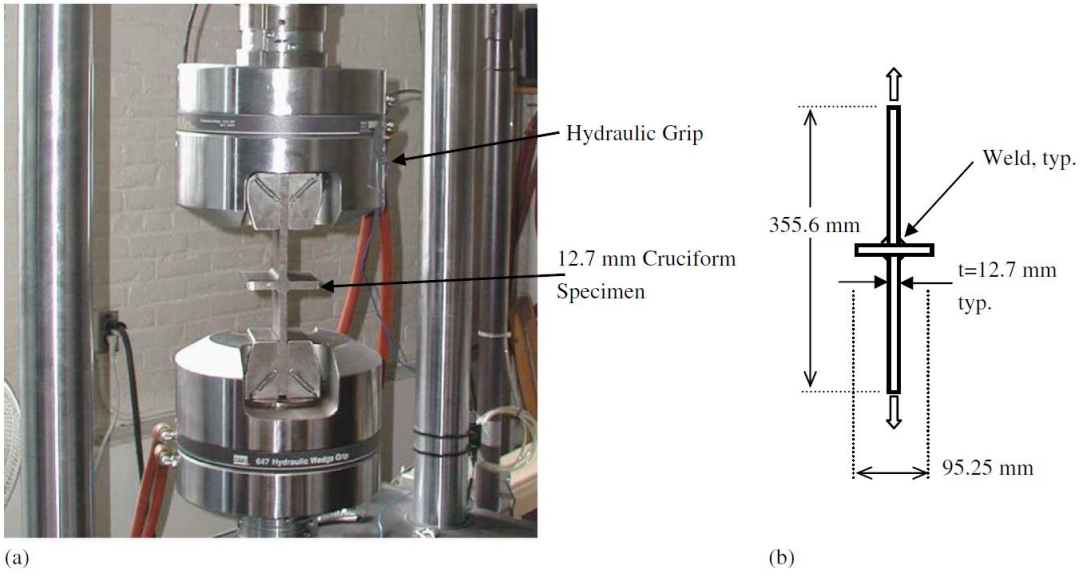

Figure 2.17 *(a) fatigue test specimen in test machine. (b) dimensions of the test specimen* (Caccese et al., 2006).

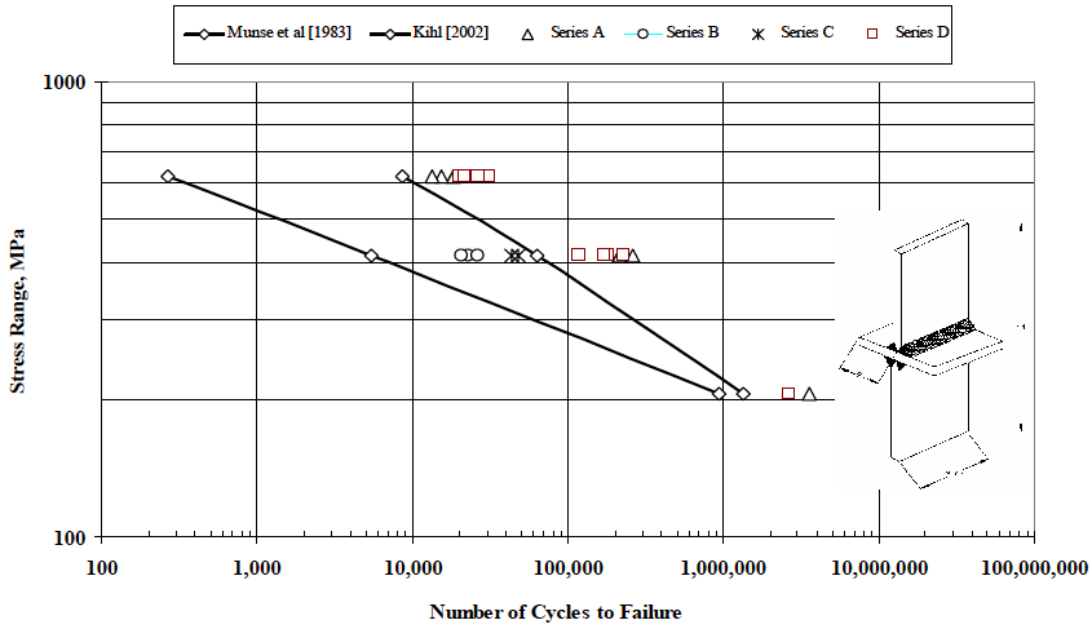

Figure 2.18 *Fatigue life of laser-welded cruciform specimens compared to conventionally welded specimens* (Abbott et al., 2007).

Bright & Smith (2004) investigated the fatigue performance of laser-welded SSD with I-section beams as a core. A deck bending test was carried out to study the performance of the laser welds directly below wheel loads (see Figure 2.19). In addition, a joggle test was conducted to simulate the web bending that might occur under offset wheel loads. In the deck bending test failure was defined as the first fatigue crack appearing at both sides of an individual weld, due to shear stress in the weld metal. When compared with mean S-N curves for weld classes published in BS5400 (1980), the tests indicated Class C for details with two linear stake welds per flange. In the joggle test the laser welds never failed. Instead, failure always occurred

in the parent metal of the I-beam web. Altogether, it was concluded that the tests indicated considerable fatigue strength of the SSD's.

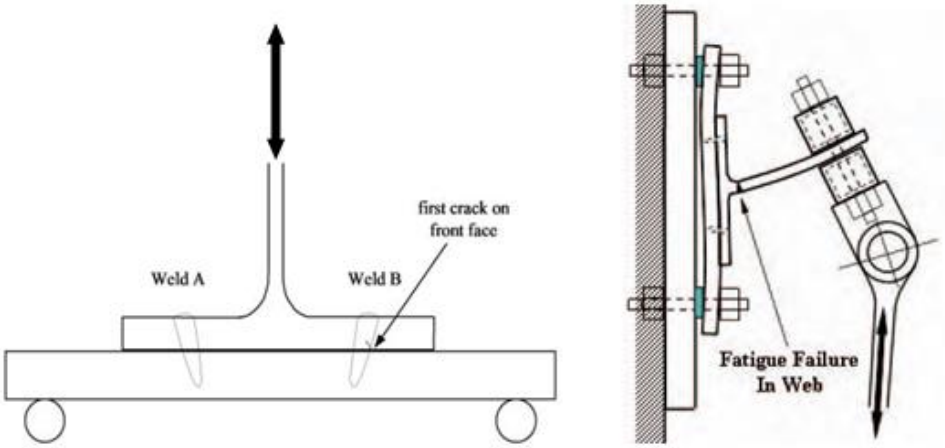

Figure 2.19 Test setup and first crack occurrence in deck bending test (left) and joggle test (right) (Bright & Smith, 2007).

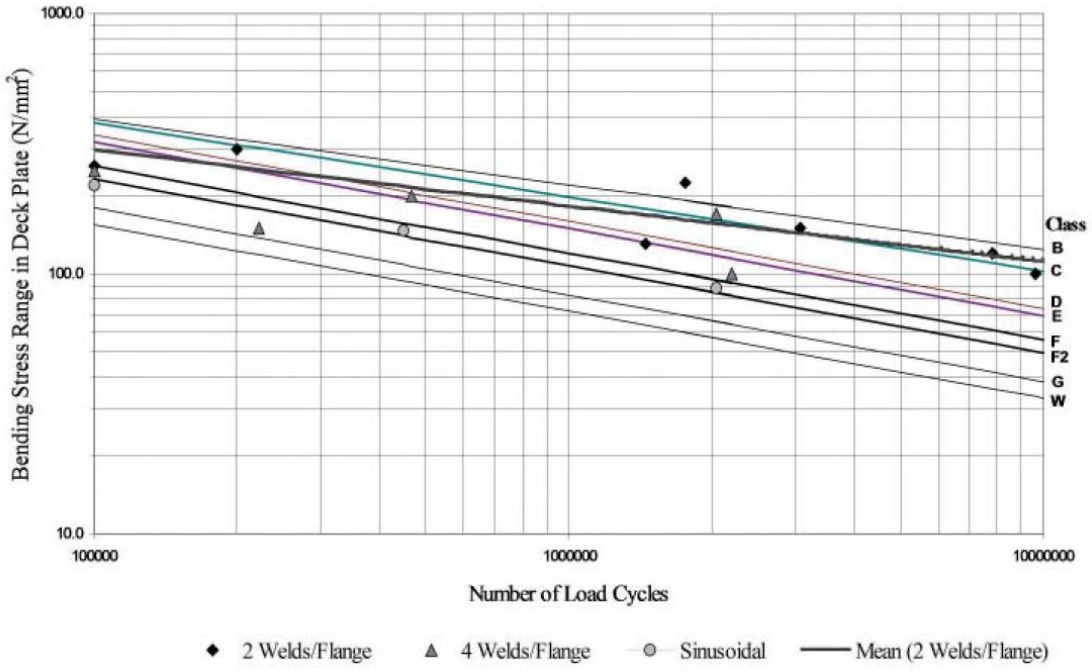

Figure 2.20 Comparison of deck bending test results with BS 5400 mean S-N curves (Bright & Smith, 2004).

3 Preliminary design

3.1 Introduction

The purpose of the preliminary design was to find a low-weight cross-sectional configuration to use in the more detailed analysis in Chapter 4. Different configurations of the SSD and distances between the transverse girders L_1 were investigated (see figure 3.1). The total width of bridge was 11.25 m and the distance between the main girders B_1 was kept constant at 6 m, as in the existing bridge over Bergeforsen.

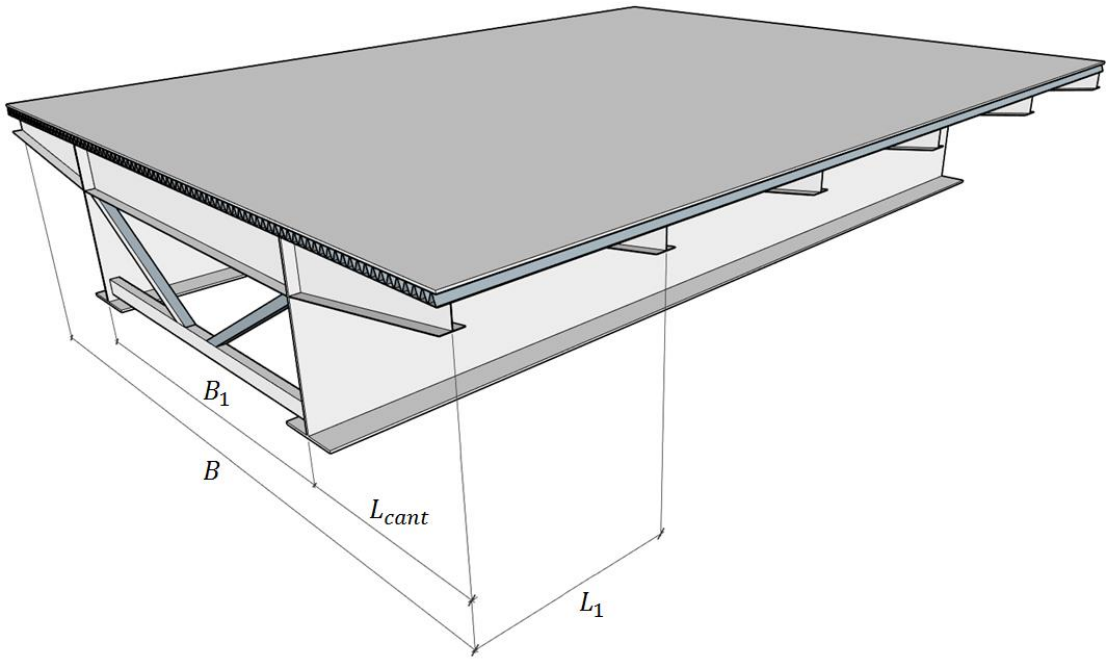

Figure 3.1 Superstructure of the bridge (without edge beams).

A part of the bridge deck was analysed with a finite element (FE) model to check that the deflection of the SSD was below the requirement. In the analysis the 3D SSD was idealised as a homogeneous orthotropic thick plate in order to reduce the modelling and calculation times. The elastic stiffness constants of the idealised plate was calculated with the optimisation routine from Beneus & Koc (2014), but had to be further developed to account for unsymmetrical SSD's. Moreover, the optimisation routine optimised the cross-sectional area of a SSD using the bending stiffness in x-direction D_x as a constraint. However, in the preliminary design the SSD was designed to fulfil the deflection limit between the transverse and main girders, meaning that the stiffness in both directions will influence the results. Therefore, the plate deflection formula in section 2.6 was included in the optimisation routine in order to optimise the area of the SSD constrained by a deflection limit.

A preliminary design of the main girders and the transverse girders was also conducted, in order to see how the dimension of the SSD and distance between transverse girders L_1 affected the dimensions of the girders, and in turn the total steel volume in the bridge.

3.1.1 Verification of agreement between analytical and numerical solution

The analytical solution for deflection of a simply supported plate, in section 2.6 was compared with the ESL-model using general shell section and eight node shell elements with reduced integration. Since the investigated deflection was caused by out-of-plane loading only, the ESL was modelled with the lamina material model as well for comparison and verification of the general shell section. The deflection in the middle of the plate was calculated for different SSD configurations and plate geometries. The geometries of the different SSD's are shown in Table 3.1 together with the stiffnesses and corresponding engineering constants in Table 3.2. The analytical deflection $w_{analytical}$, the numerical deflection with general shell stiffness $w_{ESL.GSS}$ and the numerical deflection with lamina material model $w_{ESL.LAM}$ for plates with different lengths and widths are shown in Table 3.3. A uniformly distributed load of 10 kN/m^2 was applied in all analyses.

Table 3.1 Geometries for the different SSD's considered in the verification.

Plate no.	h_c [mm]	$t_{f.top}$ [mm]	$t_{f.bot}$ [mm]	t_c [mm]	α [deg]	f [mm]
1	100.0	8.3	8.3	5.0	60	42.3
2	120.0	5.0	5.0	3.0	80	98.8

Table 3.2 Stiffnesses and corresponding engineering constants for the different SSD's considered in the verification.

Plate no.	D_x [Nm] E_x^e [Pa]	D_y [Nm] E_y^e [Pa]	D_{xy} [Nm] G_{xy}^e [Pa]	D_{Qx} [N/m] G_{xz}^e [Pa]	D_{Qy} [N/m] G_{yz}^e [Pa]
1	1.33e7 1.09e11	1.13e7 9.32e10	8.56e6 3.5e10	3.26e8 3.45e9	2.95e7 3.13e8
2	1.11e7 6.3e10	8.71e6 4.98e10	6.55e6 1.8e10	1.49e8 1.39e9	5.00e5 4.69e6

Table 3.3 Analytical and numerical deflections for different plate geometries.

BxL [m]	Plate no.	$w_{analytical}$ [mm]	$w_{ESL.GSS}$ [mm]	Difference	$w_{ESL.LAM}$ [mm]
1x6	1	0.053	0.053	0.00%	0.053
	2	1.168	1.166	-0.17%	1.166
2x4	1	0.255	0.255	0.00%	0.255
	2	1.672	1.669	-0.18%	1.669
4x6	1	1.976	1.978	0.10%	1.978
	2	9.455	9.441	-0.15%	9.441
10x10	1	33.071	33.080	0.03%	33.080
	2	76.935	76.893	-0.05%	76.893

As can be seen in Table 3.3 the analytical and numerical deflection of the simply supported plate corresponded well. The numerical deflection was identical when using general shell section and lamina material model as expected. This confirms that the part of the stiffness matrix in the general shell section associated with out-of plane loading corresponds to the lamina model for out-of plane loading.

In order to compare the lamina model and general shell section for in-plane loading, the ESL was loaded with an axial tension force of 10kN/m and an in-plane shear force of 1kN/m (see Figure 3.2). The plate was prevented from translation in all directions at the left edge and prevented from translation in the z-direction on the other three edges.

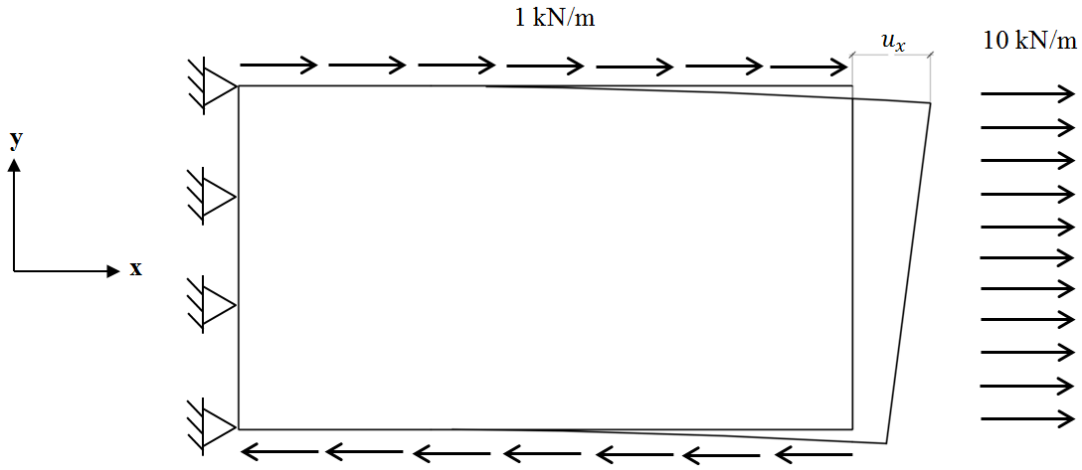

Figure 3.2 *Loading and boundary conditions for general shell section and lamina material model comparison.*

Table 3.4 shows the translation in the x-direction at the top right corner of the plate, with general shell section $u_{x.GSS}$ and lamina material model $u_{x.LAM}$, for the two different SSD geometries.

Table 3.4 *Comparision between the lamina model and general shell section for in-plane loading.*

BxL [m]	Plate no.	$u_{x.GSS}$ [mm]	$u_{x.LAM}$[mm]	Difference
4x6	1	0.0174	0.0174	0.00%
	2	0.0276	0.0276	0.00%

The translation was identical in both cases which confirmed that the in-plane part of the general shell section stiffness matrix corresponded to the lamina model for in-plane loading. The general shell section was used in the further analyses since the bridge deck was subjected to both in-plane and out-of-plane loads.

3.2 Load model 1

The preliminary configuration of the SSD was designed to meet the deflection limit under traffic load. Load model 1 (LM1) in SS-EN 1991-2 (2003) was used for the analysis, and consists of two partial systems. The first is a tandem system (TS) with double-axle concentrated loads, where each axle has the weight $\alpha_Q Q_k$. The second consists of uniformly distributed loads (UDL) with the weight $\alpha_q q_k$. The adjustment factors α_Q and α_q are national parameters.

The width of the carriageway B determines the number of notational lanes and the location of each lane should be chosen to yield the most unfavourable effect. The bridge over Bergeforsen had a carriageway width of 11.25 meters, which gave three notational lanes each having a width of 3 meters (see Figure 3.3).

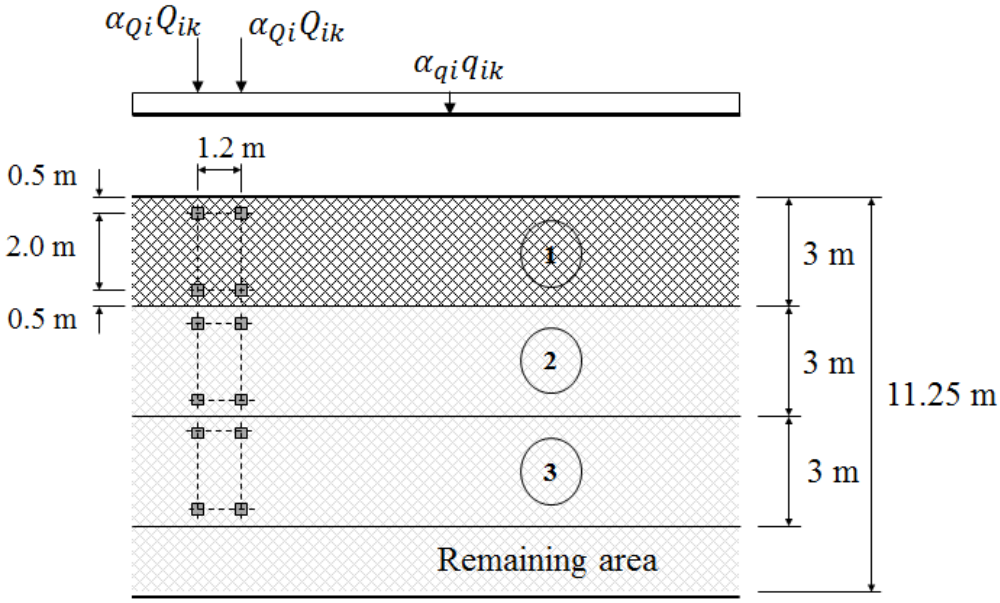

Figure 3.3 Notational lanes and wheel load position.

According to LM1 the wheels have a contact area of 400x400 mm^2. However, the contact area on the SSD is larger due to a 45º spread through the asphalt (see Figure 3.4). With an assumed asphalt cover of 50 mm the contact area on the SSD became 500x 500 mm^2.

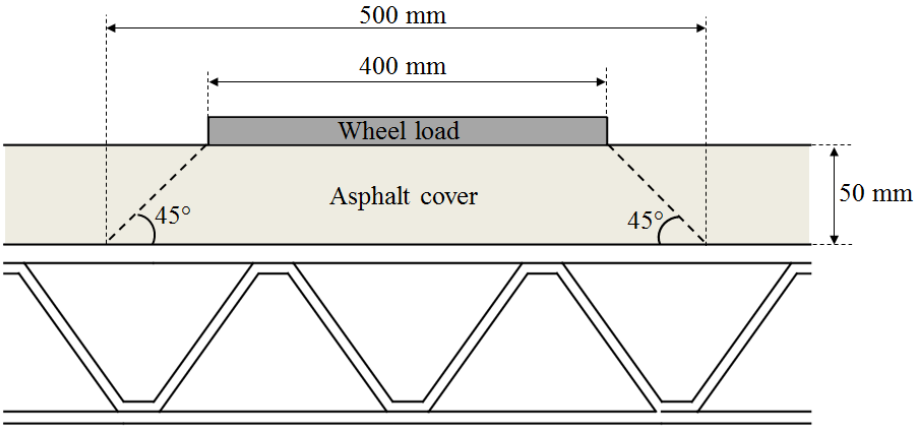

Figure 3.4 Contact surface on SSD from wheel load.

According to TRVK Bro 11 (2011) the deflection of a bridge should be determined under the frequent combination of traffic loads. For the frequent load combination the axle loads and uniformly distributed loads should be reduced with the factors $\psi_{1.TS}$ and $\psi_{1.UDL}$ respectively. The factors for frequent load combination, as well as the adjustment factors α_Q and α_q, was conservatively chosen to 1.0 in the preliminary design. The traffic loads for each lane are shown in Table 3.5.

Table 3.5 Traffic loads used in the preliminary design.

Lane	Q_{ik} [kN]	q_{ik} [kN/m^2]	$\psi_{1.TS}$	$\psi_{1.UDL}$	α_Q	α_q	$\psi_{1.TS}\alpha_Q Q_{ik}$ [kN]	$\psi_{1.UDL}\alpha_q q_{ik}$ [kN/m^2]
1	300	9.0	1.0	1.0	1.0	1.0	300	9.0
2	200	2.5	1.0	1.0	1.0	1.0	200	2.5
3	100	2.5	1.0	1.0	0	1.0	100	2.5
Remaining	0	2.5	-	1.0	-	1.0	0	2.5

3.3 SSD configuration

The preliminary configuration of the SSD was designed to meet the deflection limit between the main and transverse girders w_{mid} (see Figure 3.5). It was assumed that the deflection of the cantilever part w_{cant} could be reduced with an edge beam, and therefore this deflection was not governing in the preliminary design of the SSD.

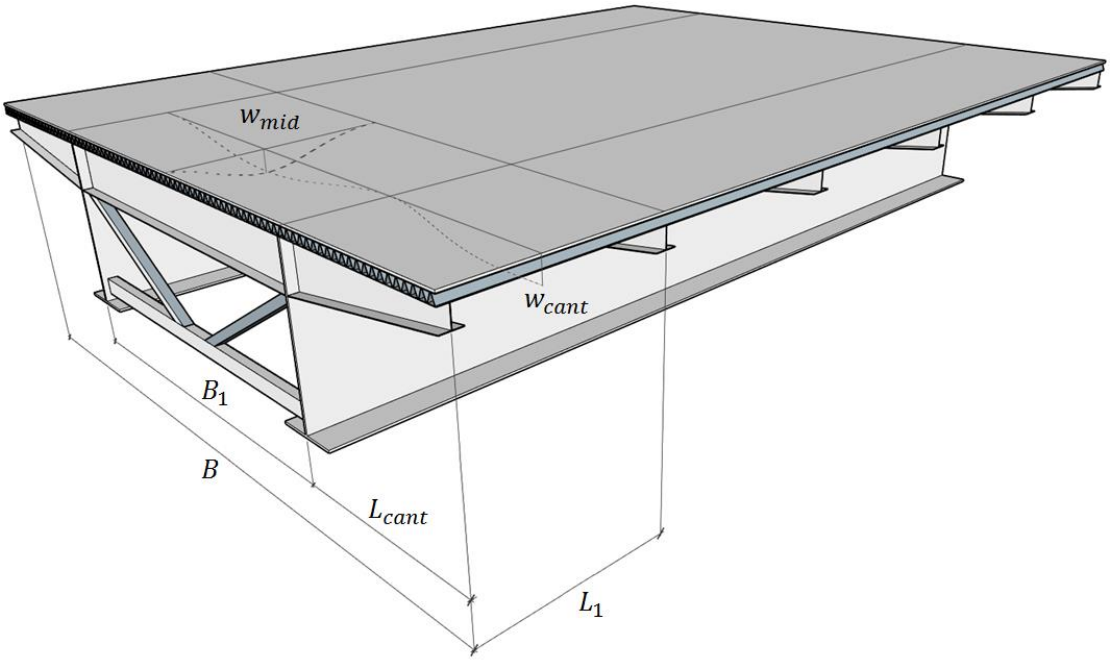

Figure 3.5 Deflection of SSD.

The flowchart for the preliminary design procedure is shown in Figure 3.6 and can be divided into the following steps:

1. The cross-sectional area of the SSD was minimised for given lengths between the transverse girders L_1 and the main girders B_1. The optimisation was constrained by the deflection limit of a simply supported plate. The output from the area optimisation was the dimensions h_c, $t_{f.top}, t_{f.bot}$, t_c, α, f together with the stiffnesses $E_x, E_y, G_{xy}, D_x, D_{xy}, D_{Qx}, D_{Qy}$.
2. A FE-analysis was carried out for a part of the bridge to get the deflection between the main girders w_{mid}. The SSD was modelled as an ESL with shell elements, using stiffnesses from the area optimisation. Boundary conditions were applied at the position of the main and transverse girders.
3. If the deflection between the main girders w_{mid} did not correspond to the deflection limit $\delta_{lim.ESL}$, the deflection limit constraint in the area optimisation was adjusted and new stiffnesses and dimensions were calculated. This was repeated until the $\delta_{lim.ESL}$ was reached.

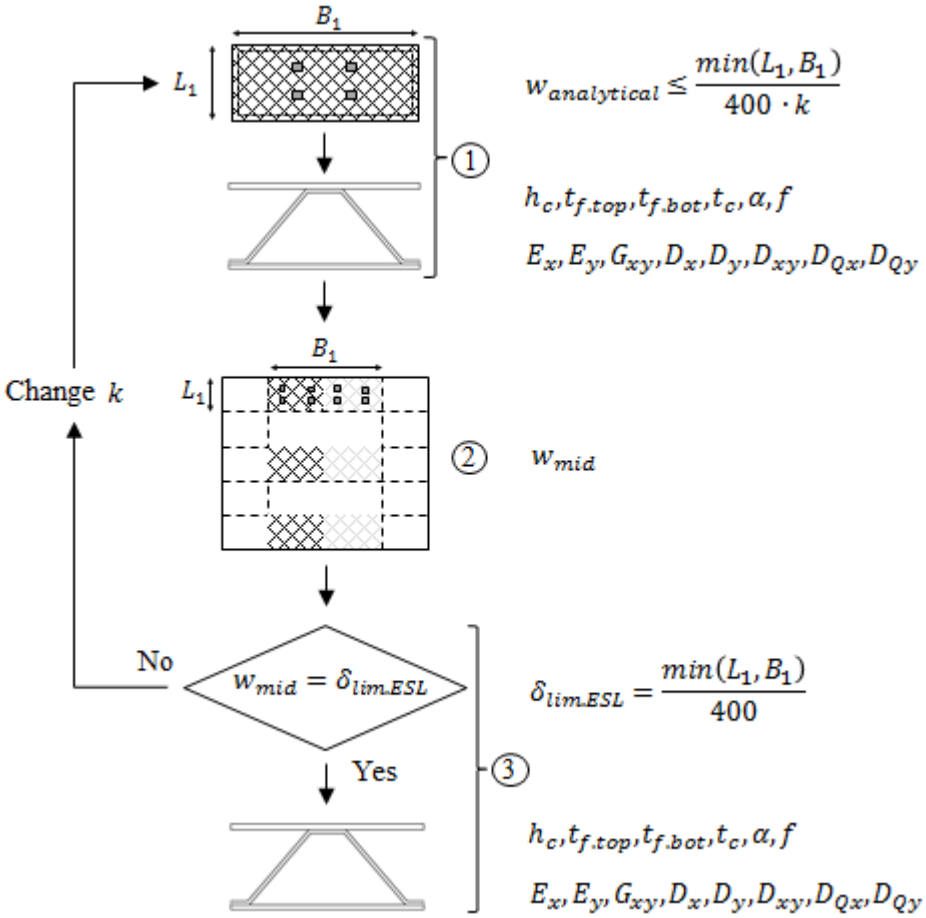

Figure 3.6 Flow chart of the preliminary design procedure.

3.3.1 Area optimisation of SSD, step 1

In order to optimise the SSD with a deflection limit constraint, equation (2.34) was included in the optimisation routine developed by Beneus & Koc (2014) (see Appendix A). The optimisation routine generated a combination of the following geometric parameters, with the lowest cross-sectional area (shown in Figure 3.7):

h_c Height of corrugation, [m]
$t_{f.top}$ Thickness of top face plate, [m]
$t_{f.bot}$ Thickness of bottom face plate, [m]
t_c Thickness of corrugation, [m]
α Angle of corrugation, [deg]
f Length of horizontal corrugation segment, [m]

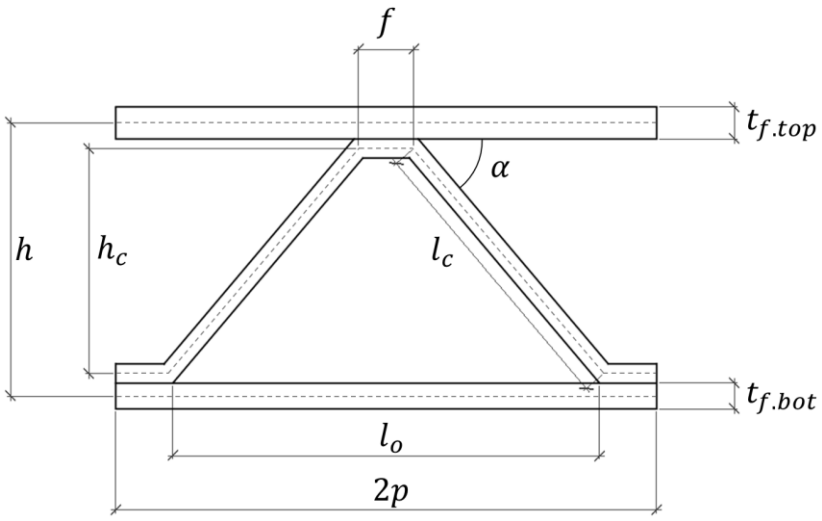

Figure 3.7 Dimensions of SSD.

In addition to the deflection limit, four other constraints were included in the analytical optimisation. The first constraint prevented the SSD from buckling locally, by assuring that the plates had a cross section in class 3. The maximum length-to-thickness ratios according to SS-EN 1993-1-1 (2005) are given below:

$$\frac{l_o}{t_{f.top}} \leq 42\varepsilon \qquad \frac{l_o}{t_{f.bot}} \leq 42\varepsilon \qquad \frac{l_c}{t_c} \leq 42\varepsilon \tag{3.1}$$

where:

l_o	Length of corrugation opening, [m]
l_c	Length of inclined leg of the corrugation, [m]
$\varepsilon = \sqrt{\frac{235MPa}{f_y}}$	Coefficient considering the yield strength, [-]
f_y	Yield strength, [Pa]

The second constraint limited the local deflection of the top face plate to $2p/400$. A part of the top plate with the length $2p$ was considered as a fixed beam subjected to the largest wheel load, as shown in Figure 3.8. Beneus & Koc (2014) also included an approximate fatigue stress constraint. Furthermore, f had to be larger than 20 mm due to production aspects.

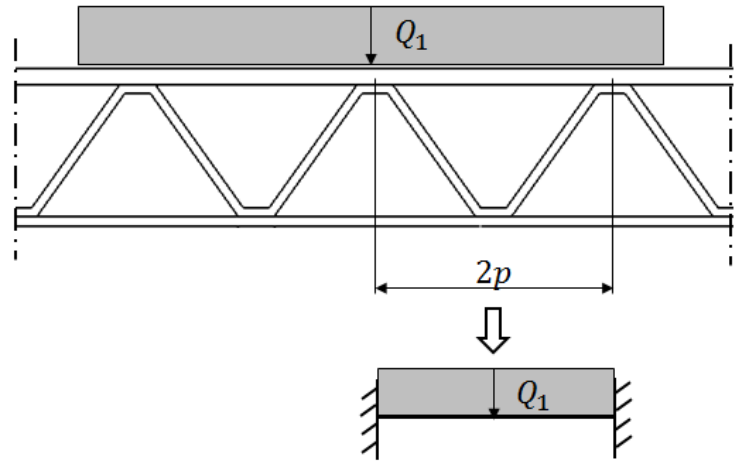

Figure 3.8 Model used to calculate the local deflection of the top plate.

LM1 was used for calculating the analytical deflection $w_{analytical}$, but with some modifications. In the analytical solution from equation (2.34), the distributed load needs to be constant over the plate. Therefore LM1 was modified to one distributed load of 9 kN/m^2 acting on the whole plate and four point loads of 150 kN around the centre of the plate (see Figure 3.9).

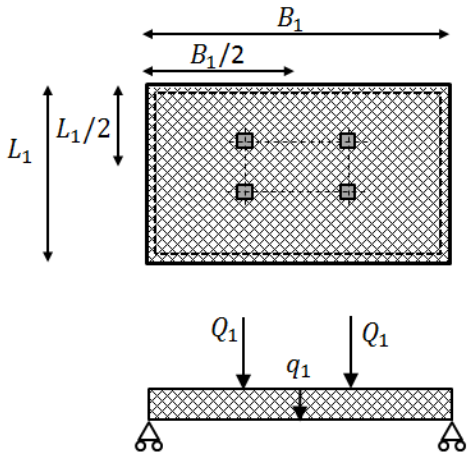

Figure 3.9 Load case used for calculating the deflection in the analytical optimisation.

Equation (2.34) was derived for a simply supported plate. This is not true for a plate segment in the bridge since it is continuous over the transverse and main girders. Due to the boundary conditions, the optimisation routine gave a stiffer SSD than what was necessary to fulfil the requirement in step 2. This was accounted for by adjusting the deflection limit in the optimisation routine in step 3, until the utilisation ratio, in terms of deflection, was 1 in the FE-model. The fact that LM1 was not correctly applied to the simply supported plate in the optimisation could therefore be disregarded, since the deflection limit constraint had to be adjusted anyway.

3.3.2 FE-model for checking deflections of SSD, step 2

The FE-software Abaqus/CAE was used for checking the deflections of the SSD. The models were created using Python scripts, to simplify the running of many analyses with different SSD configurations and geometries (see Appendix E and F). The whole width of the bridge was included together with a length equal to five times the distance between the transverse girders. The main and transverse girders were not included in the model at this stage. Instead, boundary conditions were applied so that the plate was prevented to move in the vertical direction at the position of the main girders. Two different load cases were considered, one to get the maximum deflection in the cantilever part w_{cant} and one to get the maximum deflection in between the main girders w_{mid}. In the FE-model, the modifications to LM1 described in Section 3.3.1 were no longer necessary, and the different load cases considered are shown in Figure 3.10.

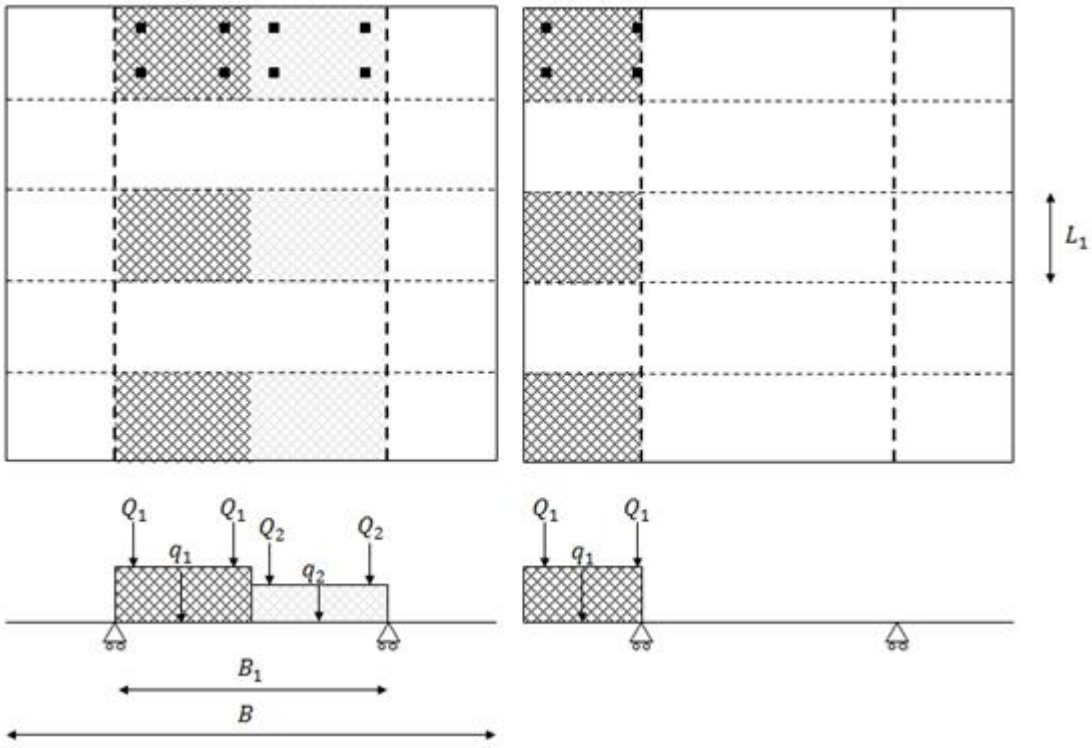

Figure 3.10 Load cases considered when checking w_{mid} (left) and w_{cant} (right) in the FE-model.

The SSD needs to be closed at the edges of the deck. The preferable way would be to have the edge beam between the face plates of the SSD. If the deflection of the cantilever part needs to be reduced, the edge beams could be extended and connected to the transverse girders as shown in Figure 3.11. However, the cantilever deflection was not governing in the preliminary design and the configuration with the edge beam between the face plates was therefore used. The edge beam had a width b_{EB}=100 mm and a thickness t_{EB}=12 mm.

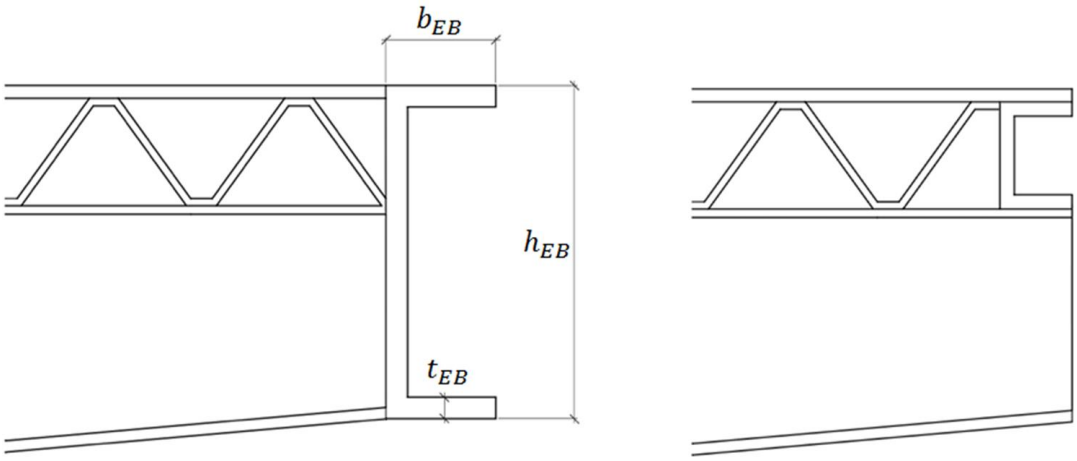

Figure 3.11 Different configurations of the edge beam.

In preliminary analyses, the distance between the transverse girders L_1 was varied between 2 m and 9 m. The dimensions obtained from the area optimisation are shown in Table 3.6, together with the stiffnesses in Table 3.7. The deflections from the FE-analyses together with the utilisation ratios are shown in Table 3.8. As can be seen in Table 3.8 the deflection limit of the cantilever part was not fulfilled, but this was not considered until the more detailed analysis in Chapter 4.

Table 3.6 SSD dimensions used in the preliminary design, obtained from the area optimisation.

$L_1 \times B_1$	h_c [mm]	$t_{f.top}$ [mm]	$t_{f.bot}$ [mm]	t_c [mm]	α [deg]	f [mm]	A [m^2/m]	Deflection limit constraint
2x6	82.4	3.4	2.4	2.6	69.2	20.0	0.0112	$L_1/(0.98 \cdot 400)$
3x6	107.6	4.5	3.4	3.4	65.9	20.0	0.0149	$L_1/(0.87 \cdot 400)$
4x6	121.8	5.2	4.0	4.0	64.3	20.0	0.0170	$L_1/(0.83 \cdot 400)$
5x6	128.9	5.6	4.4	4.2	63.3	20.0	0.0182	$L_1/(0.80 \cdot 400)$
6x6	131.8	5.8	4.6	4.3	62.6	20.0	0.0187	$B_1/(0.78 \cdot 400)$
7x6	139.9	6.2	4.9	4.6	62.0	20.0	0.0199	$B_1/(0.78 \cdot 400)$
8x6	145.5	6.5	5.2	4.8	61.6	20.0	0.0208	$B_1/(0.78 \cdot 400)$
9x6	149.9	6.7	5.4	5.0	61.3	20.0	0.0215	$B_1/(0.89 \cdot 400)$

Table 3.7 Stiffnesses for the SSD's used in the prelimnary design.

$L_1 \times B_1$	D_x [Nm]	D_y [Nm]	D_{xy} [Nm]	D_{Qx} [N/m]	D_{Qy} [N/m]
2x6	3.21e6	2.37e6	1.77e6	2.90e8	9.45e6
3x6	7.25e6	5.52e6	4.14e6	3.93e8	2.79e7
4x6	1.07e7	8.30e6	6.24e6	4.45e8	4.75e7
5x6	1.29e7	1.01e7	7.60e6	4.66e8	6.20e7
6x6	1.39e7	1.10e7	8.28e6	4.72e8	7.03e7
7x6	1.68e7	1.33e7	1.00e7	5.01e8	8.92e7
8x6	1.90e7	1.51e7	1.14e7	5.21e8	1.04e8
9x6	2.08e7	1.66e7	1.25e7	5.37e8	1.17e8

Table 3.8 Deflections and utilisation ratios from the preliminary design.

$L_1 \times B_1$	B_{TG}	w_{mid} [mm]	η_{mid}	w_{cant} [mm]	η_{cant}
2x6	*B*	4.96	0.99	3.78	0.76
3x6	*B*	7.47	1.00	8.28	1.26
4x6	*B*	9.99	1.00	12.78	1.95
5x6	*B*	12.44	1.00	17.69	2.70
6x6	*B*	14.99	1.00	22.77	3.47
7x6	*B*	14.84	0.99	23.79	3.63
8x6	*B*	14.89	0.99	24.83	3.78
9x6	*B*	14.91	0.99	25.58	3.90

3.4 Main girders

A preliminary design of the main girders was also carried out, in order to see how the dimension of the SSD and the distance between the transverse girders L_1 affected the dimensions of the main girders (see Appendix A). The main girder dimensions obtained in the preliminary design were never used in the more detailed analysis in Chapter 4. Instead, they were included for the volume comparison in Section 3.6.

The main girders were designed to meet the deflection limit under characteristic traffic load and the bridge was modelled as a continuous beam, considering half of the cross section of the most loaded girder. This was done by treating the bridge deck in the transverse direction as a beam resting on two supports being the main girders (see Figure 3.12).

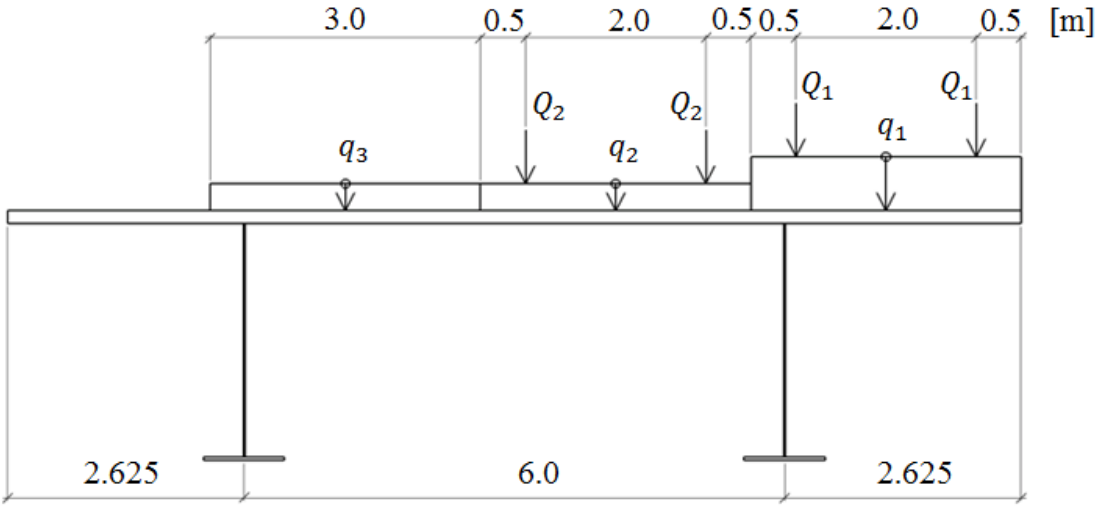

Figure 3.12 Model used to calculate the lane factors used in the preliminary design of the main girder.

The load was placed to obtain the largest reaction force in one main girder. The proportion of the load carried by that main girder, called lane factor ξ_{lf}, was calculated for distributed traffic loads and axle loads separately. The lane factor was then used to calculate the load acting on one main girder (see Table 3.9). The load cases considered in the preliminary design of the main girders is shown in Figure 3.13.

Table 3.9 Traffic loads and lane factors used in the preliminary design of the main girders.

Lane	w_{lane} [m]	Q_{ik} [kN]	q_{ik} [kN/m^2]	α_Q	α_q	ξ_{lfQ}	ξ_{lfq}	$\alpha_Q\xi_{lfQ}Q_{ik}$ [kN]	$\alpha_q\xi_{lfq}w_{lane}q_{ik}$ [kN/m]
1	3	300	9.0	1.0	1.0	0.99	0.92	296.3	38.6
2	3	200	2.5	1.0	1.0	0.99	0.92	197.5	6.9
3	3	0	2.5	0	1.0	0.99	0.92	0.0	6.9
							Sum	493.8	38.6

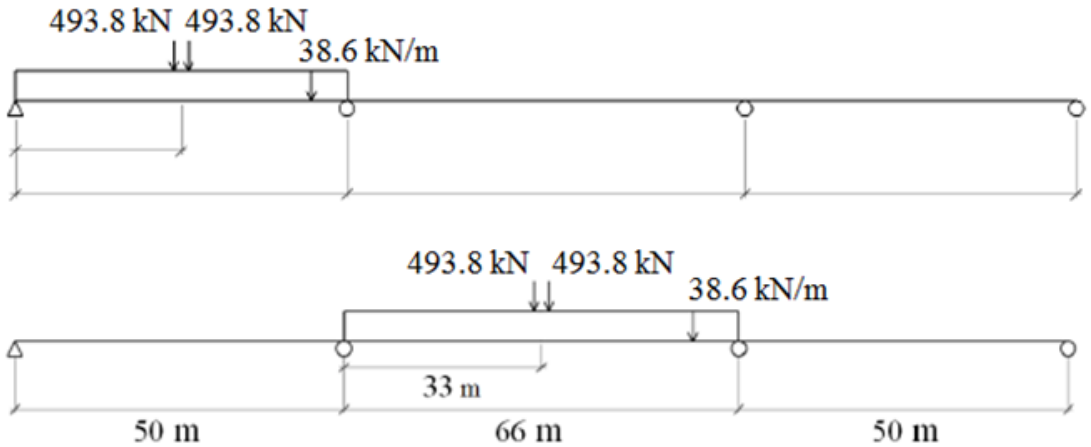

Figure 3.13 Load cases considered in the preliminary design of the main girders.

In the preliminary design of the main girders, the dimensions of the bottom flange were optimised while the thickness of the web $t_{MG.w}$ and total height were kept constant. The bottom flange thickness $t_{MG.bf}$ was constrained by the cross section class three requirement. Since the thickness of the web was kept constant at 18 mm and the total height of the main girder was kept constant at 2.6 m, the cross section of the web was in class four. However, the reduction of the cross-sectional constants was omitted since the dimensions only were used for the volume comparison in Section 3.10.

The effective width of the SSD acting as top flange was investigated with equation (2.2), given by Zou et al. (2011) (see Section 2.1.1). Equation (2.2) was derived for a girder with symmetrical top flange, which was not the case for the investigated cross section. In order to get an approximate value of the effective width the main girder web was assumed to be in the middle of the top flange, when using equation (2.2) (see Figure 3.14).

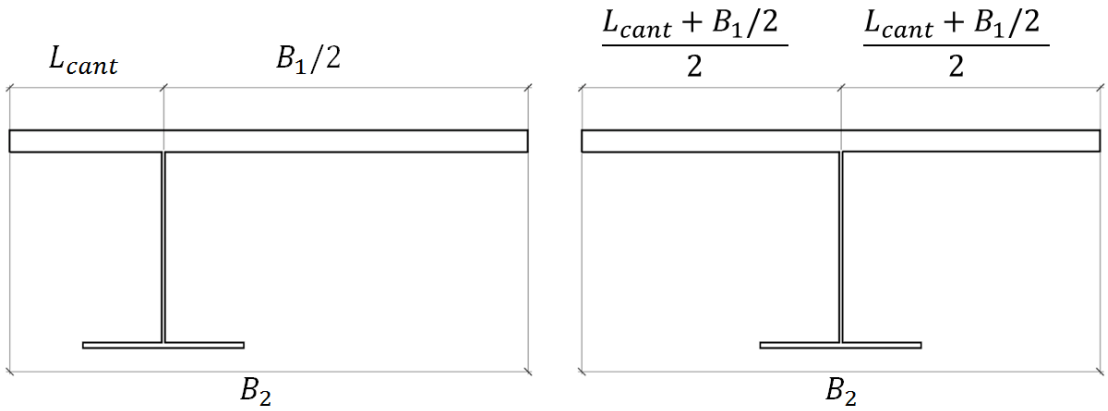

Figure 3.14 Real position of main girder (left) and position used in the calculation of the effective width (right).

The effective width b_e in the first span L_{span1} was calculated for two different lengths between the transverse girders L_1 (see Table 3.10). The dimensions for the two SSD configurations can be seen in Table 3.10. A decrease in the axial stiffness to in-plane shear stiffness ratio E_x/G_{xy}, while keeping the width to span length ratio B_2/L_{span1} constant, only lead to a small increase of the effective width. The reason for this is that the B_1/L ratio has greater influence than the E_x/G_{xy} ratio on the effective width. Since the effective width was an approximation, a conservative b_e/B_2 ratio of 0.8 was chosen for all SSD configurations in the preliminary design of the main girders. The dimensions of the main girders from the preliminary design are shown in Table 3.11.

Table 3.10 Effective widths for different lengths between the transverse girders.

$L_1 \times B_1$	B_2 [m]	L_{span1} [m]	B_2/L_{span1}	E_x/G_{xy}	b_e[m]	b_e/B_2
3x6	5.565	50	0.111	4.030	5.347	0.961
9x6	5.565	50	0.111	3.773	5.360	0.963

Table 3.11 Main girder dimensions for different distances between the transverse girders.

$L_1 \times B_1$	$h_{MG.w}$[mm]	$t_{MG.w}$ [mm]	$b_{MG.bf}$ [mm]	$t_{MG.bf}$ [mm]
2x6	2550	18	1156	50
3x6	2557	18	1001	43
4x6	2559	18	942	41
5x6	2561	18	916	39
6x6	2561	18	905	39
7x6	2562	18	881	38
8x6	2563	18	866	37
9x6	2563	18	855	37

3.5 Transverse girders

A preliminary design of the transverse girders was also conducted, in order to see how the dimension of the SSD and the distance between the transverse girders L_1 affected the dimensions of the transverse girders (see Appendix A). The results were included in the volume comparison in Section 3.10 and also used when modelling the bridge in the more detailed analysis carried out in Chapter 4.

The dimensions of the transverse girders were optimised with the constraint that the stress in the bottom flange should be below the yield strength. Furthermore, the dimensions were constrained by the cross section class three requirements. The transverse girder was modelled as a simply supported beam and the loading consisted of self-weight and traffic load in the ultimate limit state according to equation (4.2). The load case considered is shown in Figure 3.15.

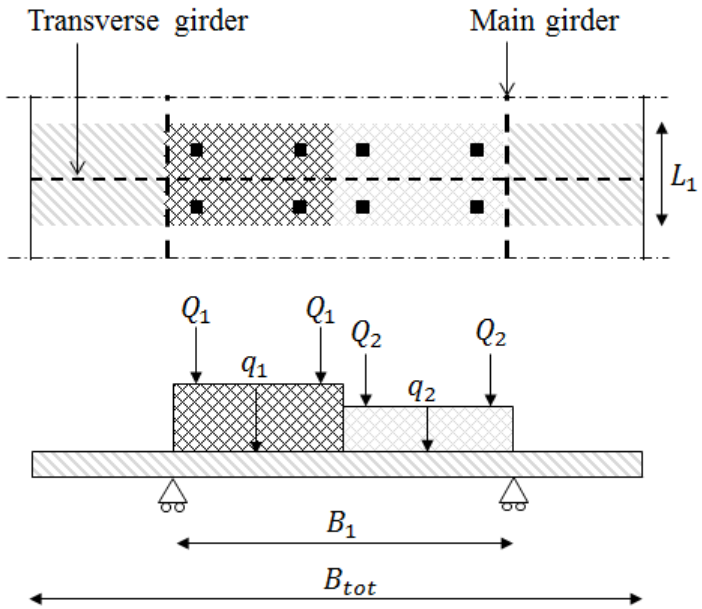

Figure 3.15 Load case considered for the preliminary design of the transverse girders.

The dimensions shown in Figure 3.16 were optimised to give the lowest cross-sectional area within the given constraints. The ratio between the height of the web at the edge and in the middle was chosen to 0.4

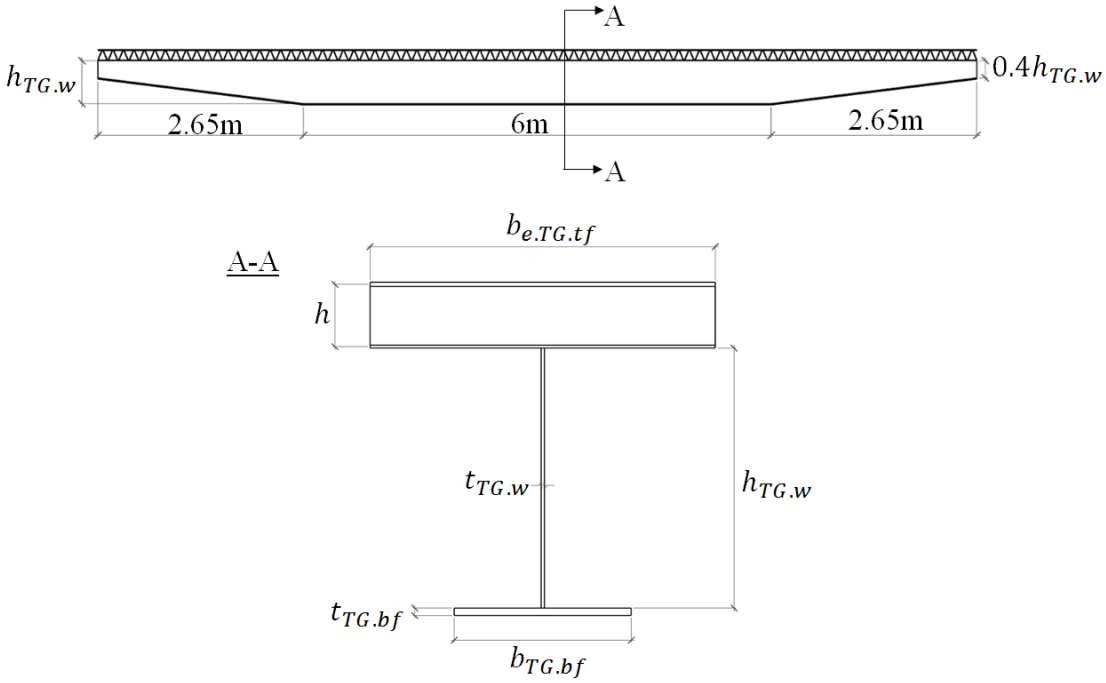

Figure 3.16 Dimensions of the transverse girders.

In the preliminary design of the transverse girders, an effective width of the SSD acting as top flange had to be calculated. Since the top plate of the SSD is compressed when the transverse girder bends, the effective width was approximated as:

$$b_{e.TG.tf} = \chi_{TG} L_1 \tag{3.2}$$

The reduction factor χ_{TG} was calculated according to SS-EN1993-1-1 (2005) for column buckling of a one meter wide strip of the top plate, with length l_o and thickness $t_{f.top}$ (see Figure 3.17).

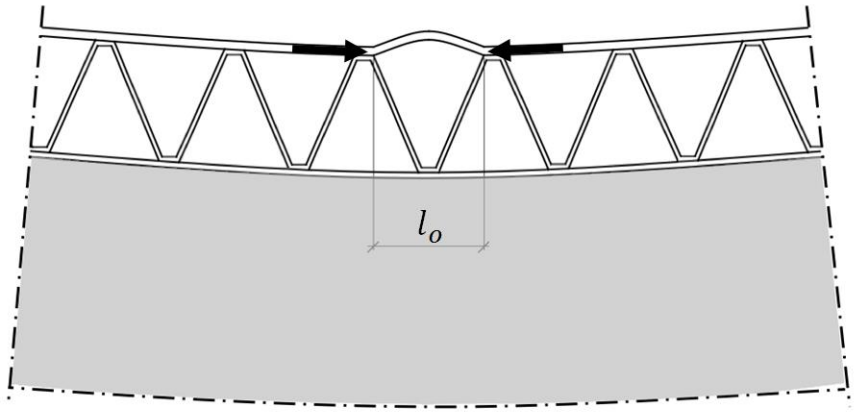

Figure 3.17 Compressive stresses in the SSD due to bending of the transverse girder.

The dimensions on the transverse girders from the preliminary design are shown in Table 3.12.

Table 3.12 Transverse girder dimensions for different distances between the transverse girders.

$L_1 \times B_1$	$h_{TG.w}$ [mm]	$t_{TG.w}$ [mm]	$b_{TG.bf}$ [mm]	$t_{TG.bf}$ [mm]
2x6	707	10	339	14
3x6	718	9	318	14
4x6	840	8	295	13
5x6	603	6	354	15
6x6	555	6	374	16
7x6	556	7	371	16
8x6	557	7	370	16
9x6	558	8	372	16

3.6 Choice of configuration for further analysis

The volume per unit length of the bridge was calculated for the SSD, the main girders and the transverse girders in order to find the SSD configuration and distance between transverse girders L_1 with the lowest weight. The volume per unit length for different L_1 are shown in Table 3.13 and Figure 3.18.

Table 3.13 Volume per unit width of the different components for different distances between the transverse girders.

$L_1 \times B_1$	V_{SSP}[m^3/m]	V_{MG}[m^3/m]	V_{TG}[m^3/m]	V_{tot}[m^3/m]
2x6	0.1264	0.2073	0.0627	0.3964
3x6	0.1672	0.1784	0.0373	0.3830
4x6	0.1914	0.1685	0.0275	0.3874
5x6	0.2043	0.1643	0.0192	0.3878
6x6	0.2101	0.1626	0.0169	0.3896
7x6	0.2241	0.1590	0.0151	0.3981
8x6	0.2337	0.1567	0.0136	0.4041
9x6	0.2414	0.1551	0.0125	0.4089

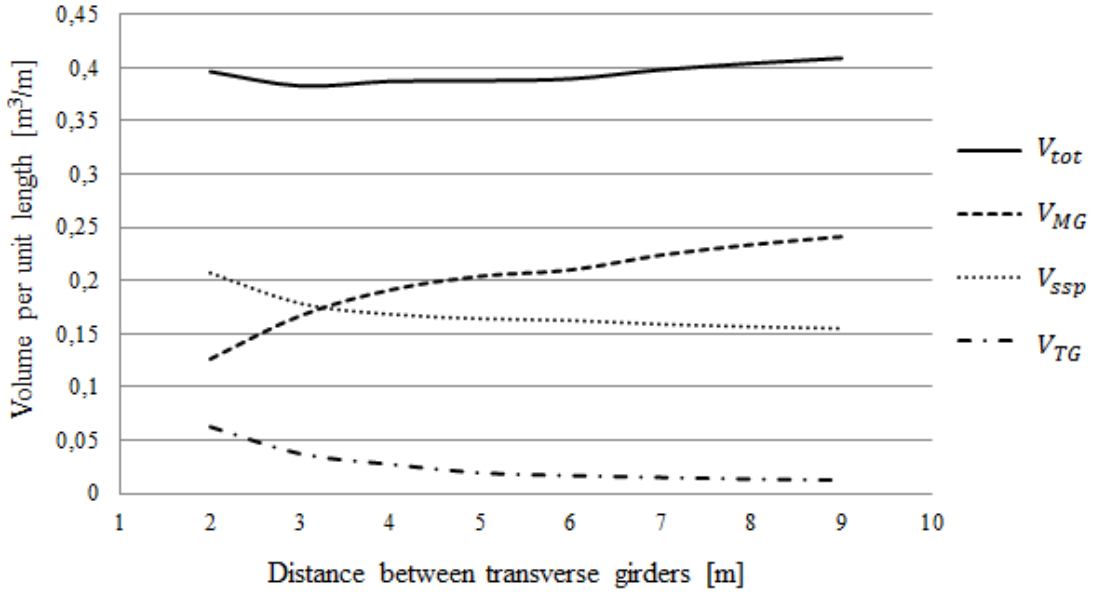

Figure 3.18 Volume per unit width of the different components for different distances between the transverse girders.

The lowest volume per unit length was obtained with a transverse girder spacing of 3 m. However, the volume per unit length only increased with 7 % when the distance between transverse girders increased from 3 m to 9 m. The labour cost for adding the additional transvers girders was therefore expected to exceed the savings in material cost from reducing the transverse girder spacing. On the other hand, if cross bracings only are used with the same distance as the transverse girders, there could be stability problems if the distance is too large. With this in mind, a girder spacing of 8.3 m was chosen to get equally spaced girders on the bridge. The dimensions, stiffnesses, deflections and utilisation ratios of the chosen configuration are shown in Table 3.14 to 3.16. Furthermore, the dimensions of the transverse girders are shown in Table 3.17.

Table 3.14 Dimensions of the chosen SSD configuration.

$L_1 \times B_1$	h_c [mm]	$t_{f.top}$ [mm]	$t_{f.bot}$ [mm]	t_c [mm]	α [deg]	f [mm]	A [m^2/m]
8.3x6	146.0	6.5	5.5	5.0	62.7	20.0	0.0217

Table 3.15 Stiffnesses of the chosen SSD configuration.

$L_1 \times B_1$	E_x [N/m]	E_y [N/m]	G_{xy} [N/m]	D_x [Nm]	D_y [Nm]	D_{xy} [Nm]	D_{Qx} [N/m]	D_{Qy} [N/m]
8.3x6	4.55e9	2.63e9	1.18e9	1.99e7	1.58e7	1.19e7	5.67e8	1.10e8

Table 3.16 Deflections and utilisation ratios of the chosen SSD configuration.

$L_1 \times B_1$	B_{TG}	w_{mid} [mm]	η_{mid}	w_{cant} [mm]	η_{cant}
8.3x6	*B*	14.70	0.98	24.79	3.78

Table 3.17 Dimensions of the transverse girders.

$L_1 \times B_1$	$h_{TG.w}$ [mm]	$t_{TG.w}$ [mm]	$b_{TG.bf}$ [mm]	$t_{TG.bf}$ [mm]
8.3x6	557	7	370	16

4 Verification of the SSD performance

4.1 Introduction

In order verify that the SSD from the preliminary design could be a viable option to concrete decking, the whole bridge was modelled and analysed in Abaqus/CAE. A FE-model of the existing composite bridge over Bergeforsen was created as well, in order to be able to compare stresses in the main girder bottom flanges of the two bridges. First, the dimensions of the bottom flanges in the SSD bridge were adjusted until the bottom flange stresses in the two models corresponded. Next, the edge beam was designed so that the cantilever part of the SSD met the local deflection requirement. In addition to designing the main girders and the edge beams, verification of the SSD capacity was carried out at some critical sections. Furthermore, it was verified that the capacity of the main girders during launching was sufficient.

After checking stresses in the top plate under wheel loads in Section 4.6.1, it was decided to increase the thickness of the top plate from 6.5 mm to 7.0 mm. The dimensions of the new SSD are shown in Table 4.1 together with the corresponding stiffnesses in Table 4.2. This deck configuration was used throughout all analysis of this chapter.

Table 4.1 Dimensions of the SSD after increasing the top plate thickness.

h_c [mm]	$t_{f.top}$ [mm]	$t_{f.bot}$ [mm]	t_c [mm]	α [deg]	f [mm]	A [m^2/m]
146.0	7.0	5.5	5.0	62.7	20.0	0.0222

Table 4.2 Stiffnesses of the SSD after increasing the top plate thickness.

E_x [N/m]	E_y [N/m]	G_{xy} [N/m]	D_x [Nm]	D_y [Nm]	D_{xy} [Nm]	D_{Qx} [N/m]	D_{Qy} [N/m]
4.65e9	2.73e9	1.22e9	2.05e7	1.63e7	1.30e7	5.70e8	1.20e8

4.2 FE-model

Three bridge models were created, one of the existing composite bridge and two of the SSD bridge. In the analyses for which the local stresses in the SSD was irrelevant, the whole bridge deck was modelled as an ESL. This model was used for the design of the main girders and the buckling analysis. In the second SSD bridge model the bridge deck was modelled with 3D SSD's at some critical sections, in order to obtain local stresses and deflections. All models were scripted in Python (see Appendix G to I).

4.2.1 Composite bridge

Eight node shell elements with reduced integration were used to model the concrete deck. For the main and transverse girders four node shell elements were used since the eight node elements should be used for thick shells only (Abaqus, 2014). Furthermore, linear Timoshenko beam elements were used for the cross bracings. An isotropic material model were used for all elements, with an elastic modulus and Poisson's ratio of $E_s = 210$ GPa and $\nu_s = 0.3$ for steel and $E_{conc} = 34$ GPa and $\nu_{conc} = 0.2$ for uncracked concrete.

The concrete deck in the bridge over Bergeforsen had varying thickness over the width of the bridge. In the FE-model this was simplified by assigning an equivalent constant thickness to the deck. The equivalent thickness was calculated by dividing the total cross-sectional area including the edge beams with the total width of the bridge. In order to account for reduced stiffness due to cracking of concrete at the interior supports, different sections were assigned. The support section of the deck was modelled as a thin steel plate with the same cross-sectional area as the reinforcement, and a length of $0.15(L_{span1} + L_{span2})$ according to SS-EN 1994-2 (2005). In the design of the existing bridge, a steel area of 1% of the concrete area was assumed in the global analysis. The same steel amount was therefore used in the following analyses.

In the existing composite bridge the main girders had a constant total height of 2.6 m, while the dimensions on the flanges and webs varied (see Table 4.3 and Figure 4.1).

Table 4.3 Main girder dimensions in the existing composite bridge

Element	$h_{MG.w.C}$ [mm]	$t_{MG.w.C}$ [mm]	$b_{MG.bf.C}$ [mm]	$t_{MG.bf.C}$ [mm]	$b_{MG.tf.C}$ [mm]	$t_{MG.tf.C}$ [mm]	l_{el} [m]
e1	2554	19	800	26	500	20	11
e2	2530	18	900	40	600	30	18
e3	2516	21	1050	44	600	40	15
e4	2474	23	1150	63	780	63	11
e5	2508	21	1000	46	600	46	10
e6	2545	18	900	32	600	23	18

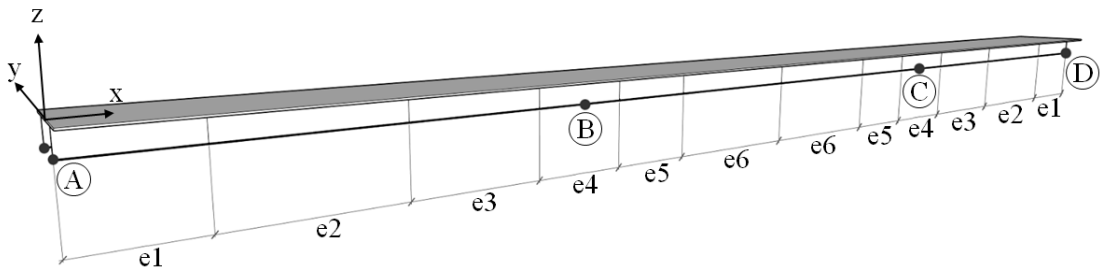

Figure 4.1 Different main girder sections.

To simplify the modelling of the bridge, the width of the top and bottom flanges was kept constant. Instead, the thicknesses were increased to give the same total area (see

Table 4.4). Since the shell elements were modelled from the centrelines, the height of the web was kept constant even if the flange thicknesses changed.

Table 4.4 Main girder dimensions used in the FE-model, with the height measured from centerline top flange to centerline bottom flange.

Element	$h_{MG.w.C}$ [mm]	$t_{MG.w.C}$ [mm]	$b_{MG.bf.C}$ [mm]	$t_{MG.bf.C}$ [mm]	$b_{MG.tf.C}$ [mm]	$t_{MG.tf.C}$ [mm]	l_{el} [m]
e1	2561	19	900	23	600	17	11
e2	2561	18	900	40	600	30	18
e3	2561	21	900	51	600	40	15
e4	2561	23	900	81	600	82	11
e5	2561	21	900	51	600	46	10
e6	2561	18	900	32	600	23	18

$h_{MG.w.C}$ Height of web

$t_{MG.w.C}$ Thickness of web

$b_{MG.bf.C}$ Width of bottom flange

$t_{MG.bf.C}$ Thickness of bottom flange

$b_{MG.tf.C}$ Width of top flange

$t_{MG.tf.C}$ Thickness of top flange

l_{el} Length of main girder element

The composite bridge had transverse girders at each support, with different dimensions for the interior and end supports (see Figure 4.2 and Table 4.5.)

Table 4.5 Dimensions of the transverse support girders in the existing composite bridge.

Support	$h_{TGS.w}$ [mm]	$t_{TGS.w}$ [mm]	$b_{TGS.bf}$ [mm]	$t_{TGS.bf}$ [mm]	$b_{TGS.tf}$ [mm]	$t_{TGS.tf}$ [mm]
A, D	1100	15	350	20	20	15
B, C	1890	25	450	30	350	25

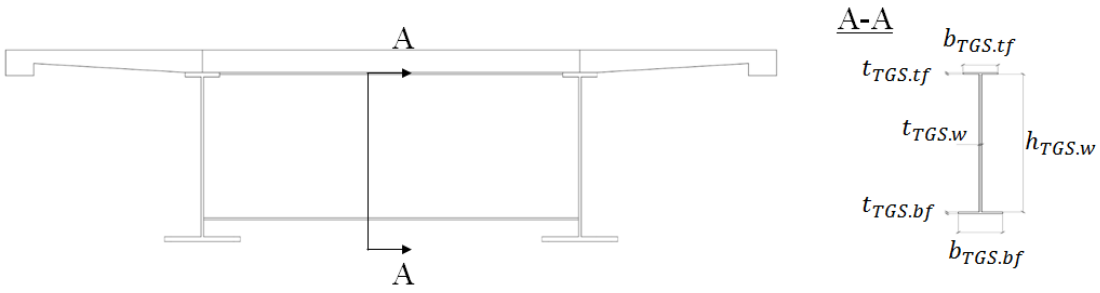

Figure 4.2 Dimensions of the transverse support girders in the existing composite bridge.

In addition, there were cross bracings consisting of KKR profiles every 7-8 m. The vertical stiffeners at each cross bracing were omitted in the model since their effect on the stress in the bottom flanges was negligible.

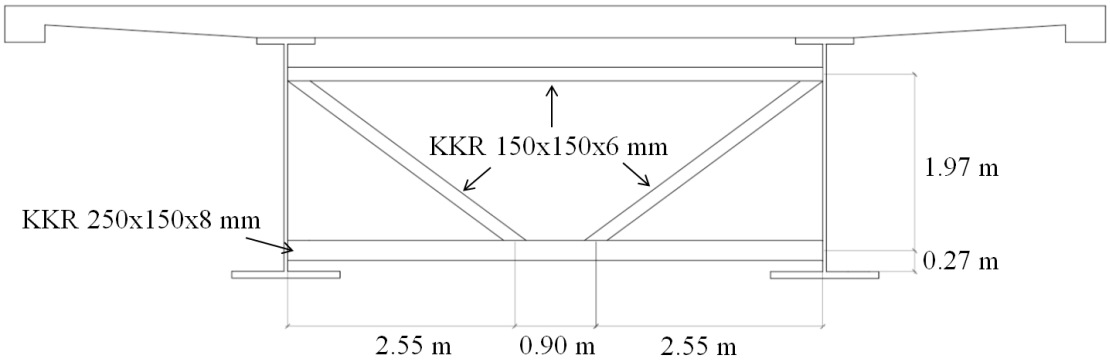

Figure 4.3 Dimensions of cross bracings in existing composite bridge.

The supports were modelled with reference points coupled to support surfaces on the bottom flanges of the main girders. Support A was prevented to move in x, y and z-direction and support B, C and D was prevented to move in y and z-direction (see Figure 4.1). The concrete deck was connected to the main and transverse girders with full interaction.

4.2.2 SSD bridge

For the main girder design and global buckling analysis, the whole bridge deck was modelled as an ESL. However, to get the local stresses in the SSD a 3D model was required. In order to reduce the computational time the SSD was only modelled in 3D in some sections, while the remaining parts were modelled as an ESL. Based on where the highest stresses and local deflections were expected, the 3D SSD was modelled at support A and B and in the middle of span AB and BC (see Figure 4.4). The length of the 3D SSD at support A and in span BC was increased, in order to span between two transverse girders.

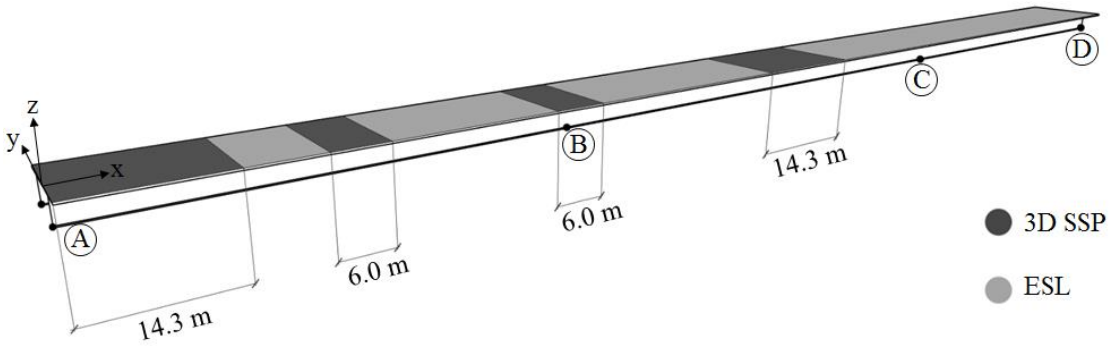

Figure 4.4 Parts of the bridge deck modelled as 3D SSD and ESL respectively.

The 3D SSD, main girders and transverse girders were modelled with four node shell elements, while the ESL was modelled with eight node shell elements with reduced integration. Moreover, the cross bracings were modelled with beam elements. An isotropic material model, with $E_s = 210$ GPa and $\nu_s = 0.3$, was used for the 3D SSD, main girders, transverse girders and cross bracings. The ESL was modelled with general shell sections, using the elastic constants in Table 4.2. The different parts were connected with full interaction.

The spacing and dimensions of the transverse girders was obtained from the preliminary design (see Section 3.10). In order to increase the stability of the compressed part of the bottom flange, cross bracings were added in connection to the transverse girders. The same KKR profiles as in the existing composite bridge were used, as shown in Figure 4.5

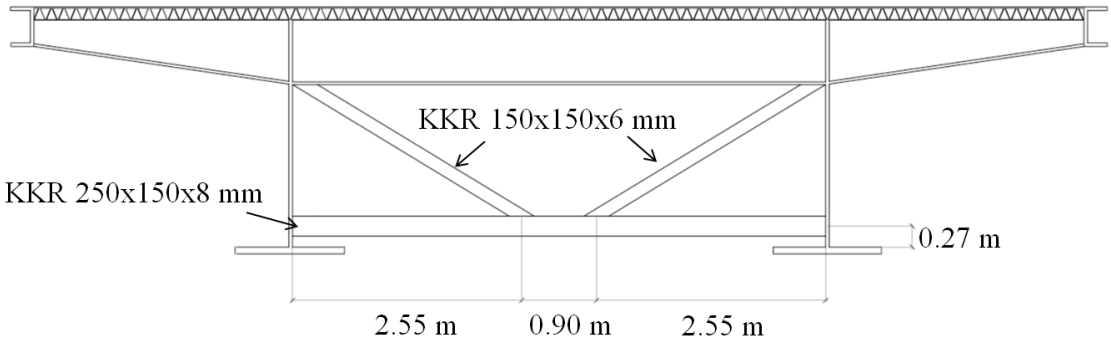

Figure 4.5 Dimensions of cross bracings in SSD bridge.

The transverse support girders had the same dimensions as in the existing composite bridge but without the top flange (see Figure 4.6 and Table 4,6). In addition, cantilever parts with the same dimensions as the regular transverse girders were used (see Table 3.17).

Table 4.6 Dimensions of transverse support girders in SSD bridge.

Support	$h_{TGS.w}$ [mm]	$t_{TGS.w}$ [mm]	$b_{TGS.bf}$ [mm]	$t_{TGS.bf}$ [mm]
A, D	1115	15	350	20
B, C	1915	25	450	30

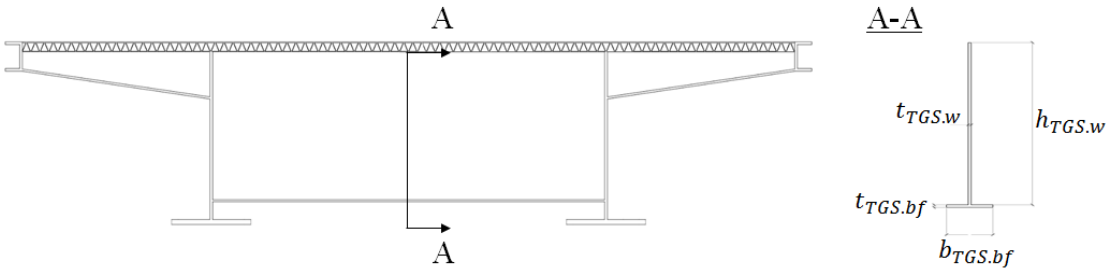

Figure 4.6 Dimensions of transverse support girders in SSD bridge.

4.2.3 Verification of ESL model

A verification was performed in order to confirm that the ESL reflected the behaviour of the 3D SSD as top flange to the main girders in the bridge. Therefore two I-beam models were analysed and compared, one with the ESL as top flange and the other with the 3D SSD. The width of the top flange was 10 m and a uniformly distributed load of 10 kN/m^2 was applied (see Figure 4.7).

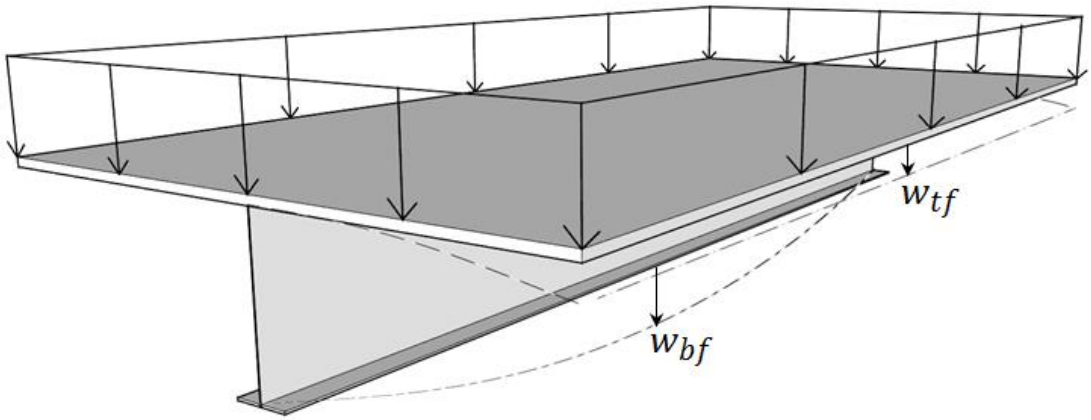

Figure 4.7 Model used to verify the ESL model.

The deflection of the bottom flange w_{bf}, deflection of top flange w_{tf} and stress in the middle of the bottom flange were compared and are shown in Table 4.7. The ESL-model gave results with less than 0.5% difference compared to the 3D SSD.

Table 4.7 Results from the verification of the ESL model.

Model	w_{bf} [mm]	w_{tf} [mm]	$\sigma_{vM.bf}$ [MPa]
ESL	6.55	51.52	39.77
3D SSD	6.54	51.66	39.66

4.2.4 Mesh convergence

Mesh convergence studies were carried out for all analyses and are presented in Appendix J.

4.3 Loads

The loads considered in the analyses were self-weight and traffic loads. The self-weights of the main girders, transverse girders and cross bracings were applied as gravity loads in all models, with a steel density of 7850 kg/m^3. The self-weight of the SSD was applied as a surface load since gravity load could not be applied to a general shell section. The self-weight of the concrete deck was applied as a surface load to the top flanges of the main girder, due to reasons described in Section 4.4. The surface loads of the SSD and concrete deck, together with the weight of the covers are shown in Table 4.8.

Table 4.8 Self-weights of the bridge decks.

Part	Bridge	A [m^2/m]	γ [kN/m^3]	g_k [kN/m^2]
Deck	SSD	0.0222	77	1.7
	Composite	0.3282	25	8.2
Cover	SSD	0.0500	23	1.2
	Composite	0.1100	25	2.8

Load model 1 (see Section 3.2) was used in the analysis with the adjustment factors α_Q and α_q according to TRVFS (2011) (see Table 4.9).

Table 4.9 Traffic loads used in the verification of the SSD performance.

Lane	Q_{ik} [kN]	q_{ik} [kN/m^2]	α_Q	α_q	$\alpha_Q Q_{ik}$ [kN]	$\alpha_q q_{ik}$ [kN/m^2]
1	300	9.0	0.9	0.7	270	6.3
2	200	2.5	0.9	1.0	180	2.5
3	100	2.5	0	1.0	0	2.5
Remaining	0	2.5	-	1.0	-	2.5

4.3.1 Load combination

Load combination of the self-weight and traffic loads in the ultimate limit state (ULS) and service limit state (SLS), was done according to SS-EN 1990 (2002). The ULS combinations were considered for analysing stresses in the main girders and SSD, as well as for the global buckling analysis. The local deflection of the SSD was checked in SLS for the frequent load combination.

For load combinations in ULS the most unfavourable of equation (4.1) and (4.2) was used. In equation (4.1) the permanent loads are dominant while equation (4.2) considers the variable actions as dominant. For the analyses considered, equation (4.2) caused the most unfavourable effects.

$$\sum_{j\geq 1} \gamma_G G_{k,j} + \gamma_Q \psi_{0,1} Q_{k,1} \tag{4.1}$$

$$\sum_{j\geq 1} \xi\, \gamma_G G_{k,j} + \gamma_Q Q_{k,1} \tag{4.2}$$

where:

$G_{k,j}$ Self-weight

$Q_{k,1}$ Traffic loads, both uniformly distributed q_{ik} and axle loads Q_{ik} with corresponding adjustment factors α_q and α_Q

γ_G Partial coefficient for permanent action equal to 1.35

γ_Q Partial coefficient for variable action equal to 1.5

ξ Reduction factor for self-weight equal to 0.89

$\psi_{0,1}$ Factor equal to 0.75 for tandem systems and 0.4 for uniformly distributed traffic load

For the frequent load combination in SLS, equation (4.3) was used.

$$\sum_{j\geq 1} G_{k,j} + \psi_{1,1} Q_{k,1} \tag{4.3}$$

where:

$\psi_{1,1}$ Coefficient equal to 0.75 for tandem systems and 0.4 for uniformly distributed traffic load

4.4 Stresses in bottom flange of main girder

The stresses obtained from the FE-model of the existing composite bridge were used to design the main girders of the SSD bridge. Due to the construction process of the composite bridge, the stress analysis had to be performed in two steps in order to get the correct stresses. To begin with the main girders were subjected to the self-weight of the concrete deck and main girders only, without composite action between the

deck and girders. This was done in order to simulate the casting of the concrete before composite action was obtained. The next step was to apply the traffic load and the self-weight of the asphalt cover and analyse the bridge when composite action had been obtained. The stresses from the two analysis steps were then added together. Two load cases, shown in Figure 4.8 and 4.9, were considered in second step in order to get the maximum span moment and support moment respectively. The results are shown in Table 4.10.

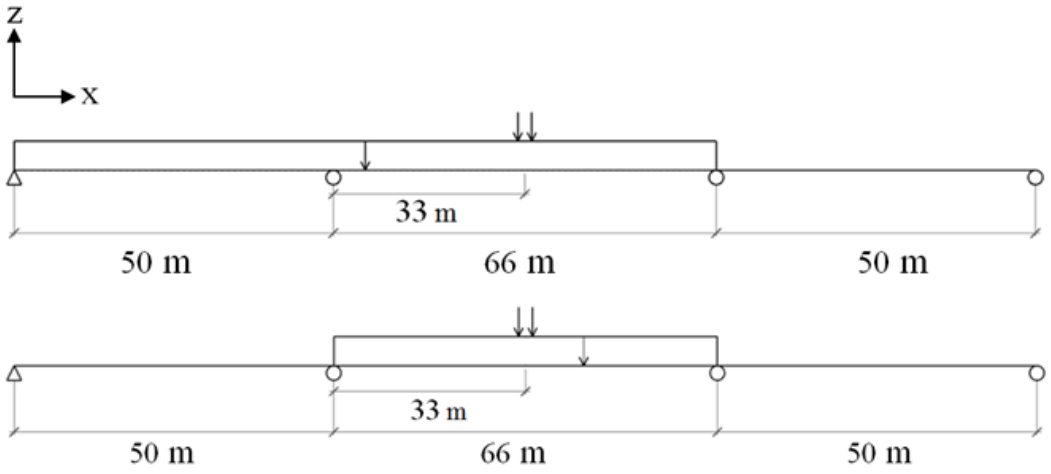

Figure 4.8 *Load cases causing the largest stresses in the bottom flange over the support (top) and in the middle span (bottom).*

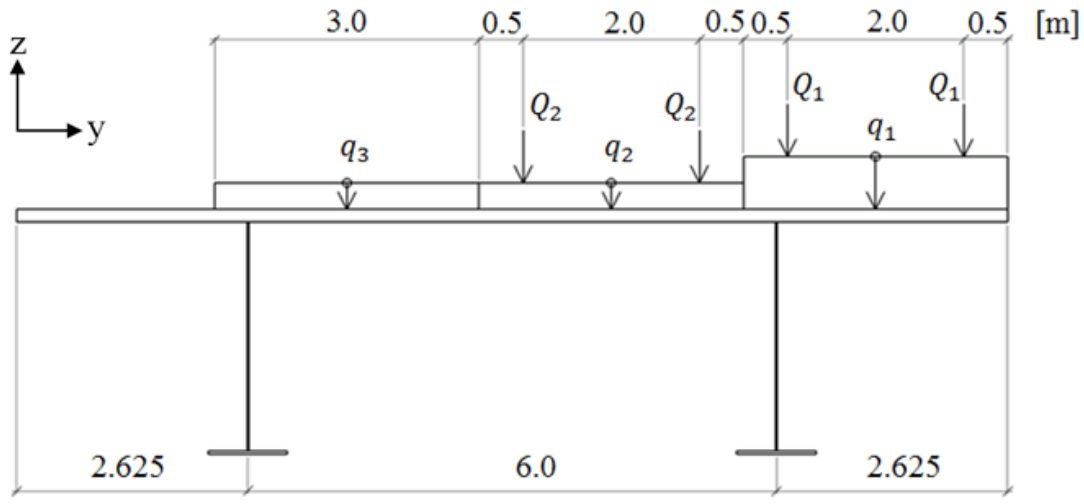

Figure 4.9 *Load placement in the transverse direction causing the largest stresses in the bottom flange.*

Table 4.10 Bottom flange stresses in the existing composite bridge.

Section	Stress before composite action [MPa]	Stress after composite action [MPa]	Total stress [MPa]
Middle span	157	212	369
Support	189	106	294

When designing the main girders of the SSD bridge, the model with the whole bridge deck as an ESL was used. The thicknesses of the web and bottom flanges, together with the ratios between the areas of the bottom flanges in each section, were kept the same as in the existing composite bridge. The width of the bottom flanges was then adjusted until the stress in the span was the same as for the composite bridge. The final dimensions are shown in Table 4.12 and the corresponding stresses are shown in Table 4.11.

Table 4.11 Bottom flange stresses in the SSD bridge.

Section	Stress in SSD bridge [MPa]
Middle span	369
Support	250

Table 4.12 Main girder dimensions in the SSD bridge.

Element	$h_{MG.w}$ [mm]	$t_{MG.w}$ [mm]	$b_{MG.bf}$ [mm]	$t_{MG.bf}$ [mm]	l_{el} [m]
1	2574	19	436	26	11
2	2560	18	490	40	18
3	2556	21	572	44	15
4	2537	23	626	63	11
5	2554	21	544	46	10
6	2568	18	490	32	18

The results showed that the dimensions of the main girders could be significantly reduced when using a SSD instead of concrete (compare with Table 4.3). A comparison of the axial stiffnesses of the decks is shown in Table 4.13, in which the effective widths were calculated with equation (2.1) from Zou et al. (2011). The axial stiffness of the concrete deck in the span was larger than the axial stiffness of the SSD. However, the self-weight of the deck was lowered from 11.0 kN/m^2 to 2.9 kN/m^2 when using the SSD. Moreover, the stiffness of the cracked concrete over the support is only 7 % of the uncracked stiffness while the SSD is fully active.

Even though the main girder in the SSD bridge was less utilised over support compared to the composite bridge, the dimensions were kept since it would be beneficial in verification of the capacity during launching.

Table 4.13 Axial stiffness of the bridge decks.

Section		A [m^2/m]	E [GPa]	b_e/b	EA [N/m]
Span	SSD bridge	0.0222	210	0.85	3.96e9
	Composite bridge	0.3282	34	0.88	9.82e9
Support	SSD bridge	0.0222	210	0.76	3.54e9
	Composite bridge	0.0033	210	1.00	6.89e8

4.5 Local deflection and edge beam dimensions

In order for the cantilever part of the SSD to fulfil the deflection requirement $w_{cant} \leq L_{cant}/400$, the edge beam dimensions were adjusted. The largest deflection of the SSD occurred in the end span between two transverse girders, for the load cases shown in Figure 4.10 and 4.11. Furthermore, the deflection between the main girders w_{mid} was checked as well.

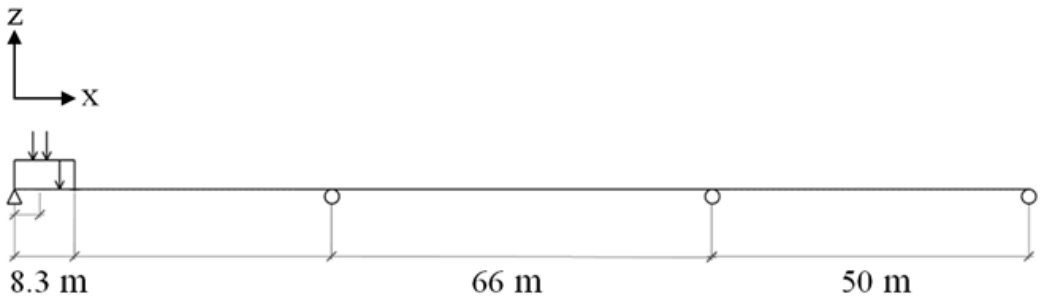

Figure 4.10 Load case resulting causing the largest deflection of the SSD.

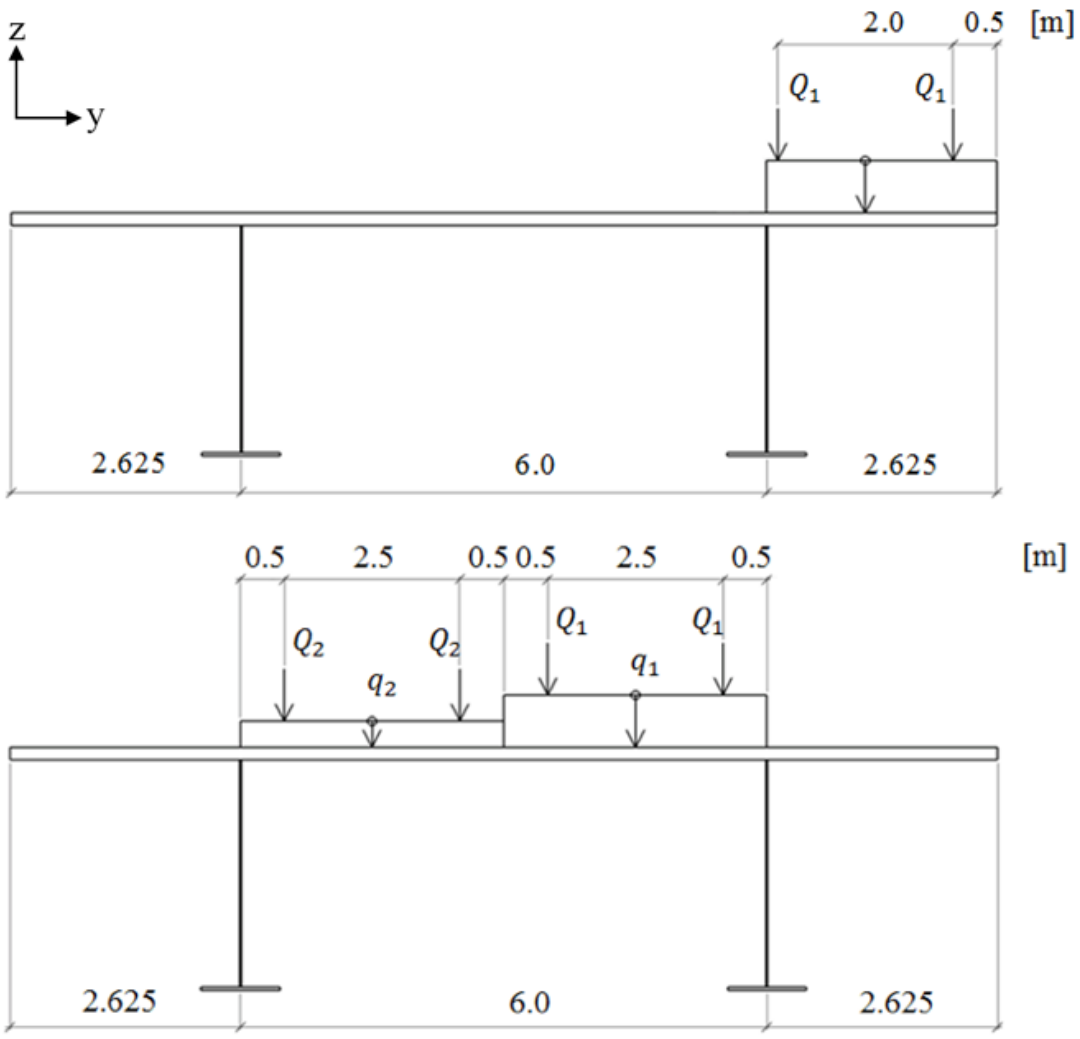

Figure 4.11 Load placement in the transverse direction considered when checking w_{cant} (top) and w_{mid} (bottom).

It was necessary to use the edge beam design described in Section 3.3.2, in which the edge beam was extended and connected to the transverse girders. The dimensions and utilisation ratios are shown in Table 4.14.

Table 4.14 Edge beam dimensions and deflection of the SSD.

h_{EB} [mm]	b_{EB} [mm]	t_{EB} [mm]	w_{cant} [mm]	η_{cant}	w_{mid} [mm]	η_{mid}
402	300	20	6.38	0.97	9.18	0.61

Finally, it was verified that the local deflection of the top plate w_{loc}, under the wheel, fulfilled the deflection requirement $2p/400$ (see Figure 4.12). The results are shown in Table 4.15.

Table 4.15 Local deflection of the SSD.

w_{loc} [mm]	η_{loc}
0.10	0.21

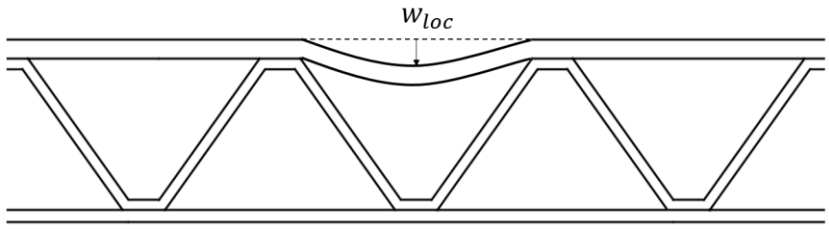

Figure 4.12 Local deflection of SSD.

4.6 Stresses in the SSD

The largest local stresses in the SSD occurred in the top plate under the wheel loads for the load case shown in Figure 4.13 and 4.14. The tandem system was placed in the middle between two transverse girders instead of in the middle of the span. The same load case resulted in the largest compressive stresses in the bottom plate, when considering the risk of face wrinkling, described in Section 4.6.2.

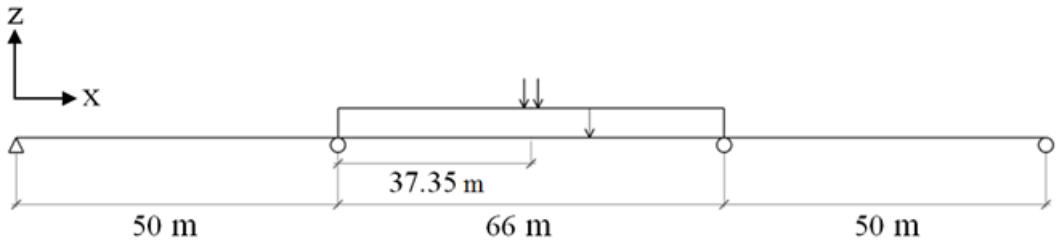

Figure 4.13 Load resulting in the largest stresses in the SSD.

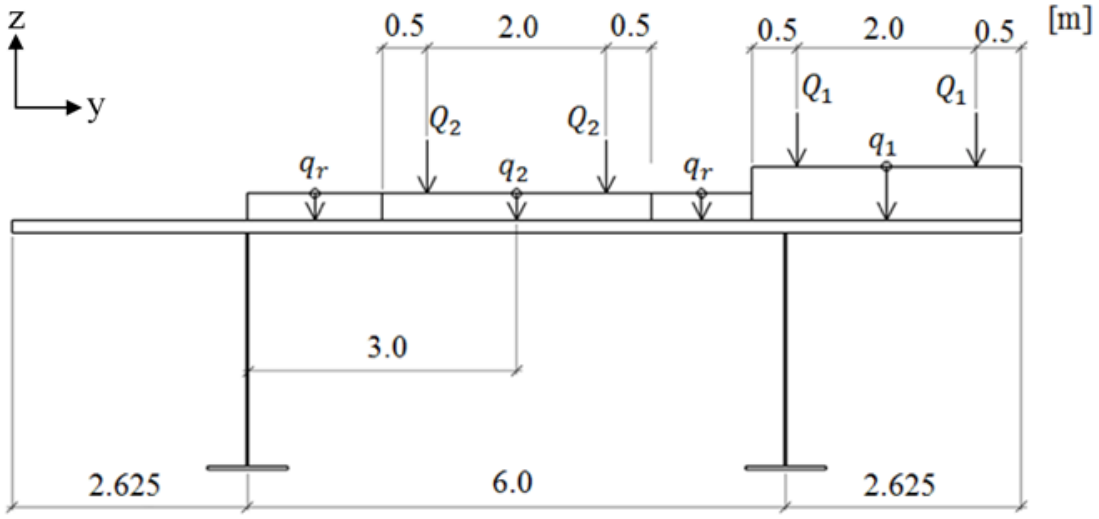

Figure 4.14 Transverse load placement causing the largest stresses in the SSD.

Moreover, the largest stresses in x-direction over the support and in the span were presented in Section 4.6.3, for the load case shown in Figure 4.15 and 4.16. Finally, the plastic collapse load of the corrugation was calculated in Section 4.6.4, using the largest stress in x-direction in the top plate.

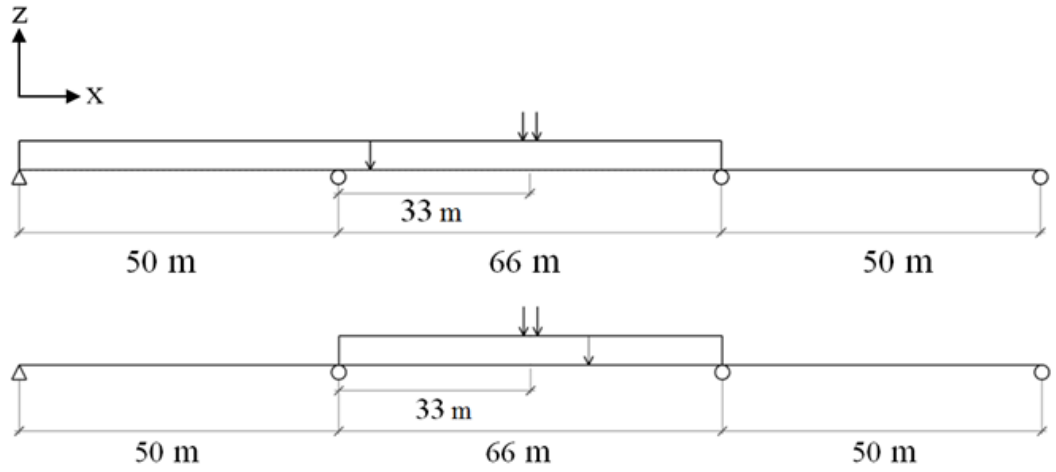

Figure 4.15 Load cases causing the largest stresses in x-direction over the support (top) and in the span (bottom).

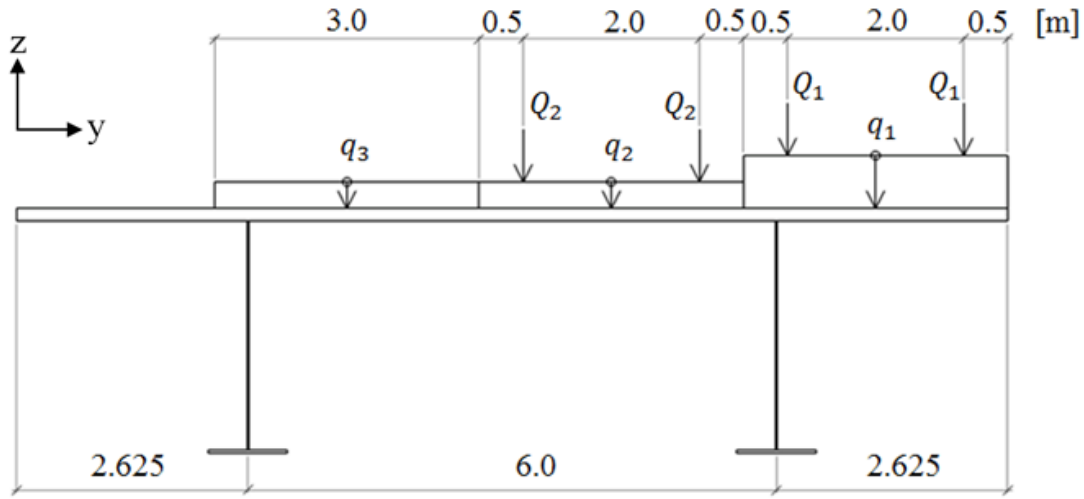

Figure 4.16 Transverse load placement resulting in the largest stresses in x-direction.

4.6.1 Top plate under wheel load

The largest stresses in the top plate of the SSD occurred under the wheel load closest to the main girder. The position of the wheel load, together with the path considered for plotting stresses, is shown in Figure 4.17.

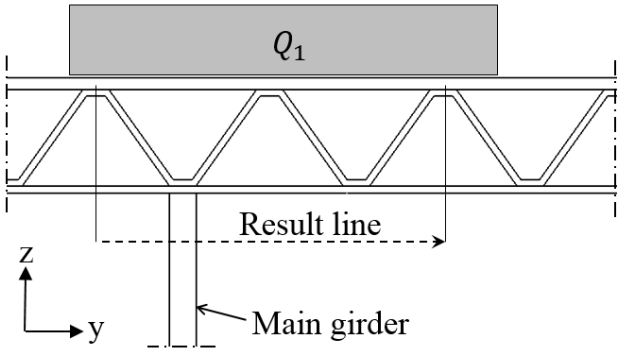

Figure 4.17 Result line considered for the maximum stresses in the top plate.

The largest stress in the y-direction $\sigma_{y.f.top}$ was found in the outer fibre of the plate and are shown in Figure 4.18.

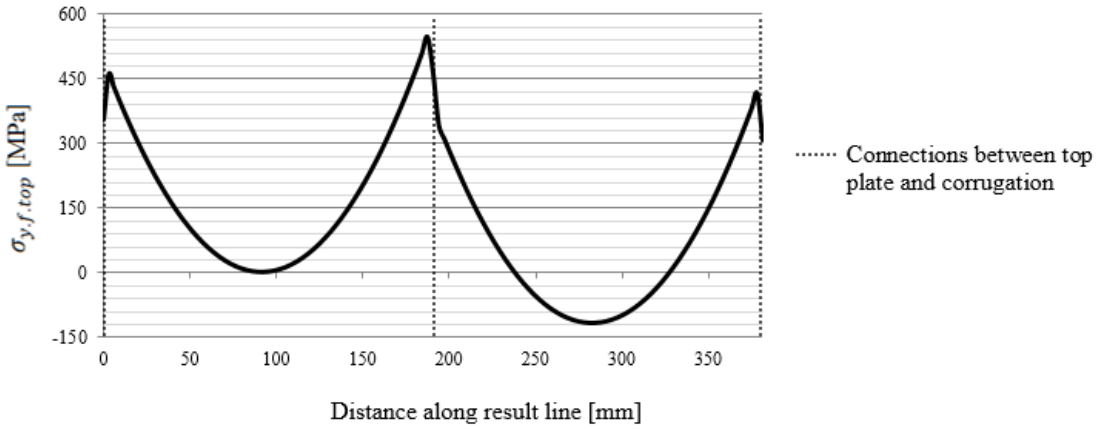

Figure 4.18 Stress in y-direction along the result line.

The von Mises stress $\sigma_{vM.top}$, shown in Figure 4.19, is an equivalent tensile stress that considers the multiaxial loading condition and was used to predict if the top plate would yield. The highest von Mises stress was obtained in the outer fibre of the plate and was 20 MPa lower than $\sigma_{y.f.top}$.

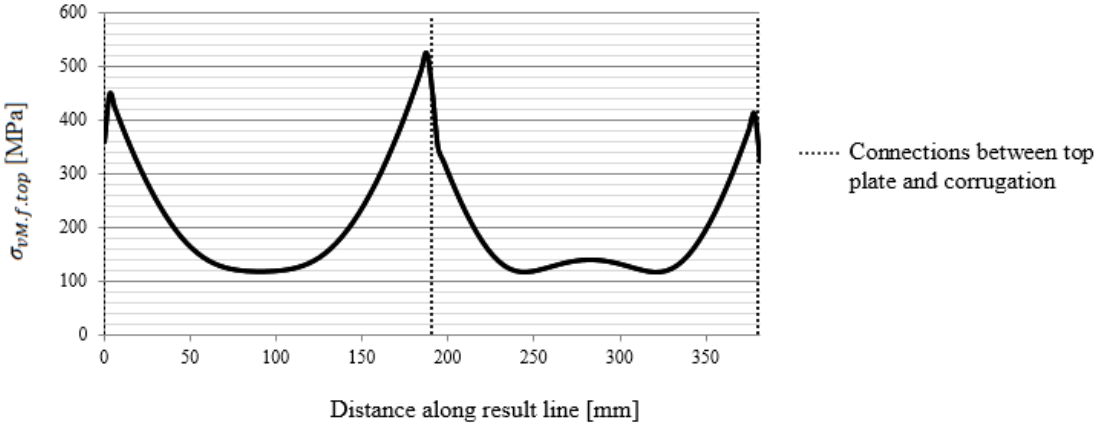

Figure 4.19 von Mises stress along the path.

In Figure 4.20, $\sigma_{vM.top}$ is plotted for different element sizes, and it clearly shows that the peak stress was mesh dependent.

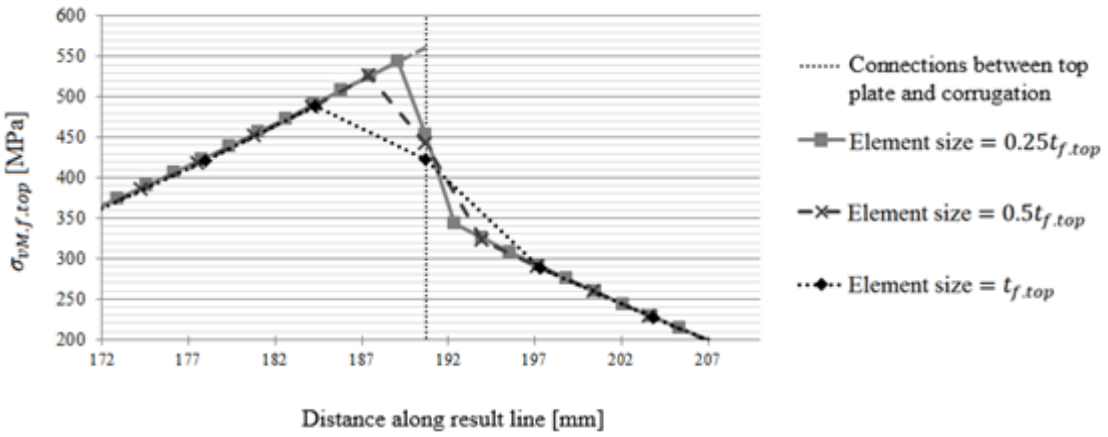

Figure 4.20 von Mises stress along the result line for different mesh sizes.

To get the accurate stress, the graph was extrapolated using the stress gradient between the stresses at a distance of $t_{f.top}$ and $0.5t_{f.top}$ from the intersection. The peak stress arises due to the fact that the face plates and corrugation are connected at single node points with full interaction, but in reality the transition would be smoother due to yielding and stress redistribution. It was therefore decided that the stress at a distance $t_{f.top}$ from the intersection should not exceed the yield stress $f_{y.f.top}$, while the peak stress should not exceed the ultimate strength $f_{u.f.top}$. In this case it would have required S690 steel, which may be problematic when it comes to weldability (Collin & Johansson, 2005). Instead, the thickness of the top plate was increased from 6.5 mm to 7.0 mm to allow for the use of S460 steel.

The values of $\sigma_{vM.f.top}$ from the analysis with a top plate thickness of 7.0 mm are shown in Figure 4.21 and summarised in Table 4.16, together with the largest stresses in the x- and y-direction

Table 4.16 Stresses in the top plate.

Position	$\sigma_{x.f.top}$ [MPa]	$\sigma_{y.f.top}$ [MPa]	$\sigma_{vM.f.top}$ [MPa]	Allowed stress
$t_{f.top}$ from tie	-174	454	444	$f_{y.f.top} = 460$ MPa
Peak value	-194	530	510	$f_{u.f.top} = 540$ MPa

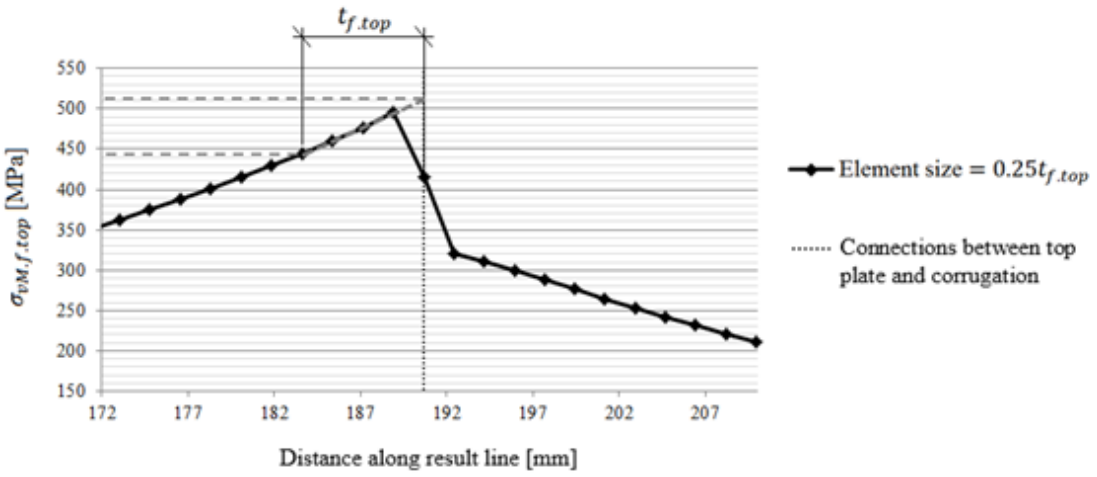

Figure 4.21 Extrapolated von Mises peak stress.

4.6.2 Compressive stresses in the bottom plate

Due to bending of the SSD in the y-direction there is a risk of face wrinkling in the bottom plate of the SSD, as described in Section 2.8.1. The largest compressive normal forces per unit width N_{Ed} occurred at the bottom plate segment next to the main girder (see Figure 4.22).

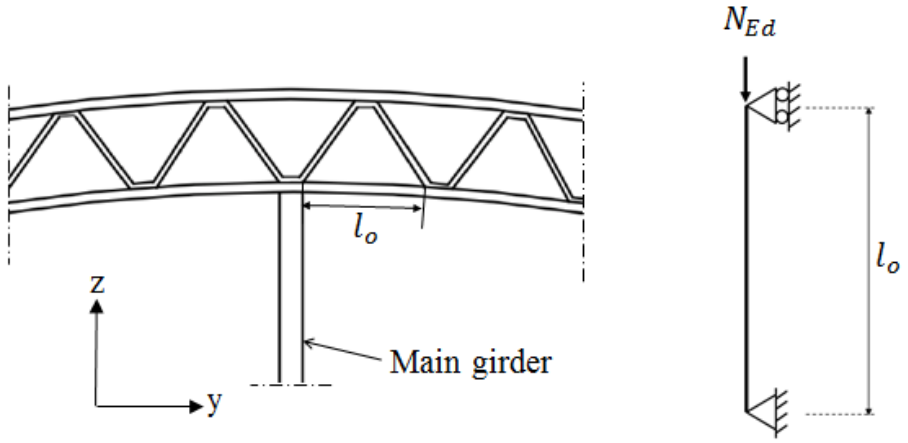

Figure 4.22 Verification of buckling resistance in the compressed part of the bottom plate.

The bottom flange was verified against buckling according to equation (4.4):

$$\frac{N_{Ed}}{N_{b,Rd}} \leq 1.0 \tag{4.4}$$

By treating the bottom plate segment as a simply supported column with a length of one corrugation opening l_o (see Figure 4.22), the buckling resistance $N_{b,Rd}$ could be calculated with equation (4.5) according to SS-EN 1993-1-1 (2005):

$$N_{b,Rd} = \frac{\chi A_{f.bot} f_{y.f.bot}}{\gamma_{M1}} \quad (4.5)$$

where:

χ	Reduction factor for simply supported column, [-]
$A_{f.bot}$	Cross section area of the bottom plate, [m^2/m]
$f_{y.f.bot}$	Yield strength of the bottom plate, [Pa]
γ_{M1}	Partial factor for instability checks equal to 1, [-]

The results from the calculations in Appendix B are shown in Table 4.17.

Table 4.17 Results from the verification of buckling capacity in bottom plate.

N_{Ed} [kN/m]	$N_{b,Rd}$ [kN/m]	$N_{Ed}/N_{b,Rd}$
617	677	0.91

4.6.3 Largest stresses in x-direction

The largest stresses in x-direction in the top plate $\sigma_{x.f.top}$ and in the bottom plate $\sigma_{x.f.bot}$ are shown in Table 4.18. The largest stresses over support and in the span were considered. Furthermore, the stress at a distance of the plate thickness away from the connection between the face plate and corrugation, as well as the peak value was calculated.

Table 4.18 Largest stersses in x-direction.

Section	$\sigma_{x.f.top}$ [MPa]		$\sigma_{x.f.bot}$ [MPa]	
	$t_{f.top}$ from connection	Peak value	$t_{f.bot}$ from connection	Peak value
Span	-177	-196	-131	-133
Support	129	130	105	107

4.6.4 Plastic collapse of the corrugation

When the SSD is subjected to high patch loads from the wheel loads there is a risk for plastic collapse of the corrugation, as described in Section 2.8.1. The plastic collapse load P_{plc} was analytically calculated with equation (2.52) and plotted against the ratio between the stress in the top plate $\sigma_{x.f.top}$ and the yield strength of the corrugation $f_{y.c} = 355$ MPa (see Figure 4.23).

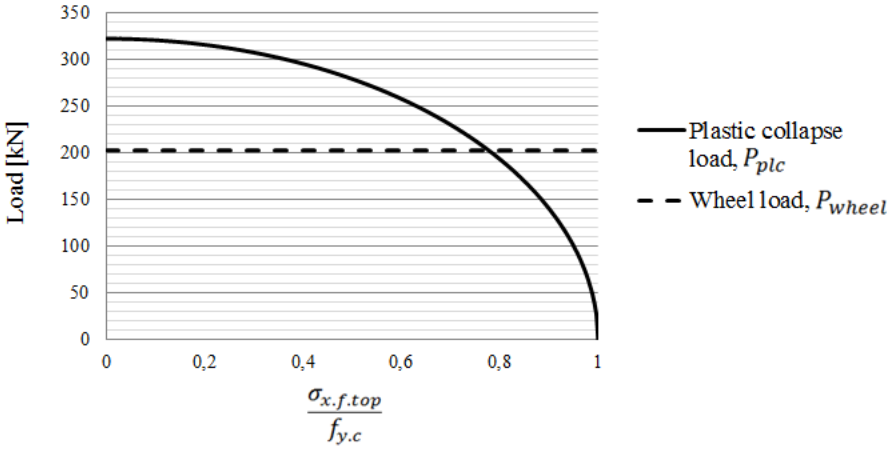

Figure 4.23 Plastic collapse load for different $\sigma_{x.f.top}/f_{y.c}$ ratios.

The wheel load from LM1 was compared with the plastic collapse load and it was found that the $\sigma_{x.f.top}/f_{y.c}$ ratio needed to be smaller than 0.77 for the corrugation to have enough capacity against plastic collapse (see Appendix B for calculations).

A $\sigma_{x.f.top}/f_{y.c}$ ratio was calculated for the largest stress in the top plate under the wheel load $\sigma_{x.f.top}$. The largest stress under the wheel load was the same as the largest stress in Section 4.6.3, resulting in a $\sigma_{x.f.top}/f_{y.c}$ ratio equal to 0.55. The results are showed in Table 4.19.

Table 4.19 Stress in top plate and utilisation ratio with respect to plastic collapse.

$\sigma_{x.f.top}$ [MPa]	$\sigma_{x.f.top}/f_{y.c}$	P_{wheel}/P_{plc}
-196	0.55	0.75

4.7 Buckling analysis

In order to capture the real buckling behaviour of the SSD bridge, a non-linear buckling analysis with the deck modelled in 3D is required. However, a sufficiently high value of the buckling load in a linear buckling analysis could indicate that the bridge has enough buckling resistance. A linear buckling analysis was therefore performed.

The Lanczos eigensolver in Abaqus/CEA was used for the buckling analysis to obtain the buckling mode and the load factor λ. The buckling mode indicates how the deck will buckle and the load factor is the ratio between the buckling load and applied load.

The load case shown in Figure 4.8 and 4.9, with the uniformly distributed load in the span only, gave the highest compressive stress in the SSD and was therefore used in the buckling analysis. The first buckling mode occurred in the web of the main girder with a load factor of $\lambda = 1.44$. Since the cross section of the main girder web was in class 4 early local buckling was expected. The first buckling mode in the SSD occurred at a load factor of λ=13.29, which indicated that the SSD had enough buckling capacity. The buckling mode is shown in Figure 4.24

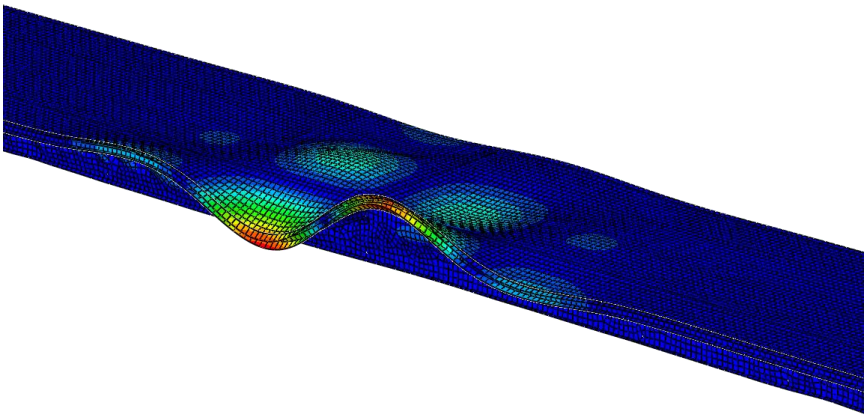

Figure 4.24 First buckling mode in the SSD.

4.8 Launching

During the launching procedure large moments and vertical patch loads arises at the supports. The moments can cause lateral torsional buckling, local buckling and yielding of the girders, while the patch loads can lead to local buckling of the web and local yielding of the bottom flange. The verification of the capacity was done according to SS-EN 1993-1-5 (2006).

Two load cases were considered where the moments M_{Ed} and reaction forces F_{Ed} were calculated at support A and support B, right before the launching nose had reached support B and support C respectively (see Figure 4.25). The launching nose was assumed to have a length L_{LN} equal to one fourth of span AB and a weight corresponding to half the weight of the main girders, according to an example from Lebet & Hirt (2013).

Figure 4.25 Launching stages considered.

The utilisation ratio for bending η_1 was calculated with equation (4.6), in which the moment resistance M_{Rd} was calculated with equation (4.7). In the equation (4.7), the area of the main girder web was reduced to account for local buckling, which gave the effective section modulus W_{eff}.

$$\eta_1 = \frac{M_{Ed}}{M_{Rd}} \leq 1.0 \tag{4.6}$$

$$M_{Rd} = \frac{W_{eff} f_y}{\gamma_{M0}} \tag{4.7}$$

The patch load resistance F_{Rd} depends mainly on the thickness of the web $t_{MG.w}$ and the length of the support. It was assumed that the SSD bridge had a support length of 0.5 m and no vertical stiffeners. The patch load resistance was verified with equation (4.8).

$$\eta_2 = \frac{F_{Ed}}{F_{Rd}} \leq 1.0 \tag{4.8}$$

Since the support section of the bridge was subjected to both bending moment and patch loading, the interaction was checked with equation (4.9).

$$\eta_2 + 0.8\eta_1 \leq 1.4 \tag{4.9}$$

Furthermore, the resistance against lateral torsional buckling was verified with equation (4.10). The moment resistance reduced for lateral torsional buckling $M_{b,Rd}$ was calculated with equation (4.11).

$$\eta_{LT} = \frac{M_{Ed}}{M_{b.Rd}} \leq 1.0 \tag{4.10}$$

$$M_{b,Rd} = \frac{\chi_{LT} W_{eff} f_y}{\gamma_{M1}} \tag{4.11}$$

The reduction factor for lateral torsional buckling χ_{LT} was calculated in a simplified manner, by treating the bottom flange of the main girder as a simply supported column that buckles in the lateral direction. The length of the bottom flange column was given by the distance between cross bracings L_1, and it was assumed that the compressive force from the bending moment at the support was constant along the length.

The calculations in Appendix C showed that bridge had enough capacity during launching and the utilisation ratios are summarised in Table 4.20.

Table 4.20 Utilisation ratios during launching.

Launching stage	$\eta_1 \leq 1$	$\eta_2 \leq 1$	$\eta_2 + 0.8\eta_1 \leq 1.4$	$\eta_{LT} \leq 1$
Launching nose at support B	0.45	0.24	0.59	0.65
Launching nose at support C	0.61	0.53	1.02	0.83

4.9 Volume and weight comparison

The total volumes of the different parts were calculated in Appendix D and are shown in Table 4.21. Moreover, the launching weights and total weights of bridges are shown in table 4.22. The steel volume in the SSD bridge, if the SSD was excluded, could be reduced with 8 m^3 or 20% compared to the existing composite bridge. With

the SSD included the total volume of steel was 74 m^3 compared to 40 m^3 in the composite bridge, which means that the launching weight was increased by 84%. However, the total weight of the SSD bridge was only 32% of the total weight of the composite bridge.

Table 4.21 Total volume of the different parts.

Part	Bridge	Total volume [m^3]
Deck	SSD	41.39
	Composite	648.42
Edge beams	SSD	4.53
	Composite	5.96
Main girders	SSD	24.02
	Composite	37.31
Cross bracings	SSD	0.99
	Composite	1.60
Transverse support girders	SSD	1.11
	Composite	1.15
Transverse girders	SSD	1.78

Table 4.22 Launching weights and total weights of the bridges.

Bridge	Launching weight [MN]	Total weight [MN]
SSD	5.68	7.83
Composite	3.09	24.49

5 Discussion

The purpose of the preliminary design was to find a weight-optimised configuration of the SSD, which could be further analysed and evaluated. In order to carry out the preliminary design, the 3D SSD was idealised as a homogeneous orthotropic thick plate with equivalent stiffness constants. Some parts of the deck were modelled as an equivalent single layer (ESL) in the more detailed analysis as well, in order to save time when running the analyses. In Section 4.2.3 it was verified that the ESL could simulate the behaviour of the 3D SSD as a top flange to the main girders. The choice to model the SSD with an ESL, when local stresses in the SSD were of no interest, could therefore be justified.

In the optimisation routine, the deflection limit constraint had to be changed manually in order to get an utilisation ratio close to one in the FE-model. Since the FE-analysis was carried out using Python scripts, it would serve the purpose of the preliminary design to incorporate the optimisation routine in the script. This was not possible due to the fact that Mathcad was used for the analytical optimisation. However, in the end the same results were obtained even though time could be saved if the deflection limit constraint were not changed manually.

It was assumed that a SSD that fulfilled the constraints in the optimisation, described in Section 3.3.1, also would have sufficient capacity in other aspects. The results from the analysis of local stresses under the wheel loads in Section 4.6.1 indicated that the deflection constraints only might be insufficient. However, the thickness of the top plate only had to be increased with 0.5 mm, which indicates that no major changes of the preliminary dimensions are needed.

Moreover, fatigue was not considered in the verification of the performance. It is possible that consideration of the fatigue strength would result in further modifications of the design.

The results showed that the dimensions of the main girders could be significantly reduced when replacing the concrete deck with SSD's. A complete design of the main girders was not carried out but since both the existing composite bridge and the SSD bridge were modelled in Abaqus/CAE, the stresses in the bottom flange could be compared for the load cases considered. The axial stiffness of the uncracked concrete deck was higher than the axial stiffness of the SSD. However, a lower self-weight of the deck together with the fact that the concrete is cracked over the supports explains why the dimensions of the main girder could be reduced.

The formulation for the plastic collapse load was verified by Naar (1997) for a simply supported SSD. However, the SSD considered in this thesis was not simply supported and worked as a top flange to the main girder. Some uncertainties were therefore associated with the plastic collapse load P_{plc}. To verify that the corrugation of the SSD has enough resistance against plastic collapse a non-linear buckling analysis could be performed. However the utilization of the SSD was 75%, which gave some margin for errors in the plastic collapse load.

The capacity of the main girders during launching was verified for the launching stages that caused the largest moments and reaction forces. However, it is possible that other stages could be critical, since the main girder had varying dimensions along the bridge. In a more thorough launching investigation, the moments and reaction forces for all possible positions of the bridge should have been calculated. On the

other hand, if the bridge would have insufficient capacity in other sections than the ones studied, it is possible to adjust the length on the launching nose to lower the section forces. In addition, the approach for calculating the lateral torsional buckling was conservative since the web of the main girder would contribute to the stiffness.

It is not possible to draw conclusions whether the total cost will be reduced if a SSD deck is used, based only on the results from this thesis. Material savings were possible in the main girder primarily, but the cost for producing the SSD has to be compared to the cost for casting the concrete deck. However, it is certain that the construction time is reduced when the SSD is launched together with the main girders. In urban areas this is a considerable advantage.

6 Conclusions

In this thesis a literature study on the structural behaviour and performance of SSD's was conducted in order to understand the potential of SSD decks as a replacement for concrete decks in composite bridges. In the preliminary design, an optimisation of a SSD deck was carried out to reduce the weight with maintained structural performance. Moreover, the structural performance of the SSD deck was verified and compared with an existing composite bridge using Abaqus/CAE.

The conclusions from the thesis, based on the results and discussion, were:

- The SSD configuration from the preliminary had sufficient capacity, except for minor changes of the top plate thickness under the given limitations.
- The main girder dimensions and total weight of the bridge could be significantly reduced due to the high stiffness-to-weight ratio of the SSD deck.
- Calculations indicated that it is feasible to launch the SSD deck together with the main girders.

Based on the verifications it was concluded that the SSD deck could be a valid alternative to concrete decks in composite bridges, especially when reduction of the construction time is of significance.

6.1 Recommendations for further studies

In future studies a cost comparison could be carried out to further establish the concept of SSD decks, as a cost efficient alternative to concrete decking in composite bridges. The comparison should include the construction cost for the bridge and take into account the cost for society, regarding disturbance during the construction time. Furthermore, the concept could be applied to other bridge types as well. The advantages of SSD decks are not limited to medium span bridges.

A thorough study on the fatigue strength is also necessary for the concept to be fully verified. Moreover, connections between the elements were not considered in the thesis. These details can be crucial for the performance of the bridge as a whole and should therefore be studied further.

7 References

Abaqus (2014): *Abaqus/CAE 6.14 Documentation*. Providance: Dassault Systèmes.

Abbott, S. P., Caccese, V., Thompson, L., Blomquist, P. A. & Hansen, E. E. (2007): *Automated Laser Welded High Performance Steel Sandwich Bridge Deck Development*. Brunswick: PLSystems.

Alwan, U. & Järve, D. (2012): *New Concept for industrial bridge construction*. Göteborg: Chalmers University of Technology.

Beneus, E. & Koc, I. (2014): *Innovative road bridges with steel sandwich decks*. Göteborg: Chalmers University of Technology.

Biagi, R. (2010): *The mechanical response of corrugated core sandiwch columns*. Charlottesville: University of Virginia.

Biagi, R. & Bart-Smith, H. (2012): In-plane column response of metallic corrugated core sandwich panels. *International Journal of Solids and Structures*, 49, pp.3901–3914.

Blaauwendraad, J. (2010): *Plates and FEM*. Dordrecht: Springer.

Bright, S.R. & Smith, J.W. (2007): A new design for steel bridge decks. *The Structural Engineer*, (November), pp.49–57.

Bright, S.R. & Smith, J.W. (2004): Fatigue performance of laser-welded steel bridge decks. *The Structural Engineer*, (November), pp.31–39.

BS 5400-10 (1980): *Steel, concrete and composite bridges*: *Code of practice for fatigue.*

Caccese, V., Blomquist, P. A., Berube, K. A., Webber, S. R. & Orozco, N. J. (2006): Effect of weld geometric profile on fatigue life of cruciform welds made by laser/GMAW processes. *Marine Structures*, 19, pp.1–22.

Caccese, V. & Yorulmaz, S. (2009): *Laser welded steel sandwich panel bridge deck development: finite element analysis and stake weld strength tests*. Orono: University of Maine.

Chang, W., Ventsel, E., Krauthammer, T. & John, J. (2005): Bending behavior of corrugated-core sandwich plates. *Composite Structures*, 70, pp.81–89.

Chang, W. (2004): *Elasto-plastic analysis of corrugated sandwich steel panels*. Pennsylvania: The Pensylvania State University.

Collin, P. & Johansson, B. (2005): Design of welds in high strength steel. In *4:th European Conference on Steel and Composite Structures*. Maastricht.

Collings, D. (2008): *ICE manual of bridge engineering*. London: ICE Publishing.

Kihl, D.P. (2002): *Fatigue strength of HSLA-65 weldments*. Naval Surface Warfare Center – Carderock Division.

Kozak, J. (2005): Strength tests of steel sandwich panel. *Maritime Transportaton and Exploitation of Ocean and Coastal Resources*, pp.471–476.

Kujala, P., Romanoff, J., Tabri, K. & Ehlers, S. (2004): All steel sandwich panels - design challenges for practical application on ships. In *9th Symposium on*

Practical Design of Ships and Other Floating structures. Luebeck-Travemuende, pp. 915–922.

Kujala, P. (1998): Ultimate strength analysis of all steel sandwich panels. *Rakenteiden Mekaniikka*, 31, pp.32–45.

Lebet, J.P. & Hirt, M. (2013): *Steel bridges: conceptual and structural design of steel and steel-concrete composite bridges*. Luasanne: EPFL Press.

Libove, C. & Batdorf, S.B. (1948): *A general small-deflection theory for flat sandwich plates*. NACA.

Libove, C. & Hubka, R.E. (1951): *Elastic constants for corrugated-core sandwich plates*. Washington: Langley Aeronautical Laboratory.

Lok, T.S. & Cheng, Q.H. (1999): Elastic Deflection of Thin-Walled Sandwich Panel. *Journal of Sandwich Structures and Materials*, 1, pp.279–298.

Moffatt, K. & Dowling, P. (1975): Shear lag in Box Girder Bridges. *The Structural Engineer*, 53(10), pp.308–313.

Munse, W. H., Wilbur, T. W., Tellalian, M. L., Nicoll, K. & Wilson, K. (1983): *Fatigue characterization of fabricated ship details for design.* Springfield: Ship Structure Committee.

Naar, H. (1997): *All steel corrugated core sandwich panels under patch loading*. Tallin: Tallin Technical University.

Oñate, E. (2013): *Structural analysis with the finite element method*. Barcelona: CIMNE.

Philips, A.L. (1961): *Welding handbook* 4th edition. New York: American Welding Society.

Romanoff, J. & Varsta, P. (2006): Bending response of web-core sandwich beams. *Composite Structures*, 73, pp.478–487.

Romanoff, J., Varsta, P. & Remes, H. (2007): Laser-welded web-core sandwich plates under patch loading. *Marine Structures*, 20, pp.25–48.

Saleh, Y. & Duan, L. (2000): Steel-concrete composite box girder bridges. In *Bridge engineering handbook*, Ed. W. Chen & L. Duan, Boca Raton: CRC Press.

SS-EN 1990 (2002): *Eurocode – Basis of structural design*.

SS-EN 1991-2 (2003): *Eurocode 1: Actions on structures – Part 2: Traffic loads on bridges*.

SS-EN 1993-1-1 (2005): *Eurocode 3: Design of steel structures – Part 1-1: General rules and rules for buildings*.

SS-EN 1993-1-5 (2006): *Eurocode 3: Design of steel structures – Part 1-5: Plated structural elements*.

SS-EN 1994-2 (2005): *Eurocode 4 – Design of composite steel and concrete structures – Part 2: General rules and rules for bridges*.

Tan, K.H., Montague, P. & Norris, C. (1989): Steel sandwich panels: finite element, closed solution, and experimental comparisons, on a 6m x 2 .lm panel. *The Structural Engineer*, 67(9), pp.159–166.

Tenchev, R.T. (1996): Shear lag in orthotropic beam flanges and plates with stiffeners. *International Journal of Solids and Structures*, 33(9), pp.1317–1334.

TRVFS (2011:12): *Trafikverkets författningssamling*.

TRVK Bro 11 (2011): *Trafikverkets tekniska krav Bro*.

Vayas, I. & Iliopoulos, A. (2014): *Design of steel-concrete composite bridges to eurocodes*. Boca Raton: CRC Press.

Zenkert, D. (1997): *The handbook of sandwich construction*. Cradley Heath: EMAS.

Zenktert, D. (1995): *An introduction to sandwich structures*. Cradley Heath: EMAS.

Zou, B., Chen, A., Davalos, J. F. & Salim, H. A. (2011): Evaluation of effective flange width by shear lag model for orthotropic FRP bridge decks. *Composite Structures*, 93(2), pp.474–482.

APPENDIX A

Analytical optimisation of SSP

Appendix A - Analytical optimisation of SSP

Contents

1. Input data

1.1. Bridge geometry

$B_{tot} := 11.25m$ Total free witdh of bridge

$L_1 := 8m$ Distance between transverse girders

$B_1 := 6m$ Distance between main girders

$L_{cant} := \frac{B_{tot} - B_1}{2} = 2.625\,m$ Length of cantilever part

$L_{span1} := 50m$ Length of side span

$L_{span2} := 66m$ Length of middle span

1.2. Material properties

$\nu := 0.3$ Poisson's ratio

$\rho := 7850\frac{kg}{m^3}$ Density of steel

$E := 210GPa$ Modulus of elasticity

$G_c := \frac{E}{2\cdot(1+\nu)} = 80.769\cdot GPa$ Shear modulus of elasticity

$f_y := 355MPa$ Yield stress

$\varepsilon_3 := \sqrt{\frac{235MPa}{f_y}} = 0.814$ Coefficient considering the yield stress for cross-section class assignment

1.3. Loads

Reduction factors

$\alpha_{Q1} := 1.0$ $\alpha_{q1} := 1.0$

$\psi_{0.UDL} := 1.0$ $\psi_{0.TS} := 1.0$

All reductionn factors are chosen to 1.0 in the preliminary design

Partial coefficients

For ULS

$\gamma_G := 1.35$ $\xi := 0.85$

$\gamma_{Q.1} := 1.5$

Permanent loads

$t_{cover} := 50mm$ Thickness of the asphalt cover

$a_c := 500mm$ Contact area of the wheel taking the asphalt cover into consideration

$\gamma_{cover} := 23\frac{kN}{m^3}$ Asphalt density

$q_{cover} := \gamma_{cover} \cdot t_{cover} \cdot a_c = 0.575 \cdot \frac{kN}{m}$ Load from asphalt cover

Variable loads

$q_{1k} := 9\frac{kN}{m^2}$ Distributed traffic load lane 1

$q_{2k} := 2.5\frac{kN}{m^2}$ Distributed traffic load lane 2

$q_{3k} := 2.5\frac{kN}{m^2}$ Distributed traffic load lane 3

$q_{rk} := 2.5\frac{kN}{m^2}$ Distributed traffic load remaining lane

$Q_{1k} := 300kN$ Load from axel in lane 1

$Q_{2k} := 200kN$ Load from axel in lane 2

$Q_{3k} := 0kN$ Load from axel in lane 3

$d_{axel.LM1} := 1.2m$ Distance between axels

$d_{wheel.LM1} := 2.0m$ Distance between wheels

$w_{lane} := 3.0m$ Width of traffic lanes

2. SSP

2.1. Geometry

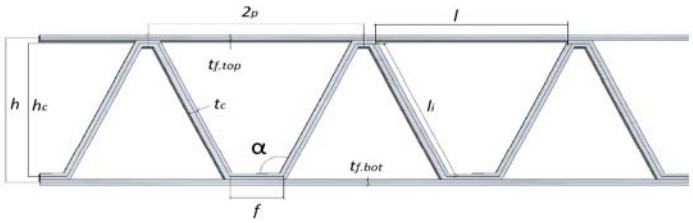

Height of the cross-section

Measured from centreline of top plate to centreline of bottom plate

$$h_{ssp}\left(h_{c.ssp}, t_{f.top}, t_{f.bot}, t_{c.ssp}\right) := h_{c.ssp} + \frac{t_{f.top}}{2} + \frac{t_{f.bot}}{2} + t_{c.ssp}$$

Measured from top to bottom of SSP

$$h_{ssp.tot}\left(h_{c.ssp}, t_{f.top}, t_{f.bot}, t_{c.ssp}\right) := h_{c.ssp} + t_{f.top} + t_{f.bot} + t_{c.ssp}$$

Length of the inclined corrrugation leg

$$l_{c.ssp}\left(h_{c.ssp}, \alpha_{ssp}\right) := \frac{h_{c.ssp}}{\sin\left(\alpha_{ssp}\right)}$$

Length of corrugation opening

$$l_o\left(h_{c.ssp}, \alpha_{ssp}, f_{ssp}\right) := 2\, l_{c.ssp}\left(h_{c.ssp}, \alpha_{ssp}\right)\cdot\cos\left(\alpha_{ssp}\right) + f_{ssp}$$

Half of the corrugation pitch

$$p_{ssp}\left(h_{c.ssp}, \alpha_{ssp}, f_{ssp}\right) := \frac{f_{ssp}}{2} + \frac{l_o\left(h_{c.ssp}, \alpha_{ssp}, f_{ssp}\right)}{2}$$

Length of cross-section

$$l_{ssp}\left(h_{c.ssp}, \alpha_{ssp}, f_{ssp}\right) := 2\cdot p_{ssp}\left(h_{c.ssp}, \alpha_{ssp}, f_{ssp}\right)$$

2.2. Cross-sectional constants

Area

Area of top flange:

$$A_{f.top}(t_{f.top}, h_{c.ssp}, \alpha_{ssp}, f_{ssp}) := t_{f.top} \cdot l_{ssp}(h_{c.ssp}, \alpha_{ssp}, f_{ssp})$$

Area of bottom flange

$$A_{f.bot}(t_{f.bot}, h_{c.ssp}, \alpha_{ssp}, f_{ssp}) := t_{f.bot} \cdot l_{ssp}(h_{c.ssp}, \alpha_{ssp}, f_{ssp})$$

Area of the core:

$$A_{c.ssp}(t_{c.ssp}, h_{c.ssp}, \alpha_{ssp}, f_{ssp}) := 2 \cdot f_{ssp} \cdot t_{c.ssp} + 2 \cdot t_{c.ssp} \cdot l_{c.ssp}(h_{c.ssp}, \alpha_{ssp})$$

Area of the core per unit width:

$$A_{C.ssp}(t_{c.ssp}, h_{c.ssp}, \alpha_{ssp}, f_{ssp}) := \frac{A_{c.ssp}(t_{c.ssp}, h_{c.ssp}, \alpha_{ssp}, f_{ssp})}{l_{ssp}(h_{c.ssp}, \alpha_{ssp}, f_{ssp})}$$

Total Area:

$$\begin{aligned} A_{tot.ssp}(h_{c.ssp}, t_{f.top}, t_{f.bot}, t_{c.ssp}, \alpha_{ssp}, f_{ssp}) := {} & A_{f.top}(t_{f.top}, h_{c.ssp}, \alpha_{ssp}, f_{ssp}) \dots \\ & + A_{f.bot}(t_{f.bot}, h_{c.ssp}, \alpha_{ssp}, f_{ssp}) \dots \\ & + A_{c.ssp}(t_{c.ssp}, h_{c.ssp}, \alpha_{ssp}, f_{ssp}) \end{aligned}$$

Total area per unit width:

$$A_{ssp}(h_{c.ssp}, t_{f.top}, t_{f.bot}, t_{c.ssp}, \alpha_{ssp}, f_{ssp}) := \frac{A_{tot.ssp}(h_{c.ssp}, t_{f.top}, t_{f.bot}, t_{c.ssp}, \alpha_{ssp}, f_{ssp})}{l_{ssp}(h_{c.ssp}, \alpha_{ssp}, f_{ssp})}$$

Neutral axis

$$z_{na.ssp}(h_{c.ssp}, t_{f.top}, t_{f.bot}, t_{c.ssp}, \alpha_{ssp}, f_{ssp}) := \frac{\left[\begin{array}{l} t_{c.ssp} \cdot f_{ssp} \cdot \left(t_{f.top} + \frac{t_{c.ssp}}{2}\right) \dots \\ + 2 \cdot t_{c.ssp} \cdot l_{c.ssp}(h_{c.ssp}, \alpha_{ssp}) \cdot \left(\frac{h_{c.ssp}}{2} + \frac{t_{f.top}}{2} + \frac{t_{c.ssp}}{2}\right) \dots \\ + t_{c.ssp} \cdot f_{ssp} \cdot \left(\frac{t_{f.top}}{2} + \frac{t_{c.ssp}}{2} + h_{c.ssp}\right) \dots \\ + A_{f.bot}(t_{f.bot}, h_{c.ssp}, \alpha_{ssp}, f_{ssp}) \cdot (h_{ssp}(h_{c.ssp}, t_{f.top}, t_{f.bot}, t_{c.ssp})) \end{array}\right]}{A_{tot.ssp}(h_{c.ssp}, t_{f.top}, t_{f.bot}, t_{c.ssp}, \alpha_{ssp}, f_{ssp})}$$

Moment of inertia

X-direction

Moment of inertia of the top flange:

$$I_{f.top.ssp.x}\left(h_{c.ssp}, t_{f.top}, t_{f.bot}, t_{c.ssp}, \alpha_{ssp}, f_{ssp}\right) := \frac{l_{ssp}\left(h_{c.ssp}, \alpha_{ssp}, f_{ssp}\right)\cdot t_{f.top}^{3}}{12} \ldots + l_{ssp}\left(h_{c.ssp}, \alpha_{ssp}, f_{ssp}\right)\cdot t_{f.top}\cdot\left(z_{na.ssp}\left(h_{c.ssp}, t_{f.top}, t_{f.bot}, t_{c.ssp}, \alpha_{ssp}, f_{ssp}\right)\right)^{2}$$

Moment of inertia of the top horisontal part of the core:

$$I_{c.top.ssp.x}\left(h_{c.ssp}, t_{f.top}, t_{f.bot}, t_{c.ssp}, \alpha_{ssp}, f_{ssp}\right) := \frac{f_{ssp}\cdot t_{c.ssp}^{3}}{12} \ldots + f_{ssp}\cdot t_{c.ssp}\cdot\left(\begin{array}{l} z_{na.ssp}\left(h_{c.ssp}, t_{f.top}, t_{f.bot}, t_{c.ssp}, \alpha_{ssp}, f_{ssp}\right) \ldots \\ +-\frac{t_{f.top}}{2} - \frac{t_{c.ssp}}{2} \end{array}\right)^{2}$$

Moment of inertia of the inclined part of the core:

$$I_{inc.ssp.x}\left(h_{c.ssp}, t_{f.top}, t_{f.bot}, t_{c.ssp}, \alpha_{ssp}, f_{ssp}\right) := 2\cdot\frac{t_{c.ssp}\cdot l_{c.ssp}\left(h_{c.ssp}, \alpha_{ssp}\right)^{3}}{12}\cdot\sin\left(\alpha_{ssp}\right)^{2} \ldots + 2t_{c.ssp}\cdot l_{c.ssp}\left(h_{c.ssp}, \alpha_{ssp}\right)\cdot\left(\begin{array}{l} \frac{t_{f.top}}{2} + \frac{t_{c.ssp}}{2} + \frac{h_{c.ssp}}{2} \ldots \\ +-z_{na.ssp}\left(h_{c.ssp}, t_{f.top}, t_{f.bot}, t_{c.ssp}, \alpha_{ssp}, f_{ssp}\right) \end{array}\right)^{2}$$

Moment of inertia of the bottom part of the core:

$$I_{c.bot.ssp.x}\left(h_{c.ssp}, t_{f.top}, t_{f.bot}, t_{c.ssp}, \alpha_{ssp}, f_{ssp}\right) := \frac{f_{ssp}\cdot t_{c.ssp}^{3}}{12} \ldots + f_{ssp}\cdot t_{c.ssp}\cdot\left(\begin{array}{l} \frac{t_{f.top}}{2} + \frac{t_{c.ssp}}{2} + h_{c.ssp} \ldots \\ +-z_{na.ssp}\left(h_{c.ssp}, t_{f.top}, t_{f.bot}, t_{c.ssp}, \alpha_{ssp}, f_{ssp}\right) \end{array}\right)^{2}$$

Moment of inertia of the bottom flange:

$$I_{f.bot.ssp.x}\left(h_{c.ssp}, t_{f.top}, t_{f.bot}, t_{c.ssp}, \alpha_{ssp}, f_{ssp}\right) := \frac{l_{ssp}\left(h_{c.ssp}, \alpha_{ssp}, f_{ssp}\right)\cdot t_{f.bot}^{3}}{12} \ldots + l_{ssp}\left(h_{c.ssp}, \alpha_{ssp}, f_{ssp}\right)\cdot t_{f.bot}\cdot\left(\begin{array}{l} h_{ssp}\left(h_{c.ssp}, t_{f.top}, t_{f.bot}, t_{c.ssp}\right) \ldots \\ +-z_{na.ssp}\left(h_{c.ssp}, t_{f.top}, t_{f.bot}, t_{c.ssp}, \alpha_{ssp}, f_{ssp}\right) \end{array}\right)^{2}$$

Total moment of inertia of SSP in x-direction:

$$I_{tot.ssp.x}\left(h_{c.ssp}, t_{f.top}, t_{f.bot}, t_{c.ssp}, \alpha_{ssp}, f_{ssp}\right) := I_{f.top.ssp.x}\left(h_{c.ssp}, t_{f.top}, t_{f.bot}, t_{c.ssp}, \alpha_{ssp}, f_{ssp}\right) \cdots + I_{c.top.ssp.x}\left(h_{c.ssp}, t_{f.top}, t_{f.bot}, t_{c.ssp}, \alpha_{ssp}, f_{ssp}\right) \cdots + I_{inc.ssp.x}\left(h_{c.ssp}, t_{f.top}, t_{f.bot}, t_{c.ssp}, \alpha_{ssp}, f_{ssp}\right) \cdots + I_{c.bot.ssp.x}\left(h_{c.ssp}, t_{f.top}, t_{f.bot}, t_{c.ssp}, \alpha_{ssp}, f_{ssp}\right) \cdots + I_{f.bot.ssp.x}\left(h_{c.ssp}, t_{f.top}, t_{f.bot}, t_{c.ssp}, \alpha_{ssp}, f_{ssp}\right)$$

Y-direction

Moment of inertia of the top flange:

$$I_{f.top.ssp.y}\left(h_{c.ssp}, t_{f.top}, t_{f.bot}, t_{c.ssp}, \alpha_{ssp}, f_{ssp}\right) := \frac{l_{ssp}\left(h_{c.ssp}, \alpha_{ssp}, f_{ssp}\right) \cdot t_{f.top}^{3}}{12} \cdots + l_{ssp}\left(h_{c.ssp}, \alpha_{ssp}, f_{ssp}\right) \cdot t_{f.top} \cdot \left(z_{na.ssp}\left(h_{c.ssp}, t_{f.top}, t_{f.bot}, t_{c.ssp}, \alpha_{ssp}, f_{ssp}\right)\right)^{2}$$

Moment of inertia of the bottom flange:

$$I_{f.bot.ssp.y}\left(h_{c.ssp}, t_{f.top}, t_{f.bot}, t_{c.ssp}, \alpha_{ssp}, f_{ssp}\right) := \frac{l_{ssp}\left(h_{c.ssp}, \alpha_{ssp}, f_{ssp}\right) \cdot t_{f.bot}^{3}}{12} \cdots + l_{ssp}\left(h_{c.ssp}, \alpha_{ssp}, f_{ssp}\right) \cdot t_{f.bot} \cdot \left(\begin{array}{l} h_{ssp}\left(h_{c.ssp}, t_{f.top}, t_{f.bot}, t_{c.ssp}\right) \cdots \\ + -z_{na.ssp}\left(h_{c.ssp}, t_{f.top}, t_{f.bot}, t_{c.ssp}, \alpha_{ssp}, f_{ssp}\right) \end{array}\right)^{2}$$

Total moment of inertia of SSP:

$$I_{tot.ssp.y}\left(h_{c.ssp}, t_{f.top}, t_{f.bot}, t_{c.ssp}, \alpha_{ssp}, f_{ssp}\right) := I_{f.top.ssp.y}\left(h_{c.ssp}, t_{f.top}, t_{f.bot}, t_{c.ssp}, \alpha_{ssp}, f_{ssp}\right) \cdots + I_{f.bot.ssp.y}\left(h_{c.ssp}, t_{f.top}, t_{f.bot}, t_{c.ssp}, \alpha_{ssp}, f_{ssp}\right)$$

Moment of inertia in x- and y-direction per unit width [m^4/m]

$$I_{ssp.x}\left(h_{c.ssp}, t_{f.top}, t_{f.bot}, t_{c.ssp}, \alpha_{ssp}, f_{ssp}\right) := \frac{I_{tot.ssp.x}\left(h_{c.ssp}, t_{f.top}, t_{f.bot}, t_{c.ssp}, \alpha_{ssp}, f_{ssp}\right)}{l_{ssp}\left(h_{c.ssp}, \alpha_{ssp}, f_{ssp}\right)}$$

$$I_{ssp.y}\left(h_{c.ssp}, t_{f.top}, t_{f.bot}, t_{c.ssp}, \alpha_{ssp}, f_{ssp}\right) := \frac{I_{tot.ssp.y}\left(h_{c.ssp}, t_{f.top}, t_{f.bot}, t_{c.ssp}, \alpha_{ssp}, f_{ssp}\right)}{l_{ssp}\left(h_{c.ssp}, \alpha_{ssp}, f_{ssp}\right)}$$

2.3. Elastic stiffness constants

The elastic stiffness constants are calculated in order to treat the SSP as an equivalent single layer. The elastic constants are calculated according to "*Elastic constants for corrugated-core*" by C.Libove & R.Hubka. All constants are calculated per unit width of the plate.

2.3.1. Axial Stiffness, Ex & Ey

Axial stiffness in the stiff direction per unit width:

$$E_{x.ssp}\left(h_{c.ssp}, t_{f.top}, t_{f.bot}, t_{c.ssp}, \alpha_{ssp}, f_{ssp}\right) := E \cdot A_{ssp}\left(h_{c.ssp}, t_{f.top}, t_{f.bot}, t_{c.ssp}, \alpha_{ssp}, f_{ssp}\right)$$

Axial stiffness in the weak direction per unit width:

$$E_{y.ssp}\left(h_{c.ssp}, t_{f.top}, t_{f.bot}, t_{c.ssp}, \alpha_{ssp}, f_{ssp}\right) := \frac{E \cdot \left(t_{f.top} + t_{f.bot}\right)}{1 - \nu^2 \left[1 - \frac{E \cdot \left(t_{f.top} + t_{f.bot}\right)}{E_{x.ssp}\left(h_{c.ssp}, t_{f.top}, t_{f.bot}, t_{c.ssp}, \alpha_{ssp}, f_{ssp}\right)}\right]}$$

2.3.2. Horizontal shear stiffness, Gxy

$$GA\left(h_{c.ssp}, t_{f.top}, t_{f.bot}, t_{c.ssp}, \alpha_{ssp}, f_{ssp}\right) := G_c \cdot t_{f.top} + \frac{G_c \cdot t_{c.ssp}^{\,2}}{A_{C.ssp}\left(t_{c.ssp}, h_{c.ssp}, \alpha_{ssp}, f_{ssp}\right)} + G_c \cdot t_{f.bot}$$

Horizontal shear stiffness per unit width:

$$G_{xy}\left(h_{c.ssp}, t_{f.top}, t_{f.bot}, t_{c.ssp}, \alpha_{ssp}, f_{ssp}\right) := GA\left(h_{c.ssp}, t_{f.top}, t_{f.bot}, t_{c.ssp}, \alpha_{ssp}, f_{ssp}\right)$$

2.3.3. Bending Stiffness, Dx & Dy

Bending stiffness in the stiff direction per unit width

$$D_{x.ssp}\left(h_{c.ssp}, t_{f.top}, t_{f.bot}, t_{c.ssp}, \alpha_{ssp}, f_{ssp}\right) := E \cdot I_{ssp.x}\left(h_{c.ssp}, t_{f.top}, t_{f.bot}, t_{c.ssp}, \alpha_{ssp}, f_{ssp}\right)$$

Bending stiffness in the weak direction per unit width

$$D_{y.ssp}\left(h_{c.ssp}, t_{f.top}, t_{f.bot}, t_{c.ssp}, \alpha_{ssp}, f_{ssp}\right) := \frac{E \cdot I_{ssp.y}\left(h_{c.ssp}, t_{f.top}, t_{f.bot}, t_{c.ssp}, \alpha_{ssp}, f_{ssp}\right)}{1 - \nu^2 \left(1 - \frac{E \cdot I_{ssp.y}\left(h_{c.ssp}, t_{f.top}, t_{f.bot}, t_{c.ssp}, \alpha_{ssp}, f_{ssp}\right)}{D_{x.ssp}\left(h_{c.ssp}, t_{f.top}, t_{f.bot}, t_{c.ssp}, \alpha_{ssp}, f_{ssp}\right)}\right)}$$

2.3.4. Torsional stiffness, Dxy

$$k_c = \frac{1}{2}\cdot\left(1 + \frac{A_1 - A_2}{2\cdot p\cdot h}\right)$$

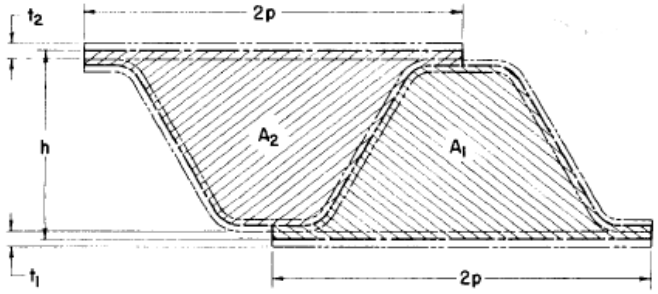

$$k_c\left(h_{c.ssp}, t_{f.top}, t_{f.bot}, t_{c.ssp}\right) := \frac{1}{2}\left(1 + \frac{t_{f.bot} - t_{f.top}}{2\cdot h_{ssp}\left(h_{c.ssp}, t_{f.top}, t_{f.bot}, t_{c.ssp}\right)}\right)$$

$$k_{GJ}\left(h_{c.ssp}, t_{f.top}, t_{f.bot}, t_{c.ssp}, \alpha_{ssp}, f_{ssp}\right) := \frac{\frac{G_c\cdot t_{c.ssp}^{\,2}\cdot k_c\left(h_{c.ssp}, t_{f.top}, t_{f.bot}, t_{c.ssp}\right)}{A_{C.ssp}\left(t_{c.ssp}, h_{c.ssp}, \alpha_{ssp}, f_{ssp}\right)} + G_c\cdot t_{f.bot}}{GA\left(h_{c.ssp}, t_{f.top}, t_{f.bot}, t_{c.ssp}, \alpha_{ssp}, f_{ssp}\right)}$$

$$GJ\left(h_{c.ssp}, t_{f.top}, t_{f.bot}, t_{c.ssp}, \alpha_{ssp}, f_{ssp}\right) :=$$

$$\left[\begin{array}{l} G_c\cdot t_{f.top}\cdot k_{GJ}\left(h_{c.ssp}, t_{f.top}, t_{f.bot}, t_{c.ssp}, \alpha_{ssp}, f_{ssp}\right)^2 \cdots \\ + \frac{G_c\cdot t_{c.ssp}^{\,2}}{A_{C.ssp}\left(t_{c.ssp}, h_{c.ssp}, \alpha_{ssp}, f_{ssp}\right)}\cdot\left(\begin{array}{l} k_{GJ}\left(h_{c.ssp}, t_{f.top}, t_{f.bot}, t_{c.ssp}, \alpha_{ssp}, f_{ssp}\right) \cdots \\ + -k_c\left(h_{c.ssp}, t_{f.top}, t_{f.bot}, t_{c.ssp}\right) \end{array}\right)^2 \cdots \\ + G_c\cdot t_{f.bot}\cdot\left(1 - k_{GJ}\left(h_{c.ssp}, t_{f.top}, t_{f.bot}, t_{c.ssp}, \alpha_{ssp}, f_{ssp}\right)\right)^2 \end{array}\right]\cdot h_{ssp}\left(h_{c.ssp}, t_{f.top}, t_{f.bot}, t_{c.ssp}\right)^2$$

Torsional stiffness per unit width:

$$D_{xy.ssp}\left(h_{c.ssp}, t_{f.top}, t_{f.bot}, t_{c.ssp}, \alpha_{ssp}, f_{ssp}\right) := 2\cdot GJ\left(h_{c.ssp}, t_{f.top}, t_{f.bot}, t_{c.ssp}, \alpha_{ssp}, f_{ssp}\right)$$

2.3.5. Dimensions needed for DQx and DQy

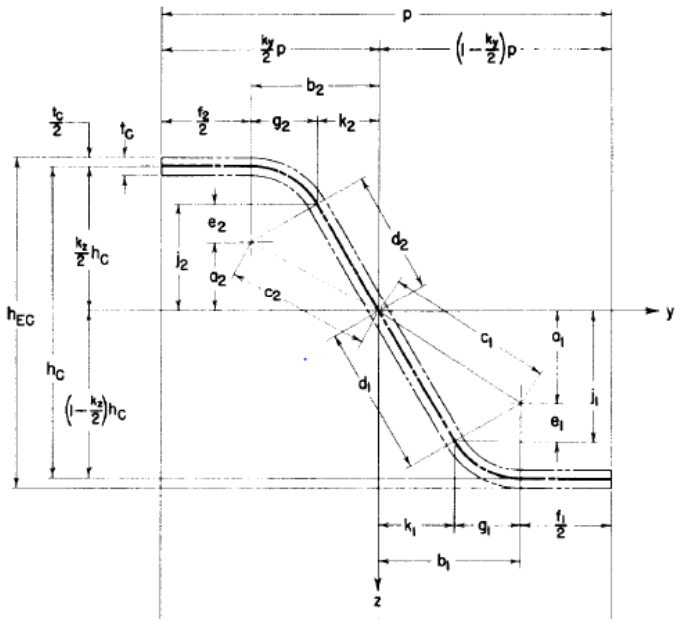

Symmetrical corrugation k.y=k.z --> K.Ay and K.Az vanish

$k_y := 1$ $k_z := 1$ $K_{Ay} := 0$ $K_{Az} := 0$

$R_{C1} := 0mm$ No radius on the corrugation

$$a_1\left(h_{c.ssp}, R_{C1}\right) := \left(1 - \frac{k_z}{2}\right) \cdot h_{c.ssp} - R_{C1}$$

$$b_1\left(h_{c.ssp}, \alpha_{ssp}, f_{ssp}\right) := \left(1 - \frac{k_y}{2}\right) \cdot p_{ssp}\left(h_{c.ssp}, \alpha_{ssp}, f_{ssp}\right) - \frac{f_{ssp}}{2}$$

$$c_1\left(h_{c.ssp}, \alpha_{ssp}, f_{ssp}, R_{C1}\right) := \left(a_1\left(h_{c.ssp}, R_{C1}\right)^2 + b_1\left(h_{c.ssp}, \alpha_{ssp}, f_{ssp}\right)^2\right)^{\frac{1}{2}}$$

$$\alpha_1\left(h_{c.ssp}, \alpha_{ssp}, f_{ssp}, R_{C1}\right) := \operatorname{atan}\left(\frac{a_1\left(h_{c.ssp}, R_{C1}\right)}{b_1\left(h_{c.ssp}, \alpha_{ssp}, f_{ssp}\right)}\right)$$

$$\beta_1\left(h_{c.ssp}, \alpha_{ssp}, f_{ssp}, R_{C1}\right) := \operatorname{asin}\left(\frac{R_{C1}}{c_1\left(h_{c.ssp}, \alpha_{ssp}, f_{ssp}, R_{C1}\right)}\right)$$

$$d_1\left(h_{c.ssp},\alpha_{ssp},f_{ssp},R_{C1}\right) := \left(c_1\left(h_{c.ssp},\alpha_{ssp},f_{ssp},R_{C1}\right)^2 - {R_{C1}}^2\right)^{\frac{1}{2}}$$

$$\theta\left(h_{c.ssp},\alpha_{ssp},f_{ssp},R_{C1}\right) := \alpha_1\left(h_{c.ssp},\alpha_{ssp},f_{ssp},R_{C1}\right) + \beta_1\left(h_{c.ssp},\alpha_{ssp},f_{ssp},R_{C1}\right)$$

$$e_1\left(h_{c.ssp},\alpha_{ssp},f_{ssp},R_{C1}\right) := R_{C1}\cdot\cos\left(\theta\left(h_{c.ssp},\alpha_{ssp},f_{ssp},R_{C1}\right)\right)$$

$$g_1\left(h_{c.ssp},\alpha_{ssp},f_{ssp},R_{C1}\right) := R_{C1}\cdot\sin\left(\theta\left(h_{c.ssp},\alpha_{ssp},f_{ssp},R_{C1}\right)\right)$$

$$j_1\left(h_{c.ssp},\alpha_{ssp},f_{ssp},R_{C1}\right) := a_1\left(h_{c.ssp},R_{C1}\right) + e_1\left(h_{c.ssp},\alpha_{ssp},f_{ssp},R_{C1}\right)$$

$$k_1\left(h_{c.ssp},\alpha_{ssp},f_{ssp},R_{C1}\right) := b_1\left(h_{c.ssp},\alpha_{ssp},f_{ssp}\right) - g_1\left(h_{c.ssp},\alpha_{ssp},f_{ssp},R_{C1}\right)$$

Height of radius (z-direction)

$$l_1\left(h_{c.ssp},\alpha_{ssp},f_{ssp},R_{C1}\right) := \frac{h_{c.ssp}}{2} - j_1\left(h_{c.ssp},\alpha_{ssp},f_{ssp},R_{C1}\right)$$

Length of one corrugation leg

$$l_s\left(h_{c.ssp},\alpha_{ssp},f_{ssp},R_{C1}\right) := f_{ssp} + 2.R_{C1}\cdot\theta\left(h_{c.ssp},\alpha_{ssp},f_{ssp},R_{C1}\right) + 2\cdot d_1\left(h_{c.ssp},\alpha_{ssp},f_{ssp},R_{C1}\right)$$

2.3.6. Transverse shear stiffness parallel to the corrugation, DQx

Area, per unit width, of the corrugation cross-section, [m^2/m]

$$A_{c.ssp.x}\left(h_{c.ssp},t_{c.ssp},\alpha_{ssp},f_{ssp},R_{C1}\right) := \frac{l_s\left(h_{c.ssp},\alpha_{ssp},f_{ssp},R_{C1}\right)\cdot t_{c.ssp}}{p_{ssp}\left(h_{c.ssp},\alpha_{ssp},f_{ssp}\right)}$$

Transverse shear stiffness parallel to the corrugation per unit width

$$D_{Qx}\left(h_{c.ssp},t_{f.top},t_{f.bot},t_{c.ssp},\alpha_{ssp},f_{ssp}\right) := \frac{G_c\cdot {t_{c.ssp}}^2}{A_{c.ssp.x}\left(h_{c.ssp},t_{c.ssp},\alpha_{ssp},f_{ssp},R_{C1}\right)}\cdot\left(\frac{h_{ssp}\left(h_{c.ssp},t_{f.top},t_{f.bot},t_{c.ssp}\right)}{p_{ssp}\left(h_{c.ssp},\alpha_{ssp},f_{ssp}\right)}\right)^2$$

2.3.7. Transverse shear stiffness perpendicular to the corrugation, DQy

The tranverse shear stiffness perpendicular to the corrugation per unit width is calculated as

$$D_{Qy} = S \cdot h_{ssp} \left(\frac{E}{1 - \nu_c^{\,2}} \right) \left(\frac{t_c}{h_c} \right)^3$$

where S is a non-dimensional cofieceint.

Nondimensional coefficient S

The non-dimensional coefficient S is calculated for symmetrical corrugation of the SSP but allows for different thicknesses of the top and bottom plate.

K values

The K values are non-dimensional functions of the corrugation shape

$$\begin{aligned} K_{Iz}(h_{c.ssp}, \alpha_{ssp}, f_{ssp}, R_{C1}) := {} & \frac{2}{3} \cdot \left(\frac{k_1(h_{c.ssp}, \alpha_{ssp}, f_{ssp}, R_{C1})}{h_{c.ssp}} \right)^2 \cdot \frac{d_1(h_{c.ssp}, \alpha_{ssp}, f_{ssp}, R_{C1})}{h_{c.ssp}} \dots \\ & + \frac{2}{3} \cdot \left[\frac{1}{8} \cdot \left(\frac{p_{ssp}(h_{c.ssp}, \alpha_{ssp}, f_{ssp})}{h_{c.ssp}} \right)^3 - \left(\frac{b_1(h_{c.ssp}, \alpha_{ssp}, f_{ssp})}{h_{c.ssp}} \right)^3 \right] \dots \\ & + 2 \cdot \frac{R_{C1}}{h_{c.ssp}} \cdot \left[\frac{b_1(h_{c.ssp}, \alpha_{ssp}, f_{ssp})}{h_{c.ssp}} \cdot \left[\theta(h_{c.ssp}, \alpha_{ssp}, f_{ssp}, R_{C1}) \cdot \frac{b_1(h_{c.ssp}, \alpha_{ssp}, f_{ssp})}{h_{c.ssp}} \dots \right] \dots \right. \\ & \left. + \frac{1}{2} \cdot \left[\theta(h_{c.ssp}, \alpha_{ssp}, f_{ssp}, R_{C1}) \cdot \left(\frac{R_{C1}}{h_{c.ssp}} \right)^2 \dots \right] \right] \end{aligned}$$

$$K_{Iyz}\left(h_{c.ssp},\alpha_{ssp},f_{ssp},R_{C1}\right) := \frac{2}{3}\cdot\frac{j_1\left(h_{c.ssp},\alpha_{ssp},f_{ssp},R_{C1}\right)}{h_{c.ssp}}\cdot\frac{k_1\left(h_{c.ssp},\alpha_{ssp},f_{ssp},R_{C1}\right)}{h_{c.ssp}}\cdot\frac{d_1\left(h_{c.ssp},\alpha_{ssp},f_{ssp},R_{C1}\right)}{h_{c.ssp}} \dots$$
$$+\frac{1}{2}\cdot\left[\frac{1}{4}\cdot\left(\frac{p_{ssp}\left(h_{c.ssp},\alpha_{ssp},f_{ssp}\right)}{h_{c.ssp}}\right)^2-\left(\frac{b_1\left(h_{c.ssp},\alpha_{ssp},f_{ssp}\right)}{h_{c.ssp}}\right)^2\right] \dots$$
$$+2\cdot\frac{R_{C1}}{h_{c.ssp}}\cdot\left[\frac{a_1\left(h_{c.ssp},R_{C1}\right)}{h_{c.ssp}}\cdot\left(\begin{array}{l}\theta\left(h_{c.ssp},\alpha_{ssp},f_{ssp},R_{C1}\right)\cdot\dfrac{b_1\left(h_{c.ssp},\alpha_{ssp},f_{ssp}\right)}{h_{c.ssp}} \dots\\ +\dfrac{e_1\left(h_{c.ssp},\alpha_{ssp},f_{ssp},R_{C1}\right)}{h_{c.ssp}}-\dfrac{R_{C1}}{h_{c.ssp}}\end{array}\right) \dots\right.$$
$$\left.+\frac{g_1\left(h_{c.ssp},\alpha_{ssp},f_{ssp},R_{C1}\right)}{h_{c.ssp}}\cdot\left(\begin{array}{l}\dfrac{b_1\left(h_{c.ssp},\alpha_{ssp},f_{ssp}\right)}{h_{c.ssp}} \dots\\ +-\dfrac{1}{2}\cdot\dfrac{g_1\left(h_{c.ssp},\alpha_{ssp},f_{ssp},R_{C1}\right)}{h_{c.ssp}}\end{array}\right)\right]$$

$$K_{Iy}\left(h_{c.ssp},\alpha_{ssp},f_{ssp},R_{C1}\right) := \frac{2}{3}\cdot\left(\frac{j_1\left(h_{c.ssp},\alpha_{ssp},f_{ssp},R_{C1}\right)}{h_{c.ssp}}\right)^2\cdot\frac{d_1\left(h_{c.ssp},\alpha_{ssp},f_{ssp},R_{C1}\right)}{h_{c.ssp}}+\frac{1}{4}\cdot\frac{f_{ssp}}{h_{c.ssp}} \dots$$
$$+2\cdot\frac{R_{C1}}{h_{c.ssp}}\cdot\left[\frac{a_1\left(h_{c.ssp},R_{C1}\right)}{h_{c.ssp}}\cdot\left(\begin{array}{l}\theta\left(h_{c.ssp},\alpha_{ssp},f_{ssp},R_{C1}\right)\cdot\dfrac{a_1\left(h_{c.ssp},R_{C1}\right)}{h_{c.ssp}} \dots\\ +2\cdot\dfrac{g_1\left(h_{c.ssp},\alpha_{ssp},f_{ssp},R_{C1}\right)}{h_{c.ssp}}\end{array}\right) \dots\right.$$
$$\left.+\frac{1}{2}\cdot\left[\theta\left(h_{c.ssp},\alpha_{ssp},f_{ssp},R_{C1}\right)\cdot\left(\frac{R_{C1}}{h_{c.ssp}}\right)^2 \dots+\frac{g_1\left(h_{c.ssp},\alpha_{ssp},f_{ssp},R_{C1}\right)}{h_{c.ssp}}\cdot\frac{e_1\left(h_{c.ssp},\alpha_{ssp},f_{ssp},R_{C1}\right)}{h_{c.ssp}}\right]\right]$$

$$K_L\left(h_{c.ssp},\alpha_{ssp},f_{ssp},R_{C1}\right) := 2\cdot\frac{d_1\left(h_{c.ssp},\alpha_{ssp},f_{ssp},R_{C1}\right)}{h_{c.ssp}}+2\cdot\theta\left(h_{c.ssp},\alpha_{ssp},f_{ssp},R_{C1}\right)\cdot\frac{R_{C1}}{h_{c.ssp}}+\frac{f_{ssp}}{h_{c.ssp}}$$

$$K_{Ly}\left(h_{c.ssp},\alpha_{ssp},f_{ssp},R_{C1}\right) := \frac{f_{ssp}}{h_{c.ssp}}+2\cdot\frac{d_1\left(h_{c.ssp},\alpha_{ssp},f_{ssp},R_{C1}\right)}{h_{c.ssp}}\cdot\cos\left(\theta\left(h_{c.ssp},\alpha_{ssp},f_{ssp},R_{C1}\right)\right)^2 \dots$$
$$+\frac{R_{C1}}{h_{c.ssp}}\cdot\left(\begin{array}{l}\theta\left(h_{c.ssp},\alpha_{ssp},f_{ssp},R_{C1}\right) \dots\\ +\sin\left(\theta\left(h_{c.ssp},\alpha_{ssp},f_{ssp},R_{C1}\right)\right)\cdot\cos\left(\theta\left(h_{c.ssp},\alpha_{ssp},f_{ssp},R_{C1}\right)\right)\end{array}\right)$$

$$K_{Lyz}\left(h_{c.ssp},\alpha_{ssp},f_{ssp},R_{C1}\right) := 2\cdot\frac{d_1\left(h_{c.ssp},\alpha_{ssp},f_{ssp},R_{C1}\right)}{h_{c.ssp}}\cdot\sin\left(\theta\left(h_{c.ssp},\alpha_{ssp},f_{ssp},R_{C1}\right)\right)\cdot\cos\left(\theta\left(h_{c.ssp},\alpha_{ssp},f_{ssp},R_{C1}\right)\right) \dots$$
$$+\frac{R_{C1}}{h_{c.ssp}}\cdot\sin\left(\theta\left(h_{c.ssp},\alpha_{ssp},f_{ssp},R_{C1}\right)\right)^2$$

$$K_{Lz}\left(h_{c.ssp},\alpha_{ssp},f_{ssp},R_{C1}\right) := 2\cdot\frac{d_1\left(h_{c.ssp},\alpha_{ssp},f_{ssp},R_{C1}\right)}{h_{c.ssp}}\cdot\sin\left(\theta\left(h_{c.ssp},\alpha_{ssp},f_{ssp},R_{C1}\right)\right)^2 \ldots$$
$$+\frac{R_{C1}}{h_{c.ssp}}\cdot\left(\begin{array}{l}\theta\left(h_{c.ssp},\alpha_{ssp},f_{ssp},R_{C1}\right) \ldots\\ +-\sin\left(\theta\left(h_{c.ssp},\alpha_{ssp},f_{ssp},R_{C1}\right)\right)\cdot\cos\left(\theta\left(h_{c.ssp},\alpha_{ssp},f_{ssp},R_{C1}\right)\right)\end{array}\right)$$

C values

$$C_1\left(h_{c.ssp},t_{f.top},t_{c.ssp},\alpha_{ssp},f_{ssp},R_{C1}\right) := K_L\left(h_{c.ssp},\alpha_{ssp},f_{ssp},R_{C1}\right) + \frac{1}{3}\cdot\left(\frac{t_{c.ssp}}{t_{f.top}}\right)^3\cdot\frac{p_{ssp}\left(h_{c.ssp},\alpha_{ssp},f_{ssp}\right)}{h_{c.ssp}}$$

$$C_2\left(h_{c.ssp},\alpha_{ssp},f_{ssp},R_{C1}\right) := \frac{k_y}{2}\cdot\frac{p_{ssp}\left(h_{c.ssp},\alpha_{ssp},f_{ssp}\right)}{h_{c.ssp}}\cdot K_L\left(h_{c.ssp},\alpha_{ssp},f_{ssp},R_{C1}\right)$$

$$C_3\left(h_{c.ssp},t_{c.ssp},\alpha_{ssp},f_{ssp},R_{C1}\right) := K_{Iz}\left(h_{c.ssp},\alpha_{ssp},f_{ssp},R_{C1}\right) \ldots$$
$$+k_y\cdot\frac{p_{ssp}\left(h_{c.ssp},\alpha_{ssp},f_{ssp}\right)}{h_{c.ssp}}\cdot\left(\frac{k_y}{4}\cdot\frac{p_{ssp}\left(h_{c.ssp},\alpha_{ssp},f_{ssp}\right)}{h_{c.ssp}}\cdot K_L\left(h_{c.ssp},\alpha_{ssp},f_{ssp},R_{C1}\right)\right) \ldots$$
$$+\frac{1}{12}\cdot\left(\frac{t_{c.ssp}}{h_{c.ssp}}\right)^2\cdot K_{Lz}\left(h_{c.ssp},\alpha_{ssp},f_{ssp},R_{C1}\right)$$

$$C_4\left(h_{c.ssp},t_{f.top},t_{c.ssp},\alpha_{ssp},f_{ssp},R_{C1}\right) := K_{Iyz}\left(h_{c.ssp},\alpha_{ssp},f_{ssp},R_{C1}\right) \ldots$$
$$+\frac{1}{2}\cdot\left[k_z+\left(1+\frac{t_{f.top}}{t_{c.ssp}}\right)\cdot\frac{t_{c.ssp}}{h_{c.ssp}}\right]\cdot\left(\frac{k_y}{2}\cdot\frac{p_{ssp}\left(h_{c.ssp},\alpha_{ssp},f_{ssp}\right)}{h_{c.ssp}}\cdot K_L\left(h_{c.ssp},\alpha_{ssp},f_{ssp},R_{C1}\right)\right) \ldots$$
$$+-\frac{1}{12}\cdot\left(\frac{t_{c.ssp}}{h_{c.ssp}}\right)^2\cdot K_{Lyz}\left(h_{c.ssp},\alpha_{ssp},f_{ssp},R_{C1}\right)$$

$$C_5\left(h_{c.ssp},t_{f.top},t_{c.ssp},\alpha_{ssp},f_{ssp},R_{C1}\right) := \frac{1}{2}\cdot\left[k_z+\left(1+\frac{t_{f.top}}{t_{c.ssp}}\right)\cdot\frac{t_{c.ssp}}{h_{c.ssp}}\right]\cdot K_L\left(h_{c.ssp},\alpha_{ssp},f_{ssp},R_{C1}\right)$$

$$C_6\left(h_{c.ssp},t_{f.top},t_{c.ssp},\alpha_{ssp},f_{ssp},R_{C1}\right) := K_{Iy}\left(h_{c.ssp},\alpha_{ssp},f_{ssp},R_{C1}\right) \ldots$$
$$+\left[k_z+\left(1+\frac{t_{f.top}}{t_{c.ssp}}\right)\cdot\frac{t_{c.ssp}}{h_{c.ssp}}\right]\cdot\left[\frac{1}{4}\cdot\left[k_z+\left(1+\frac{t_{f.top}}{t_{c.ssp}}\right)\cdot\frac{t_{c.ssp}}{h_{c.ssp}}\right]\cdot K_L\left(h_{c.ssp},\alpha_{ssp},f_{ssp},R_{C1}\right)\right] \ldots$$
$$+\frac{1}{12}\cdot\left(\frac{t_{c.ssp}}{h_{c.ssp}}\right)^2\cdot K_{Ly}\left(h_{c.ssp},\alpha_{ssp},f_{ssp},R_{C1}\right)$$

$$C_7\left(t_{f.bot},t_{c.ssp}\right) := \left(\frac{t_{f.bot}}{t_{c.ssp}}\right)^3$$

Non-dimensional cofficient S

$$S\left(h_{c.ssp}, t_{f.top}, t_{f.bot}, t_{c.ssp}, \alpha_{ssp}, f_{ssp}, R_{C1}\right) :=$$

$$\frac{\begin{aligned}&3\cdot\frac{h_{c.ssp}}{p_{ssp}\left(h_{c.ssp},\alpha_{ssp},f_{ssp}\right)}\cdot C_7\left(t_{f.bot},t_{c.ssp}\right)\cdot\left(C_2\left(h_{c.ssp},\alpha_{ssp},f_{ssp},R_{C1}\right)^2-C_1\left(h_{c.ssp},t_{f.top},t_{c.ssp},\alpha_{ssp},f_{ssp},R_{C1}\right)\cdot C_3\left(h_{c.ssp},t_{c.ssp},\alpha_{ssp},f_{ssp},R_{C1}\right)\right)\cdots\\&+-C_3\left(h_{c.ssp},t_{c.ssp},\alpha_{ssp},f_{ssp},R_{C1}\right)+\frac{p_{ssp}\left(h_{c.ssp},\alpha_{ssp},f_{ssp}\right)}{h_{c.ssp}}\cdot\left(2\cdot C_2\left(h_{c.ssp},\alpha_{ssp},f_{ssp},R_{C1}\right)-\frac{p_{ssp}\left(h_{c.ssp},\alpha_{ssp},f_{ssp}\right)}{h_{c.ssp}}\cdot C_1\left(h_{c.ssp},t_{f.top},t_{c.ssp},\alpha_{ssp},f_{ssp},R_{C1}\right)\right)\end{aligned}}{12\cdot\left[\begin{aligned}&2\cdot\frac{p_{ssp}\left(h_{c.ssp},\alpha_{ssp},f_{ssp}\right)}{h_{c.ssp}}\cdot\left[\frac{p_{ssp}\left(h_{c.ssp},\alpha_{ssp},f_{ssp}\right)}{h_{c.ssp}}\cdot\begin{pmatrix}C_1\left(h_{c.ssp},t_{f.top},t_{c.ssp},\alpha_{ssp},f_{ssp},R_{C1}\right)\cdot C_4\left(h_{c.ssp},t_{f.top},t_{c.ssp},\alpha_{ssp},f_{ssp},R_{C1}\right)\cdots\\+-C_2\left(h_{c.ssp},\alpha_{ssp},f_{ssp},R_{C1}\right)\cdot C_5\left(h_{c.ssp},t_{f.top},t_{c.ssp},\alpha_{ssp},f_{ssp},R_{C1}\right)\end{pmatrix}\cdots\right]\cdots\\&+\frac{h_{c.ssp}}{h_{ssp}\left(h_{c.ssp},t_{f.top},t_{f.bot},t_{c.ssp}\right)}\cdot\left[\begin{aligned}&3\cdot C_7\left(t_{f.bot},t_{c.ssp}\right)\cdot\left[\begin{aligned}&C_4\left(h_{c.ssp},t_{f.top},t_{c.ssp},\alpha_{ssp},f_{ssp},R_{C1}\right)\cdot\left(\begin{aligned}&C_1\left(h_{c.ssp},t_{f.top},t_{c.ssp},\alpha_{ssp},f_{ssp},R_{C1}\right)\cdot C_4\left(h_{c.ssp},t_{f.top},t_{c.ssp},\alpha_{ssp},f_{ssp},R_{C1}\right)\cdots\\&+-2\cdot C_2\left(h_{c.ssp},\alpha_{ssp},f_{ssp},R_{C1}\right)\cdot C_5\left(h_{c.ssp},t_{f.top},t_{c.ssp},\alpha_{ssp},f_{ssp},R_{C1}\right)\end{aligned}\right)\cdots\\&+C_3\left(h_{c.ssp},t_{c.ssp},\alpha_{ssp},f_{ssp},R_{C1}\right)\cdot C_5\left(h_{c.ssp},t_{f.top},t_{c.ssp},\alpha_{ssp},f_{ssp},R_{C1}\right)^2\cdots\\&+-C_6\left(h_{c.ssp},t_{f.top},t_{c.ssp},\alpha_{ssp},f_{ssp},R_{C1}\right)\cdot\begin{pmatrix}C_1\left(h_{c.ssp},t_{f.top},t_{c.ssp},\alpha_{ssp},f_{ssp},R_{C1}\right)\cdot C_3\left(h_{c.ssp},t_{c.ssp},\alpha_{ssp},f_{ssp},R_{C1}\right)\cdots\\+-C_2\left(h_{c.ssp},\alpha_{ssp},f_{ssp},R_{C1}\right)^2\end{pmatrix}\end{aligned}\right]\cdots\\&+\frac{p_{ssp}\left(h_{c.ssp},\alpha_{ssp},f_{ssp}\right)}{h_{c.ssp}}\cdot\left(C_4\left(h_{c.ssp},t_{f.top},t_{c.ssp},\alpha_{ssp},f_{ssp},R_{C1}\right)^2-C_3\left(h_{c.ssp},t_{c.ssp},\alpha_{ssp},f_{ssp},R_{C1}\right)\cdot C_6\left(h_{c.ssp},t_{f.top},t_{c.ssp},\alpha_{ssp},f_{ssp},R_{C1}\right)\right)\cdots\\&+2\cdot\left(\frac{p_{ssp}\left(h_{c.ssp},\alpha_{ssp},f_{ssp}\right)}{h_{c.ssp}}\right)^2\cdot\begin{pmatrix}C_2\left(h_{c.ssp},\alpha_{ssp},f_{ssp},R_{C1}\right)\cdot C_6\left(h_{c.ssp},t_{f.top},t_{c.ssp},\alpha_{ssp},f_{ssp},R_{C1}\right)\cdots\\+-C_4\left(h_{c.ssp},t_{f.top},t_{c.ssp},\alpha_{ssp},f_{ssp},R_{C1}\right)\cdot C_3\left(h_{c.ssp},t_{f.top},t_{c.ssp},\alpha_{ssp},f_{ssp},R_{C1}\right)\end{pmatrix}\cdots\\&+\left(\frac{p_{ssp}\left(h_{c.ssp},\alpha_{ssp},f_{ssp}\right)}{h_{c.ssp}}\right)^3\cdot\begin{pmatrix}C_5\left(h_{c.ssp},t_{f.top},t_{c.ssp},\alpha_{ssp},f_{ssp},R_{C1}\right)^2\cdots\\+-C_1\left(h_{c.ssp},t_{f.top},t_{c.ssp},\alpha_{ssp},f_{ssp},R_{C1}\right)\cdot C_6\left(h_{c.ssp},t_{f.top},t_{c.ssp},\alpha_{ssp},f_{ssp},R_{C1}\right)\end{pmatrix}\end{aligned}\right]\\&+\frac{h_{ssp}\left(h_{c.ssp},t_{f.top},t_{f.bot},t_{c.ssp}\right)}{h_{c.ssp}}\cdot\frac{p_{ssp}\left(h_{c.ssp},\alpha_{ssp},f_{ssp}\right)}{h_{c.ssp}}\cdot\left(C_2\left(h_{c.ssp},\alpha_{ssp},f_{ssp},R_{C1}\right)^2-C_1\left(h_{c.ssp},t_{f.top},t_{c.ssp},\alpha_{ssp},f_{ssp},R_{C1}\right)\cdot C_3\left(h_{c.ssp},t_{c.ssp},\alpha_{ssp},f_{ssp},R_{C1}\right)\right)\end{aligned}\right]}$$

<u>Transverse shear stiffness perpendicular to the corrugation per unit width</u>

$$D_{Qy}\left(h_{c.ssp}, t_{f.top}, t_{f.bot}, t_{c.ssp}, \alpha_{ssp}, f_{ssp}\right) :=$$

$$S\left(h_{c.ssp}, t_{f.top}, t_{f.bot}, t_{c.ssp}, \alpha_{ssp}, f_{ssp}, R_{C1}\right)\cdot h_{ssp}\left(h_{c.ssp}, t_{f.top}, t_{f.bot}, t_{c.ssp}\right)\cdot\left(\frac{E}{1-\nu^2}\right)\left(\frac{t_{c.ssp}}{h_{c.ssp}}\right)^3$$

3. Local deflection and fatigue load

3.1. Local deflection

The local deflection of the top plate is calulated by treating the top plate as a fixed beam with the same width as the wheel load and the length of 2p. Only traffic load is considered in the deflection calculation

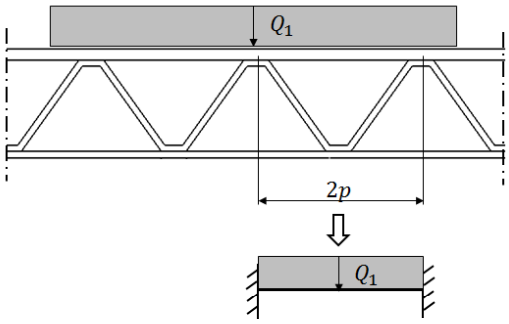

$$Q_{wheel} := \frac{Q_{1k} \cdot \alpha_{Q1}}{2a_c} = 300 \cdot \frac{kN}{m}$$ One wheel load

$$I_{top}(t_{f.top}) := \frac{a_c \cdot t_{f.top}^{3}}{12}$$ Moment of inertia of top flange strip

Local deflection:

$$\delta_I(h_{c.ssp}, t_{f.top}, \alpha_{ssp}, f_{ssp}) := \frac{Q_{wheel} \cdot I_{ssp}(h_{c.ssp}, \alpha_{ssp}, f_{ssp})^4}{384 \cdot E \cdot I_{top}(t_{f.top})}$$

3.2. Fatigue load

The fatigue load consists of self weight and traffic loads according to load model 3. The fatigue limit constraint used later in the optimisation is approximative since no detail category exists in Eurocode for laser welded sandwich panels.

Total weight of the section:

$$G_{ssp}(h_{c.ssp}, t_{f.top}, t_{f.bot}, t_{c.ssp}, \alpha_{ssp}, f_{ssp}) := A_{ssp}(h_{c.ssp}, t_{f.top}, t_{f.bot}, t_{c.ssp}, \alpha_{ssp}, f_{ssp}) \cdot \rho$$

Self-weight per unit width:

$$q_{self}(h_{c.ssp}, t_{f.top}, t_{f.bot}, t_{c.ssp}, \alpha_{ssp}, f_{ssp}) := G_{ssp}(h_{c.ssp}, t_{f.top}, t_{f.bot}, t_{c.ssp}, \alpha_{ssp}, f_{ssp}) \cdot g \cdot a_c$$

Total permanent load:

$$q(h_{c.ssp}, t_{f.top}, t_{f.bot}, t_{c.ssp}, \alpha_{ssp}, f_{ssp}) := q_{self}(h_{c.ssp}, t_{f.top}, t_{f.bot}, t_{c.ssp}, \alpha_{ssp}, f_{ssp}) + q_{cover}$$

Traffic LM3:

$$q_{w.LM3} := \frac{120kN}{2 \cdot a_c} = 120 \cdot \frac{kN}{m}$$

Total load for calculation of the fatigue stress:

$$q_{tot}(h_{c.ssp}, t_{f.top}, t_{f.bot}, t_{c.ssp}, \alpha_{ssp}, f_{ssp}) := q_{w.LM3} + q(h_{c.ssp}, t_{f.top}, t_{f.bot}, t_{c.ssp}, \alpha_{ssp}, f_{ssp})$$

4. Deflection of SSP

The deflection of the SSP between main and transveres girders is calculated with the analytical solution for deflection of a simply supported plate. The analytical solution was obtained from " *Elasto-plasto analysis of corrugated sandwich steel panels*" W.Chang.

Loads

Loads according to LM1

Characteristic load combination is used in the optimisation of the SSP

$q_{1d} := q_{1k} = 9 \cdot \frac{kN}{m^2}$ Distributed load

$Q_{1d} := \frac{Q_{1k}}{2} = 150 \cdot kN$ One wheel load

Uniformly distributed load

Load used in the optimisation:

$$q_{ijC}(i,j) := \frac{4 \cdot q_{1d}}{i \cdot j \, \pi^2} \cdot \left[1 - (-1)^i\right] \cdot \left[1 - (-1)^j\right]$$

Wheel loads

The wheel loads are placed symmetrically around the centre of the plate. The distance between axels is 1.2 m and the distance between wheels in one axel is 2.0 m

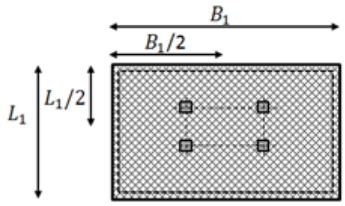

Wheel load 1

$x_1 := \frac{L_1}{2} + 0.6m = 4.6\,m \qquad y_1 := \frac{B_1}{2} - 1m = 2\,m$

$$Q_1(i,j) := \frac{4 \cdot Q_{1d}}{L_1 \cdot B_1} \cdot \sin\left(\frac{i \cdot \pi \cdot x_1}{L_1}\right) \cdot \sin\left(\frac{j \cdot \pi \cdot y_1}{B_1}\right)$$

Wheel load 2

$$x_2 := \frac{L_1}{2} + 0.6\text{m} = 4.6\,\text{m} \qquad y_2 := \frac{B_1}{2} + 1\text{m} = 4\,\text{m}$$

$$Q_2(i,j) := \frac{4 \cdot Q_{1d}}{L_1 \cdot B_1} \cdot \sin\left(\frac{i \cdot \pi \cdot x_2}{L_1}\right) \cdot \sin\left(\frac{j \cdot \pi \cdot y_2}{B_1}\right)$$

Wheel load 3

$$x_3 := \frac{L_1}{2} - 0.6\text{m} = 3.4\,\text{m} \qquad y_3 := \frac{B_1}{2} - 1\text{m} = 2\,\text{m}$$

$$Q_3(i,j) := \frac{4 \cdot Q_{1d}}{L_1 \cdot B_1} \cdot \sin\left(\frac{i \cdot \pi \cdot x_3}{L_1}\right) \cdot \sin\left(\frac{j \cdot \pi \cdot y_3}{B_1}\right)$$

Wheel load 4

$$x_4 := \frac{L_1}{2} - 0.6\text{m} = 3.4\,\text{m} \qquad y_4 := \frac{B_1}{2} + 1\text{m} = 4\,\text{m}$$

$$Q_4(i,j) := \frac{4 \cdot Q_{1d}}{L_1 \cdot B_1} \cdot \sin\left(\frac{i \cdot \pi \cdot x_4}{L_1}\right) \cdot \sin\left(\frac{j \cdot \pi \cdot y_4}{B_1}\right)$$

Deflection

Poisson's ratios

$$\nu_{xy} := \nu = 0.3$$

$$\nu_{yx}\left(h_{c.ssp}, t_{f.top}, t_{f.bot}, t_{c.ssp}, \alpha_{ssp}, f_{ssp}\right) := \nu_{xy} \cdot \frac{D_{y.ssp}\left(h_{c.ssp}, t_{f.top}, t_{f.bot}, t_{c.ssp}, \alpha_{ssp}, f_{ssp}\right)}{D_{x.ssp}\left(h_{c.ssp}, t_{f.top}, t_{f.bot}, t_{c.ssp}, \alpha_{ssp}, f_{ssp}\right)}$$

$$\nu_p\left(h_{c.ssp}, t_{f.top}, t_{f.bot}, t_{c.ssp}, \alpha_{ssp}, f_{ssp}\right) := 1 - \nu_{xy}^2 \cdot \frac{D_{y.ssp}\left(h_{c.ssp}, t_{f.top}, t_{f.bot}, t_{c.ssp}, \alpha_{ssp}, f_{ssp}\right)}{D_{x.ssp}\left(h_{c.ssp}, t_{f.top}, t_{f.bot}, t_{c.ssp}, \alpha_{ssp}, f_{ssp}\right)}$$

Coefficients used in deflection formula

$$D_{xx}\left(h_{c.ssp}, t_{f.top}, t_{f.bot}, t_{c.ssp}, \alpha_{ssp}, f_{ssp}\right) := \frac{D_{x.ssp}\left(h_{c.ssp}, t_{f.top}, t_{f.bot}, t_{c.ssp}, \alpha_{ssp}, f_{ssp}\right)}{1 - \nu_{xy} \cdot \nu_{yx}\left(h_{c.ssp}, t_{f.top}, t_{f.bot}, t_{c.ssp}, \alpha_{ssp}, f_{ssp}\right)}$$

$$D_{yy}\left(h_{c.ssp}, t_{f.top}, t_{f.bot}, t_{c.ssp}, \alpha_{ssp}, f_{ssp}\right) := \frac{D_{y.ssp}\left(h_{c.ssp}, t_{f.top}, t_{f.bot}, t_{c.ssp}, \alpha_{ssp}, f_{ssp}\right)}{1 - \nu_{xy} \cdot \nu_{yx}\left(h_{c.ssp}, t_{f.top}, t_{f.bot}, t_{c.ssp}, \alpha_{ssp}, f_{ssp}\right)}$$

$$w_{ij}\left(h_{c.ssp}, t_{f.top}, t_{f.bot}, t_{c.ssp}, \alpha_{ssp}, f_{ssp}, i, j\right) :=$$

$$\frac{L_1^{2} B_1^{2} \cdot \left(\begin{array}{l} 2 \cdot D_{Qx}(h_{c.ssp}, t_{f.top}, t_{f.bot}, t_{c.ssp}, \alpha_{ssp}, f_{ssp}) \cdot D_{Qy}(h_{c.ssp}, t_{f.top}, t_{f.bot}, t_{c.ssp}, \alpha_{ssp}, f_{ssp}) \cdot L_1^{4} \cdot B_1^{4} \ldots \\ + D_{xx}(h_{c.ssp}, t_{f.top}, t_{f.bot}, t_{c.ssp}, \alpha_{ssp}, f_{ssp}) \cdot D_{xy.ssp}(h_{c.ssp}, t_{f.top}, t_{f.bot}, t_{c.ssp}, \alpha_{ssp}, f_{ssp}) \cdot \pi^{4} \cdot B_1^{4} \cdot i^{4} \ldots \\ + D_{xy.ssp}(h_{c.ssp}, t_{f.top}, t_{f.bot}, t_{c.ssp}, \alpha_{ssp}, f_{ssp}) \cdot D_{yy}(h_{c.ssp}, t_{f.top}, t_{f.bot}, t_{c.ssp}, \alpha_{ssp}, f_{ssp}) \cdot \pi^{4} \cdot L_1^{4} \cdot j^{4} \ldots \\ + D_{Qx}(h_{c.ssp}, t_{f.top}, t_{f.bot}, t_{c.ssp}, \alpha_{ssp}, f_{ssp}) \cdot D_{xy.ssp}(h_{c.ssp}, t_{f.top}, t_{f.bot}, t_{c.ssp}, \alpha_{ssp}, f_{ssp}) \cdot \pi^{2} \cdot L_1^{2} \cdot B_1^{4} \cdot i^{2} \ldots \\ + 2 \cdot D_{Qy}(h_{c.ssp}, t_{f.top}, t_{f.bot}, t_{c.ssp}, \alpha_{ssp}, f_{ssp}) \cdot D_{xx}(h_{c.ssp}, t_{f.top}, t_{f.bot}, t_{c.ssp}, \alpha_{ssp}, f_{ssp}) \cdot \pi^{2} \cdot L_1^{2} \cdot B_1^{4} \cdot i^{2} \ldots \\ + D_{Qy}(h_{c.ssp}, t_{f.top}, t_{f.bot}, t_{c.ssp}, \alpha_{ssp}, f_{ssp}) \cdot D_{xy.ssp}(h_{c.ssp}, t_{f.top}, t_{f.bot}, t_{c.ssp}, \alpha_{ssp}, f_{ssp}) \cdot \pi^{2} \cdot L_1^{4} \cdot B_1^{2} \cdot j^{2} \ldots \\ + 2 \cdot D_{Qx}(h_{c.ssp}, t_{f.top}, t_{f.bot}, t_{c.ssp}, \alpha_{ssp}, f_{ssp}) \cdot D_{yy}(h_{c.ssp}, t_{f.top}, t_{f.bot}, t_{c.ssp}, \alpha_{ssp}, f_{ssp}) \cdot \pi^{4} \cdot L_1^{4} \cdot B_1^{2} \cdot j^{2} \ldots \\ + 2 \cdot D_{xx}(h_{c.ssp}, t_{f.top}, t_{f.bot}, t_{c.ssp}, \alpha_{ssp}, f_{ssp}) \cdot D_{yy}(h_{c.ssp}, t_{f.top}, t_{f.bot}, t_{c.ssp}, \alpha_{ssp}, f_{ssp}) \cdot \pi^{4} \cdot L_1^{2} \cdot B_1^{2} \cdot i^{2} \cdot j^{2} \ldots \\ + -D_{xx}(h_{c.ssp}, t_{f.top}, t_{f.bot}, t_{c.ssp}, \alpha_{ssp}, f_{ssp}) \cdot D_{xy.ssp}(h_{c.ssp}, t_{f.top}, t_{f.bot}, t_{c.ssp}, \alpha_{ssp}, f_{ssp}) \cdot \pi^{4} \cdot L_1^{2} \cdot B_1^{2} \cdot i^{2} \cdot j^{2} \cdot \nu_{yx}(h_{c.ssp}, t_{f.top}, t_{f.bot}, t_{c.ssp}, \alpha_{ssp}, f_{ssp}) \ldots \\ + -D_{xy.ssp}(h_{c.ssp}, t_{f.top}, t_{f.bot}, t_{c.ssp}, \alpha_{ssp}, f_{ssp}) \cdot D_{yy}(h_{c.ssp}, t_{f.top}, t_{f.bot}, t_{c.ssp}, \alpha_{ssp}, f_{ssp}) \cdot \pi^{4} \cdot L_1^{2} \cdot B_1^{2} \cdot i^{2} \cdot j^{2} \cdot \nu_{xy} \ldots \\ + -2 \cdot D_{xx}(h_{c.ssp}, t_{f.top}, t_{f.bot}, t_{c.ssp}, \alpha_{ssp}, f_{ssp}) \cdot D_{yy}(h_{c.ssp}, t_{f.top}, t_{f.bot}, t_{c.ssp}, \alpha_{ssp}, f_{ssp}) \cdot \pi^{4} \cdot L_1^{2} \cdot B_1^{2} \cdot i^{2} \cdot j^{2} \cdot \nu_{xy} \cdot \nu_{yx}(h_{c.ssp}, t_{f.top}, t_{f.bot}, t_{c.ssp}, \alpha_{ssp}, f_{ssp}) \end{array} \right)}{\pi^{2} \cdot \left(\begin{array}{l} D_{Qx}(h_{c.ssp}, t_{f.top}, t_{f.bot}, t_{c.ssp}, \alpha_{ssp}, f_{ssp}) \cdot D_{xx}(h_{c.ssp}, t_{f.top}, t_{f.bot}, t_{c.ssp}, \alpha_{ssp}, f_{ssp}) \cdot D_{xy.ssp}(h_{c.ssp}, t_{f.top}, t_{f.bot}, t_{c.ssp}, \alpha_{ssp}, f_{ssp}) \cdot \pi^{4} \cdot B_1^{6} \cdot i^{6} \ldots \\ + D_{Qy}(h_{c.ssp}, t_{f.top}, t_{f.bot}, t_{c.ssp}, \alpha_{ssp}, f_{ssp}) \cdot D_{xy.ssp}(h_{c.ssp}, t_{f.top}, t_{f.bot}, t_{c.ssp}, \alpha_{ssp}, f_{ssp}) \cdot D_{yy}(h_{c.ssp}, t_{f.top}, t_{f.bot}, t_{c.ssp}, \alpha_{ssp}, f_{ssp}) \cdot \pi^{4} \cdot L_1^{6} \cdot j^{6} \ldots \\ + 2 \cdot D_{Qx}(h_{c.ssp}, t_{f.top}, t_{f.bot}, t_{c.ssp}, \alpha_{ssp}, f_{ssp}) \cdot D_{Qy}(h_{c.ssp}, t_{f.top}, t_{f.bot}, t_{c.ssp}, \alpha_{ssp}, f_{ssp}) \cdot D_{xx}(h_{c.ssp}, t_{f.top}, t_{f.bot}, t_{c.ssp}, \alpha_{ssp}, f_{ssp}) \cdot \pi^{2} \cdot L_1^{2} \cdot B_1^{6} \cdot i^{4} \ldots \\ + 2 \cdot D_{Qx}(h_{c.ssp}, t_{f.top}, t_{f.bot}, t_{c.ssp}, \alpha_{ssp}, f_{ssp}) \cdot D_{Qy}(h_{c.ssp}, t_{f.top}, t_{f.bot}, t_{c.ssp}, \alpha_{ssp}, f_{ssp}) \cdot D_{yy}(h_{c.ssp}, t_{f.top}, t_{f.bot}, t_{c.ssp}, \alpha_{ssp}, f_{ssp}) \pi^{2} \cdot L_1^{6} \cdot B_1^{2} \cdot j^{4} \ldots \\ + 4 \cdot D_{Qx}(h_{c.ssp}, t_{f.top}, t_{f.bot}, t_{c.ssp}, \alpha_{ssp}, f_{ssp}) \cdot D_{Qy}(h_{c.ssp}, t_{f.top}, t_{f.bot}, t_{c.ssp}, \alpha_{ssp}, f_{ssp}) \cdot D_{xy.ssp}(h_{c.ssp}, t_{f.top}, t_{f.bot}, t_{c.ssp}, \alpha_{ssp}, f_{ssp}) \cdot \pi^{2} \cdot L_1^{4} \cdot B_1^{4} \cdot i^{2} \cdot j^{2} \ldots \\ + D_{Qy}(h_{c.ssp}, t_{f.top}, t_{f.bot}, t_{c.ssp}, \alpha_{ssp}, f_{ssp}) \cdot D_{xx}(h_{c.ssp}, t_{f.top}, t_{f.bot}, t_{c.ssp}, \alpha_{ssp}, f_{ssp}) \cdot D_{xy.ssp}(h_{c.ssp}, t_{f.top}, t_{f.bot}, t_{c.ssp}, \alpha_{ssp}, f_{ssp}) \cdot \pi^{4} \cdot L_1^{2} \cdot B_1^{4} \cdot i^{4} \cdot j^{2} \ldots \\ + 2 \cdot D_{Qx}(h_{c.ssp}, t_{f.top}, t_{f.bot}, t_{c.ssp}, \alpha_{ssp}, f_{ssp}) \cdot D_{xx}(h_{c.ssp}, t_{f.top}, t_{f.bot}, t_{c.ssp}, \alpha_{ssp}, f_{ssp}) \cdot D_{yy}(h_{c.ssp}, t_{f.top}, t_{f.bot}, t_{c.ssp}, \alpha_{ssp}, f_{ssp}) \cdot \pi^{4} \cdot L_1^{4} \cdot B_1^{2} \cdot i^{2} \cdot j^{2} \ldots \\ + D_{Qx}(h_{c.ssp}, t_{f.top}, t_{f.bot}, t_{c.ssp}, \alpha_{ssp}, f_{ssp}) \cdot D_{xy.ssp}(h_{c.ssp}, t_{f.top}, t_{f.bot}, t_{c.ssp}, \alpha_{ssp}, f_{ssp}) \cdot D_{yy}(h_{c.ssp}, t_{f.top}, t_{f.bot}, t_{c.ssp}, \alpha_{ssp}, f_{ssp}) \cdot \pi^{4} \cdot L_1^{4} \cdot B_1^{2} \cdot i^{2} \cdot j^{4} \ldots \\ + 2 \cdot D_{Qy}(h_{c.ssp}, t_{f.top}, t_{f.bot}, t_{c.ssp}, \alpha_{ssp}, f_{ssp}) \cdot D_{xx}(h_{c.ssp}, t_{f.top}, t_{f.bot}, t_{c.ssp}, \alpha_{ssp}, f_{ssp}) \cdot D_{yy}(h_{c.ssp}, t_{f.top}, t_{f.bot}, t_{c.ssp}, \alpha_{ssp}, f_{ssp}) \cdot \pi^{4} \cdot L_1^{4} \cdot B_1^{2} \cdot i^{2} \cdot j^{4} \ldots \\ + 2 D_{Qx}(h_{c.ssp}, t_{f.top}, t_{f.bot}, t_{c.ssp}, \alpha_{ssp}, f_{ssp}) \cdot D_{Qy}(h_{c.ssp}, t_{f.top}, t_{f.bot}, t_{c.ssp}, \alpha_{ssp}, f_{ssp}) \cdot D_{xx}(h_{c.ssp}, t_{f.top}, t_{f.bot}, t_{c.ssp}, \alpha_{ssp}, f_{ssp}) \cdot \pi^{2} \cdot L_1^{4} \cdot B_1^{4} \cdot i^{2} \cdot j^{2} \cdot \nu_{yx}(h_{c.ssp}, t_{f.top}, t_{f.bot}, t_{c.ssp}, \alpha_{ssp}, f_{ssp}) \ldots \\ + 2 D_{Qx}(h_{c.ssp}, t_{f.top}, t_{f.bot}, t_{c.ssp}, \alpha_{ssp}, f_{ssp}) \cdot D_{Qy}(h_{c.ssp}, t_{f.top}, t_{f.bot}, t_{c.ssp}, \alpha_{ssp}, f_{ssp}) \cdot D_{yy}(h_{c.ssp}, t_{f.top}, t_{f.bot}, t_{c.ssp}, \alpha_{ssp}, f_{ssp}) \cdot \pi^{2} \cdot L_1^{4} \cdot B_1^{4} \cdot i^{2} \cdot j^{2} \cdot \nu_{xy} \ldots \\ + -D_{Qx}(h_{c.ssp}, t_{f.top}, t_{f.bot}, t_{c.ssp}, \alpha_{ssp}, f_{ssp}) \cdot D_{xx}(h_{c.ssp}, t_{f.top}, t_{f.bot}, t_{c.ssp}, \alpha_{ssp}, f_{ssp}) \cdot D_{xy.ssp}(h_{c.ssp}, t_{f.top}, t_{f.bot}, t_{c.ssp}, \alpha_{ssp}, f_{ssp}) \cdot \pi^{4} \cdot L_1^{2} \cdot B_1^{4} \cdot i^{4} \cdot j^{2} \cdot \nu_{yx}(h_{c.ssp}, t_{f.top}, t_{f.bot}, t_{c.ssp}, \alpha_{ssp}, f_{ssp}) \ldots \\ + -D_{Qx}(h_{c.ssp}, t_{f.top}, t_{f.bot}, t_{c.ssp}, \alpha_{ssp}, f_{ssp}) \cdot D_{xy.ssp}(h_{c.ssp}, t_{f.top}, t_{f.bot}, t_{c.ssp}, \alpha_{ssp}, f_{ssp}) \cdot D_{yy}(h_{c.ssp}, t_{f.top}, t_{f.bot}, t_{c.ssp}, \alpha_{ssp}, f_{ssp}) \cdot \pi^{4} \cdot L_1^{2} \cdot B_1^{4} \cdot i^{4} \cdot j^{2} \cdot \nu_{xy} \ldots \\ + -D_{Qy}(h_{c.ssp}, t_{f.top}, t_{f.bot}, t_{c.ssp}, \alpha_{ssp}, f_{ssp}) \cdot D_{xx}(h_{c.ssp}, t_{f.top}, t_{f.bot}, t_{c.ssp}, \alpha_{ssp}, f_{ssp}) \cdot D_{xy.ssp}(h_{c.ssp}, t_{f.top}, t_{f.bot}, t_{c.ssp}, \alpha_{ssp}, f_{ssp}) \cdot \pi^{4} \cdot L_1^{4} \cdot B_1^{2} \cdot i^{2} \cdot j^{4} \cdot \nu_{yx}(h_{c.ssp}, t_{f.top}, t_{f.bot}, t_{c.ssp}, \alpha_{ssp}, f_{ssp}) \ldots \\ + -D_{Qy}(h_{c.ssp}, t_{f.top}, t_{f.bot}, t_{c.ssp}, \alpha_{ssp}, f_{ssp}) \cdot D_{xy.ssp}(h_{c.ssp}, t_{f.top}, t_{f.bot}, t_{c.ssp}, \alpha_{ssp}, f_{ssp}) \cdot D_{yy}(h_{c.ssp}, t_{f.top}, t_{f.bot}, t_{c.ssp}, \alpha_{ssp}, f_{ssp}) \cdot \pi^{4} \cdot L_1^{4} \cdot B_1^{2} \cdot i^{2} \cdot j^{4} \cdot \nu_{xy} \ldots \\ + -2 D_{Qx}(h_{c.ssp}, t_{f.top}, t_{f.bot}, t_{c.ssp}, \alpha_{ssp}, f_{ssp}) \cdot D_{xx}(h_{c.ssp}, t_{f.top}, t_{f.bot}, t_{c.ssp}, \alpha_{ssp}, f_{ssp}) \cdot D_{yy}(h_{c.ssp}, t_{f.top}, t_{f.bot}, t_{c.ssp}, \alpha_{ssp}, f_{ssp}) \cdot \pi^{4} \cdot L_1^{4} \cdot B_1^{2} \cdot i^{2} \cdot j^{4} \cdot \nu_{xy} \cdot \nu_{yx}(h_{c.ssp}, t_{f.top}, t_{f.bot}, t_{c.ssp}, \alpha_{ssp}, f_{ssp}) \ldots \\ + 2 D_{Qy}(h_{c.ssp}, t_{f.top}, t_{f.bot}, t_{c.ssp}, \alpha_{ssp}, f_{ssp}) \cdot D_{xx}(h_{c.ssp}, t_{f.top}, t_{f.bot}, t_{c.ssp}, \alpha_{ssp}, f_{ssp}) \cdot D_{yy}(h_{c.ssp}, t_{f.top}, t_{f.bot}, t_{c.ssp}, \alpha_{ssp}, f_{ssp}) \cdot \pi^{4} \cdot L_1^{4} \cdot B_1^{2} \cdot i^{2} \cdot j^{4} \cdot \nu_{xy} \cdot \nu_{yx}(h_{c.ssp}, t_{f.top}, t_{f.bot}, t_{c.ssp}, \alpha_{ssp}, f_{ssp}) \end{array} \right)}$$

Deflection

The deflection in the middle of the plate is considered

$$X := \frac{L_1}{2} = 4\,m \qquad Y := \frac{B_1}{2} = 3\,m$$

Number of terms in the Fourier seris used in the deflection solution. Here both i and j are choosen to 1 since using more terms is more computationally demanding in the optimisation analysis.

$$i := 1 .. 1 \qquad j := 1 .. 1$$

Distributed load

$$w_{UDL}(h_{c.ssp}, t_{f.top}, t_{f.bot}, t_{c.ssp}, \alpha_{ssp}, f_{ssp}) := \sum_j \left[\sum_i \left(w_{ij}(h_{c.ssp}, t_{f.top}, t_{f.bot}, t_{c.ssp}, \alpha_{ssp}, f_{ssp}, i, j) \cdot q_{ijC}(i,j) \cdot \sin\left(\frac{i \cdot \pi \cdot X}{L_1}\right) \cdot \sin\left(\frac{j \cdot \pi \cdot Y}{B_1}\right) \right) \right]$$

Wheel loads

Wheel load 1

$$w_1(h_{c.ssp}, t_{f.top}, t_{f.bot}, t_{c.ssp}, \alpha_{ssp}, f_{ssp}) := \sum_j \left[\sum_i \left(w_{ij}(h_{c.ssp}, t_{f.top}, t_{f.bot}, t_{c.ssp}, \alpha_{ssp}, f_{ssp}, i, j) \cdot Q_1(i,j) \cdot \sin\left(\frac{i \cdot \pi \cdot X}{L_1}\right) \cdot \sin\left(\frac{j \cdot \pi \cdot Y}{B_1}\right) \right) \right]$$

Wheel load 2

$$w_2(h_{c.ssp}, t_{f.top}, t_{f.bot}, t_{c.ssp}, \alpha_{ssp}, f_{ssp}) := \sum_j \left[\sum_i \left(w_{ij}(h_{c.ssp}, t_{f.top}, t_{f.bot}, t_{c.ssp}, \alpha_{ssp}, f_{ssp}, i, j) \cdot Q_2(i,j) \cdot \sin\left(\frac{i \cdot \pi \cdot X}{L_1}\right) \cdot \sin\left(\frac{j \cdot \pi \cdot Y}{B_1}\right) \right) \right]$$

Wheel load 3

$$w_3(h_{c.ssp}, t_{f.top}, t_{f.bot}, t_{c.ssp}, \alpha_{ssp}, f_{ssp}) := \sum_j \left[\sum_i \left(w_{ij}(h_{c.ssp}, t_{f.top}, t_{f.bot}, t_{c.ssp}, \alpha_{ssp}, f_{ssp}, i, j) \cdot Q_3(i,j) \cdot \sin\left(\frac{i \cdot \pi \cdot X}{L_1}\right) \cdot \sin\left(\frac{j \cdot \pi \cdot Y}{B_1}\right) \right) \right]$$

Wheel load 4

$$w_4(h_{c.ssp}, t_{f.top}, t_{f.bot}, t_{c.ssp}, \alpha_{ssp}, f_{ssp}) := \sum_j \left[\sum_i \left(w_{ij}(h_{c.ssp}, t_{f.top}, t_{f.bot}, t_{c.ssp}, \alpha_{ssp}, f_{ssp}, i, j) \cdot Q_4(i,j) \cdot \sin\left(\frac{i \cdot \pi \cdot X}{L_1}\right) \cdot \sin\left(\frac{j \cdot \pi \cdot Y}{B_1}\right) \right) \right]$$

Total deflection in the middle of the plate

$$\begin{aligned} w_{tot}(h_{c.ssp}, t_{f.top}, t_{f.bot}, t_{c.ssp}, \alpha_{ssp}, f_{ssp}) := {} & w_{UDL}(h_{c.ssp}, t_{f.top}, t_{f.bot}, t_{c.ssp}, \alpha_{ssp}, f_{ssp}) \cdots \\ & + w_1(h_{c.ssp}, t_{f.top}, t_{f.bot}, t_{c.ssp}, \alpha_{ssp}, f_{ssp}) \cdots \\ & + w_2(h_{c.ssp}, t_{f.top}, t_{f.bot}, t_{c.ssp}, \alpha_{ssp}, f_{ssp}) \cdots \\ & + w_3(h_{c.ssp}, t_{f.top}, t_{f.bot}, t_{c.ssp}, \alpha_{ssp}, f_{ssp}) \cdots \\ & + w_4(h_{c.ssp}, t_{f.top}, t_{f.bot}, t_{c.ssp}, \alpha_{ssp}, f_{ssp}) \end{aligned}$$

5. Deflection main girder

The deflection limit of the main girder is used to design the main girders in order to see how the SSP configuration and distance between transverse girders affects the main girder dimensions.

5.1. Loads and lane factors

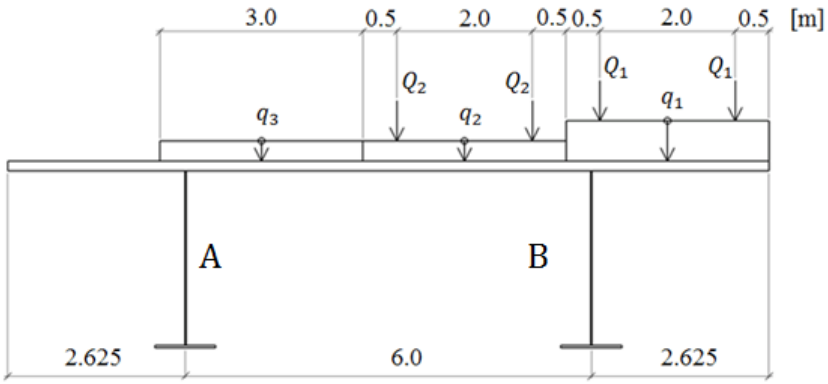

The load case resulting in the largest load on one main girder is shown in the figure above. The charateristic load combination is used.

Loads

Traffic loads, (same numbering as in picture)

$Q_{1k} = 300 \cdot kN$

$Q_{2k} = 200 \cdot kN$

$Q_{3k} = 0 \cdot kN$

$q_{1k} = 9 \cdot \frac{kN}{m^2}$

q_2 and q_3 have the same magnitude, only q_2 defined here:

$q_{2k} = 2.5 \cdot \frac{kN}{m^2}$

Lane factors

Load positions

$$l_{Q1} := B_1 + L_{cant} - \frac{d_{wheel.LM1}}{2} - 0.5m = 7.125\,m$$

$$l_{Q2} := l_{Q1} - w_{lane} = 4.125\,m$$

$$l_{Q3} := l_{Q1} - 2w_{lane} = 1.125\,m$$

$$l_{q1} := l_{Q1} = 7.125\,m$$

$$l_{q2} := \frac{B_1}{2} - \left(w_{lane} - L_{cant}\right) = 2.625\,m$$

Lane factors

$$R_{BQ} := \frac{Q_{1k}\cdot l_{Q1} + Q_{2k}\cdot l_{Q2}}{B_1} = 493.75\cdot kN$$ Reaction force at support B from axel loads

$$R_{AQ} := Q_{1k} + Q_{2k} - R_{BQ} = 6.25\cdot kN$$ Reaction force at support A from axel loads

$$lf_Q := \frac{R_{BQ}}{R_{AQ} + R_{BQ}} = 0.988$$ Lane factor for axel loads

$$R_{Bq} := \frac{q_{1k}\cdot w_{lane}\cdot l_{q1} + q_{2k}\cdot 2w_{lane}\cdot l_{q2}}{B_1} = 38.625\cdot\frac{kN}{m}$$ Reaction force at support B from uniformly distributed load

$$R_{Aq} := q_{1k}\cdot w_{lane} + q_{2k}\cdot 2w_{lane} - R_{Bq} = 3.375\cdot\frac{kN}{m}$$ Reaction force at support A from uniformly distributed load

$$lf_q := \frac{R_{Bq}}{R_{Aq} + R_{Bq}} = 0.92$$ Lane factor for uniformly distributed load

Loads on main girder B in the direction parallel to the main girders

$$Q_{lf} := lf_Q\cdot\left(Q_{1k} + Q_{2k} + Q_{3k}\right) = 493.75\cdot kN$$ Axel load

$$q_{lf} := lf_q\cdot\left(q_{1k}\cdot w_{lane} + q_{2k}\cdot 2w_{lane}\right) = 38.625\cdot\frac{kN}{m}$$ Uniformly distributed load

5.2. Cross-sectional constants

Area

SSP

The effective width is assumed to remain constant at 80 % of half the width of the bridge.

$$b_e := 0.8 \cdot \left(L_{cant} + \frac{B_1}{2} \right) = 4.5\,m$$

Area of SSP

$$A_{MG.tf}\left(h_{c.ssp}, t_{f.top}, t_{f.bot}, t_{c.ssp}, \alpha_{ssp}, f_{ssp}\right) := A_{ssp}\left(h_{c.ssp}, t_{f.top}, t_{f.bot}, t_{c.ssp}, \alpha_{ssp}, f_{ssp}\right) \cdot b_e$$

Main girder

The total height of the main girder is kept constant at 2.6 m.

$$h_{MG.w}\left(t_{MG.bf}\right) := 2.6m - t_{MG.bf}$$ Height of web

$$A_{MG.w}\left(t_{MG.bf}, t_{MG.w}\right) := h_{MG.w}\left(t_{MG.bf}\right) \cdot t_{MG.w}$$ Area web

$$A_{MG.bf}\left(b_{MG.bf}, t_{MG.bf}\right) := b_{MG.bf} \cdot t_{MG.bf}$$ Area bottom flange

Full section

$$A_{MG.tot}\left(h_{c.ssp}, t_{f.top}, t_{f.bot}, t_{c.ssp}, \alpha_{ssp}, f_{ssp}, b_{MG.bf}, t_{MG.bf}, t_{MG.w}\right) := A_{MG.tf}\left(h_{c.ssp}, t_{f.top}, t_{f.bot}, t_{c.ssp}, \alpha_{ssp}, f_{ssp}\right) \cdots + A_{MG.w}\left(t_{MG.bf}, t_{MG.w}\right) \cdots + A_{MG.bf}\left(b_{MG.bf}, t_{MG.bf}\right)$$

Moment of inertia

Centre of gravity

Measured from the top of the section

$$z_{na.MG}\left(h_{c.ssp}, t_{f.top}, t_{f.bot}, t_{c.ssp}, \alpha_{ssp}, f_{ssp}, b_{MG.bf}, t_{MG.bf}, t_{MG.w}\right) :=$$

$$\frac{\begin{aligned} &A_{MG.tf}\left(h_{c.ssp}, t_{f.top}, t_{f.bot}, t_{c.ssp}, \alpha_{ssp}, f_{ssp}\right) \cdot \left(z_{na.ssp}\left(h_{c.ssp}, t_{f.top}, t_{f.bot}, t_{c.ssp}, \alpha_{ssp}, f_{ssp}\right) + \frac{t_{f.top}}{2} \right) \cdots \\ &+ A_{MG.w}\left(t_{MG.bf}, t_{MG.w}\right) \cdot \left(h_{ssp.tot}\left(h_{c.ssp}, t_{f.top}, t_{f.bot}, t_{c.ssp}\right) + \frac{h_{MG.w}\left(t_{MG.bf}\right)}{2} \right) \cdots \\ &+ A_{MG.bf}\left(b_{MG.bf}, t_{MG.bf}\right) \cdot \left(h_{ssp.tot}\left(h_{c.ssp}, t_{f.top}, t_{f.bot}, t_{c.ssp}\right) + h_{MG.w}\left(t_{MG.bf}\right) + \frac{t_{MG.bf}}{2} \right) \end{aligned}}{A_{MG.tot}\left(h_{c.ssp}, t_{f.top}, t_{f.bot}, t_{c.ssp}, \alpha_{ssp}, f_{ssp}, b_{MG.bf}, t_{MG.bf}, t_{MG.w}\right)}$$

Moment of inertia

Top flange:

$$I_{x.MG.tf}\left(h_{c.ssp}, t_{f.top}, t_{f.bot}, t_{c.ssp}, \alpha_{ssp}, f_{ssp}, b_{MG.bf}, t_{MG.bf}, t_{MG.w}\right) :=$$

$$I_{ssp.x}\left(h_{c.ssp}, t_{f.top}, t_{f.bot}, t_{c.ssp}, \alpha_{ssp}, f_{ssp}\right) \cdot b_e \ \cdots$$
$$+ A_{MG.tf}\left(h_{c.ssp}, t_{f.top}, t_{f.bot}, t_{c.ssp}, \alpha_{ssp}, f_{ssp}\right) \cdot \left(\begin{matrix} z_{na.MG}\left(h_{c.ssp}, t_{f.top}, t_{f.bot}, t_{c.ssp}, \alpha_{ssp}, f_{ssp}, b_{MG.bf}, t_{MG.bf}, t_{MG.w}\right) \cdots \\ + -z_{na.ssp}\left(h_{c.ssp}, t_{f.top}, t_{f.bot}, t_{c.ssp}, \alpha_{ssp}, f_{ssp}\right) \end{matrix}\right)^2$$

Web:

$$I_{x.MG.w}\left(h_{c.ssp}, t_{f.top}, t_{f.bot}, t_{c.ssp}, \alpha_{ssp}, f_{ssp}, b_{MG.bf}, t_{MG.bf}, t_{MG.w}\right) :=$$

$$\frac{t_{MG.w} \cdot h_{MG.w}\left(t_{MG.bf}\right)^3}{12} \cdots$$
$$+ A_{MG.w}\left(t_{MG.bf}, t_{MG.w}\right) \cdot \left(\begin{matrix} h_{ssp.tot}\left(h_{c.ssp}, t_{f.top}, t_{f.bot}, t_{c.ssp}\right) \cdots \\ + \frac{h_{MG.w}\left(t_{MG.bf}\right)}{2} \cdots \\ + -z_{na.MG}\left(h_{c.ssp}, t_{f.top}, t_{f.bot}, t_{c.ssp}, \alpha_{ssp}, f_{ssp}, b_{MG.bf}, t_{MG.bf}, t_{MG.w}\right) \end{matrix}\right)^2$$

Bottom flange:

$$I_{x.MG.bf}\left(h_{c.ssp}, t_{f.top}, t_{f.bot}, t_{c.ssp}, \alpha_{ssp}, f_{ssp}, b_{MG.bf}, t_{MG.bf}, t_{MG.w}\right) :=$$

$$\frac{b_{MG.bf} \cdot t_{MG.bf}^3}{12} \cdots$$
$$+ A_{MG.bf}\left(b_{MG.bf}, t_{MG.bf}\right) \cdot \left(\begin{matrix} h_{ssp.tot}\left(h_{c.ssp}, t_{f.top}, t_{f.bot}, t_{c.ssp}\right) \cdots \\ + h_{MG.w}\left(t_{MG.bf}\right) + t_{MG.bf} \cdots \\ + -z_{na.MG}\left(h_{c.ssp}, t_{f.top}, t_{f.bot}, t_{c.ssp}, \alpha_{ssp}, f_{ssp}, b_{MG.bf}, t_{MG.bf}, t_{MG.w}\right) \end{matrix}\right)^2$$

Full section:

$$I_{x.MG}\left(h_{c.ssp}, t_{f.top}, t_{f.bot}, t_{c.ssp}, \alpha_{ssp}, f_{ssp}, b_{MG.bf}, t_{MG.bf}, t_{MG.w}\right) :=$$

$$I_{x.MG.tf}\left(h_{c.ssp}, t_{f.top}, t_{f.bot}, t_{c.ssp}, \alpha_{ssp}, f_{ssp}, b_{MG.bf}, t_{MG.bf}, t_{MG.w}\right) \cdots$$
$$+ I_{x.MG.w}\left(h_{c.ssp}, t_{f.top}, t_{f.bot}, t_{c.ssp}, \alpha_{ssp}, f_{ssp}, b_{MG.bf}, t_{MG.bf}, t_{MG.w}\right) \cdots$$
$$+ I_{x.MG.bf}\left(h_{c.ssp}, t_{f.top}, t_{f.bot}, t_{c.ssp}, \alpha_{ssp}, f_{ssp}, b_{MG.bf}, t_{MG.bf}, t_{MG.w}\right)$$

5.3. Deflection

Two load cases are considered; one when the uniformly distributed load is in the middle span with the axel loads in the middle, see figure below. The other with the uniformly distributed load in one side span and the axel load centred in the middle of that span.

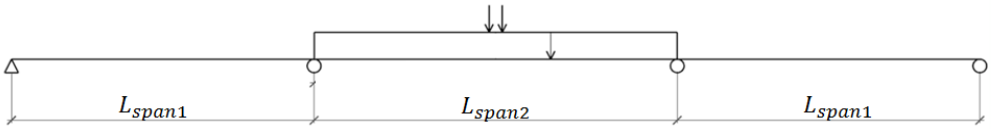

5.3.1. Deflection with load in mid span

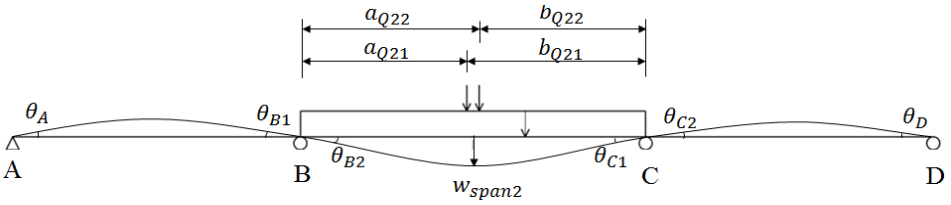

Distances to point loads and support angels for the load case when the load is in the middle span

$$a_{Q21} := \frac{L_{span2}}{2} - \frac{d_{axel.LM1}}{2} = 32.4\,m$$

$$a_{Q22} := \frac{L_{span2}}{2} + \frac{d_{axel.LM1}}{2} = 33.6\,m$$

$$b_{Q21} := L_{span2} - a_{Q21} = 33.6\,m$$

$$b_{Q22} := L_{span2} - a_{Q22} = 32.4\,m$$

Support moment

Continuity condition

$$-\theta_{B1} = \theta_{B2}$$

$$\theta_{C1} = -\theta_{C2}$$

Symmetry gives

$$\theta_{B2} = \theta_{C1}$$

$$\theta_{B1} = \theta_{C2}$$

$$M_B = M_C$$

Standard cases for beam bending gives the expressions for θ_{B1} and θ_{B2}

$$\theta_{B1} = \frac{M_B \cdot L_{span1}}{3EI}$$

$$\theta_{B2} = \frac{M_B \cdot L_{span2}}{3EI} + \frac{q_{LF} \cdot L_{span2}^{3}}{24EI} + \frac{Q_{lf} \cdot b_{Q21} \cdot L_{span2}}{6 \cdot EI} \cdot \left(1 - \frac{b_{Q21}^{2}}{L_{span2}^{2}}\right) \ldots + \frac{Q_{lf} \cdot b_{Q22} \cdot L_{span2}}{6 \cdot EI} \cdot \left(1 - \frac{b_{Q22}^{2}}{L_{span2}^{2}}\right) + \frac{M_C \cdot L_{span2}}{6EI}$$

The continuity condition gives

$$M_{B2} := \frac{\frac{q_{lf} \cdot L_{span2}^{3}}{24} + \frac{Q_{lf} \cdot b_{Q21} \cdot L_{span2}}{6} \cdot \left(1 - \frac{b_{Q21}^{2}}{L_{span2}^{2}}\right) + \frac{Q_{lf} \cdot b_{Q22} \cdot L_{span2}}{6} \cdot \left(1 - \frac{b_{Q22}^{2}}{L_{span2}^{2}}\right)}{-\left(\frac{L_{span1}}{3} + \frac{L_{span2}}{2}\right)}$$

$$M_{B2} = -1.473 \times 10^{4} \cdot kN \cdot m$$

$$M_{B2.q} := \frac{\frac{q_{lf} \cdot L_{span2}^{3}}{24}}{-\left(\frac{L_{span1}}{3} + \frac{L_{span2}}{2}\right)} = -9.316 \times 10^{3} \cdot kN \cdot m$$

$$M_{B2.Q} := \frac{\frac{Q_{lf} \cdot b_{Q21} \cdot L_{span2}}{6} \cdot \left(1 - \frac{b_{Q21}^{2}}{L_{span2}^{2}}\right) + \frac{Q_{lf} \cdot b_{Q22} \cdot L_{span2}}{6} \cdot \left(1 - \frac{b_{Q22}^{2}}{L_{span2}^{2}}\right)}{-\left(\frac{L_{span1}}{3} + \frac{L_{span2}}{2}\right)} = -5.411 \times 10^{3} \cdot kN \cdot m$$

Deflection

Deflection in the middle of the span

$$w_{span2}\left(h_{c.ssp}, t_{f.top}, t_{f.bot}, t_{c.ssp}, \alpha_{ssp}, f_{ssp}, b_{MG.bf}, t_{MG.bf}, t_{MG.w}\right) := \frac{5 \cdot q_{lf} \cdot L_{span2}^{4}}{384E \cdot I_{x.MG}\left(h_{c.ssp}, t_{f.top}, t_{f.bot}, t_{c.ssp}, \alpha_{ssp}, f_{ssp}, b_{MG.bf}, t_{MG.bf}, t_{MG.w}\right)} \ldots + 2\frac{M_{B2} \cdot L_{span2}^{2}}{16 \cdot E \cdot I_{x.MG}\left(h_{c.ssp}, t_{f.top}, t_{f.bot}, t_{c.ssp}, \alpha_{ssp}, f_{ssp}, b_{MG.bf}, t_{MG.bf}, t_{MG.w}\right)} \ldots + \frac{Q_{lf} \cdot a_{Q21} \cdot L_{span2}^{2}}{48 \cdot E \cdot I_{x.MG}\left(h_{c.ssp}, t_{f.top}, t_{f.bot}, t_{c.ssp}, \alpha_{ssp}, f_{ssp}, b_{MG.bf}, t_{MG.bf}, t_{MG.w}\right)} \cdot \left(3 - \frac{4 \cdot a_{Q21}^{2}}{L_{span2}^{2}}\right) \ldots + \frac{Q_{lf} \cdot b_{Q22} \cdot L_{span2}^{2}}{48 \cdot E \cdot I_{x.MG}\left(h_{c.ssp}, t_{f.top}, t_{f.bot}, t_{c.ssp}, \alpha_{ssp}, f_{ssp}, b_{MG.bf}, t_{MG.bf}, t_{MG.w}\right)} \cdot \left(3 - \frac{4 \cdot b_{Q22}^{2}}{L_{span2}^{2}}\right)$$

5.3.2. Deflection with load in side span

The deflection in the side span is calulated in the same manner as the deflction in the mid span. Now the distributed load is in span 1 and the axel loads in the middle of span 1

$$a_{Q11} := \frac{L_{span1}}{2} - \frac{d_{axel.LM1}}{2} = 24.4\,m$$

$$a_{Q12} := \frac{L_{span1}}{2} + \frac{d_{axel.LM1}}{2} = 25.6\,m$$

$$b_{Q11} := L_{span1} - a_{Q11} = 25.6\,m$$

$$b_{Q12} := L_{span1} - a_{Q12} = 24.4\,m$$

Support moment

Continuity condition

$$\theta_{B1} = -\theta_{B2}$$

Standard cases for beam bending gives the expressions for θ_{B1} and θ_{B2}

$$\theta_{B1} = \frac{M_B \cdot L_{span1}}{3EI} + \frac{q_{LF} \cdot L_{span1}^{3}}{24EI} + \frac{Q_{lf} \cdot a_{Q11} \cdot L_{span1}}{6 \cdot EI} \cdot \left(1 - \frac{a_{Q11}^{2}}{L_{span1}^{2}}\right) \ldots + \frac{Q_{lf} \cdot a_{Q12} \cdot L_{span1}}{6 \cdot EI} \cdot \left(1 - \frac{a_{Q12}^{2}}{L_{span1}^{2}}\right)$$

$$\theta_{B2} = \frac{M_B \cdot L_{span2}}{3EI}$$

The continuity condition gives

$$M_{B1} := \frac{\frac{q_{lf} \cdot L_{span1}^{3}}{24} + \frac{Q_{lf} \cdot a_{Q11} \cdot L_{span1}}{6} \cdot \left(1 - \frac{a_{Q11}^{2}}{L_{span1}^{2}}\right) + \frac{Q_{lf} \cdot a_{Q12} \cdot L_{span1}}{6} \cdot \left(1 - \frac{a_{Q12}^{2}}{L_{span1}^{2}}\right)}{-\frac{(L_{span2} + L_{span1})}{3}}$$

$$M_{B1} = -9.191 \times 10^{3} \cdot kN \cdot m$$

Deflection

Deflection in the middle of the span

$$w_{span1}\left(h_{c.ssp}, t_{f.top}, t_{f.bot}, t_{c.ssp}, \alpha_{ssp}, f_{ssp}, b_{MG.bf}, t_{MG.bf}, t_{MG.w}\right) :=$$

$$\frac{5 \cdot q_{lf} \cdot L_{span1}^{4}}{384 E \cdot I_{x.MG}\left(h_{c.ssp}, t_{f.top}, t_{f.bot}, t_{c.ssp}, \alpha_{ssp}, f_{ssp}, b_{MG.bf}, t_{MG.bf}, t_{MG.w}\right)} \ldots$$

$$+ \frac{M_{B1} \cdot L_{span1}^{2}}{16 \cdot E \cdot I_{x.MG}\left(h_{c.ssp}, t_{f.top}, t_{f.bot}, t_{c.ssp}, \alpha_{ssp}, f_{ssp}, b_{MG.bf}, t_{MG.bf}, t_{MG.w}\right)} \ldots$$

$$+ \frac{Q_{lf} \cdot a_{Q11} \cdot L_{span1}^{2}}{48 \cdot E \cdot I_{x.MG}\left(h_{c.ssp}, t_{f.top}, t_{f.bot}, t_{c.ssp}, \alpha_{ssp}, f_{ssp}, b_{MG.bf}, t_{MG.bf}, t_{MG.w}\right)} \cdot \left(3 - \frac{4 \cdot a_{Q11}^{2}}{L_{span1}^{2}}\right) \ldots$$

$$+ \frac{Q_{lf} \cdot b_{Q12} \cdot L_{span1}^{2}}{48 \cdot E \cdot I_{x.MG}\left(h_{c.ssp}, t_{f.top}, t_{f.bot}, t_{c.ssp}, \alpha_{ssp}, f_{ssp}, b_{MG.bf}, t_{MG.bf}, t_{MG.w}\right)} \cdot \left(3 - \frac{4 \cdot b_{Q12}^{2}}{L_{span1}^{2}}\right)$$

6. Stress in transverse girder

The yield stress in the bottom flange of the transverse girder is used as a constraint in the design of the transverse griders in order to estimate how the SSP configuration affects the transverse girder dimensions. The transverse girder is shown below.

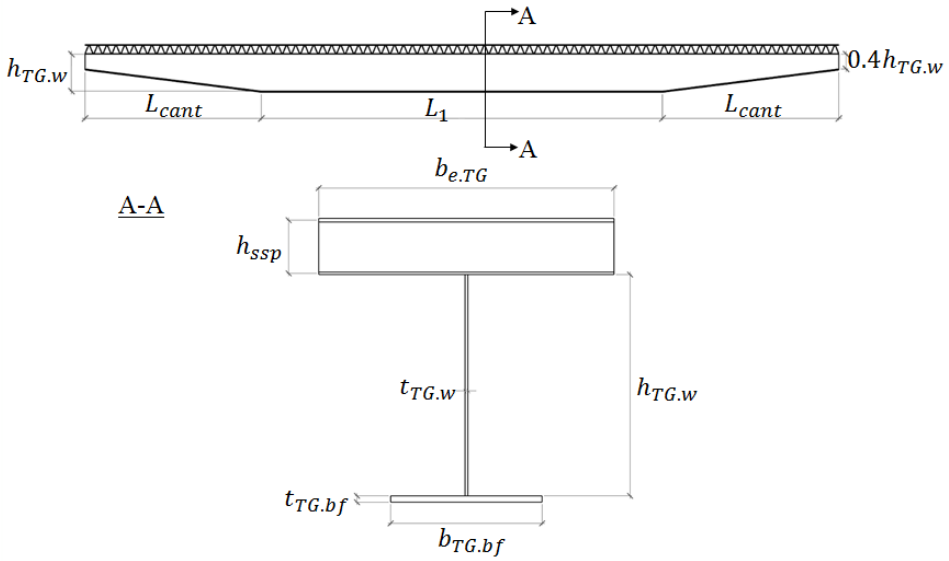

6.1. Effective width top flange

The effective witdh of the top flange is calculated by using the reduction factor for buckling of a column with length of one corrugation opening l_o, width 1 m and thickness of the top flange. The transverse girder is designed to be in CSC3.

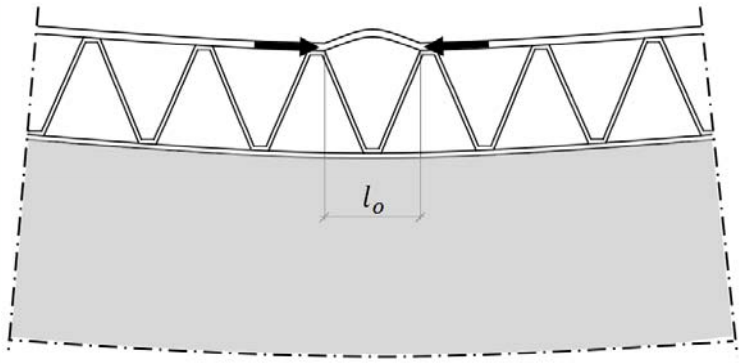

Buckling of the top plate due to bending of the transverse girder

$\alpha_{imp} := 0.49$ Imperfection factor, solid section class c

Area and moment of inertia of top flange in SSP:

$$A_{TG.tf.be}(t_{f.top}) := t_{f.top} \cdot 1m$$

$$I_{TG.tf.be}(t_{f.top}) := \frac{t_{f.top}^{3} \cdot 1m}{12}$$

Critical buckling stress:

$$N_{cr}(h_{c.ssp}, t_{f.top}, \alpha_{ssp}, f_{ssp}) := \frac{\pi \cdot E \cdot I_{TG.tf.be}(t_{f.top})}{\left(l_o(h_{c.ssp}, \alpha_{ssp}, f_{ssp})\right)^2}$$

Slenderness:

$$\lambda_{TG}(h_{c.ssp}, t_{f.top}, \alpha_{ssp}, f_{ssp}) := \sqrt{\frac{A_{TG.tf.be}(t_{f.top}) \cdot f_y}{N_{cr}(h_{c.ssp}, t_{f.top}, \alpha_{ssp}, f_{ssp})}}$$

Reduction factor:

$$\Phi_{TG}(h_{c.ssp}, t_{f.top}, \alpha_{ssp}, f_{ssp}) := 0.5 \cdot \left[1 + \alpha_{imp} \cdot \left(\lambda_{TG}(h_{c.ssp}, t_{f.top}, \alpha_{ssp}, f_{ssp}) - 0.2\right) + \lambda_{TG}(h_{c.ssp}, t_{f.top}, \alpha_{ssp}, f_{ssp})^2\right]$$

$$\chi_{TG}(h_{c.ssp}, t_{f.top}, \alpha_{ssp}, f_{ssp}) :=$$

$$\begin{cases} \dfrac{1}{\Phi_{TG}(h_{c.ssp}, t_{f.top}, \alpha_{ssp}, f_{ssp}) + \left(\sqrt{\Phi_{TG}(h_{c.ssp}, t_{f.top}, \alpha_{ssp}, f_{ssp})^2 - \lambda_{TG}(h_{c.ssp}, t_{f.top}, \alpha_{ssp}, f_{ssp})^2}\right)} & \text{if } \lambda_{TG}(h_{c.ssp}, t_{f.top}, \alpha_{ssp}, f_{ssp}) > 0.2 \\ 1 & \text{otherwise} \end{cases}$$

Effective width of top flange:

$$b_{e.TG}(h_{c.ssp}, t_{f.top}, \alpha_{ssp}, f_{ssp}) := \chi_{TG}(h_{c.ssp}, t_{f.top}, \alpha_{ssp}, f_{ssp}) \cdot L_1$$

6.2. Cross-sectional constants

Area

Area of flange (SSP), only the top an bottom plate of the SSP is assumed to contribute in bending perpendicular to the corrugation

$$A_{TG.tf}(h_{c.ssp}, t_{f.top}, t_{f.bot}, \alpha_{ssp}, f_{ssp}) := b_{e.TG}(h_{c.ssp}, t_{f.top}, \alpha_{ssp}, f_{ssp}) \cdot (t_{f.top} + t_{f.bot})$$

$A_{TG.w}(h_{TG.w}, t_{TG.w}) := h_{TG.w} \cdot t_{TG.w}$ Area of web

$A_{TG.bf}(b_{TG.bf}, t_{TG.bf}) := b_{TG.bf} \cdot t_{TG.bf}$ Area of bottom flange

Area of the mid section of the transverse girder

$$A_{TG.mid}(h_{c.ssp}, t_{f.top}, t_{f.bot}, \alpha_{ssp}, f_{ssp}, h_{TG.w}, t_{TG.w}, b_{TG.bf}, t_{TG.bf}) := A_{TG.tf}(h_{c.ssp}, t_{f.top}, t_{f.bot}, \alpha_{ssp}, f_{ssp}) \cdots + A_{TG.w}(h_{TG.w}, t_{TG.w}) \cdots + A_{TG.bf}(b_{TG.bf}, t_{TG.bf})$$

Centre of gravity

$$z_{na.TG}\left(h_{c.ssp}, t_{f.top}, t_{f.bot}, t_{c.ssp}, \alpha_{ssp}, f_{ssp}, h_{TG.w}, t_{TG.w}, b_{TG.bf}, t_{TG.bf}\right)$$

$$\frac{\left[\begin{array}{l} A_{TG.tf}\left(h_{c.ssp}, t_{f.top}, t_{f.bot}, \alpha_{ssp}, f_{ssp}\right)\cdot\left(z_{na.ssp}\left(h_{c.ssp}, t_{f.top}, t_{f.bot}, t_{c.ssp}, \alpha_{ssp}, f_{ssp}\right) + \frac{t_{f.top}}{2}\right) \dots \\ + A_{TG.w}\left(h_{TG.w}, t_{TG.w}\right)\cdot\left(h_{ssp.tot}\left(h_{c.ssp}, t_{f.top}, t_{f.bot}, t_{c.ssp}\right) + \frac{h_{TG.w}}{2}\right) \dots \\ + A_{TG.bf}\left(b_{TG.bf}, t_{TG.bf}\right)\cdot\left(h_{ssp.tot}\left(h_{c.ssp}, t_{f.top}, t_{f.bot}, t_{c.ssp}\right) + h_{TG.w} + \frac{t_{TG.bf}}{2}\right) \end{array}\right]}{A_{TG.mid}\left(h_{c.ssp}, t_{f.top}, t_{f.bot}, \alpha_{ssp}, f_{ssp}, h_{TG.w}, t_{TG.w}, b_{TG.bf}, t_{TG.bf}\right)}$$

Moment of inertia

Top flange:

$$I_{TG.tf}\left(h_{c.ssp}, t_{f.top}, t_{f.bot}, t_{c.ssp}, \alpha_{ssp}, f_{ssp}, h_{TG.w}, t_{TG.w}, b_{TG.bf}, t_{TG.bf}\right) :=$$

$$\begin{array}{l} I_{ssp.y}\left(h_{c.ssp}, t_{f.top}, t_{f.bot}, t_{c.ssp}, \alpha_{ssp}, f_{ssp}\right)\cdot b_{e.TG}\left(h_{c.ssp}, t_{f.top}, \alpha_{ssp}, f_{ssp}\right) \dots \\ + A_{TG.tf}\left(h_{c.ssp}, t_{f.top}, t_{f.bot}, \alpha_{ssp}, f_{ssp}\right)\cdot\left[\begin{array}{l} z_{na.TG}\left(h_{c.ssp}, t_{f.top}, t_{f.bot}, t_{c.ssp}, \alpha_{ssp}, f_{ssp}, h_{TG.w}, t_{TG.w}, b_{TG.bf}, t_{TG.bf}\right) \dots \\ + -\left(z_{na.ssp}\left(h_{c.ssp}, t_{f.top}, t_{f.bot}, t_{c.ssp}, \alpha_{ssp}, f_{ssp}\right) + \frac{t_{f.top}}{2}\right) \end{array}\right]^2 \end{array}$$

Web:

$$I_{TG.w}\left(h_{c.ssp}, t_{f.top}, t_{f.bot}, t_{c.ssp}, \alpha_{ssp}, f_{ssp}, h_{TG.w}, t_{TG.w}, b_{TG.bf}, t_{TG.bf}\right) :=$$

$$\begin{array}{l} \frac{t_{TG.w}\cdot h_{TG.w}^{3}}{12} \dots \\ + A_{TG.w}\left(h_{TG.w}, t_{TG.w}\right)\cdot\left(\begin{array}{l} h_{ssp.tot}\left(h_{c.ssp}, t_{f.top}, t_{f.bot}, t_{c.ssp}\right) + \frac{h_{TG.w}}{2} \dots \\ + -z_{na.TG}\left(h_{c.ssp}, t_{f.top}, t_{f.bot}, t_{c.ssp}, \alpha_{ssp}, f_{ssp}, h_{TG.w}, t_{TG.w}, b_{TG.bf}, t_{TG.bf}\right) \end{array}\right)^2 \end{array}$$

Bottom flange :

$$I_{TG.bf}\left(h_{c.ssp}, t_{f.top}, t_{f.bot}, t_{c.ssp}, \alpha_{ssp}, f_{ssp}, h_{TG.w}, t_{TG.w}, b_{TG.bf}, t_{TG.bf}\right) :$$

$$\begin{array}{l} \frac{b_{TG.bf}\cdot t_{TG.bf}^{3}}{12} \dots \\ + A_{TG.bf}\left(b_{TG.bf}, t_{TG.bf}\right)\cdot\left(\begin{array}{l} h_{ssp.tot}\left(h_{c.ssp}, t_{f.top}, t_{f.bot}, t_{c.ssp}\right) + h_{TG.w} + \frac{t_{TG.bf}}{2} \dots \\ + -z_{na.TG}\left(h_{c.ssp}, t_{f.top}, t_{f.bot}, t_{c.ssp}, \alpha_{ssp}, f_{ssp}, h_{TG.w}, t_{TG.w}, b_{TG.bf}, t_{TG.bf}\right) \end{array}\right)^2 \end{array}$$

Moment of inertia of whole tansverse beam section:

$$I_{TG}\left(h_{c.ssp}, t_{f.top}, t_{f.bot}, t_{c.ssp}, \alpha_{ssp}, f_{ssp}, h_{TG.w}, t_{TG.w}, b_{TG.bf}, t_{TG.bf}\right) :$$

$$\begin{array}{l} I_{TG.tf}\left(h_{c.ssp}, t_{f.top}, t_{f.bot}, t_{c.ssp}, \alpha_{ssp}, f_{ssp}, h_{TG.w}, t_{TG.w}, b_{TG.bf}, t_{TG.bf}\right) \dots \\ + I_{TG.w}\left(h_{c.ssp}, t_{f.top}, t_{f.bot}, t_{c.ssp}, \alpha_{ssp}, f_{ssp}, h_{TG.w}, t_{TG.w}, b_{TG.bf}, t_{TG.bf}\right) \dots \\ + I_{TG.bf}\left(h_{c.ssp}, t_{f.top}, t_{f.bot}, t_{c.ssp}, \alpha_{ssp}, f_{ssp}, h_{TG.w}, t_{TG.w}, b_{TG.bf}, t_{TG.bf}\right) \end{array}$$

6.3 Cross section class

In the preliminary design of the transverse girders the web is forced to be in cross section class 3. The following ratios needs to be lower than $h_{TG.w}/t_{TG.w}$ for this to be true. The bottom flange is also designed to be in cross section class 3 but this is done directly in the optimastion .

Web span section

$$\psi_{TG.span}\left(h_{c.ssp}, t_{f.top}, t_{f.bot}, t_{c.ssp}, \alpha_{ssp}, f_{ssp}, h_{TG.w}, t_{TG.w}, b_{TG.bf}, t_{TG.bf}\right) :=$$

$$-\frac{h_{TG.w} + h_{ssp.tot}\left(h_{c.ssp}, t_{f.top}, t_{f.bot}, t_{c.ssp}\right) - z_{na.TG}\left(h_{c.ssp}, t_{f.top}, t_{f.bot}, t_{c.ssp}, \alpha_{ssp}, f_{ssp}, h_{TG.w}, t_{TG.w}, b_{TG.bf}, t_{TG.bf}\right)}{z_{na.TG}\left(h_{c.ssp}, t_{f.top}, t_{f.bot}, t_{c.ssp}, \alpha_{ssp}, f_{ssp}, h_{TG.w}, t_{TG.w}, b_{TG.bf}, t_{TG.bf}\right) - h_{ssp.tot}\left(h_{c.ssp}, t_{f.top}, t_{f.bot}, t_{c.ssp}\right)}$$

$$\beta_{TG.web.span}\left(h_{c.ssp}, t_{f.top}, t_{f.bot}, t_{c.ssp}, \alpha_{ssp}, f_{ssp}, h_{TG.w}, t_{TG.w}, b_{TG.bf}, t_{TG.bf}\right) :=$$

$$\begin{cases} \dfrac{42\varepsilon_3}{0.67 + 0.33\cdot\psi_{TG.span}\left(h_{c.ssp}, t_{f.top}, t_{f.bot}, t_{c.ssp}, \alpha_{ssp}, f_{ssp}, h_{TG.w}, t_{TG.w}, b_{TG.bf}, t_{TG.bf}\right)} & \text{if } \psi_{TG.span}\left(h_{c.ssp}, t_{f.top}, t_{f.bot}, t_{c.ssp}, \alpha_{ssp}, f_{ssp}, h_{TG.w}, t_{TG.w}, b_{TG.bf}, t_{TG.bf}\right) > -1 \\ 62\cdot\varepsilon_3\cdot\left(1 - \psi_{TG.span}\left(h_{c.ssp}, t_{f.top}, t_{f.bot}, t_{c.ssp}, \alpha_{ssp}, f_{ssp}, h_{TG.w}, t_{TG.w}, b_{TG.bf}, t_{TG.bf}\right)\right)\cdot\sqrt{-\psi_{TG.span}\left(h_{c.ssp}, t_{f.top}, t_{f.bot}, t_{c.ssp}, \alpha_{ssp}, f_{ssp}, h_{TG.w}, t_{TG.w}, b_{TG.bf}, t_{TG.bf}\right)} & \text{otherwise} \end{cases}$$

Web support section

$$\psi_{TG.support}\left(h_{c.ssp}, t_{f.top}, t_{f.bot}, t_{c.ssp}, \alpha_{ssp}, f_{ssp}, h_{TG.w}, t_{TG.w}, b_{TG.bf}, t_{TG.bf}\right) :=$$

$$-\frac{z_{na.TG}\left(h_{c.ssp}, t_{f.top}, t_{f.bot}, t_{c.ssp}, \alpha_{ssp}, f_{ssp}, h_{TG.w}, t_{TG.w}, b_{TG.bf}, t_{TG.bf}\right) - h_{ssp.tot}\left(h_{c.ssp}, t_{f.top}, t_{f.bot}, t_{c.ssp}\right)}{h_{TG.w} + h_{ssp.tot}\left(h_{c.ssp}, t_{f.top}, t_{f.bot}, t_{c.ssp}\right) - z_{na.TG}\left(h_{c.ssp}, t_{f.top}, t_{f.bot}, t_{c.ssp}, \alpha_{ssp}, f_{ssp}, h_{TG.w}, t_{TG.w}, b_{TG.bf}, t_{TG.bf}\right)}$$

$$\beta_{TG.web.support}\left(h_{c.ssp}, t_{f.top}, t_{f.bot}, t_{c.ssp}, \alpha_{ssp}, f_{ssp}, h_{TG.w}, t_{TG.w}, b_{TG.bf}, t_{TG.bf}\right) :=$$

$$\begin{cases} \dfrac{42\varepsilon_3}{0.67 + 0.33\cdot\psi_{TG.support}\left(h_{c.ssp}, t_{f.top}, t_{f.bot}, t_{c.ssp}, \alpha_{ssp}, f_{ssp}, h_{TG.w}, t_{TG.w}, b_{TG.bf}, t_{TG.bf}\right)} & \text{if } \psi_{TG.support}\left(h_{c.ssp}, t_{f.top}, t_{f.bot}, t_{c.ssp}, \alpha_{ssp}, f_{ssp}, h_{TG.w}, t_{TG.w}, b_{TG.bf}, t_{TG.bf}\right) > -1 \\ 62\cdot\varepsilon_3\cdot\left(1 - \psi_{TG.support}\left(h_{c.ssp}, t_{f.top}, t_{f.bot}, t_{c.ssp}, \alpha_{ssp}, f_{ssp}, h_{TG.w}, t_{TG.w}, b_{TG.bf}, t_{TG.bf}\right)\right)\cdot\sqrt{-\psi_{TG.support}\left(h_{c.ssp}, t_{f.top}, t_{f.bot}, t_{c.ssp}, \alpha_{ssp}, f_{ssp}, h_{TG.w}, t_{TG.w}, b_{TG.bf}, t_{TG.bf}\right)} & \text{otherwise} \end{cases}$$

6.4. Bending stress in bottom flange

Loads

The transverse girder is desiged in ULS using equation 6.10b in EN 1990 since this gives the highest variable laod

$\gamma_{G} \cdot \xi \cdot G + \gamma_{Q.1} \cdot Q$ (6.10b)

The load case used are shown in the figure below. It is assumed that the transverse girder carries all load from traffic and self-weight of the SSP from an area corresponding to L_1 x B_{tot}

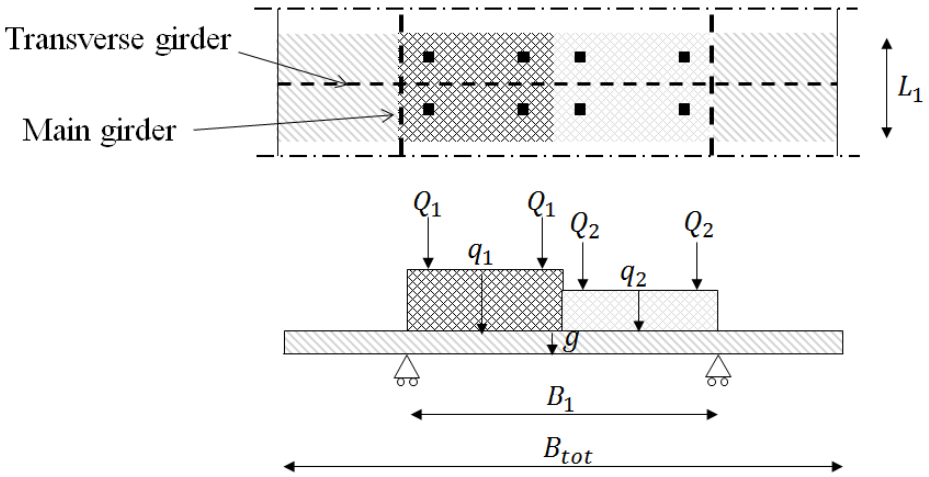

Self-weight

Cantilever part:

$g_{TG.cant}(h_{c.ssp}, t_{f.top}, t_{f.bot}, t_{c.ssp}, \alpha_{ssp}, f_{ssp}, h_{TG.w}, t_{TG.w}, b_{TG.bf}, t_{TG.bf}) :=$

$$\gamma_{G} \cdot \xi \cdot \left(\begin{matrix} A_{ssp}(h_{c.ssp}, t_{f.top}, t_{f.bot}, t_{c.ssp}, \alpha_{ssp}, f_{ssp}) \cdot L_1 \dots \\ + t_{TG.w} \cdot 0.4 \cdot h_{TG.w} + b_{TG.bf} \cdot t_{TG.bf} + t_{TG.w} \cdot 0.6 \cdot h_{TG.w} \end{matrix} \right) \cdot g \cdot \rho$$

Middle part:

$$g_{TG.mid}\left(h_{c.ssp}, t_{f.top}, t_{f.bot}, t_{c.ssp}, \alpha_{ssp}, f_{ssp}, h_{TG.w}, t_{TG.w}, b_{TG.bf}, t_{TG.bf}\right) :=$$

$$\gamma_G \cdot \xi \cdot \left(\begin{array}{l} A_{ssp}\left(h_{c.ssp}, t_{f.top}, t_{f.bot}, t_{c.ssp}, \alpha_{ssp}, f_{ssp}\right) \cdot L_1 \cdots \\ + A_{TG.mid}\left(h_{c.ssp}, t_{f.top}, t_{f.bot}, \alpha_{ssp}, f_{ssp}, h_{TG.w}, t_{TG.w}, b_{TG.bf}, t_{TG.bf}\right) \end{array} \right) \cdot g \cdot \rho$$

Traffic load

Two lanes between main girders

$q_{TG.1} := \gamma_{Q.1} \cdot q_{1k} \cdot L_1 = 108 \cdot \frac{kN}{m}$ Lane 1

$q_{TG.2} := \gamma_{Q.1} \cdot q_{2k} \cdot L_1 = 30 \cdot \frac{kN}{m}$ Lane 2

Wheel loads

$Q_{TG.1} := \gamma_{Q.1} \cdot Q_{1k} = 450 \cdot kN$ One axel lane 1

$Q_{TG.2} := \gamma_{Q.1} \cdot Q_{2k} = 300 \cdot kN$ One axel lane 2

$d_{axel.LM1} = 1.2\,m$ Distance between axels

$d_{wheel.LM1} = 2\,m$ Distance between wheels

$w_{lane} = 3\,m$ Width of traffic lanes

Moment

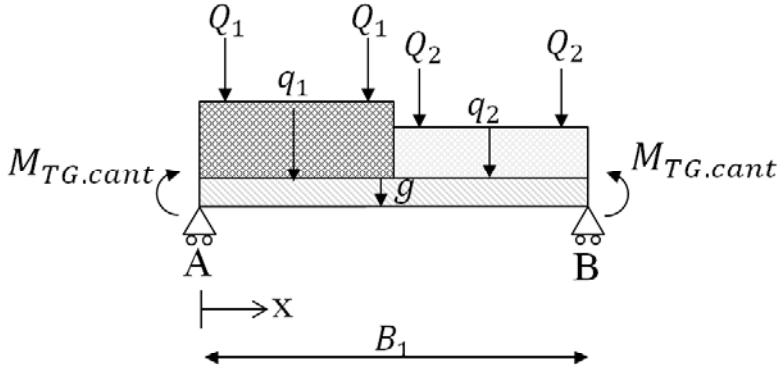

The maximum moment in the span of the transverse girder are calculated by treating it as a simply supported beam with support moments from the weight of the cantilevering part

Support moment

The support moments are determined by the self-weight on the cantilever part, they are equal due to symmetry

$$M_{TG.cant}\left(h_{c.ssp}, t_{f.top}, t_{f.bot}, t_{c.ssp}, \alpha_{ssp}, f_{ssp}, h_{TG.w}, t_{TG.w}, b_{TG.bf}, t_{TG.bf}\right) :=$$

$$-\gamma_G \cdot \xi \cdot \left(A_{ssp}\left(h_{c.ssp}, t_{f.top}, t_{f.bot}, t_{c.ssp}, \alpha_{ssp}, f_{ssp}\right) \cdot L_1 \cdot \frac{L_{cant}^2}{2} + t_{TG.w} \cdot 0.4 \cdot h_{TG.w} \cdot \frac{L_{cant}^2}{2} + b_{TG.bf} \cdot t_{TG.bf} \cdot \frac{L_{cant}^2}{2} + t_{TG.w} \cdot 0.6 \cdot h_{TG.w} \cdot \frac{L_{cant}^2}{6} \right) \cdot g \cdot \rho$$

Span moment

Taking the moment equlibrium around A gives the reaction force at support B, R_B

$$R_B\left(h_{c.ssp}, t_{f.top}, t_{f.bot}, t_{c.ssp}, \alpha_{ssp}, f_{ssp}, h_{TG.w}, t_{TG.w}, b_{TG.bf}, t_{TG.bf}\right) :=$$

$$\frac{\begin{bmatrix} g_{TG.mid}\left(h_{c.ssp}, t_{f.top}, t_{f.bot}, t_{c.ssp}, \alpha_{ssp}, f_{ssp}, h_{TG.w}, t_{TG.w}, b_{TG.bf}, t_{TG.bf}\right) \cdot \frac{B_1^2}{2} \dots \\ + g_{TG.cant}\left(h_{c.ssp}, t_{f.top}, t_{f.bot}, t_{c.ssp}, \alpha_{ssp}, f_{ssp}, h_{TG.w}, t_{TG.w}, b_{TG.bf}, t_{TG.bf}\right) \cdot L_{cant} \cdot \left(B_1 + \frac{L_{cant}}{2}\right) \dots \\ + -g_{TG.cant}\left(h_{c.ssp}, t_{f.top}, t_{f.bot}, t_{c.ssp}, \alpha_{ssp}, f_{ssp}, h_{TG.w}, t_{TG.w}, b_{TG.bf}, t_{TG.bf}\right) \cdot \frac{L_{cant}^2}{2} \dots \\ + q_{TG.1} \cdot \frac{w_{lane}^2}{2} + q_{TG.2} \cdot w_{lane} \cdot \left(w_{lane} + \frac{w_{lane}}{2}\right) + Q_{TG.1} \cdot 0.5m + Q_{TG.1} \cdot \left(w_{lane} - 0.5m\right) \dots \\ + Q_{TG.2} \cdot \left(w_{lane} + 0.5m\right) + Q_{TG.2} \cdot \left(2 \cdot w_{lane} - 0.5m\right) \end{bmatrix}}{B_1}$$

Vertical equlibrium gives the reaction force at support A, R_A

$$R_A\left(h_{c.ssp}, t_{f.top}, t_{f.bot}, t_{c.ssp}, \alpha_{ssp}, f_{ssp}, h_{TG.w}, t_{TG.w}, b_{TG.bf}, t_{TG.bf}\right) :=$$

$$\begin{aligned} & g_{TG.mid}\left(h_{c.ssp}, t_{f.top}, t_{f.bot}, t_{c.ssp}, \alpha_{ssp}, f_{ssp}, h_{TG.w}, t_{TG.w}, b_{TG.bf}, t_{TG.bf}\right) \cdot B_1 \dots \\ & + 2\, g_{TG.cant}\left(h_{c.ssp}, t_{f.top}, t_{f.bot}, t_{c.ssp}, \alpha_{ssp}, f_{ssp}, h_{TG.w}, t_{TG.w}, b_{TG.bf}, t_{TG.bf}\right) \cdot L_{cant} \dots \\ & + q_{TG.1} \cdot w_{lane} + q_{TG.2} \cdot w_{lane} + 2 \cdot Q_{TG.1} + 2 \cdot Q_{TG.2} \dots \\ & + -R_B\left(h_{c.ssp}, t_{f.top}, t_{f.bot}, t_{c.ssp}, \alpha_{ssp}, f_{ssp}, h_{TG.w}, t_{TG.w}, b_{TG.bf}, t_{TG.bf}\right) \end{aligned}$$

Span moment calulated for different parts

The x-coordinate is starting from support A

Part 1: $0 < x < 0.5m$

$$M_{TG1}\left(h_{c.ssp}, t_{f.top}, t_{f.bot}, t_{c.ssp}, \alpha_{ssp}, f_{ssp}, h_{TG.w}, t_{TG.w}, b_{TG.bf}, t_{TG.bf}, x\right)$$

$$\begin{aligned} & R_A\left(h_{c.ssp}, t_{f.top}, t_{f.bot}, t_{c.ssp}, \alpha_{ssp}, f_{ssp}, h_{TG.w}, t_{TG.w}, b_{TG.bf}, t_{TG.bf}\right) \cdot x \dots \\ & + M_{TG.cant}\left(h_{c.ssp}, t_{f.top}, t_{f.bot}, t_{c.ssp}, \alpha_{ssp}, f_{ssp}, h_{TG.w}, t_{TG.w}, b_{TG.bf}, t_{TG.bf}\right) \dots \\ & + -\frac{q_{TG.1} \cdot x^2}{2} - \frac{g_{TG.mid}\left(h_{c.ssp}, t_{f.top}, t_{f.bot}, t_{c.ssp}, \alpha_{ssp}, f_{ssp}, h_{TG.w}, t_{TG.w}, b_{TG.bf}, t_{TG.bf}\right) \cdot x^2}{2} \end{aligned}$$

Part 2: 0.5< x < 2.5 m

$$M_{TG2}(h_{c.ssp}, t_{f.top}, t_{f.bot}, t_{c.ssp}, \alpha_{ssp}, f_{ssp}, h_{TG.w}, t_{TG.w}, b_{TG.bf}, t_{TG.bf}, x) :=$$
$$R_A(h_{c.ssp}, t_{f.top}, t_{f.bot}, t_{c.ssp}, \alpha_{ssp}, f_{ssp}, h_{TG.w}, t_{TG.w}, b_{TG.bf}, t_{TG.bf}) \cdot x \ldots$$
$$+ M_{TG.cant}(h_{c.ssp}, t_{f.top}, t_{f.bot}, t_{c.ssp}, \alpha_{ssp}, f_{ssp}, h_{TG.w}, t_{TG.w}, b_{TG.bf}, t_{TG.bf}) \ldots$$
$$+ -\frac{q_{TG.1} \cdot x^2}{2} - \frac{g_{TG.mid}(h_{c.ssp}, t_{f.top}, t_{f.bot}, t_{c.ssp}, \alpha_{ssp}, f_{ssp}, h_{TG.w}, t_{TG.w}, b_{TG.bf}, t_{TG.bf}) \cdot x^2}{2} \ldots$$
$$+ -Q_{TG.1} \cdot (x - 0.5m)$$

Part 3: 2.5< x < 3.0 m

$$M_{TG3}(h_{c.ssp}, t_{f.top}, t_{f.bot}, t_{c.ssp}, \alpha_{ssp}, f_{ssp}, h_{TG.w}, t_{TG.w}, b_{TG.bf}, t_{TG.bf}, x) :=$$
$$R_A(h_{c.ssp}, t_{f.top}, t_{f.bot}, t_{c.ssp}, \alpha_{ssp}, f_{ssp}, h_{TG.w}, t_{TG.w}, b_{TG.bf}, t_{TG.bf}) \cdot x \ldots$$
$$+ M_{TG.cant}(h_{c.ssp}, t_{f.top}, t_{f.bot}, t_{c.ssp}, \alpha_{ssp}, f_{ssp}, h_{TG.w}, t_{TG.w}, b_{TG.bf}, t_{TG.bf}) \ldots$$
$$+ -\frac{q_{TG.1} \cdot x^2}{2} - \frac{g_{TG.mid}(h_{c.ssp}, t_{f.top}, t_{f.bot}, t_{c.ssp}, \alpha_{ssp}, f_{ssp}, h_{TG.w}, t_{TG.w}, b_{TG.bf}, t_{TG.bf}) \cdot x^2}{2} \ldots$$
$$+ -Q_{TG.1} \cdot (x - 0.5m) - Q_{TG.1} \cdot \left[x - (w_{lane} - 0.5m)\right]$$

Part 4: 3.0< x < 3.5 m

$$M_{TG4}(h_{c.ssp}, t_{f.top}, t_{f.bot}, t_{c.ssp}, \alpha_{ssp}, f_{ssp}, h_{TG.w}, t_{TG.w}, b_{TG.bf}, t_{TG.bf}, x) :=$$
$$R_A(h_{c.ssp}, t_{f.top}, t_{f.bot}, t_{c.ssp}, \alpha_{ssp}, f_{ssp}, h_{TG.w}, t_{TG.w}, b_{TG.bf}, t_{TG.bf}) \cdot x \ldots$$
$$+ M_{TG.cant}(h_{c.ssp}, t_{f.top}, t_{f.bot}, t_{c.ssp}, \alpha_{ssp}, f_{ssp}, h_{TG.w}, t_{TG.w}, b_{TG.bf}, t_{TG.bf}) \ldots$$
$$+ -q_{TG.1} \cdot w_{lane} \cdot \left(x - \frac{w_{lane}}{2}\right) - \frac{g_{TG.mid}(h_{c.ssp}, t_{f.top}, t_{f.bot}, t_{c.ssp}, \alpha_{ssp}, f_{ssp}, h_{TG.w}, t_{TG.w}, b_{TG.bf}, t_{TG.bf}) \cdot x^2}{2} \ldots$$
$$+ -Q_{TG.1} \cdot (x - 0.5m) - Q_{TG.1} \cdot \left[x - (w_{lane} - 0.5m)\right] - q_{TG.2} \cdot \frac{(x - w_{lane})^2}{2}$$

Maximum moment in span

Function that transform a range variale to a vector, needed to use max function in Mathcad

$$x_{vec}(s_1, s_2, e) :=$$
Count ← ORIGIN
for $i \in s_1, s_2 .. e$
  $Vec_{Count} \leftarrow i$
  Count ← Count + 1
Vec

Defining x-ranges

$n_{step} := 0.01m$ Step

$x_{TG1} := x_{vec}(0m, 0m + n_{step}, 0.5m)$

$x_{TG2} := x_{vec}(0.5m, 0.5m + n_{step}, 2.5m)$

$x_{TG3} := x_{vec}(2.5m, 2.5m + n_{step}, 3.0m)$

$x_{TG4} := x_{vec}(3.0m, 3.0m + n_{step}, 3.5m)$

Finding maximum moment

By testing the maximum moment was found to be in the range 2.5<x<3.0

$M_{TG.max}(h_{c.ssp}, t_{f.top}, t_{f.bot}, t_{c.ssp}, \alpha_{ssp}, f_{ssp}, h_{TG.w}, t_{TG.w}, b_{TG.bf}, t_{TG.bf})$

$$\max(M_{TG3}(h_{c.ssp}, t_{f.top}, t_{f.bot}, t_{c.ssp}, \alpha_{ssp}, f_{ssp}, h_{TG.w}, t_{TG.w}, b_{TG.bf}, t_{TG.bf}, x_{TG3}))$$

Bending stress

$\sigma_{TG.bf}(h_{c.ssp}, t_{f.top}, t_{f.bot}, t_{c.ssp}, \alpha_{ssp}, f_{ssp}, h_{TG.w}, t_{TG.w}, b_{TG.bf}, t_{TG.bf}) :=$

$$\frac{M_{TG.max}(h_{c.ssp}, t_{f.top}, t_{f.bot}, t_{c.ssp}, \alpha_{ssp}, f_{ssp}, h_{TG.w}, t_{TG.w}, b_{TG.bf}, t_{TG.bf})}{I_{TG}(h_{c.ssp}, t_{f.top}, t_{f.bot}, t_{c.ssp}, \alpha_{ssp}, f_{ssp}, h_{TG.w}, t_{TG.w}, b_{TG.bf}, t_{TG.bf})} \cdot \left(\begin{matrix} h_{ssp.tot}(h_{c.ssp}, t_{f.top}, t_{f.bot}, t_{c.ssp}) + h_{TG.w} + t_{TG.bf} \cdots \\ + -z_{na.TG}(h_{c.ssp}, t_{f.top}, t_{f.bot}, t_{c.ssp}, \alpha_{ssp}, f_{ssp}, h_{TG.w}, t_{TG.w}, b_{TG.bf}, t_{TG.bf}) \end{matrix} \right)$$

7. Total steel volume in bridge section

SSP

$$V_{ssp}(h_{c.ssp}, t_{f.top}, t_{f.bot}, t_{c.ssp}, \alpha_{ssp}, f_{ssp}) := A_{ssp}(h_{c.ssp}, t_{f.top}, t_{f.bot}, t_{c.ssp}, \alpha_{ssp}, f_{ssp}) \cdot B_{tot}$$

Main girders

$$V_{MG}(b_{MG.bf}, t_{MG.bf}, t_{MG.w}) := 2 \cdot \left(A_{MG.bf}(b_{MG.bf}, t_{MG.bf}) + A_{MG.w}(t_{MG.bf}, t_{MG.w})\right)$$

Transverse girders

Middle part :

$$V_{TG.mid}(h_{TG.w}, t_{TG.w}, b_{TG.bf}, t_{TG.bf}) := B_1 \cdot \left(h_{TG.w} \cdot t_{TG.w} + b_{TG.bf} \cdot t_{TG.bf}\right)$$

Cantilever part :

$$L_{TG.edge}(h_{TG.w}) := \sqrt{(L_{cant})^2 + (0.6 \cdot h_{TG.w})^2}$$

$$V_{TG.edge}(h_{TG.w}, t_{TG.w}, b_{TG.bf}, t_{TG.bf}) := L_{cant} \cdot \frac{0.4 h_{TG.w} + h_{TG.w}}{2} \cdot t_{TG.w} + L_{TG.edge}(h_{TG.w}) \cdot b_{TG.bf} \cdot t_{TG.bf}$$

Total volume:

$$V_{TG}(h_{TG.w}, t_{TG.w}, b_{TG.bf}, t_{TG.bf}) := \frac{V_{TG.mid}(h_{TG.w}, t_{TG.w}, b_{TG.bf}, t_{TG.bf}) + 2\, V_{TG.edge}(h_{TG.w}, t_{TG.w}, b_{TG.bf}, t_{TG.bf})}{L_1}$$

Total volume of bridge section per unit length

$$V_{tot}(h_{c.ssp}, t_{f.top}, t_{f.bot}, t_{c.ssp}, \alpha_{ssp}, f_{ssp}, b_{MG.bf}, t_{MG.bf}, t_{MG.w}, h_{TG.w}, t_{TG.w}, b_{TG.bf}, t_{TG.bf}) :$$

$$V_{ssp}(h_{c.ssp}, t_{f.top}, t_{f.bot}, t_{c.ssp}, \alpha_{ssp}, f_{ssp}) \cdots$$
$$+ V_{MG}(b_{MG.bf}, t_{MG.bf}, t_{MG.w}) \cdots$$
$$+ V_{TG}(h_{TG.w}, t_{TG.w}, b_{TG.bf}, t_{TG.bf})$$

8. Optimisation

In the optimisation the cross-secional area of the SSP was minimised within given constraints. Furthemore, preliminary dimensions of the main and transverse girder were calculated for the optimised SSP.

$CTOL := 1 \cdot 10^{-6}$ Tolerance the minimising iteration

8.1. SSP

Definition of constraints

$w \le \frac{\min(B_1, L_1)}{400}$ The global deflection in the mid span should be limited to the shortest of B_1 and L_1 divided by 400.

$\frac{l_{c.ssp}}{t_{c.ssp}} \le 42 \cdot \varepsilon_3$

$\frac{l_o}{t_{f.top}} \le 42 \cdot \varepsilon_3$ Maximum width to thickness ratios for compression parts must be in cross-section class 3.

$\frac{l_o}{t_{f.bot}} \le 42 \varepsilon_3$

$20mm \le f_{ssp}$ The length of the horizontal corrugated segment has to be a small as possible to minimize the resulting moments which cause local buckling in the face plate.

$\delta_I \le \frac{l_{ssp}}{400}$ The local deflection of the top plate needs to fulfill the required control l.ssp/400. Taken from TRVFS 2011:12, pg. 64.

$71MPa \ge \frac{q_{w.LM3} \cdot l_{ssp}^2}{1m \cdot 2 \cdot t_{f.top}^2}$ To check the fatigue strength of the welded joints the stress in the joints needs to be less than the stress value from the detail category given in EN_1993-1-9. There is no detail category in Eurocode for the laser weld detail connection that is used in a SSP so 71MPa is taken as a reference since it's a reasonable stress value used for toe cracking of weld. Load Model 3 was used for the fatigue loads acting on the deck.

Calculating deflection limit

Shortest of B_1 and L_1

$$\delta_{lim.mid} := \begin{cases} \delta_{lim.mid} \leftarrow \frac{B_1}{400 \cdot 0.78} & \text{if } B_1 \le L_1 \\ \delta_{lim.mid} \leftarrow \frac{L_1}{400 \cdot 0.78} & \text{otherwise} \end{cases}$$

Minimising SSP area

Predefined values

$h_{c.ssp} := 180mm$ $t_{f.top} := 7mm$ $\alpha_{ssp} := 65 \cdot deg$

$t_{c.ssp} := 7mm$ $t_{f.bot} := 7mm$ $f_{ssp} := 20mm$

Constraints

Given

$$0 \le \frac{l_o(h_{c.ssp}, \alpha_{ssp}, f_{ssp})}{t_{f.bot}} \le 42\varepsilon_3 \qquad 0 \le \frac{l_o(h_{c.ssp}, \alpha_{ssp}, f_{ssp})}{t_{f.top}} \le 42\varepsilon_3$$

$$0 \le \frac{l_{c.ssp}(h_{c.ssp}, \alpha_{ssp})}{t_{c.ssp}} \le 42 \cdot \varepsilon_3$$

$20mm \le f_{ssp}$

$$w_{tot}(h_{c.ssp}, t_{f.top}, t_{f.bot}, t_{c.ssp}, \alpha_{ssp}, f_{ssp}) \le \delta_{lim.mid}$$

$$71MPa \ge \frac{q_{w.LM3} \cdot l_{ssp}(h_{c.ssp}, \alpha_{ssp}, f_{ssp})^2}{\left(1m\, t_{f.top}^{\,2} \cdot 2\right)}$$

$$\frac{l_{ssp}(h_{c.ssp}, \alpha_{ssp}, f_{ssp})}{400} \ge \delta_I(h_{c.ssp}, t_{f.top}, \alpha_{ssp}, f_{ssp})$$

Minimising SSP area

$$\begin{pmatrix} h_{c.sspA} \\ t_{f.topA} \\ t_{f.botA} \\ t_{c.sspA} \\ \alpha_{sspA} \\ f_{sspA} \end{pmatrix} := \text{Minimize}(V_{ssp}, h_{c.ssp}, t_{f.top}, t_{f.bot}, t_{c.ssp}, \alpha_{ssp}, f_{ssp})$$

8.2. Main girders

Definition of constraints

$w_{span1} \leq \frac{L_{span1}}{400}$

$w_{span2} \leq \frac{L_{span2}}{400}$

The deflections in span1 and span2 are limited to L/400

$t_{MG.w} = 18mm$

The web of the main girder of the web was fixed to 18mm, which was used in the composite bridge over Bergforsen. With this thickness the web is in CSC 4, and a reduction of the area should be made. This area reduction is omitted since the purpose of preliminary design of the main girders only is to estimate of the steel volume of the bridge.

$\frac{\frac{b_{MG.bf} - t_{MG.w}}{2}}{t_{MG.bf}} = 14 \cdot \varepsilon_3$

The web and bottom flange of the main girder must be in cross section class 3.

Minimising area of main girders

Predefined values

$b_{MG.bf} := 800mm \quad t_{MG.bf} := 18mm \quad t_{MG.w} := 20mm$

Constraints

Given

$w_{span1}\left(h_{c.sspA}, t_{f.topA}, t_{f.botA}, t_{c.sspA}, \alpha_{sspA}, f_{sspA}, b_{MG.bf}, t_{MG.bf}, t_{MG.w}\right) \leq \frac{L_{span1}}{400}$

$w_{span2}\left(h_{c.sspA}, t_{f.topA}, t_{f.botA}, t_{c.sspA}, \alpha_{sspA}, f_{sspA}, b_{MG.bf}, t_{MG.bf}, t_{MG.w}\right) \leq \frac{L_{span2}}{400}$

$t_{MG.w} = 18mm$

$\frac{\frac{b_{MG.bf} - t_{MG.w}}{2}}{t_{MG.bf}} = 14 \cdot \varepsilon_3$

Minimising area of main girders within given constraints

$$\begin{pmatrix} b_{MG.bfA} \\ t_{MG.bfA} \\ t_{MG.wA} \end{pmatrix} := \text{Minimize}\left(V_{MG}, b_{MG.bf}, t_{MG.bf}, t_{MG.w}\right)$$

8.3. Transverse girders

Definition of constraints

$\sigma_{TG.bf} \le f_y$ The stress in the bottom flange must be below the yield stress

$\frac{h_{TG.w}}{t_{TG.w}} \le \beta_{TG}$

$\frac{\frac{b_{TG.bf} - t_{TG.w}}{2}}{t_{TG.bf}} = 14 \cdot \varepsilon_3$ The web and bottom flange of the main girder must be in cross section class 3.

Minimising area of transverse girders

Predefined values

$h_{TG.w} := 1100mm \quad b_{TG.bf} := 233mm \quad t_{TG.bf} := 4.6mm \quad t_{TG.w} := 9mm$

Constraints

Given

$$0 \le \frac{h_{TG.w}}{t_{TG.w}} \le \beta_{TG.web.span}\left(h_{c.sspA}, t_{f.topA}, t_{f.botA}, t_{c.sspA}, \alpha_{sspA}, f_{sspA}, h_{TG.w}, t_{TG.w}, b_{TG.bf}, t_{TG.bf}\right)$$

$$0 \le \frac{h_{TG.w}}{t_{TG.w}} \le \beta_{TG.web.support}\left(h_{c.sspA}, t_{f.topA}, t_{f.botA}, t_{c.sspA}, \alpha_{sspA}, f_{sspA}, h_{TG.w}, t_{TG.w}, b_{TG.bf}, t_{TG.bf}\right)$$

$$\frac{\frac{b_{TG.bf} - t_{TG.w}}{2}}{t_{TG.bf}} = 14 \cdot \varepsilon_3$$

$$\sigma_{TG.bf}\left(h_{c.sspA}, t_{f.topA}, t_{f.botA}, t_{c.sspA}, \alpha_{sspA}, f_{sspA}, h_{TG.w}, t_{TG.w}, b_{TG.bf}, t_{TG.bf}\right) < f_y$$

Minimising area of transverse girders within given constraints

$$\begin{pmatrix} h_{TG.wA} \\ t_{TG.wA} \\ b_{TG.bfA} \\ t_{TG.bfA} \end{pmatrix} := \text{Minimize}\left(V_{TG}, h_{TG.w}, t_{TG.w}, b_{TG.bf}, t_{TG.bf}\right)$$

9. Elastic constants for SSP

9.1. Change in dimensions of SSP

The plate thicknesses of the chosen configuration are rounded up to whole or half millimeters. The new dimensions are checked to fulfill the given requirements. $t_{f.top}$ was changed to 7 mm since the FE-analysis showed that 6.5 mm did not provide enough capaciy for local stress under wheel loads.

Change in dimensions

$h_{c.ssp}$	$t_{f.top}$	$t_{f.bot}$
$n_{hc} := 146mm - h_{c.sspA}$	$n_{ttop} := 7.0mm - t_{f.topA}$	$n_{tbot} := 5.5mm - t_{f.botA}$
$t_{c.ssp}$	α_{ssp}	f_{ssp}
$n_{tc} := 5mm - t_{c.sspA}$	$n_{\alpha} := 1.094414 - \alpha_{sspA}$	$n_f := 0mm$

New dimensions	Dimensions from the optimisation
$h_{c.sspN} := h_{c.sspA} + n_{hc} = 146 \cdot mm$	$h_{c.sspA} = 145.4607 \cdot mm$
$t_{f.topN} := t_{f.topA} + n_{ttop} = 7 \cdot mm$	$t_{f.topA} = 6.497 \cdot mm$
$t_{f.botN} := t_{f.botA} + n_{tbot} = 5.5 \cdot mm$	$t_{f.botA} = 5.188 \cdot mm$
$t_{c.sspN} := t_{c.sspA} + n_{tc} = 5 \cdot mm$	$t_{c.sspA} = 4.839 \cdot mm$
$\alpha_{sspN} := \alpha_{sspA} + n_{\alpha} = 1.094$	$\alpha_{sspA} = 1.075191$
$\alpha_{sspN} \cdot \frac{180}{\pi} = 62.705$	$\alpha_{sspA} \cdot \frac{180}{\pi} = 61.604$
$f_{sspN} := f_{sspA} + n_f = 20 \cdot mm$	$f_{sspA} = 20 \cdot mm$

9.2 Elastic constants

All the elastic constants are calulated per unit width

Axial stiffness parallel to the corrugation:

$$E_{xN} := E_{x.ssp}\left(h_{c.sspN}, t_{f.topN}, t_{f.botN}, t_{c.sspN}, \alpha_{sspN}, f_{sspN}\right) = 4.655 \times 10^{9} \cdot \frac{N}{m}$$

Axial stiffness perpendicular to the corrugation:

$$E_{yN} := E_{y.ssp}\left(h_{c.sspN}, t_{f.topN}, t_{f.botN}, t_{c.sspN}, \alpha_{sspN}, f_{sspN}\right) = 2.732 \times 10^{9} \cdot \frac{N}{m}$$

Horizontal shear stiffness:

$$G_{xyN} := G_{xy}\left(h_{c.sspN}, t_{f.topN}, t_{f.botN}, t_{c.sspN}, \alpha_{sspN}, f_{sspN}\right) = 1.219 \times 10^{9} \cdot \frac{N}{m}$$

Bending stiffness parallel to the corrugation

$$D_{xN} := D_{x.ssp}\left(h_{c.sspN}, t_{f.topN}, t_{f.botN}, t_{c.sspN}, \alpha_{sspN}, f_{sspN}\right) = 2.05 \times 10^{7} \cdot N \cdot m$$

Bending stiffness perpendicular to the corrugation:

$$D_{yN} := D_{y.ssp}\left(h_{c.sspN}, t_{f.topN}, t_{f.botN}, t_{c.sspN}, \alpha_{sspN}, f_{sspN}\right) = 1.637 \times 10^{7} \cdot N \cdot m$$

Torsional stiffness:

$$D_{xyN} := D_{xy.ssp}\left(h_{c.sspN}, t_{f.topN}, t_{f.botN}, t_{c.sspN}, \alpha_{sspN}, f_{sspN}\right) = 1.233 \times 10^{7} \cdot N \cdot m$$

Transverse shear stiffness parallel to the corrugation

$$D_{QxN} := D_{Qx}\left(h_{c.sspN}, t_{f.topN}, t_{f.botN}, t_{c.sspN}, \alpha_{sspN}, f_{sspN}\right) = 5.684 \times 10^{8} \cdot \frac{N}{m}$$

Transverse shear stiffness perpendicular to the corrugation

$$D_{QyN} := D_{Qy}\left(h_{c.sspN}, t_{f.topN}, t_{f.botN}, t_{c.sspN}, \alpha_{sspN}, f_{sspN}\right) = 1.135 \times 10^{8} \cdot \frac{N}{m}$$

9.3. Additional constants

Engineering constants

The engineering constants are used when the SSP is modelled with the lamina model in Abaqus

Total height of SSP

From centreline top plate to centreline of bottom plate:

$$h_N := h_{ssp}\left(h_{c.sspN}, t_{f.topN}, t_{f.botN}, t_{c.sspN}\right) = 0.157\ m$$

Engineering constants

$$E_{xeN} := \frac{12 \cdot D_{xN}}{h_N^{3}} = 6.33 \times 10^{10} \cdot Pa$$

$$E_{yeN} := \frac{12 \cdot D_{yN}}{h_N^{3}} = 5.05 \times 10^{10} \cdot Pa$$

$$G_{xyeN} := \frac{6 \cdot D_{xyN}}{h_N^{3}} = 1.9 \times 10^{10} \cdot Pa$$

$$G_{xzeN} := \frac{D_{QxN}}{\left(\frac{5}{6}\right) \cdot h_N} = 4.337 \times 10^{9} \cdot Pa$$

$$G_{yzeN} := \frac{D_{QyN}}{\left(\frac{5}{6}\right) \cdot h_N} = 8.66 \times 10^{8} \cdot Pa$$

Area, center of gravity and moment of inertia SSP

The constants calculated here are needed for the check of the local stresses in the SSP and launching see Appendix B and Appendix C.

$$A_{sspN} := A_{ssp}\left(h_{c.sspN}, t_{f.topN}, t_{f.botN}, t_{c.sspN}, \alpha_{sspN}, f_{sspN}\right) = 0.022 \cdot \frac{m^{2}}{m}$$

Center of gravity

$$z_{na.sspN} := z_{na.ssp}\left(h_{c.sspN}, t_{f.topN}, t_{f.botN}, t_{c.sspN}, \alpha_{sspN}, f_{sspN}\right) = 0.074\,\text{m}$$

Moment of inertia

Parallel to the corrugation:

$$I_{ssp.xN} := I_{ssp.x}\left(h_{c.sspN}, t_{f.topN}, t_{f.botN}, t_{c.sspN}, \alpha_{sspN}, f_{sspN}\right) = 9.763 \times 10^{-5}\cdot\frac{\text{m}^4}{\text{m}}$$

Perpendicular to the corrugation:

$$I_{ssp.yN} := I_{ssp.y}\left(h_{c.sspN}, t_{f.topN}, t_{f.botN}, t_{c.sspN}, \alpha_{sspN}, f_{sspN}\right) = 7.644 \times 10^{-5}\cdot\frac{\text{m}^4}{\text{m}}$$

9.4 Control of new dimensions

The new dimensions are controlled for local deflection and cross section class

Local deflection

Length of cross-section (2p):

$$l_{sspN} := l_{ssp}\left(h_{c.sspN}, \alpha_{sspN}, f_{sspN}\right) = 190.678\cdot\text{mm}$$

Local deflection:

$$\delta_{IN} := \delta_I\left(h_{c.sspN}, t_{f.topN}, \alpha_{sspN}, f_{sspN}\right) = 0.344\cdot\text{mm}$$

Control

$$\delta_{IN} = 0.344\cdot\text{mm} \quad < \quad \frac{l_{sspN}}{400} = 0.477\cdot\text{mm} \quad \text{OK}$$

Cross section class

All parts of the SSP should be in CSC3

Length of the inclined leg of the core:

$$l_{c.sspN} := l_{c.ssp}\left(h_{c.sspN}, \alpha_{sspN}\right) = 164.292\cdot\text{mm}$$

Length of corrugation opening

$$l_{oN} := l_o\left(h_{c.sspN}, \alpha_{sspN}, f_{sspN}\right) = 170.678\cdot\text{mm}$$

Control

Corrugation	$\frac{l_{c.sspN}}{t_{c.sspN}} = 32.858$	<	$42\cdot\varepsilon_3 = 34.172$	OK
Top flange	$\frac{l_{oN}}{t_{f.topN}} = 24.383$	<	$42\cdot\varepsilon_3 = 34.172$	OK
Bottom flange	$\frac{l_{oN}}{t_{f.botN}} = 31.032$	<	$42\cdot\varepsilon_3 = 34.172$	OK

10. Steel volume

The steel volume of the SSP, main girders and transverse girders is calculated. This is done in order to see how different SSP configurations and distances between transverse girders affects the steel volume. The volume calculation is done for the optimised dimensions i.e before changes. The volume is calculated per unit length of the bridge.

Main girder dimensions

$$\begin{pmatrix} b_{MG.bfA} \\ t_{MG.bfA} \\ t_{MG.wA} \end{pmatrix} = \begin{pmatrix} 866.09 \\ 37.228 \\ 18 \end{pmatrix} \cdot mm$$

Transverse girder dimensions

$$\begin{pmatrix} h_{TG.wA} \\ t_{TG.wA} \\ b_{TG.bfA} \\ t_{TG.bfA} \end{pmatrix} = \begin{pmatrix} 557.455 \\ 5.798 \\ 370.103 \\ 16.081 \end{pmatrix} \cdot mm$$

Volume SSP:

$$V_{ssp}\left(h_{c.sspA}, t_{f.topA}, t_{f.botA}, t_{c.sspA}, \alpha_{sspA}, f_{sspA}\right) = 0.23375 \cdot \frac{m^3}{m}$$

Volume main girder:

$$V_{MG}\left(b_{MG.bfA}, t_{MG.bfA}, t_{MG.wA}\right) = 0.15674 \cdot \frac{m^3}{m}$$

Volume transverse girder:

$$V_{TG}\left(h_{TG.wA}, t_{TG.wA}, b_{TG.bfA}, t_{TG.bfA}\right) = 0.01231 \cdot \frac{m^3}{m}$$

Total steel volume:

$$V_{tot}\left(h_{c.sspA}, t_{f.topA}, t_{f.botA}, t_{c.sspA}, \alpha_{sspA}, f_{sspA}, b_{MG.bfA}, t_{MG.bfA}, t_{MG.wA}, h_{TG.wA}, t_{TG.wA}, b_{TG.bfA}, t_{TG.bfA}\right) = 0.403 \cdot \frac{m^3}{m}$$

11. Vector imported to FE-model

The elastic constants calculated in the optimisation swere used in FE-analyses, in which the SSP was modeled as an equivalent singel layer. Since a lot of different and configurations of the SSP wereanalysed the model was scripted. This section gives a vector of the results from the optimsiation, which can be saved as comma seperated values and imported to Abaqus.

The constants used in the vector are

V_N = [h.c.ssp t.f.top t.f.bot t.c.ssp α.ssp f.ssp A.ssp h Ex Ey Gxy D.x D.y D.xy D.Qx D.Qy Exe Eye Gxye Gxze Gyze w_mid w_cant]

Both the elastic stiffness constants and the engineering constants are included since both the general shell section and lamina model was used. The deflection in span w_mid and at the cantilever w_cant is put to zero in this vector. When the FE-analysis is finished the deflections are recorded and written to the two empty places.

$$V_N := \left(\frac{h_{c.sspN}}{mm} \; \frac{t_{f.topN}}{mm} \; \frac{t_{f.botN}}{mm} \; \frac{t_{c.sspN}}{mm} \; \alpha_{sspN} \; \frac{f_{sspN}}{mm} \; \frac{A_{sspN}}{m} \; \frac{h_N}{m} \; \frac{E_{xN}}{\frac{N}{m}} \; \frac{E_{yN}}{\frac{N}{m}} \; \frac{G_{xyN}}{\frac{N}{m}} \; \frac{D_{xN}}{N \cdot m} \; \frac{D_{yN}}{N \cdot m} \; \frac{D_{xyN}}{N \cdot m} \; \frac{D_{QxN}}{\frac{N}{m}} \; \frac{D_{QyN}}{\frac{N}{m}} \; \frac{E_{xeN}}{Pa} \; \frac{E_{yeN}}{Pa} \; \frac{G_{xyeN}}{Pa} \; \frac{G_{xzeN}}{Pa} \; \frac{G_{yzeN}}{Pa} \; 0 \; 0 \right)$$

Vector imported to FE-model

V_N =

	0	1	2	3	4
0	146	7	5.5	5	...

APPENDIX B

Local stresses in SSP

Appendix B- Local stresses in SSP

Contents

References

[1] *EN 1993-1-1*

[2] *EN 1993-1-5*

[3] *Formulations for the strength analsysis of all steel sandwich panels J. Romanoff and P.Kuljala*

[4] *TRVK BRO 2011*

[5] *Formulations for the strength analsysis of all steel sandwich panels J. Romanoff and P.Kuljala*

1. Input data

1.1. Geometry

Bridge

$B_{tot} := 11.25m$ Total free witdh of bridge

$L_1 := 8m$ Distance between transverse girders

$B_1 := 6m$ Distance between main girders

$L_{cant} := \frac{B_{tot} - B_1}{2} = 2.625\,m$ Length of cantilever part

$L_{span1} := 50m$ Length of side span

$L_{span2} := 66m$ Length of middle span

$L_{tot} := 2 \cdot L_{span1} + L_{span2} = 166\,m$ Total length of the bridge

SSP

$h_{c.ssp} := 146mm$

$t_{f.top} := 7.0mm$

$t_{f.bot} := 5.5mm$

$t_{c.ssp} := 5mm$

$\alpha_{ssp} := 1.094414$

$f_{ssp} := 20mm$

$h_{ssp1} := h_{c.ssp} + \frac{t_{f.top}}{2} + \frac{t_{f.bot}}{2} + t_{c.ssp} = 0.157\,m$

$h_{ssp} := h_{ssp1} + \frac{t_{f.top}}{2} + \frac{t_{f.bot}}{2} = 0.164\,m$ Total height of SSP (top topplate to bottom bottom plate)

$l_{buck} := \frac{h_{c.ssp}}{\tan(\alpha_{ssp})} \cdot 2 + f_{ssp} = 0.171\,m$ Lenght of corrugation opening

$p_{ssp} := \frac{l_{buck}}{2} + \frac{f_{ssp}}{2} = 0.095\,m$

$A_{ssp} := 0.022165\,\frac{m^2}{m}$ Cross-sectional area/unit width of SSP from optimisation

$z_{na.ssp} := 0.07355\ m = 0.074\,m$ Center of gravity SSP

$I_{x.ssp} := 9.461 \times 10^{-5}\,\frac{m^4}{m}$ Moment of inertia SSP

$I_{y.ssp} := 7.6441 \times 10^{-5} \frac{m^4}{m}$ Moment of inertia SSP

$l_o := \frac{h_{c.ssp}}{\tan(\alpha_{ssp})} \cdot 2 + f_{ssp} = 0.171\,m$ Lenght of corrugation opening

1.2. Material Properties

$\nu := 0.3$ Poisson's ratio

$\rho := 7850 \frac{kg}{m^3}$ Density of steel

$E := 210GPa$ Modulus of elasticity

$G_c := \frac{E}{2 \cdot (1 + \nu)} = 80.769 \cdot GPa$ Shear modulus of elasticity

$f_{y.f.top} := 460MPa$ Yield stress top plate of SSP

$f_{y.c} := 355MPa$ Yield stress corrugation of SSP

$f_{y.f.bot} := 355MPa$ Yield stress bottom plate of SSP

$\gamma_{M1} := 1.0$ Partial factor for instablity checks

1.3. Loads

Self-weight

$\gamma_g := 1.35$ Partial cofficeint for self-weight in ULS

$\xi := 0.89$ Reduction factor for self-weight

Asphalt cover

$t_{cover} := 50mm$ Thickness of the asphalt cover

$\gamma_{cover} := 23 \frac{kN}{m^3}$ Asphalt density in [kN/m^3] *[4] p45*

$g_{k.cover} := t_{cover} \cdot \gamma_{cover} = 1.15 \cdot \frac{kN}{m^2}$ Asphalt load

SSP

$g_{k.ssp} := \rho \cdot g \cdot A_{ssp} = 1.706 \cdot \frac{kN}{m^2}$

SSP and cover

$g_d := \xi \cdot \gamma_g \cdot (g_{k.ssp} + g_{k.cover}) = 3.432 \cdot \frac{kN}{m^2}$

Traffic load

$\gamma_Q := 1.5$ Partial factor variable load

UDL

$q_k := 9 \frac{kN}{m^2}$

$\alpha_q := 0.7$ Reduction factor for UDL traffic

$q_d := \gamma_Q \cdot \alpha_q \cdot q_k = 9.45 \cdot \frac{kN}{m^2}$

Axel load

$Q_k := 300kN$ One axel load

$\alpha_Q := 0.9$ Reduction factor for axel load

$Q_d := \gamma_Q \cdot \alpha_Q \cdot Q_k = 405 \cdot kN$

$d_{axel} := 2.0m$ Distance between axels

$w_{lane} := 3.0m$ Lane width

1.4. Results from FE-analysis

Normal stress component in top plateom bending in y-direction

$\sigma_{x.yn.top.FEM} := 126MPa$

Bending stress component in top plate from bending in y-direction

$\sigma_{x.yb.top.FEM} := 404MPa$

Normal force in y-direction in bottom plate of SSP, per unit width.

$N_{Ed.y.bot.FEM} := 617 \frac{kN}{m}$

Stress in the top plate from global bending

$\sigma_{x.f.top.FEM} := 196MPa$

2. Local stresses in top plate

The local stress in the top plate was obtained under the wheel load next to the main girder. The stress has two componets; normal stress from bending of the cantilever part of the SSP and local stress from bending of the top plate between corrugations. This control was made in order to se if it was possibe to include the local stress in the top plate as a constraint in the optimisation.

2.1. Normal stress from global bending over main

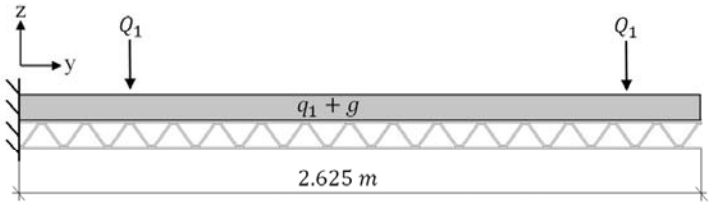

The SSP was treated as a cantilever fixed at the main girder. The stress under the wheel load closest to the main girder was calculated

Moment

Effecitve width of the SSP

$w_{beam} := 8.9m$ Assumed value

Moment

$$M(x) := \begin{cases} \left(q_d \cdot w_{beam} + g_d \cdot w_{beam}\right) \cdot \frac{x^2}{2} & \text{if } 0m \le x < 0.5m \\ \left(q_d \cdot w_{beam} + g_d \cdot w_{beam}\right) \cdot \frac{x^2}{2} + Q_d \cdot (x - 0.5m) & \text{if } 0.5m \le x < d_{axel} + 0.5m \\ \left(q_d \cdot w_{beam} + g_d \cdot w_{beam}\right) \cdot \frac{x^2}{2} + Q_d \cdot (x - 0.5m) + Q_d \cdot \left(x - 0.5m - d_{axel}\right) & \text{if } d_{axel} + 0.5m \le x \le L_{cant} \end{cases}$$

$M_B := M\left(d_{axel} + 0.5m\right) = 1.168 \times 10^{3} \cdot kN \cdot m$

Cross sectional constants

$I_{tot.y} := w_{beam} \cdot I_{y.ssp} = 6.803 \times 10^{-4} m^4$

Normal stress top plate

$W_{top} := \frac{I_{tot.y}}{z_{na.ssp}} = 9.25 \times 10^{-3} \cdot m^3$ Section modulus

$\sigma_{x.yn.top} := \frac{M_B}{W_{top}} = 126.303 \cdot MPa$

Normal stress from FE-analysis:

$\sigma_{x.yn.top.FEM} = 126\,MPa$

2.2. Local bending stress under wheel load

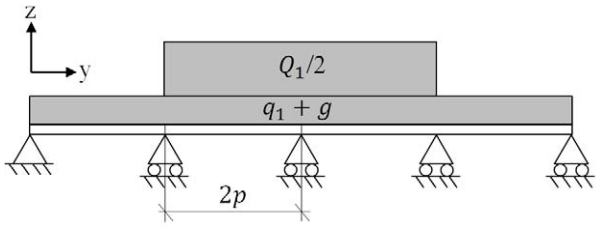

The local stress from bending was calcualted by treating the top plate as a continuous beam supported on the corrugation.

Moment

Belastningsfall		Max fältmoment (Faktor: qL^2)					Stödmoment (Faktor: qL^2)			
		M_1	M_2	M_3	M_4	M_5	M_B	M_C	M_D	M_E
4 fack	A 1 B 2 C 3 D 4 E	0,0772	0,0364	0,0364	0,0772		−0,1071	−0,0714	−0,1071	
			0,0561	0,0561			−0,0357	−0,1072	−0,0357	

The highest support moment was calulated using the beams shown in the table above.

$$M_{B.loc} := 0.0714 \cdot \left(q_d + \xi \cdot \gamma_g \cdot g_{k.cover}\right) \cdot \left(2 \cdot p_{ssp}\right)^2 + 0.1072 \cdot \left[\frac{Q_d}{(2 \cdot 0.5m \cdot 0.5m)}\right] \cdot \left(2 \cdot p_{ssp}\right)^2 = 3.185 \cdot \frac{kN \cdot m}{m}$$

Cross-sectional constant

$$W_{tf.top} := \frac{t_{f.top}^2}{6} = 8.167 \times 10^{-6} \cdot \frac{m^3}{m}$$

Stress from local bending in top plate

$$\sigma_{x.yb.top} := \frac{M_{B.loc}}{W_{tf.top}} = 390.021 \cdot MPa$$

Bending stress from FE-analysis:

$$\sigma_{x.yb.top.FEM} = 404\,MPa$$

3. Compressive stress in bottom plate

Due to bending of the SSP deck in the y-direction there is a risk of face wrinkling in the bottom plate of the SSP. The largest compresive force from the FE-model occured in the bottom plate next to the main girder, see figure below.

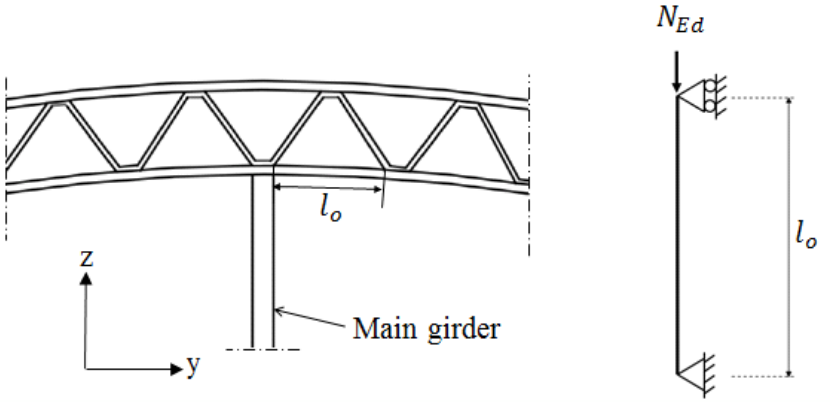

In order to calulated the buckling resistance of the bottom flange in the y-direction, it was treated as a simply supported column with length of one corrugation opening l_o.

3.1. Reduction factor for buckling

$A_{f.bot} := t_{f.bot} = 5.5 \times 10^{-3} \cdot \frac{m^2}{m}$ Cross section area of a unit width strip of the bottom plate

$I_{f.bot.y} := \frac{t_{f.bot}^3}{12} = 1.386 \times 10^{-8} \cdot \frac{m^4}{m}$ Moment of inertia

$N_{cr} := \frac{\pi^2 \cdot E \cdot I_{f.bot.y}}{l_o^2} = 986.438 \cdot \frac{kN}{m}$ Critical buckling force

$\alpha_{imp} := 0.49$ Imperfection factor for solid section buckling curve c *[1] Table 6.1*

$\lambda := \sqrt{\frac{A_{f.bot} \cdot f_{y.f.bot}}{N_{cr}}} = 1.407$ Slenderness *[1] (6.49)*

$\Phi_1 := 0.5 \cdot \left[1 + \alpha_{imp} \cdot (\lambda - 0.2) + \lambda^2\right] = 1.785$

$\chi_c := \frac{1}{\Phi_1 + \sqrt{\Phi_1^2 - \lambda^2}} = 0.347$ Reduction factor

$\chi_c := \begin{cases} 1 & \text{if } \chi_c \geq 1 \\ \chi_c & \text{otherwise} \end{cases} = 0.347$

3.2 Buckling resistance of bottom plate

Buckling resistance:

$$N_{b.Rd} := \frac{A_{f.bot} \cdot f_{y.f.bot} \cdot \chi_c}{\gamma_{M1}} = 676.887 \cdot \frac{kN}{m} \qquad [1] \ (6.47)$$

Normal force in y-direction from FE-analysis:

$$N_{Ed.y.bot.FEM} = 617 \cdot \frac{kN}{m}$$

$$\frac{N_{Ed.y.bot.FEM}}{N_{b.Rd}} = 0.912 \quad < 1.0$$

The bottom flange has sufficent capacity

4. Plastic collapse of corrugation

When the SSP is subjected to high patch loads from the wheels there is a risk for plastic collapse of the corrugation. The plastic collapse load can be determined from:

$$P_{plc}(\sigma_{ratio}) = 2\left[4\cdot\frac{M_t}{\beta} + 4\cdot\frac{M_w}{\beta}\cdot\left(\frac{k_1\cdot\beta\cdot c + \frac{M_t}{2\cdot M_w}}{1 + k_1\cdot k_3\cdot t_{c.ssp}}\right)\right]\cdot\left[1 - \left(\frac{\sigma_{x.f.top}}{f_{y.c}}\right)^2\right]^{0.5}$$

where:

$c := 0.5m$ Load lenght of the corrugation, in this case the length of one wheel

$f_{y.f.top} = 460\cdot MPa$ Yield stress top plate of SSP

$f_{y.c} = 355\cdot MPa$ Yield stress corrugation of SSP

$$M_t := \frac{f_{y.f.top}\cdot p_{ssp}\cdot t_{f.top}^2}{2} = 1.074\times 10^3\cdot N\cdot m$$ *[1] (187)*

$$M_w := \frac{f_{y.c}\cdot t_{c.ssp}^2}{4} = 2.219\times 10^3\,\frac{1}{m}\cdot N\cdot m$$ *[5] (188)*

$$I_t := \frac{p_{ssp}\cdot t_{f.top}^3}{6} = 5.45\times 10^{-9}\,m^4$$ *[5] (189)*

$$k_2 := \frac{M_t^2}{12\cdot E\cdot I_t\cdot M_w} = 0.038$$ *[5] (190)*

$$\phi := \operatorname{atan}\left(\frac{2\cdot k_2\cdot\sin(\alpha_{ssp})^2}{\sin(\alpha_{ssp})^2 - k_2^2}\right) = 0.076$$ *[5] (191)*

$$k_1 := \frac{f_{y.f.top}}{40\cdot t_{c.ssp}\cdot f_{y.c}}\cdot\sqrt{\frac{\sin(\alpha_{ssp})^2 - \sin(\phi)^2}{\sin(\phi)\cdot\cos(\phi)}} = 20.881\,\frac{1}{m}$$ *[5] (192)*

$$\beta := \sqrt{\frac{M_t}{4\cdot M_w\cdot k_1}} = 0.076\,m$$ *[5] (193)*

$$k_3 := \sqrt{\sin(\alpha_{ssp})^2 + \frac{27}{4}\cdot\cos(\alpha_{ssp})^2} = 1.486$$ *[5] (194)*

Plotting plastic collapse load

The plastic collapse load of the corrugation is plotted against the ratio between the stress in the top plate and yeild stress of the corrugation, in order to see how the stress in the top plate affects the plastic collapse load.

$$P_{plc}(\sigma_{ratio}) := 2\left[4\cdot\frac{M_t}{\beta} + 4\cdot\frac{M_w}{\beta}\cdot\left(\frac{k_1\cdot\beta\cdot c + \frac{M_t}{2\cdot M_w}}{1 + k_1\cdot k_3\cdot t_{c.ssp}}\right)\right]\cdot\left[1 - (\sigma_{ratio})^2\right]^{0.5} \qquad \textit{[5] (186)}$$

Function that transforms a range variale to a vector

$$x_{vec}(s_1, s_2, e) := \left|\begin{array}{l} Count \leftarrow ORIGIN \\ \text{for } i \in s_1, s_2 .. e \\ \quad \left|\begin{array}{l} Vec_{Count} \leftarrow i \\ Count \leftarrow Count + 1 \end{array}\right. \\ Vec \end{array}\right.$$

Creating vector with top plate stresses from 0 to the yield stress of the corrugation with steps of 1MPa

$$\sigma_{x.f.top.vec} := x_{vec}(0MPa, 1MPa, f_{y.c})$$

Ratio between top plate stress and yeild stress of corrugation

$$\sigma_{ratio} := \frac{\sigma_{x.f.top.vec}}{f_{y.c}}$$

Load from one wheel

The wheel load in ULS is included in the plot in order to see which ratio that is needed for the SSP to have sufficent capacity against plastic collapse.

$$P_{wheel} := \gamma_Q\cdot\alpha_Q\cdot\frac{Q_k}{2} = 202.5\cdot kN$$ One axel load

Ratio at which plastic collapse occures

Given

$\sigma_{ratio.int} := 0.1$ Start guess

$P_{plc}(\sigma_{ratio.int}) = P_{wheel}$

$\sigma_{ratio.int} := \text{Find}(\sigma_{ratio.int}) = 0.778$

The $\sigma_{x.f.top}/f_{y.c}$ ratio needs to be smaller than 0.778.

Plot

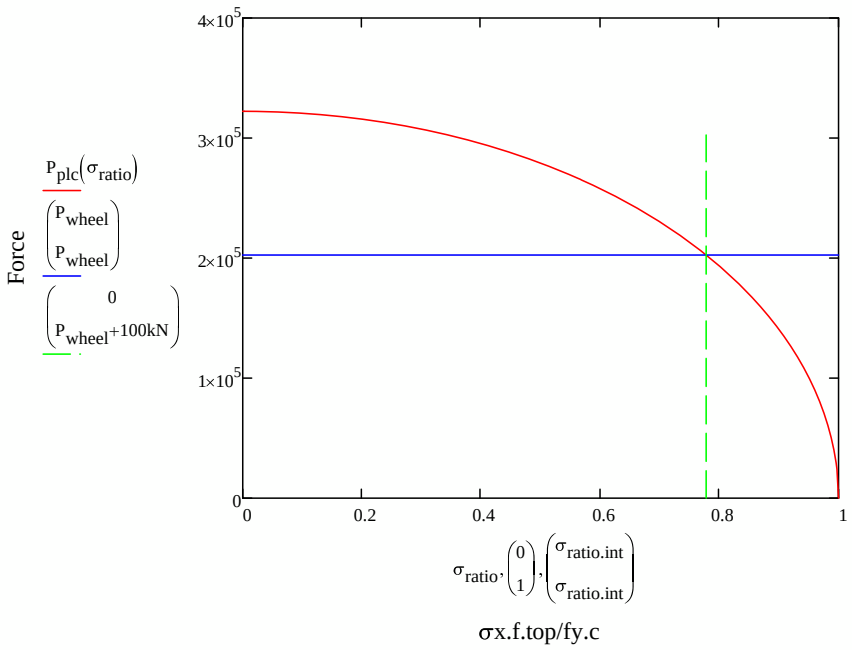

Plastic collapse load

With the stress in the top plate, obtained in FE-analysis

$\sigma_{x.f.top.FEM} = 196 \cdot MPa$

The plastic collapse load is:

$$P_{plc} := 2\left[4\cdot\frac{M_t}{\beta} + 4\cdot\frac{M_w}{\beta}\cdot\left(\frac{k_1\cdot\beta\cdot c + \frac{M_t}{2\cdot M_w}}{1 + k_1\cdot k_3\cdot t_{c.ssp}}\right)\right]\cdot\left[1 - \left(\frac{\sigma_{x.f.top.FEM}}{f_{y.c}}\right)^2\right]^{0.5} = 268.622\cdot kN$$

Giving the utilisation ratio of the SSP

$\frac{P_{wheel}}{P_{plc}} = 0.754$ <1.0 OK

APPENDIX C

Capacity during launching

Appendix C - Capacity during launching

Contents

References

[1] *EN 1993-1-1*

[2] *EN 1993-1-5*

1. Input Data

1.1 Geometry

Bridge

$B_{tot} := 11.25m$ Total free witdh of bridge

$B_{ssp} := 6m$ Distance between main girders

$L_{ssp} := 8.3m$ Distance between transverse girders

$L_{cant} := \frac{B_{tot} - B_{ssp}}{2} = 2.625\,m$ Length of cantilever part

$L_{span1} := 50m$ Length of side span

$L_{span2} := 66m$ Length of middle span

$L_{tot} := 2 \cdot L_{span1} + L_{span2} = 166\,m$ Total length of the bridge

SSP

$A_{ssp} := 0.022165\ \frac{m^2}{m}$ Cross-sectional area/unit width of SSP, from optimisation

$h_{c.ssp} := 146mm$

$t_{f.top} := 7.0mm$

$t_{f.bot} := 5.5mm$

$t_{c.ssp} := 5mm$

$\alpha_{ssp} := 1.094414$

$f_{ssp} := 20mm$

$h_{ssp1} := h_{c.ssp} + \frac{t_{f.top}}{2} + \frac{t_{f.bot}}{2} + t_{c.ssp} = 0.157\,m$

$h_{ssp} := h_{ssp1} + \frac{t_{f.top}}{2} + \frac{t_{f.bot}}{2} = 0.164\,m$ Total height of SSP (top topplate to bottom bottom plate)

$l_{buck} := \frac{h_{c.ssp}}{\tan(\alpha_{ssp})} \cdot 2 + f_{ssp} = 0.171\,m$ Lenght of corrugation oppening

$I_{x.ssp} := 9.461 \times 10^{-5}\ \frac{m^4}{m}$ Moment of inertia SSP

$z_{na.ssp} := 0.07355\ m + \frac{t_{f.top}}{2} = 0.077\,m$ Center of gravity mesaured from the top of the top plate

Main girder

The section used depends on the length of the launching nose and which support that is considered.

Support A		Support B	
Length of launching nose:	Main girder element:	Length of launching nose:	Main girder element:
0-6 m	4	0-1 m	6
6-21 m	3	1-11 m	5
		11-22 m	4

Element 3:

$b_{MG.bf.3} := 572mm$

$t_{MG.bf.3} := 44mm$

$h_{MG.w.3} := 2.6m - t_{MG.bf.3} = 2.556 \cdot m$

$t_{MG.w.3} := 21mm$

Element 4:

$b_{MG.bf.4} := 626mm$

$t_{MG.bf.4} := 63mm$

$h_{MG.w.4} := 2.6m - t_{MG.bf.4} = 2.537\,m$

$t_{MG.w.4} := 23mm$

Element 5:

$b_{MG.bf.5} := 544mm$

$t_{MG.bf.5} := 46mm$

$h_{MG.w.5} := 2.6m - t_{MG.bf.5} = 2.554 \cdot m$

$t_{MG.w.5} := 21mm$

Element 6:

$b_{MG.bf.6} := 490mm$

$t_{MG.bf.6} := 32mm$

$h_{MG.w.6} := 2.6m - t_{MG.bf.6} = 2.568 \cdot m$

$t_{MG.w.6} := 18mm$

$L_{LN} := \frac{L_{span1}}{4} = 12.5\,m$ Length of launching nose

Support A

$b_{MG.bf.A} := b_{MG.bf.3} = 572 \cdot mm$ Width bottom flange

$t_{MG.bf.A} := t_{MG.bf.3} = 44 \cdot mm$ Thickness bottom flange

$h_{MG.w.A} := h_{MG.w.3} = 2.556 \cdot m$ Height of web

$t_{MG.w.A} := t_{MG.w.3} = 21 \cdot mm$ Thickness of web

Support B

$b_{MG.bf.B} := b_{MG.bf.4} = 626 \cdot mm$ Width bottom flange

$t_{MG.bf.B} := t_{MG.bf.4} = 63 \cdot mm$ Thickness bottom flange

$h_{MG.w.B} := h_{MG.w.4} = 2.537 \cdot m$ Height of web

$t_{MG.w.B} := t_{MG.w.4} = 23 \cdot mm$ Thickness of web

Transverse girder

$h_{TG.w} := 557mm$

$t_{TG.w} := 7mm$

$b_{TG.bf} := 370mm$

$t_{TG.bf} := 16mm$

Edge beam

$h_{EB} := 402mm$

$b_{EB} := 300mm$

$t_{EB} := 20mm$

1.2. Material properties

$\nu := 0.3$ Poisson's ratio

$\rho_S := 7850 \frac{kg}{m^3}$ Density of steel

$E_s := 210GPa$ Modulus of elasticity steel

$G_c := \frac{E_s}{2 \cdot (1 + \nu)} = 80.769 \cdot GPa$ Shear modulus of elasticity steel

$f_y := 460MPa$ Yield strength

$\varepsilon_{bf} := \sqrt{\frac{235}{460}} = 0.715$

$\varepsilon_w := \sqrt{\frac{235}{355}} = 0.814$

$\gamma_{M0} := 1.0$ Partial coefficient for cross-section resistance checks

$\gamma_{M1} := 1.0$ Partial coefficient for instability checks

2. Loads

SSP

One girder with half of the SSP as top flange is considered.

$V_{ssp} := A_{ssp} \cdot \frac{B_{tot}}{2} = 0.125 \cdot \frac{m^3}{m}$ Volume per unit lenght of the bridge

$g_{k.ssp} := \rho_S \cdot g \cdot V_{ssp} = 9.598 \cdot \frac{kN}{m}$ Self -weight per unit length

Main girders

$V_{MG.tot} := 24.016 m^3$ Total volume of the main girders

$V_{MG} := \frac{V_{MG.tot}}{2 \cdot L_{tot}} = 0.072 \cdot \frac{m^3}{m}$ Average volume of one main girder per unit length of the bridge

$g_{k.MG} := \rho_S \cdot g \cdot V_{MG} = 5.569 \cdot \frac{kN}{m}$ Self-weight per unit length

Transverse girders and cross-bracings

$V_{TG.tot} := 3.777 m^3$ Total volume of the transverse girders and cross bracings

$V_{TG} := \frac{V_{TG.tot}}{2 \cdot L_{tot}} = 0.011 \cdot \frac{m^3}{m}$ Volume per unit length considering half of the transverse girders and cross bracings

$g_{k.TG} := \rho_S \cdot g \cdot V_{TG} = 0.876 \cdot \frac{kN}{m}$ Self-weight per unit length

Edge beams

$V_{EB.tot} := 4.528 m^3$ Total volume of the edge beams

$V_{EB} := \frac{V_{EB.tot}}{2 \cdot L_{tot}} = 0.014 \cdot \frac{m^3}{m}$ Volume per unit length considering one edge beam

$g_{k.EB} := \rho_S \cdot g \cdot V_{TG} = 0.876 \cdot \frac{kN}{m}$ Self-weight per unit length

Total self weight in ULS

$\gamma_G := 1.35$ Partial cofficient

$g_d := \gamma_G \cdot \left(g_{k.ssp} + g_{k.MG} + g_{k.TG} + g_{k.EB} \right) = 22.84 \cdot \frac{kN}{m}$

Weight launching nose

$g_{d.LN} := \gamma_G \cdot \frac{g_{k.MG}}{2} = 3.759 \cdot \frac{kN}{m}$

3. Moment and support reactions

The two load cases considerd are shown in the figure below

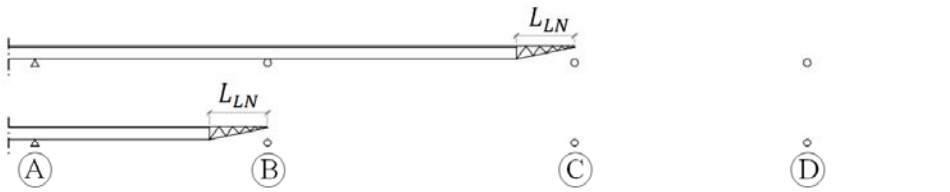

At support A

The moment and reaction force at support A is calculated right before the launching nose has reached support B.

Moment equlibrium around A gives

$$M_A := -g_d \cdot \frac{\left(L_{span1} - L_{LN}\right)^2}{2} - g_{d.LN} \cdot L_{LN} \cdot \left(L_{span1} - \frac{L_{LN}}{2}\right) = -1.811 \times 10^4 \cdot kN \cdot m$$

Vertical equlibrium gives

$$R_A := g_d \cdot \left(L_{span1} - L_{LN}\right) + g_{d.LN} \cdot L_{LN} = 903.473 \cdot kN$$

At support B

The moment and reaction force at support B is calculated right before the launching nose has reached support C

Moment equlibrium around B gives

$$M_B := -g_d \cdot \frac{\left(L_{span2} - L_{LN}\right)^2}{2} - g_{d.LN} \cdot L_{LN} \cdot \left(L_{span2} - \frac{L_{LN}}{2}\right) = -3.549 \times 10^4 \cdot kN \cdot m$$

Moment equlibrium around A gives

$$R_{B1} := \frac{\frac{g_d \cdot L_{span1}^2}{2} - M_B}{L_{span1}} = 1.281 \times 10^3 \cdot kN$$

$$R_{B2} := g_d \cdot \left(L_{span2} - L_{LN}\right) + g_{d.LN} \cdot L_{LN} = 1.269 \times 10^3 \cdot kN$$

$$R_B := R_{B1} + R_{B2} = 2.55 \times 10^3 \cdot kN$$

4. Resistance to patch loading

The reistance can be calulcated as

$$F_{Rd} = \frac{f_y \cdot L_{eff} \cdot t_w}{\gamma_{M1}}$$ *[2] (6.1)*

$s_s := 0.5m$ Assumed width of support

Effective loaded length

Support A:

$$m_{1.A} := \frac{f_y \cdot b_{MG.bf.A}}{f_y \cdot t_{MG.w.A}} = 27.238$$ *[2] (6.8)*

$m_{2.A} := 0$ λ_F <= 0.5

$$m_{2.A} := 0.02 \cdot \left(\frac{h_{MG.w.A}}{t_{MG.bf.A}}\right)^2 = 67.491$$ λ_F > 0.5 *[2] (6.9)*

$$l_{y.A} := s_s + 2 \cdot t_{MG.bf.A} \cdot \left(1 + \sqrt{m_{1.A} + m_{2.A}}\right) = 1.444\,m$$ *[2] (6.10)*

Support B:

$$m_{1.B} := \frac{f_y \cdot b_{MG.bf.B}}{f_y \cdot t_{MG.w.B}} = 27.217$$ *[2] (6.8)*

$m_{2.B} := 0$ λ_F <= 0.5

$$m_{2.B} := 0.02 \cdot \left(\frac{h_{MG.w.B}}{t_{MG.bf.B}}\right)^2 = 32.433$$ λ_F > 0.5 *[2] (6.9)*

$$l_{y.B} := s_s + 2 \cdot t_{MG.bf.B} \cdot \left(1 + \sqrt{m_{1.B} + m_{2.B}}\right) = 1.599\,m$$ *[2] (6.10)*

Reduction factor for effective length

Support A:

Theoretical critcal buckling stress

$k_{F.A} := 6$ No vertical stiffeners [2] Figure 6.1

$$F_{cr.A} := 0.9 \cdot k_{F.A} \cdot E_s \cdot \frac{t_{MG.w.A}^3}{h_{MG.w.A}} = 4.109 \times 10^3 \cdot kN$$

Relative slenderness

$$\lambda_{F.A} := \sqrt{\frac{l_{y.A} \cdot t_{MG.w.A} \cdot f_y}{F_{cr.A}}} = 1.843$$

$$\chi_{F.A} := \frac{0.5}{\lambda_{F.A}} = 0.271$$

Support B:

Theoretical critcal buckling stress

$k_{F.B} := 6$ No vertical stiffeners [2] Figure 6.1

$$F_{cr.B} := 0.9 \cdot k_{F.B} \cdot E_s \cdot \frac{t_{MG.w.B}^3}{h_{MG.w.B}} = 5.438 \times 10^3 \cdot kN$$

Relative slenderness

$$\lambda_{F.B} := \sqrt{\frac{l_{y.B} \cdot t_{MG.w.B} \cdot f_y}{F_{cr.B}}} = 1.764$$

$$\chi_{F.B} := \frac{0.5}{\lambda_{F.B}} = 0.283$$

Design resistance

Support A:

$L_{eff.A} := \chi_{F.A} \cdot l_{y.A} = 0.392\,m$ Effective length

$$F_{Rd.A} := \frac{f_y \cdot L_{eff.A} \cdot t_{MG.w.A}}{\gamma_{M1}} = 3.786 \times 10^3 \cdot kN$$

Support B:

$L_{eff.B} := \chi_{F.B} \cdot l_{y.B} = 0.453\,m$ Effective length

$$F_{Rd.B} := \frac{f_y \cdot L_{eff.B} \cdot t_{MG.w.B}}{\gamma_{M1}} = 4.796 \times 10^3 \cdot kN$$

5. Moment resistance

5.1. Cross-sectional constants

Area

Top flange, SSP

It is asssumed that no shear lag occurs.

$$A_{tf} := A_{ssp} \cdot \frac{B_{tot}}{2} = 0.125\,m^2$$

Web

$A_{w.A} := h_{MG.w.A} \cdot t_{MG.w.A} = 0.054\,m^2$ Support A

$A_{w.B} := h_{MG.w.B} \cdot t_{MG.w.B} = 0.058\,m^2$ Support B

Bottom flange

$A_{bf.A} := b_{MG.bf.A} \cdot t_{MG.bf.A} = 0.025\,m^2$ Support A

$A_{bf.B} := b_{MG.bf.B} \cdot t_{MG.bf.B} = 0.039\,m^2$ Support B

Total area

$A_{tot.A} := A_{tf} + A_{w.A} + A_{bf.A} = 0.204\,m^2$ Support A

$A_{tot.B} := A_{tf} + A_{w.B} + A_{bf.B} = 0.222\,m^2$ Support B

Center of gravity

Distances from top plate of SSP to each parts center of gravity

$z_{tf} := z_{na.ssp} = 0.077\,m$

Support A:

$$z_{w.A} := h_{ssp} + \frac{h_{MG.w.A}}{2} = 1.442\,m$$

$$z_{bf.A} := h_{ssp} + h_{MG.w.A} + \frac{t_{MG.bf.A}}{2} = 2.741\,m$$

$$z_{na.A} := \frac{A_{tf} \cdot z_{tf} + A_{w.A} \cdot z_{w.A} + A_{bf.A} \cdot z_{bf.A}}{A_{tot.A}} = 0.766\,m$$

Support B:

$$z_{w.B} := h_{ssp} + \frac{h_{MG.w.B}}{2} = 1.432\,\text{m}$$

$$z_{bf.B} := h_{ssp} + h_{MG.w.B} + \frac{t_{MG.bf.B}}{2} = 2.732\,\text{m}$$

$$z_{na.B} := \frac{A_{tf}\cdot z_{tf} + A_{w.B}\cdot z_{w.B} + A_{bf.B}\cdot z_{bf.B}}{A_{tot.B}} = 0.903\,\text{m}$$

Moment of inertia

Top flange

$$I_{tf.A} := I_{x.ssp}\cdot\frac{B_{tot}}{2} + A_{tf}\cdot\left(z_{na.A} - z_{tf}\right)^2 = 0.06\,\text{m}^4$$ Support A

$$I_{tf.B} := I_{x.ssp}\cdot\frac{B_{tot}}{2} + A_{tf}\cdot\left(z_{na.B} - z_{tf}\right)^2 = 0.086\,\text{m}^4$$ Support B

Web

$$I_{w.A} := \frac{t_{MG.w.A}\cdot h_{MG.w.A}^3}{12} + A_{w.A}\cdot\left(z_{na.A} - z_{w.A}\right)^2 = 0.054\,\text{m}^4$$ Support A

$$I_{w.B} := \frac{t_{MG.w.B}\cdot h_{MG.w.B}^3}{12} + A_{w.B}\cdot\left(z_{na.B} - z_{w.B}\right)^2 = 0.048\,\text{m}^4$$ Support B

Bottom flange

$$I_{bf.A} := \frac{b_{MG.bf.A}\cdot t_{MG.bf.A}^3}{12} + A_{bf.A}\cdot\left(z_{na.A} - z_{bf.A}\right)^2 = 0.098\,\text{m}^4$$ Support A

$$I_{bf.B} := \frac{b_{MG.bf.B}\cdot t_{MG.bf.B}^3}{12} + A_{bf.B}\cdot\left(z_{na.B} - z_{bf.B}\right)^2 = 0.132\,\text{m}^4$$ Support B

Whole section

$$I_A := I_{tf.A} + I_{w.A} + I_{bf.A} = 0.212\,\text{m}^4$$ Support A

$$I_B := I_{tf.B} + I_{w.B} + I_{bf.B} = 0.265\,\text{m}^4$$ Support B

5.2. Effective cross-sectional constants

Reduction factor web

Suppport A:

$$\psi_{MG.w.A} := -\frac{z_{na.A} - h_{ssp}}{h_{MG.w.A} + h_{ssp} - z_{na.A}} = -0.309$$

$$k_{\sigma.A} := 7.81 - 6.29\cdot\psi_{MG.w.A} + 9.78\cdot\psi_{MG.w.A}^{2} = 10.684$$

$$\lambda_{p.A} := \frac{\frac{h_{MG.w.A}}{t_{MG.w.A}}}{28.4\cdot\varepsilon_{w}\cdot\sqrt{k_{\sigma.A}}} = 1.612$$

$$\rho_A := \frac{\lambda_{p.A} - 0.055\cdot\left(3 + \psi_{MG.w.A}\right)}{\lambda_{p.A}^{2}} = 0.564$$

Suppport B:

$$\psi_{MG.w.B} := -\frac{z_{na.B} - h_{ssp}}{h_{MG.w.B} + h_{ssp} - z_{na.B}} = -0.411$$

$$k_{\sigma.B} := 7.81 - 6.29\cdot\psi_{MG.w.B} + 9.78\cdot\psi_{MG.w.B}^{2} = 12.054$$

$$\lambda_{p.B} := \frac{\frac{h_{MG.w.B}}{t_{MG.w.B}}}{28.4\cdot\varepsilon_{w}\cdot\sqrt{k_{\sigma.B}}} = 1.375$$

$$\rho_B := \frac{\lambda_{p.B} - 0.055\cdot\left(3 + \psi_{MG.w.B}\right)}{\lambda_{p.B}^{2}} = 0.652$$

Effective height of web

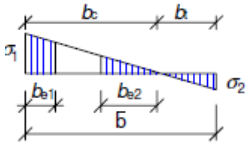

Support A:

$$h_{MG.w.A.e1} := 0.4\cdot\rho_A\cdot\frac{h_{MG.w.A}}{1 - \psi_{MG.w.A}} = 0.44\,\text{m}$$

$$h_{MG.w.A.e2} := 0.6\cdot\rho_A\cdot\frac{h_{MG.w.A}}{1 - \psi_{MG.w.A}} = 0.66\,\text{m}$$

Support B:

$$h_{MG.w.B.e1} := 0.4 \cdot \rho_B \cdot \frac{h_{MG.w.B}}{1 - \psi_{MG.w.B}} = 0.469\,m$$

$$h_{MG.w.B.e2} := 0.6 \cdot \rho_B \cdot \frac{h_{MG.w.B}}{1 - \psi_{MG.w.B}} = 0.703\,m$$

Area

Web

Support A:

$$A_{w.A.e1} := h_{MG.w.A.e1} \cdot t_{MG.w.A} = 9.245 \times 10^{-3}\,m^2$$

$$A_{w.A.e2} := \left(h_{MG.w.A} - \frac{h_{MG.w.A}}{1 - \psi_{MG.w.A}} + h_{MG.w.A.e2} \right) \cdot t_{MG.w.A} = 0.027\,m^2$$

Support B:

$$A_{w.B.e1} := h_{MG.w.B.e1} \cdot t_{MG.w.B} = 0.011\,m^2$$

$$A_{w.B.e2} := \left(h_{MG.w.B} - \frac{h_{MG.w.B}}{1 - \psi_{MG.w.B}} + h_{MG.w.B.e2} \right) \cdot t_{MG.w.B} = 0.033\,m^2$$

Total area

$$A_{tot.A.e} := A_{tf} + A_{w.A.e1} + A_{w.A.e2} + A_{bf.A} = 0.186\,m^2 \qquad \text{Support A}$$

$$A_{tot.B.e} := A_{tf} + A_{w.B.e1} + A_{w.B.e2} + A_{bf.B} = 0.208\,m^2 \qquad \text{Support B}$$

Center of gravity

Support A:

$$z_{w.A.e1} := h_{ssp} + h_{MG.w.A} - \frac{h_{MG.w.A.e1}}{2} = 2.499\,m$$

$$z_{w.A.e2} := h_{ssp} + \frac{h_{MG.w.A} - \frac{h_{MG.w.A}}{1 - \psi_{MG.w.A}} + h_{MG.w.A.e2}}{2} = 0.795\,m$$

$$z_{na.A.e} := \frac{A_{tf} \cdot z_{tf} + A_{w.A.e1} \cdot z_{w.A.e1} + A_{w.A.e2} \cdot z_{w.A.e2} + A_{bf.A} \cdot z_{bf.A}}{A_{tot.A.e}} = 0.662\,m$$

Support B:

$$z_{w.B.e1} := h_{ssp} + h_{MG.w.B} - \frac{h_{MG.w.B.e1}}{2} = 2.466\,\text{m}$$

$$z_{w.B.e2} := h_{ssp} + \frac{h_{MG.w.B} - \frac{h_{MG.w.B}}{1 - \psi_{MG.w.B}} + h_{MG.w.B.e2}}{2} = 0.885\,\text{m}$$

$$z_{na.B.e} := \frac{A_{tf}\cdot z_{tf} + A_{w.B.e1}\cdot z_{w.B.e1} + A_{w.B.e2}\cdot z_{w.B.e2} + A_{bf.B}\cdot z_{bf.B}}{A_{tot.B.e}} = 0.833\,\text{m}$$

Moment of inertia

Top flange

$$I_{tf.A.e} := I_{x.ssp}\cdot\frac{B_{tot}}{2} + A_{tf}\cdot\left(z_{na.A.e} - z_{tf}\right)^2 = 0.043\,\text{m}^4$$ Support A

$$I_{tf.B.e} := I_{x.ssp}\cdot\frac{B_{tot}}{2} + A_{tf}\cdot\left(z_{na.B.e} - z_{tf}\right)^2 = 0.072\,\text{m}^4$$ Support B

Web

Support A:

$$I_{w.A.e1} := \frac{t_{MG.w.A}\cdot h_{MG.w.A.e1}^{3}}{12} + A_{w.A.e1}\cdot\left(z_{na.A.e} - z_{w.A.e1}\right)^2 = 0.031\,\text{m}^4$$

$$I_{w.A.e2} := \frac{t_{MG.w.A}\cdot h_{MG.w.A.e2}^{3}}{12} + A_{w.A.e2}\cdot\left(z_{na.A.e} - z_{w.A.e2}\right)^2 = 9.77\times10^{-4}\,\text{m}^4$$

Support B:

$$I_{w.B.e1} := \frac{t_{MG.w.B}\cdot h_{MG.w.B.e1}^{3}}{12} + A_{w.B.e1}\cdot\left(z_{na.B.e} - z_{w.B.e1}\right)^2 = 0.029\,\text{m}^4$$

$$I_{w.B.e2} := \frac{t_{MG.w.B}\cdot h_{MG.w.B.e2}^{3}}{12} + A_{w.B.e2}\cdot\left(z_{na.B.e} - z_{w.B.e2}\right)^2 = 7.56\times10^{-4}\,\text{m}^4$$

Bottom flange

$$I_{bf.A.e} := \frac{b_{MG.bf.A}\cdot t_{MG.bf.A}^{3}}{12} + A_{bf.A}\cdot\left(z_{na.A.e} - z_{bf.A}\right)^2 = 0.109\,\text{m}^4$$ Support A

$$I_{bf.B.e} := \frac{b_{MG.bf.B}\cdot t_{MG.bf.B}^{3}}{12} + A_{bf.B}\cdot\left(z_{na.B.e} - z_{bf.B}\right)^2 = 0.142\,\text{m}^4$$ Support B

Whole section

$I_{A.e} := I_{tf.A.e} + I_{w.A.e1} + I_{w.A.e2} + I_{bf.A.e} = 0.184\,m^4$ Support A

$I_{B.e} := I_{tf.B.e} + I_{w.B.e1} + I_{w.B.e2} + I_{bf.B.e} = 0.244\,m^4$ Support B

5.3. Moment resistance

Calculated for the bottom flange

$$M_{Rd.A} := \frac{\frac{f_y}{\gamma_{M0}} \cdot I_{A.e}}{\left(h_{ssp} + h_{MG.w.A} + t_{MG.bf.A} - z_{na.A.e}\right)} = 4.035 \times 10^4 \cdot kN \cdot m$$

$$M_{Rd.B} := \frac{\frac{f_y}{\gamma_{M0}} \cdot I_{B.e}}{\left(h_{ssp} + h_{MG.w.B} + t_{MG.bf.B} - z_{na.B.e}\right)} = 5.807 \times 10^4 \cdot kN \cdot m$$

6. Lateral torsional buckling

The bottom flange of the section is treated as a simply supported column and a reduction factor for buckling is calculated. The reduction factor is used to calculate the capacity of the composite section against lateral torsional buckling

Area of bottom flange

$A_{bf.A} = 0.025\,m^2$

$A_{bf.B} = 0.039\,m^2$

Moment of inertia of bottom flange

$$I_{bf.LT.A} := \frac{t_{MG.bf.A} \cdot b_{MG.bf.A}^{3}}{12} = 6.862 \times 10^{-4}\,m^4$$

$$I_{bf.LT.B} := \frac{t_{MG.bf.B} \cdot b_{MG.bf.B}^{3}}{12} = 1.288 \times 10^{-3}\,m^4$$

Crictical buckling force

Buckling length, distance between bracings

$L_{cr} := 8.3m$

Crictical buckling force

$$N_{cr.A} := \frac{\pi^2 \cdot E_s \cdot I_{bf.LT.A}}{L_{cr}^{2}} = 2.065 \times 10^{4} \cdot kN$$

$$N_{cr.B} := \frac{\pi^2 \cdot E_s \cdot I_{bf.LT.B}}{L_{cr}^{2}} = 3.875 \times 10^{4} \cdot kN$$

Reduction factor

Slenderness

$$\lambda_{LT.A} := \sqrt{\frac{A_{bf.A} \cdot f_y}{N_{cr.A}}} = 0.749$$ [1] (6.50)

$$\lambda_{LT.B} := \sqrt{\frac{A_{bf.B} \cdot f_y}{N_{cr.B}}} = 0.684$$

Imperfection factor c welded I-profile

$\alpha_{LT} := 0.49$ [1] Table 6.3

$$\Phi_{LT.A} := 0.5 \cdot \left[1 + \alpha_{LT} \cdot \left(\lambda_{LT.A} - 0.2\right) + \lambda_{LT.A}^{2}\right] = 0.915$$

$$\Phi_{LT.B} := 0.5 \cdot \left[1 + \alpha_{LT} \cdot \left(\lambda_{LT.B} - 0.2\right) + \lambda_{LT.B}^{2}\right] = 0.853$$

Reduction factor support A:

$$\chi_{LT.A} := \frac{1}{\Phi_{LT.A} + \sqrt{\Phi_{LT.A}^{2} - \lambda_{LT.A}^{2}}} = 0.694$$

Reduction factor support B:

$$\chi_{LT.B} := \frac{1}{\Phi_{LT.B} + \sqrt{\Phi_{LT.B}^{2} - \lambda_{LT.B}^{2}}} = 0.734$$

Moment resistance reduced for lateral torsional buckling

$$M_{b.Rd.A} := \chi_{LT.A} \cdot M_{Rd.A} = 2.801 \times 10^{4} \cdot kN \cdot m$$

$$M_{b.Rd.B} := \chi_{LT.B} \cdot M_{Rd.B} = 4.265 \times 10^{4} \cdot kN \cdot m$$

7. CAPACITY CHECKS

Patch loading

Support A

$M_{Ed.A} := |M_A| = 1.811 \times 10^4 \cdot kN \cdot m$

$\eta_{1.A} := \frac{M_{Ed.A}}{M_{Rd.A}} = 0.449$

$F_{Ed.A} := R_A = 903.473 \cdot kN$

$\eta_{2.A} := \frac{F_{Ed.A}}{F_{Rd.A}} = 0.239$

$\eta_{2.A} + 0.8 \cdot \eta_{1.A} = 0.598$ < 1,4

Support B

$M_{Ed.B} := |M_B| = 3.549 \times 10^4 \cdot kN \cdot m$

$\eta_{1.B} := \frac{M_{Ed.B}}{M_{Rd.B}} = 0.611$ < 1,0

$F_{Ed.B} := R_B = 2.55 \times 10^3 \cdot kN$

$\eta_{2.B} := \frac{F_{Ed.B}}{F_{Rd.B}} = 0.532$ < 1,0

$\eta_{2.B} + 0.8 \cdot \eta_{1.B} = 1.021$ < 1,4 [2] (7.2)

Lateral torsional buckling

Support A

$\frac{M_{Ed.A}}{M_{b.Rd.A}} = 0.647$ < 1,0

Support B

$\frac{M_{Ed.B}}{M_{b.Rd.B}} = 0.832$ < 1,0

APPENDIX D

Volume and weight comparison

Appendix D - Volume and weight comparison

Contents

1. SSP bridge

1.1. Main girders

Dimensions of the different sections

Element 1:

$b_{MG.bf.1} := 436mm$

$t_{MG.bf.1} := 26mm$

$h_{MG.w.1} := 2.6m - t_{MG.bf.1} = 2.574 \cdot m$

$t_{MG.w.1} := 19mm$

$l_{el.1} := 11m$

$A_{MG.1} := h_{MG.w.1} \cdot t_{MG.w.1} + b_{MG.bf.1} \cdot t_{MG.bf.1} \ldots = 0.06\,m^2$

Element 2:

$b_{MG.bf.2} := 490mm$ Width bottom flange

$t_{MG.bf.2} := 40mm$ Thickness bottom flange

$h_{MG.w.2} := 2.6m - t_{MG.bf.2} = 2.56\,m$ Height web

$t_{MG.w.2} := 18mm$ Thickness web

$l_{el.2} := 18m$ Length of element

$A_{MG.2} := h_{MG.w.2} \cdot t_{MG.w.2} + b_{MG.bf.2} \cdot t_{MG.bf.2} \ldots = 0.066\,m^2$ Cross-sectional area

Element 3:

$b_{MG.bf.3} := 572mm$

$t_{MG.bf.3} := 44mm$

$h_{MG.w.3} := 2.6m - t_{MG.bf.3} = 2.556 \cdot m$

$t_{MG.w.3} := 21mm$

$l_{el.3} := 15m$

$A_{MG.3} := h_{MG.w.3} \cdot t_{MG.w.3} + b_{MG.bf.3} \cdot t_{MG.bf.3} \ldots = 0.079\,m^2$

Element 4:

$b_{MG.bf.4} := 626mm$

$t_{MG.bf.4} := 63mm$

$h_{MG.w.4} := 2.6m - t_{MG.bf.4} = 2.537\,m$

$t_{MG.w.4} := 23mm$

$l_{el.4} := 11m$

$A_{MG.4} := h_{MG.w.4} \cdot t_{MG.w.4} + b_{MG.bf.4} \cdot t_{MG.bf.4} \ldots = 0.098\,m^2$

Element 5:

$b_{MG.bf.5} := 544mm$

$t_{MG.bf.5} := 46mm$

$h_{MG.w.5} := 2.6m - t_{MG.bf.5} = 2.554 \cdot m$

$t_{MG.w.5} := 21mm$

$l_{el.5} := 10m$

$A_{MG.5} := h_{MG.w.5} \cdot t_{MG.w.5} + b_{MG.bf.5} \cdot t_{MG.bf.5} \ldots = 0.079\,m^2$

Element 6:

$b_{MG.bf.6} := 490mm$

$t_{MG.bf.6} := 32mm$

$h_{MG.w.6} := 2.6m - t_{MG.bf.6} = 2.568 \cdot m$

$t_{MG.w.6} := 18mm$

$l_{el.6} := 18m$

$A_{MG.6} := h_{MG.w.6} \cdot t_{MG.w.6} + b_{MG.bf.6} \cdot t_{MG.bf.6} \ldots = 0.062\,m^2$

Total volume

$V_{MG.tot} := 4\left(A_{MG.1} \cdot l_{el.1} + A_{MG.2} \cdot l_{el.2} + A_{MG.3} \cdot l_{el.3} + A_{MG.4} \cdot l_{el.4} + A_{MG.5} \cdot l_{el.5} + A_{MG.6} \cdot l_{el.6}\right) = 24.016 \cdot m^3$

1.2. Cross bracings

Cross-sectional areas

$A_{KKR150} := 0.00346m^2$ KKR 150x150x6 profile

$A_{KKR250} := 0.00614m^2$ KKR 250x150x8 profile

$l_{bot} := 6m$ Length of bottom bracing

$l_{diag} := 3.080m$ Length of diagonal bracing

Total volume

$n_{CB} := 17$ Number of cross bracings

$V_{CB.tot} := n_{CB}\cdot\left(2A_{KKR150}\cdot l_{diag} + A_{KKR250}\cdot l_{bot}\right) = 0.989\cdot m^3$

1.3. Transverse girders

Dimensions

$B := 11.25m$ Total free width of bridge

$B_1 := 6m$ Distance between main girders

$L_{cant} := \frac{B - B_1}{2} = 2.625\,m$ Length of cantilever part

$h_{TG.w} := 557mm$ Height web

$h_{TG.we} := 0.4\cdot h_{TG.w} = 223\cdot mm$ Height of web at the edge

$t_{TG.w} := 7mm$ Thickness web

$b_{TG.bf} := 370mm$ Width bottom flange

$t_{TG.bf} := 16mm$ Thickness bottom flange

Volumes

Middle part :

$V_{TG.mid} := B_1\cdot\left(h_{TG.w}\cdot t_{TG.w} + b_{TG.bf}\cdot t_{TG.bf}\right) = 0.059\cdot m^3$

Cantilever part :

$L_{TG.edge} := \sqrt{\left(L_{cant}\right)^2 + \left(0.6\cdot h_{TG.w}\right)^2} = 2.646\,m$

$V_{TG.edge} := L_{cant}\cdot\frac{0.4h_{TG.w} + h_{TG.w}}{2}\cdot t_{TG.w} + L_{TG.edge}\cdot b_{TG.bf}\cdot t_{TG.bf} = 0.023\cdot m^3$

Total volume:

$n_{TG} := 17$ Number of transverse girders

$V_{TG.tot} := n_{TG}\left(V_{TG.mid} + 2V_{TG.edge}\right) = 1.778 \cdot m^3$

1.4. Transverse support girders

Dimensions

Support A & D:	Support B & C:	
$h_{TGS.AD.w} := 1115mm$	$h_{TGS.BC.w} := 1915mm$	Height web
$t_{TGS.AD.w} := 15mm$	$t_{TGS.BC.w} := 25mm$	Thickness web
$b_{TGS.AD.bf} := 350mm$	$b_{TGS.BC.bf} := 450mm$	Width bottom flange
$t_{TGS.AD.bf} := 20mm$	$t_{TGS.BC.bf} := 30mm$	Thickness bottom flange

Total volume

$V_{TGS.tot} := 2 \cdot B_1 \cdot \left(h_{TGS.AD.w} \cdot t_{TGS.AD.w} + b_{TGS.AD.bf} \cdot t_{TGS.AD.bf}\right) \ldots = 1.113 \cdot m^3$
$+ 2 \cdot B_1 \cdot \left(h_{TGS.BC.w} \cdot t_{TGS.BC.w} + b_{TGS.BC.bf} \cdot t_{TGS.BC.bf}\right) \ldots$
$+ 4 \cdot V_{TG.edge}$

1.5. Edge beams

Dimensions

$L_{tot} := 166m$ Total length of bridge

$h_{EB} := 402mm$ Height

$b_{EB} := 300mm$ Width flanges

$t_{EB} := 20mm$ Thickness

$A_{EB} := t_{EB} \cdot \left[h_{EB} + \left(b_{EB} - t_{EB}\right)\right] = 0.014\,m^2$ Cross-sectional area

Total volume

$V_{EB.tot} := 2 \cdot L_{tot} \cdot A_{EB} = 4.528 \cdot m^3$

1.6. Deck

Dimensions

$B := 11.25m$

$A_{ssp} := 0.022165 \frac{m^2}{m}$

$t_{cover} := 50mm$

Total volume

$V_{SSP.tot} := A_{ssp} \cdot B \cdot L_{tot} = 41.393 \cdot m^3$

$V_{cover.tot} := t_{cover} \cdot B \cdot L_{tot} = 93.375 \cdot m^3$

2. Composite bridge

2.1. Main girders

Dimensions of the different sections

Element 1:

$b_{MG.bf.1} := 800mm$

$t_{MG.bf.1} := 26mm$

$b_{MG.tf.1} := 500mm$

$t_{MG.tf.1} := 20mm$

$h_{MG.w.1} := 2.6m - t_{MG.bf.1} - t_{MG.tf.1} = 2.554 \cdot m$

$t_{MG.w.1} := 19mm$

$l_{el.1} := 11m$

$A_{MG.1} := h_{MG.w.1} \cdot t_{MG.w.1} \cdots = 0.079\,m^2$
$+ b_{MG.bf.1} \cdot t_{MG.bf.1} \cdots$
$+ b_{MG.tf.1} \cdot t_{MG.tf.1}$

Element 2:

$b_{MG.bf.2} := 900mm$ Width bottom flange

$t_{MG.bf.2} := 40mm$ Thickness bottom flange

$b_{MG.tf.2} := 600mm$ Width top flange

$t_{MG.tf.2} := 30mm$ Thickness top flange

$h_{MG.w.2} := 2.6m - t_{MG.bf.2} - t_{MG.tf.2} = 2.53\,m$ Height web

$t_{MG.w.2} := 18mm$ Thickness web

$l_{el.2} := 18m$ Length of element

$A_{MG.2} := h_{MG.w.2} \cdot t_{MG.w.2} \cdots = 0.1\,m^2$ Cross-sectional area
$+ b_{MG.bf.2} \cdot t_{MG.bf.2} \cdots$
$+ b_{MG.tf.2} \cdot t_{MG.tf.2}$

Element 3:

$b_{MG.bf.3} := 1050mm$

$t_{MG.bf.3} := 44mm$

$b_{MG.tf.3} := 600mm$

$t_{MG.tf.3} := 40mm$

$h_{MG.w.3} := 2.6m - t_{MG.bf.3} - t_{MG.tf.3} = 2.516 \cdot m$

$t_{MG.w.3} := 21mm$

$l_{el.3} := 15m$

$A_{MG.3} := h_{MG.w.3} \cdot t_{MG.w.3} \cdots = 0.123\,m^2$
$+ b_{MG.bf.3} \cdot t_{MG.bf.3} \cdots$
$+ b_{MG.tf.3} \cdot t_{MG.tf.3}$

Element 4:

$b_{MG.bf.4} := 1150mm$

$t_{MG.bf.4} := 63mm$

$b_{MG.tf.4} := 780mm$

$t_{MG.tf.4} := 63mm$

$h_{MG.w.4} := 2.6m - t_{MG.bf.4} - t_{MG.tf.4} = 2.474\,m$

$t_{MG.w.4} := 23mm$

$l_{el.4} := 11m$

$A_{MG.4} := h_{MG.w.4} \cdot t_{MG.w.4} \cdots = 0.178\,m^2$
$+ b_{MG.bf.4} \cdot t_{MG.bf.4} \cdots$
$+ b_{MG.tf.4} \cdot t_{MG.tf.4}$

Element 5:

$b_{MG.bf.5} := 1000mm$

$t_{MG.bf.5} := 46mm$

$b_{MG.tf.5} := 600mm$

$t_{MG.tf.5} := 46mm$

$h_{MG.w.5} := 2.6m - t_{MG.bf.5} - t_{MG.tf.5} = 2.508 \cdot m$

$t_{MG.w.5} := 21mm$

$l_{el.5} := 10m$

$A_{MG.5} := h_{MG.w.5} \cdot t_{MG.w.5} \cdots = 0.126\,m^2$
$+ b_{MG.bf.5} \cdot t_{MG.bf.5} \cdots$
$+ b_{MG.tf.5} \cdot t_{MG.tf.5}$

Element 6:

$b_{MG.bf.6} := 900mm$

$t_{MG.bf.6} := 32mm$

$b_{MG.tf.6} := 600mm$

$t_{MG.tf.6} := 23mm$

$h_{MG.w.6} := 2.6m - t_{MG.bf.6} - t_{MG.tf.6} = 2.545 \cdot m$

$t_{MG.w.6} := 18mm$

$l_{el.6} := 18m$

$A_{MG.6} := h_{MG.w.6} \cdot t_{MG.w.6} \cdots = 0.088\,m^2$
$+ b_{MG.bf.6} \cdot t_{MG.bf.6} \cdots$
$+ b_{MG.tf.6} \cdot t_{MG.tf.6}$

Total volume

$V_{MG.C.tot} := 4\left(A_{MG.1} \cdot l_{el.1} + A_{MG.2} \cdot l_{el.2} + A_{MG.3} \cdot l_{el.3} + A_{MG.4} \cdot l_{el.4} + A_{MG.5} \cdot l_{el.5} + A_{MG.6} \cdot l_{el.6}\right) = 37.309 \cdot m^3$

2.2. Cross bracings

Cross-sectional areas

$A_{KKR150} := 0.00346m^2$ KKR 150x150x6 profile

$A_{KKR250} := 0.00614m^2$ KKR 250x150x8 profile

$l_{top} := 6m$ Length of top bracing

$l_{bot} := 6m$ Length of bottom bracing

$l_{diag} := 3.219m$ Length of diagonal bracing

Total volume

$n_{CB} := 20$ Number of cross bracings

$V_{CB.C.tot} := n_{CB} \cdot \left(A_{KKR150} \cdot l_{top} + 2A_{KKR150} \cdot l_{diag} + A_{KKR250} \cdot l_{bot}\right) = 1.598 \cdot m^3$

2.3. Transverse support girders

Dimensions

Support A & D:	Support B & C:	
$h_{TGS.AD.w} := 1100mm$	$h_{TGS.BC.w} := 1890mm$	Height web
$t_{TGS.AD.w} := 15mm$	$t_{TGS.BC.w} := 25mm$	Thickness web
$b_{TGS.AD.bf} := 350mm$	$b_{TGS.BC.bf} := 450mm$	Width bottom flange
$t_{TGS.AD.bf} := 20mm$	$t_{TGS.BC.bf} := 30mm$	Thickness bottom flange
$b_{TGS.AD.tf} := 200mm$	$b_{TGS.BC.tf} := 350mm$	Width top flange
$t_{TGS.AD.tf} := 15mm$	$t_{TGS.BC.tf} := 25mm$	Thickness top flange

Total volume

$$V_{TGS.C.tot} := 2 \cdot B_1 \cdot \left(h_{TGS.AD.w} \cdot t_{TGS.AD.w} + b_{TGS.AD.bf} \cdot t_{TGS.AD.bf} + b_{TGS.AD.tf} \cdot t_{TGS.AD.tf} \right) \dots = 1.152 \cdot m^3$$
$$+ 2 \cdot B_1 \cdot \left(h_{TGS.BC.w} \cdot t_{TGS.BC.w} + b_{TGS.BC.bf} \cdot t_{TGS.BC.bf} + b_{TGS.BC.tf} \cdot t_{TGS.BC.tf} \right)$$

2.4. Edge beams

Total volume

$A_{EB} := 0.017946m^2$

$V_{EB.C.tot} := 2 \cdot L_{tot} \cdot A_{EB} = 5.958 \cdot m^3$

2.6. Deck

Total volume

$V_{deck.C.tot} := 654.382m^3 - V_{EB.C.tot} = 648.424 \cdot m^3$

3. Weight comparison

Self-weights

$\gamma_{concrete} := 25 \frac{kN}{m^3}$

$\gamma_{steel} := 77 \frac{kN}{m^3}$

$\gamma_{cover.ssp} := 23 \frac{kN}{m^3}$

$$G_{cover.C} := 2.77\,\frac{kN}{m^2}\cdot B\cdot L_{tot} = 5.173 \times 10^6\,N$$

Launching weigths

$$G_{L.C} := \gamma_{steel}\cdot\left(V_{MG.C.tot} + V_{CB.C.tot} + V_{TGS.C.tot}\right) = 3.085\cdot MN$$

$$G_{L.ssp} := \gamma_{steel}\cdot\left(V_{MG.tot} + V_{CB.tot} + V_{TG.tot} + V_{TGS.tot} + V_{EB.tot} + V_{SSP.tot}\right) = 5.684\cdot MN$$

$$\frac{G_{L.ssp}}{G_{L.C}} = 1.843$$

Total weights

$$G_{tot.C} := G_{L.C} + G_{cover.C} + \gamma_{concrete}\cdot V_{deck.C.tot} = 24.468\cdot MN$$

$$G_{tot.ssp} := G_{L.ssp} + \gamma_{cover.ssp}\cdot V_{cover.tot} = 7.832\cdot MN$$

$$\frac{G_{tot.ssp}}{G_{tot.C}} = 0.32$$

APPENDIX J

Mesh convergence

Mesh convergence are presented here for:

- Stress in the main girder bottom flange
- Stress in the top plate of the SSP over support
- Compressive stress in SSP bottom plate due to bending over the main girder

The mesh convergence for the local stresses in the top plate of the SSP is shown in the report. Some of the convergence studies was carried out before the increase in thickness of the top plate, therefore the stresses can differ some from the final values presented in the report. Some of the convergence studies were conducted before the top plate thickness was changed.

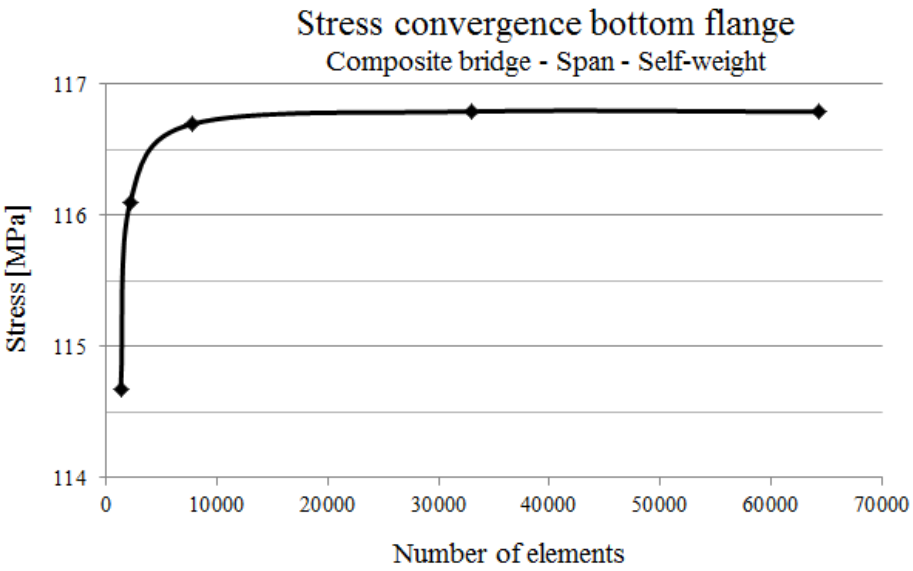

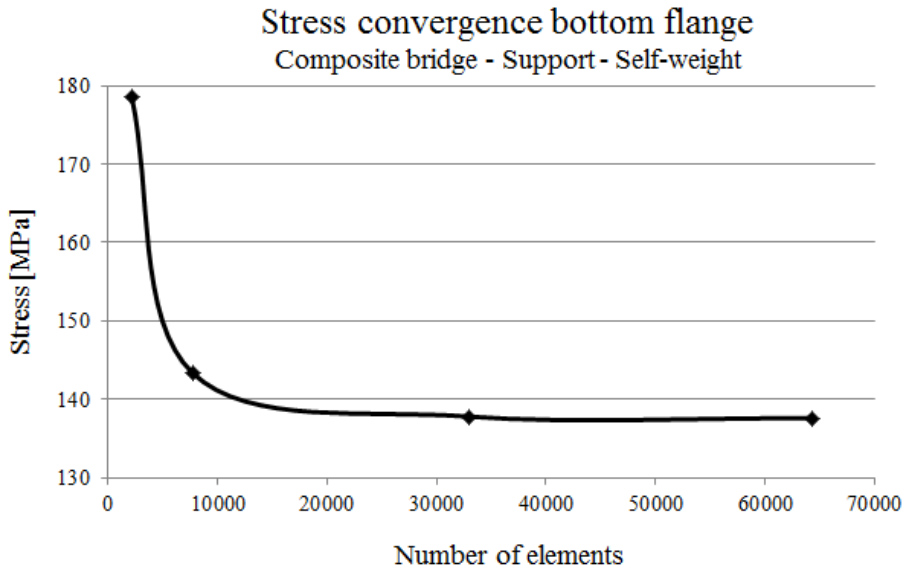

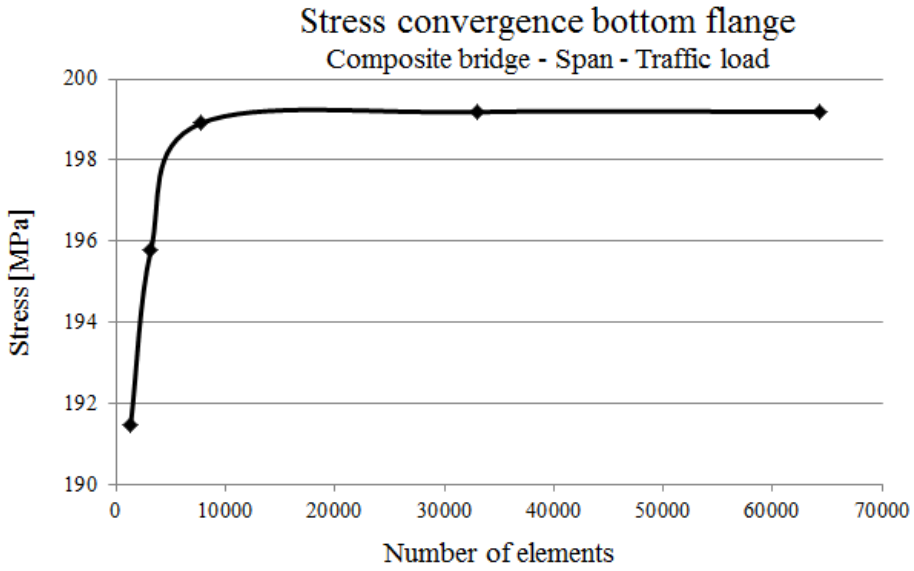
Stress convergence bottom flange
Composite bridge - Span - Traffic load
Stress [MPa]
200
198
196
194
192
190
0
10000
20000
30000
40000
50000
60000
70000
Number of elements

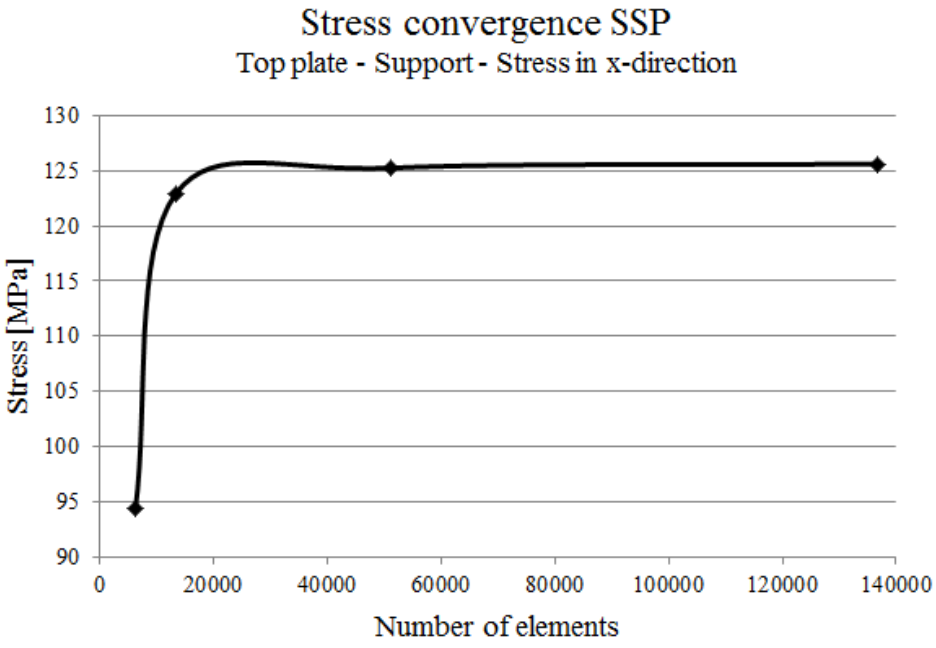
Stress convergence SSP
Top plate - Support - Stress in x-direction
Stress [MPa]
130
125
120
115
110
105
100
95
90
0
20000
40000
60000
80000
100000
120000
140000
Number of elements

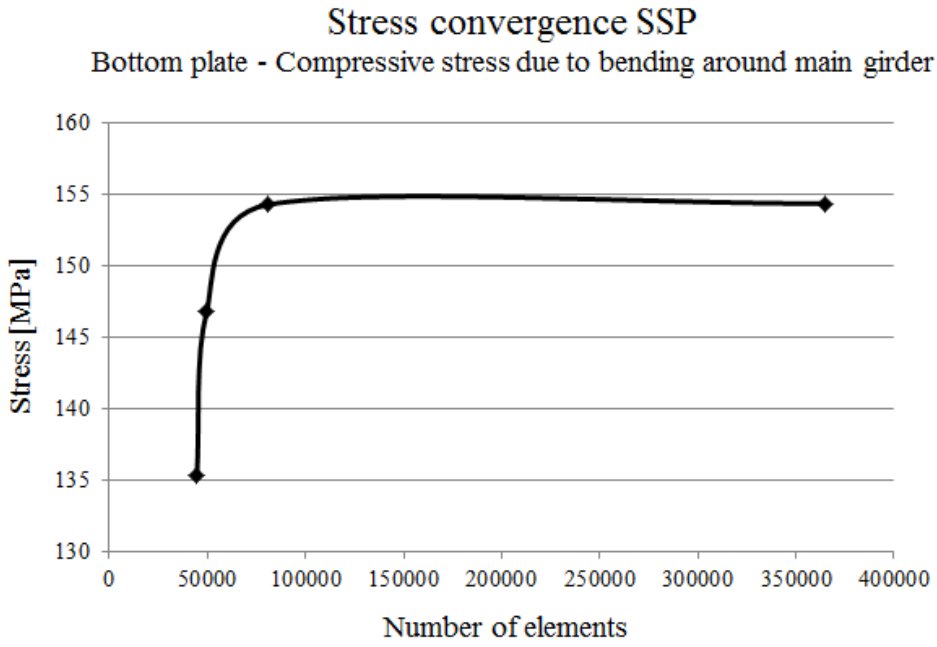
Stress convergence SSP
Bottom plate - Compressive stress due to bending around main girder
Stress [MPa]
160
155
150
145
140
135
130
0
50000
100000
150000
200000
250000
300000
350000
400000
Number of elements